Design and Synthesis of Potent Benzimidazolone HIV Non-nucleoside Reverse Transcriptase Inhibitors

by
Nicole Pribut

Dissertation presented for the degree of
Doctor of Philosophy in Chemistry
in the
Faculty of Science at
Stellenbosch University

Supervisor: Dr S.C. Pelly

Co-supervisor: Prof W.A.L. van Otterlo

December 2018

Declaration

By submitting this thesis electronically, I declare that the entirety of the work contained therein is my own, original work, that I am the authorship owner thereof (unless to the extent explicitly otherwise stated) and that I have not previously in its entirety or in part submitted it for obtaining any qualification.

Date: December 2018

Abstract

Since the 1980's, HIV has plagued the population on a global scale, with millions of newly infected individuals reported every year. However, with the introduction of combination therapy, which can significantly suppress viremia to almost undetectable levels in the infected populace, the disease can be managed to a point where the infected population can live almost normal lives. Unfortunately, although able to improve quality of life and prevent the onset of AIDS, combination therapy is not curative as issues related to drug resistance and adherence can lead to the re-emergence of high viremia, AIDS and, inevitably, death. Consequently, there remains a need for the continued development of new and superior ARVs that are effective against wild-type and resistant strains of HIV and are well tolerated for chronic use.

In an effort to address this need, our group has focused on the design and synthesis of new NNRTIs. In the clinic, NNRTIs are an important part of first-line regimens employed in the treatment of HIV. In particular, our group focused on the synthesis of a series of small benzimidazolone-containing NNRTIs which were initially designed to address lability issues exhibited by a series of potent indole-based NNRTIs. These first-generation benzimidazolones were readily synthesized over five steps and, following evaluation in an HIV whole cell assay, were found to be potent inhibitors of HIV RT, but were susceptible to clinically relevant resistant strains such as K103N and Y181C.

As a result, we synthesized a series of second-generation benzimidazolone NNRTIs which were designed to overcome, specifically, the Y181C resistant strain. Starting from 2-amino-3-nitrophenol, the benzimidazolone precursor for these compounds was synthesized over six steps. This precursor was then coupled to various aryl or heteroaryl halides by way of an Ullmann reaction or S_NAr. Of this small library, one compound in particular was found to be potent (with low nanomolar activity), not only against wild-type, but also against Y181C, Y188C and the double mutant K103N/Y181C. Furthermore, this compound, 3-chloro-5-((3-ethyl-2-oxo-1-((2-trimethylsilyl)ethoxy)methyl)-2,3-dihydro-1*H*-benzo[*d*]imidazol-4-yl)oxy)benzonitrile, exhibited only low levels of susceptibility against the most problematic K103N resistant strain.

We envisaged that by introducing additional electrostatic interactions between our potent lead compound and the NNIBP we would succeed in optimizing the efficacy of our compound against wild-type

and resistant strains of HIV. In order to achieve these additional interactions we adopted two different approaches.

The first approach focused on targeting a lysine residue located at the top of a narrow hydrophobic chimney towards the back of the NNIBP. To this end, we installed a cyanovinyl substituent onto our lead compound which, based on docking studies, would protrude into the chimney and form a hydrogen bond with the targeted lysine. Installation of the cyanovinyl substituent was achieved using the well-established Heck coupling reaction. Although this compound, (*E*)-3-(2-cyanovinyl)-5-((3-ethyl-2-oxo-2,3-dihydro-1*H*-benzo[*d*]imidazol-4-yl)oxy)benzonitrile, was also a potent inhibitor of HIV RT, it was unfortunately not significantly more potent than our existing lead compound.

The second approach employed a molecular hybridization technique to form a combination of our lead compound and efavirenz, in order to achieve additional hydrogen bonding to the backbone of Lys101. This new hybrid compound, 3-chloro-5-((4,4-dimethyl-2-oxo-1,4-dihydro-2*H*-benzo[*d*][1,3]oxazin-5-yl)oxy)benzonitrile, was successfully synthesized over seven steps and found to be slightly more potent than our lead compound with an improved selectivity index.

Uittreksel

Sedert die 1980's het MIV in 'n globale pandemie geraak waar miljoene mense jaarliks gediagnoseer word. Die gebruik van kombinasie terapie het gelei tot grootskaalse onderdrukking van viremie in so 'n mate dat dit gevolglik onopspoorbaar is, en dus sorg dat mense met HIV amper 'n normale lewe kan lei. Alhoewel die behandeling van mense met HIV hulle lewens gehalte verbeter het en die aanvang van VIGS verhoed, is hedendaagse behandeling nie genesend nie, en as gevolg van dwelm-bestandhied moontlik kan lei to die herverskyning van 'n hoë viralelading, VIGS en dan dood. As gevolg van hierdie dilemma, is daar tans 'n groot nood vir navorsing en onwikkeling vir nuwe ARV medisyne wat effektief is teen wilde-tipe en dwelm-bestande MIV stamme, tesame met minimale newe effekte wat 'n resultaat is van daaglikse gebruik.

Om die tekort aan nuwe en effektiewe antiretrovirale medisyne aan te spreek, het ons groep gefokus op om nuwe nie-nukleosied-omgekeerde transkriptase-inhibeerders (NNRTI's) te ontwerp en te sintetiseer, sedert NNRTI's beskou word as 'n belangrike gedeelte vir die behandeling van MIV. Ons groep het onder andere gefokus op die sintesise van 'n klein reeks molekules wat 'n bensimidasoloon kern bevat. Die reeks was aanvanklik gesintetiseer om probleme rakend die chemiese stabiliteit van 'n voorheen gesintetiseerde reeks indool NNRTI's, ook deur ons groep ontwikkel, aan te spreek. Die eerste generasie reeks bensimidasoloon molekules was maklik geskep oor vyf stappe, en heel sel toetse teenoor MIV omgekeerde transkriptase het getoon dat hulle kragtige inhibeerders van die ensiem was, maar was ook onder andere vatbaar vir relevante MIV stamme soos K103N en Y181C.

As gevolg daarvan het ons 'n tweede generasie reeks bensimidasoloon NNRTI's ontwerp om hierdie tekortkoming teenoor K103N en spesifiek die Y181C weerstandige stam te verbeter. Deur te begin met 2-amino-3-nitro fenol was die bensimidasoloon voorloper gesintetiseer in ses stappe. Die voorloper was dan gekoppel met menigte aromatiese en heteroaromatiese haliede deur middel van of die Ullmann-koppel reaksie of S_NAr. Een molekule uit hierdie reeks, 3-chloro-5-((3-ethyl-2-oxo-1-((2-trimethylsilyl)ethoxy)methyl)-2,3-dihydro-1*H*-benzo[*d*]imidazol-4-yl)oxy)benzonitrile, was aktief gewees met lae nanomolaar aktiwiteit teenoor die wilde-tipe MIV maar ook teenoor Y181C, Y188C en die dubbel mutant K103N/Y181C, met net 'n klein hoeveelheid weerstand teenoor die problematiese K103N MIV stam.

Deur addisionele elektrostatiese interaksies by te voeg tussen ons aktiefste molekule en die NNIBP, het ons probeer bevestig of ons die aktiwitiet teenoor die wilde tipe MIV stam sal kan verbeter. Om hierdie idee van addisionele interaksies te laat realiseer het ons twee verskillende metodes benader. In die eerste metode het ons daarop gefokus om ‘n lisien residu te teiken wat in die boonste gedeelte van die smal hidrofobiese skoorsteen in die aktiewe setel van die NNIBP geleë is. Ons het ‘n nitriel-viniel groep geïnstalleer op ons mees aktiefste molekule wat, deur middle van dokstudies, getoon het dat die nitriel-viniel groep moontlik sal inbeweeg in die skoorsteen gedeelte en ‘n waterstof-binding vorm met die lisien residu. Inkorporering van die nitriel-viniel substituent was gedoen deur die uitvoering van ‘n Heck-koppel reaksie. Alhoewel die nitriel-viniel molecule, (*E*)-3-(2-cyanovinyl)-5-((3-ethyl-2-oxo-2,3-dihydro-1*H*-benzo[*d*]imidazol-4-yl)oxy)benzonitrile, goeie aktiwiteit getoon het teenoor MIV omgekeerde transkriptase, was dit nie moontlik om die oorspronlike aktiewe molekuul se aktiwiteit drasties te verbeter nie.

Die tweede benadering het ‘n molekulêre hibridisasie tegniek ingesluit waar ons ons aktiewe molekuul en efavirenz gebaster het sodat daar moontlik ‘n addisionele waterstof-binding gemaak kan word met ‘n Lys101 residu in die aktiewe setel. Hierdie hibried molekuul, 3-chloro-5-((4,4-dimethyl-2-oxo-1,4-dihydro-2*H*-benzo[*d*][1,3]oxazin-5-yl)oxy)benzonitrile, was suksesvol gesintetiseer oor sewe stappe, en was meer aktief as die oorspronglike aktiewe molekuul, maar het ook ‘n verbeterde selektiwiteits indeks getoon in vergelyking met die oorspronklike aktiewe molekuul.

Acknowledgements

Personal Acknowledgements

First and foremost, to my supervisor, Dr. Stephen Pelly, for your unwavering support and guidance over the past couple of years and for your complete faith in my ability as a chemist. I could not have asked for a better mentor! Your enthusiasm for the lab and for Medicinal Chemistry has certainly sown my own interest in the field and has made many a bad day in the lab more tolerable. Moreover, I am eternally grateful to you for bringing to pass my time at Emory University.

To my co-supervisor, Prof. Willem van Otterlo, for all the valuable advice and aid you have provided during the course of my time at Stellenbosch University.

To Dr. Dennis Liotta, for granting me the opportunity to carry out my final graduate year in your labs at Emory University. It has been a life-changing experience and I feel incredibly privileged that you will permit me to remain a part of your amazing research team. I am looking forward to becoming a part of new and exciting projects!

To Dr. Adriaan Basson, for the amazing work that you have done for us over the past couple of years. Your knowledge in the field of HIV has been invaluable.

To Dr. Jaco Brand and Else Malherbe, for your knowledge and assistance with NMR at Stellenbosch University. To the team at CAF and Marietjie Stander at Stellenbosch University for all things relating to HRMS and LC-MS. To Dr. John Bacsa at the Emory University Crystallography Center for your contribution towards this project and to Dr. Frederick Strobel and his team at the Emory Mass Spectrometry Center for HRMS.

To the group of Organic and Medicinal Chemistry (GOMOC), my friends and peers at Stellenbosch University, you guys have truly made my time at Stellenbosch a memorable one. Thank you for all your assistance, whenever it was needed, for unforgettable group getaways and, of course, for many an afternoon of beer and laughter.

To the research team at Emory University, for many interesting and valuable discussions that made me realize how much more I still need to learn. To the team on the fifth floor especially, thank you for wholly

accepting me as a colleague and as a friend. You guys are amazing, and I look forward to spending the next year, maybe two, with you!

To my mom, losing you two years ago and having to work at a PhD while coming to terms with my grief was challenging and, at times unbearable, but here I am! Thank you for always believing in me and loving me unconditionally. To my dad, you have always been such an inspiration and a role-model, and without you I would not be where I am today. Thank you for instilling in me a love for Science! To my brother, Devin, for always having my back and for being the most generous and genuine person that you are. To Sharon, Jeanne and Sue for all your love and support over the years.

To Leon, thank you for being my rock and for being by my side through some of the toughest moments of my life. Thank you for always being so supportive, patient and understanding. You are truly a gem of a person and I am so lucky to have you in my life.

Acknowledgements for Funding

For funding, I would like to acknowledge the National Research Foundation for the generous bursary that has allowed me to continue with my studies and complete a PhD.

Finally, once again to Dr. Dennis Liotta for funding my time at Emory University. Without which, my time in the States would not have been possible.

Abbreviations:

3'-P	– 3'-processing
3TC	– lamivudine
6HB	– six-helix bundle formation
ABC	– abacavir
AIDS	– acquired immunodeficiency virus
ART	– antiretroviral therapy
ARVs	– antiretrovirals
AZT	– azidothymidine
BPI	– boosted protease inhibitor
BW	– Burroughs Wellcome Co.
CA	– capsid
CC_{50}	– half maximal cytotoxic concentration
CCD	– catalytic core domain
CDI	– carbonyldiimidazole
CDK9	– cyclin dependent kinase 9
CTD	– C-terminal binding domain
cycT1	– cyclin T1
CYP450	– cytochrome P450
d4T	– stavudine
ddC	– zalcitabine
Ddl	– didanosine
dsDNA	– double-stranded DNA
Env	– viral envelope protein
ESCRT	– endosomal sorting complex required for transport
EWG	– electron-withdrawing group
FLV	– Friend Leukemia Virus
FTC	– emtricitabine
FTIR	– fourier-transform infrared spectroscopy
GPCRs	– G-protein-coupled receptors
HAART	– highly-active antiretroviral therapy
HaSV	– Harvey Sarcoma Virus
hDNA	– host DNA
HEPT	– 1-(2-hydroxyethoxymethyl)-6-(phenylthiol)thymine
HIV	– human immunodeficiency virus
HRMS	– high resolution mass spectroscopy
HTLV-1	– human T-cell leukemia virus 1
IC_{50}	– half maximal inhibitory concentration
IN	– integrase
INSTIs	– integrase strand transfer inhibitors
LDA	– lithium diisopropyl amide
LTR	– long-terminal-repeat
MA	– matrix protein
Met-tRNA	– methionyl-tRNA
n-BuLi	– *n*-butyl lithium
NC	– nucleocapsid
NMR	– nuclear magnetic resonance spectroscopy
NMT	– N-myristoltransferase
NNIBP	– non-nucleoside inhibitor binding pocket
NNRTIs	– non-nucleoside reverse transcriptase inhibitors
NRTIs	– nucleoside reverse transcriptase inhibitors
NTD	– N-terminal binding domain

pbs – primer binding site
$Pd(OAc)_2$ – palladium diacetate
$Pd(PPh_3)_2$ – tetrakis(triphenylphosphine)palladium(0)
Pd/C – palladium on carbon
PIC – preintegration complex
Pol II – RNA polymerase II
PPh_3 – triphenyl phosphine
PR – protease
$Pr55^{Gag}$ – Gag precursor polyprotein
pre-mRNA – precursor mRNA
P-TEFb – positive transcription elongation factor
RNase H – ribonuclease H
RRE – Rev response element
RT – reverse transcriptase
RTC – reverse transcription complex
SAR – structure activity relationship
SEM – 2-(trimethylsilyl)ethoxy methyl
SIVcpz – Chimpanzee associated Simian Immunodeficiency Virus
SIVgor – Gorilla associated Simian Immunodeficiency Virus
S_NAr – aromatic nucleophilic substitution reaction
ssDNA – single-stranded DNA
ssRNA – single-stranded RNA
ST – strand-transfer
STR – single tablet regimen
TAR – transactivation response element
Tat – transcriptional transactivator protein
TBAF – tetrabutylammonium fluoride
TCDI – thiocarbonyldiimidazole
TDF – tenofovir disoproxil fumarate
TIBO – 4,5,6,7- tetrahydroimidazo[4,5,1-*jk*][1,4]benzodiazepine-2(1*H*)one
TLC – thin layer chromatography
TMS – trimethylsilyl
vDNA – viral DNA
Vpr – viral protein R
WHO – World Health Organization

Amino Acids:
Asn (N) – asparagine
Asp (D) – aspartic acid
Cys (C) – cysteine
Glu (E) – glutamic acid
Lys (K) – lysine
Phe (F) – phenylalanine
Trp (W) – tryptophan
Tyr (Y) – tyrosine
Val (V) – valine

Table of Contents

Chapter 1: A Brief Introduction to HIV and Current Therapeutic Strategies

1.1. The Discovery of HIV-1 as the Cause of AIDS

On the 3rd of January 1983, in the lab of Francoise Sinoussi, a new retrovirus was identified in a T-lymphocyte culture obtained from a man with a lymphadenopathy in the neck.[1] This new retrovirus, which we now know to be human immunodeficiency virus (HIV) and the causative agent of acquired immune-deficiency virus (AIDS), would become the most significant epidemic to plague the population on a global scale.

The discovery of HIV as the cause of AIDS was a serendipitous one at a time when it was believed that human retroviruses did not exist and that severe epidemic diseases were restricted to the "Third World".[2] As a result it was thought that other factors such as chemicals, fungi and autoimmune responses to leukocytes were responsible for the onset of AIDS. Despite this unfavourable backdrop, a few scientists remained persistent in their efforts to identify retroviruses in human cancers, particularly in breast cancer and leukemia.[3] In 1979 in the laboratory of Robert Gallo, human T-cell leukaemia virus 1 (HTLV-1), the first human retrovirus was discovered and isolated. Not long after that Luc Montagnier identified lymphotropic retroviruses in human T-cell cultures.[1-2] These discoveries were significant in establishing that human retroviruses did exist and encouraged speculation that a retrovirus could be the causative agent of AIDS. Gallo hypothesized that this retrovirus would be a close relative of HTLV-1 due to observations that HTLV-1 and AIDS manifested in a similar manner.[4] Patients with AIDS and those infected with HTLV-1 both presented with decreased levels of CD4+ T-cells and it was known that both diseases could be transmitted through blood, sexual activity and mother-to-child transmission. However, it was later discovered that HIV was not a close relative to HTLV-1, but a completely new retrovirus altogether.[2]

What followed in the years 1983 to 1987 was considered a "period of intense discovery" by Jonathon Mann of the World Health Organization (WHO).[5] Within two years of the discovery of HIV as the causative agent of AIDS the HIV genome was fully cloned and sequenced, the heterogeneity of the HIV genome described, the first blood test was made available and treatment in the form of AZT was introduced.[5-6]

The rapidity with which research progressed led to the hope and expectation that the problem of AIDS would be swiftly resolved. In fact, in 1984 the then US Secretary of Health and Human Services, Margaret M. Heckler, predicted that a vaccine and consequently a cure would become available in the next two

years.[6] However, the defences of HIV to avoid the immune response would render the development of a viable vaccine close to impossible.

1.2. The State of HIV-1 Today

Despite high expectations, 34 years after its discovery HIV still affects millions of people on a global scale. The latest statistics reported by UNAIDS and the WHO in 2017 estimated that 36.7 million people worldwide were living with HIV in 2016 and approximately 1.8 million of those reported were newly infected.[7] Sadly, of the millions of infected individuals, approximately 6% are children under the age of 15 years.[7] Most of these children became infected due to mother-to-child transmission *in utero*, during delivery or through breastfeeding.[8] For the rest of the population HIV can be transmitted through accidental contact with infected blood due to contaminated needles, blood transfusions or sexual intercourse. Individuals considered to be at high risk of infection include individuals who practise promiscuous and risky homo or heterosexual behaviour and intravenous drug users.[8] In low to middle income countries young women under the age of 24 are also associated with increased risk of infection, a consequence of gender-based violence, inequity and a lack of awareness of the disease.[8-9]

The most severely affected areas are developing countries which include most of Africa, South America, Southeast Asia and India.[7] Sub-Saharan Africa alone hosts almost 70% of the globe's infected population and of the Sub-Saharan African countries, South Africa has the highest reported incidence of HIV-positive individuals.[8]

Even though HIV-1 still poses a significant public health challenge, the acquisition of HIV is no longer a death sentence and most of the infected population can live a relatively normal life. This can largely be attributed to the introduction of antiretroviral (ARV) therapeutics (To be discussed in more detail in section **1.5.**). Today, ARVs are administered the moment a diagnosis of HIV is made regardless of age and CD4+ count.[10] Although not a cure for HIV-1, the introduction of ARVs has improved quality of life and decreased the mortality rate by controlling viral loads in the infected population. In 2016 the number of AIDS related deaths was reported to be 1.0 million, a 48% decrease from the number of deaths reported in 2005.[7] According to the 2016 UNAIDS global AIDS update approximately 17 million people infected with HIV are taking ARVs, a significant improvement on the 7.5 million reported in 2010.[11] Although a notable

achievement for the "90-90-90"* initiative against HIV, these statistics suggest that the remaining 54% of the infected population are not receiving treatment.[12] A shortfall that could be a consequence of the fact that a large number of HIV-positive individuals are not aware of their HIV status.[11]

In high-prevalence regions such as Sub-Saharan Africa, ARV coverage is less than optimal as a majority of the population are situated in resource-poor rural areas with limited access to adequate health care facilities and qualified medical staff.[10] Not only does this prevent infected individuals from seeking ARV treatment, it also affects the adherence of those already receiving ARV treatment.[13] Furthermore, deficiencies in service delivery resulting in pharmacy drug stock-outs represents another major issue for drug adherence.[14] This poses a serious problem for maintaining the suppression of viral levels in infected individuals as poor adherence would unavoidably lead to the onset of drug resistance, disease progression to AIDS and ultimately death.

Complex social, structural and economic factors need to also be recognized as impediments to the global initiative against HIV.[11] Accounts of HIV-related stigma and discrimination against HIV-positive individuals completely undermine preventative measures.[15-16] HIV-related stigma often leads to the refusal of infected individuals to seek out treatment, divulge their status to prospective partners for fear of rejection or to adhere to recommended treatment regimens.[17]

1.3. HIV Origins and Heterogeneity

The origin of HIV-1 can be traced back to a lentivirus known as simian immunodeficiency virus (SIV) isolated from the common chimpanzee (*Pan troglodytes troglodytes,* SIVcpz) found only in the Central African regions of southern Cameroon, Gabon and the Republic of Congo.[18-20] Not only did SIVcpz share a close genetic relationship to HIV-1 but in some cases manifested in the same manner with decreased CD4 levels and increased risk of death.[21] The exact means by which the primate precursor to HIV was transmitted to humans has not yet been determined. However, researchers have hypothesized that transmission of the virus to humans occurred due to accidental exposure to blood or bodily fluids of

* The 90-90-90 initiative is a UNAIDS initiative to end the AIDS epidemic. The aim of this initiative is to ensure that by 2020 90% of individuals living with HIV should know their HIV status, 90% of all individuals diagnosed with HIV will receive antiretroviral therapy and that 90% of those individuals on antiretroviral therapy will experience viral suppression.

infected chimpanzees through hunting, the preparation of bushmeat or from bites or scratches obtained from captive chimpanzees.[21]

The evolution of SIVcpz, the primate precursor of HIV, has resulted in four divergent lineages of HIV-1 termed group M (major), O (outlier), N (nonmajor) and P. Studies have determined that groups M, and N arose as a result of two independent cross-species transmission events between chimpanzees and humans in the early twentieth century.[22] Interestingly, group P was found to originate from SIVgor, a lentivirus discovered in the Western lowland gorilla of Cameroon in 2006.[23-24] Just recently, in 2015, the question as to whether group O originated from SIVcpz or SIVgor was resolved as researchers isolated a new SIVgor strain closely related to the group O virus.[25] SIVgor shares a close phylogenetic relationship with SIVcpz, suggesting that a cross-species transmission event was likely to have occurred between chimpanzees and gorillas.[21]

Group M is the predominant and pandemic form of HIV-1 affecting millions of people on a global scale. Group M was also the first HIV-1 lineage to be discovered and can be further divided into nine subtypes (A to K), as well as over 40 varying recombinant forms resulting from the recombination of subtypes in dually infected individuals.[21] Subtype C is largely found in Southern Africa, Asia and India while subtype B is predominant in Europe and the United States.[26]

Unlike group M which affects the population on a global scale, non-M group (O, N and P) associated infections have been mostly limited to individuals living in or associated with Cameroon. Group O, identified in 1989, affects less than 1% of the population located in Cameroon, Gabon and neighbouring countries.[27] Occurrence of group N, identified in 1998, is even rarer with only 13 cases reported in Cameroon.[22, 28-30] Only 2 cases of individuals infected with group P have been reported.[31] The first case was discovered in a Cameroonian woman in France in 2009.[22, 24] All HIV lineages are capable of causing a decrease of CD4+ T cells but the transmissibility of non-M groups is much lower than for group M. It has been speculated that the slower spread of non-M groups could be attributed to poorer human adaptation.

In 1986 a new variant of HIV was discovered in Western Africa and has remained largely confined to the area. This variant, now known as HIV-2, has origins that could also be traced back to SIV. However, unlike HIV-1 where the disease was traced back to SIV in chimpanzees, HIV-2 is suspected to originate from the sooty mangabey (SIVsmm).[32-33] Most individuals with HIV-2 do not progress to AIDS as the pathogenicity of HIV-2 is lower than HIV-1.[34] As a result, HIV-2 expresses lower levels of viremia than HIV-1.[34-35] Furthermore, the transmission rate of HIV-2 is inferior to HIV-1 and mother-to-child transmission for HIV-

2 is almost non-existent. It is therefore unsurprising that the prevalence of HIV-2 today is largely declining.[36]

1.4. HIV-1 Replication Cycle and Mode of Infection

As mentioned in section **1.2**, HIV is acquired through contact with infected blood or bodily fluids either by blood transfusion, sexual transmission or mother-to-child transmission. The most significant manifestation of HIV infection is the depletion of CD4 + T cells in the gastrointestinal tract, peripheral blood, lymph nodes and other lymphatic tissues, while the levels of viremia increase due to rapid viral replication.[37-38]

The HIV replication cycle comprises of several critical steps, many of which have been considered as viable targets for therapeutic intervention as shown in **Figure 1**.

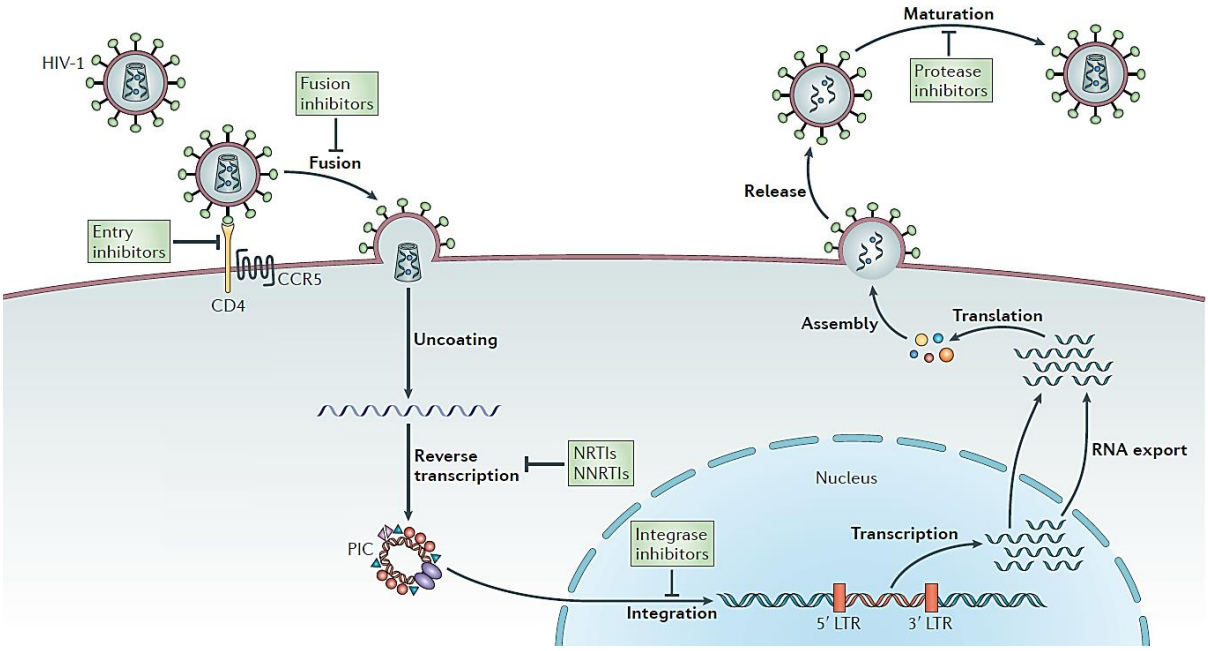

Figure 1 An overview of the HIV replication cycle indicating several steps currently targeted for therapeutic intervention. Taken from Barré-Sinoussi *et al.*[39]

1.4.1. Viral fusion and entry

The first step of the HIV replication cycle is viral fusion and entry (**Figure 1**). The primary cell surface receptor for HIV is the CD4 receptor, an integral plasma membrane glycoprotein expressed in CD4+ T cells, as well as dendritic and macrophage derived cells.[40] Adsorption of the virus to the host cell occurs due to the high affinity that CD4 has for the viral envelope protein (Env). Env is a heavily glycosylated trimer comprising of heterodimeric subunits gp120, a docking glycoprotein responsible for receptor binding and gp41, a transmembrane protein responsible for anchoring gp120 to the viral membrane and catalysing membrane fusion.[41] The binding of CD4 to gp120 elicits a conformational change in gp120 bringing the outer membranes of virus and host into close proximity in preparation for membrane fusion (**Figure 2**). However, the binding of CD4 alone is not sufficient for merging viral and host cell membranes and additional binding to a chemokine coreceptor (CCR5 or CXCR4) is required.[42]

CCR5 and CXCR4 are members of a family of G-protein-coupled receptors (GPCRs) that are expressed predominantly on T cells, monocytes, macrophages and dendritic cells.[43] HIV-1 strains that utilize CCR5, known as the R5 virus, are predominant in the early stages of the disease and are more readily transmitted than strains that use CXCR4, known as the X4 virus.[44] X4 viruses are often associated with rapid disease progression and only emerge years later after infection.[45] In some instances dual tropism occurs where HIV recruits both chemokine receptors. This is referred to as the R5X4 virus.[44]

The binding of gp120 with a coreceptor triggers a structural rearrangement in gp41. This results in the exposure and insertion of gp41 into the host cell membrane, tethering the viral membrane to the host.[41] The region of gp41 that inserts into the host membrane is a highly hydrophobic region known as the fusion peptide.[46] The ectodomain of gp41, the domain of gp41 extending into extracellular space, consists of an N-terminal and C-terminal helical region which upon tethering are brought in close proximity resulting in the formation of a six-helix bundle (6HB) as demonstrated in **Figure 2**. The 6HB is responsible for the formation, stabilization and enlargement of the fusion pore which itself permits the delivery of the viral nucleocapsid or core into the host cell cytoplasm.[47]

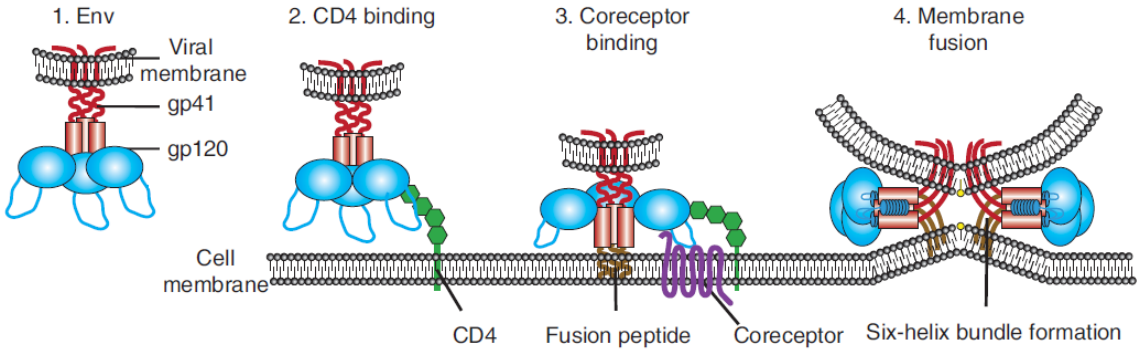

Figure 2 Overview of HIV fusion and entry. Viral envelope protein (Env) consists of subunits gp41 (red) and gp120 (blue). Gp120 is responsible for receptor and coreceptor binding while gp41 is responsible for tethering the viral membrane to the host cell membrane. Tethering results in the formation of a six-helix bundle and ultimately the fusion pore, permitting entry of the viral nucleocapsid into the host cell. Image adapted from Wilen *et al.*[41]

1.4.2. Release of viral RNA and reverse transcription

Once the viral core has been delivered into the cytoplasm of the host cell a process known as 'uncoating' occurs whereby the protective conical capsid surrounding the HIV RNA genome and viral proteome is removed.[48] Once the capsid has been removed the viral genome and most of the viral proteins remain associated forming a complex referred to as the reverse transcription complex (RTC).[38] Viral proteins observed to be associated with RTC include reverse transcriptase (RT), integrase (IN), matrix protein (MA), nucleocapsid (NC) and accessory viral protein R (Vpr).[38]

During or following the 'uncoating' process the viral single-stranded RNA (ssRNA) is converted into double-stranded DNA (dsDNA) by the viral enzyme RT.[48-49] RT exists as an asymmetric heterodimer comprising of two subunits p66 (66 kDa) and p51 (51 kDa) which share a largely similar protein sequence but adopt different tertiary structures.[38] The p66 subunit comprises of a ribonuclease H (RNase H) domain, responsible for the degradation of the viral RNA, and four pol subdomains. Three of the four pol subdomains are referred to as the palm, fingers and thumb subdomains since structurally, p66 resembles a right hand. The fourth pol subdomain is referred to as the connection domain, connecting the 'hand' to the RNase H domain.[50]

The first step of reverse transcription is the formation of the RNA/DNA hybrid at the polymerase active site located in the palm subdomain.[38] A molecule of tRNA bound to the primer binding site (pbs) acts as a primer to initiate the synthesis of the complementary DNA strand from the viral ssRNA in order to

generate the hybrid. The RNA portion of the hybrid is then degraded by RNase H.[38] Various biological steps follow from this point which ultimately result in the propagation of the 'free' single-stranded DNA (ssDNA) molecule and the synthesis and propagation of a complementary strand of DNA to generate a molecule of viral dsDNA (vDNA).[38] The newly synthesized vDNA remains associated with RTC, now referred to as the preintegration complex (PIC).[38]

1.4.3. Integration of viral DNA into the host genome

The following crucial step in the HIV replication cycle involves the integration of the newly generated vDNA into the host cell chromosome. This step is catalysed by IN, a 32 kDa protein comprising of three structural domains which include the N-terminal domain (NTD) containing a zinc-binding motif, a catalytic core domain (CCD) containing the enzymatic catalytic site and a C-terminal nonspecific DNA binding domain (CTD).[51]

Integration occurs in two parts. The first part involves the priming of vDNA for integration. This process known as 3'-processing (3'-P) is also catalysed by IN but takes place in the cytoplasm of the host cell.[51] As mentioned previously IN is one of the enzymes associated with PIC. 3'-P involves the endonucleolytic cleavage of two nucleotides (GT) from the tetranucleotide CAGT situated at the 3'-end of the vDNA. The CA dinucleotide that is subsequently exposed is highly conserved among retroviruses.[51]

Following 3'-P, PIC is transported to the nucleus where IN catalyses the insertion of vDNA into the host chromosome. This step known as strand-transfer (ST) occurs through divalent metal-mediated phosphodiester transesterification between the exposed 3'-OH groups of the CA dinucleotide and phosphodiester bonds on complementary strands of the host DNA (hDNA).[51] In this instance IN distorts the phosphodiester bonds on the backbone of the hDNA making it vulnerable to nucleophilic attack by the vDNA 3'-OH in an S_N2-like mechanism to form a new phosphodiester bond (**Figure 3**).[52-53] The metal ions involved in this step are typically two magnesium ions which coordinate to the IN catalytic triad comprising of residues Asp116 (D116), Asp64 (D64) and Glu152 (E152).[54] These metal ions aid in the stabilization of the DNA-enzyme complex and facilitate the transesterification reaction by activating the incoming nucleophile, stabilizing the pentacoordinate transition state and activating the 3'-oxoanion leaving group (**Figure 3**).[55]

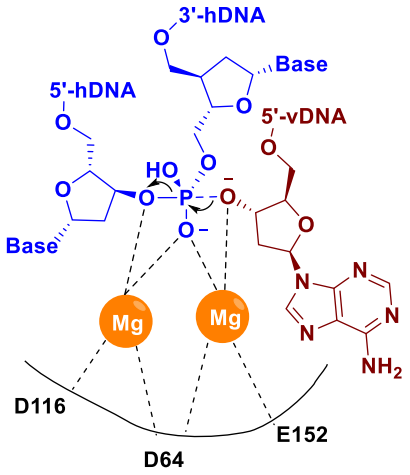

Figure 3: The second part of the integration process involves strand transfer of the vDNA (red) to a complementary strand of the hDNA (blue). This occurs through metal-mediated phosphodiester transesterification between the 3'-OH group of the vDNA and phosphodiester bonds of hDNA.

Once ST has occurred host cell DNA polymerases fill in the resulting gaps between viral and host DNA.[51] The integrated vDNA, now considered a provirus, behaves as a cellular gene functioning as a template for the transcription of new viral mRNA that is able to encode for all the necessary viral proteins to promote viral replication.[38]

1.4.4. Viral transcription and translation

Transcription of the provirus is a multistage and complex process employing both viral and cellular factors. This process is initiated and regulated at the long-terminal-repeat (LTR) region at the 5' end of the DNA provirus by promoter and enhancer elements, short segments of DNA that are able to bind to proteins to stimulate gene expression.[56] Promoter elements recruit RNA polymerase II (pol II) which initiates synthesis of viral mRNAs.[57] Enhancer elements associate with the transcriptional transactivator protein Tat which drastically increases the rate and efficiency of gene expression.[58] In order to transactivate gene expression Tat first forms a complex with a positive transcription elongation factor b (P-TEFb), a large cellular protein complex composed of proteins cyclin T1 (cycT1) and cyclin-dependent kinase 9 (CDK9).[38] The Tat/P-TEFb complex then binds with the transactivation response element (TAR) located at the 5'-end of nascent RNA resulting in the hyperphosphorylation of pol II and ultimately efficient elongation and synthesis of viral mRNA.[58]

Transcription results in the synthesis of unspliced and partially spliced mRNA in addition to the fully spliced or mature mRNA.[38] Normally unspliced and partially spliced mRNA, also known as precursor mRNA (pre-

mRNA) are degraded within the nucleus. However in the case of HIV-1, pre-mRNA are essential for encoding important viral proteins such as gag and gagpol polyprotein precursors, Env and other important accessory proteins.[59] To overcome this issue of degradation HIV-1 expresses the Rev protein which facilitates the export of the pre-mRNA from the nucleus to the cytoplasm of the host cell.[57] This is achieved by the recognition of an RNA element found only in pre-mRNA referred to as the Rev response element (RRE). Rev binds to the RRE forming a complex which enables it to utilize cellular nuclear export machinery transporting the pre-mRNA from the nucleus.[38, 59]

Once in the cytoplasm mRNA and pre-mRNA are translated to various viral proteins. This process is utterly dependent on the host cell to provide the translational machinery including ribosomes, tRNA, amino acids and all other factors relating to translational initiation, elongation and termination.[60] Depending on the mRNA each translational process is different but can be loosely divided into four stages.

The first step involves the recruitment of the 43S pre-initiation complex to the mRNA. 43S comprises of the small host cell ribosomal subunit (40S), a number of initiation factors and a molecule of methionyl-tRNA (Met-tRNA).[61] 43S scans the mRNA until it locates the initiation codon (AUG) on the mRNA through complementarity with the anticodon on Met-tRNA.[60] Following this step the large ribosomal unit (60S) is employed to 43S resulting in the formation of the 80S ribosome complex. 80S is then able to decode the mRNA and subsequently recruit the amino acids necessary to elongate and synthesize the viral protein.[61] Elongation factors introduce the required amino acids which are bound to molecules of peptidyl-tRNA, RNA-containing adapter molecules responsible for linking and matching amino acids to complementary codons on the viral mRNA and ultimately transferring the amino acids to the growing polypeptide chain.[61] Penultimately, the 80S complex reaches the termination codon which can be UGA, UAA or UAG and termination of the translational process commences. Termination is achieved through the hydrolysis of the ester bond binding the nascent polypeptide to tRNA.[62] The final step is termed ribosome recycling whereby the ribosome is dissociated from the mRNA and tRNA in preparation for the next round of translation.[63]

1.4.5. Viral assembly, budding and maturation

The final stages of the HIV-1 replication process involve assembly, budding and maturation of HIV-1, all of which takes place at the host cell plasma membrane (**Figure 4**).

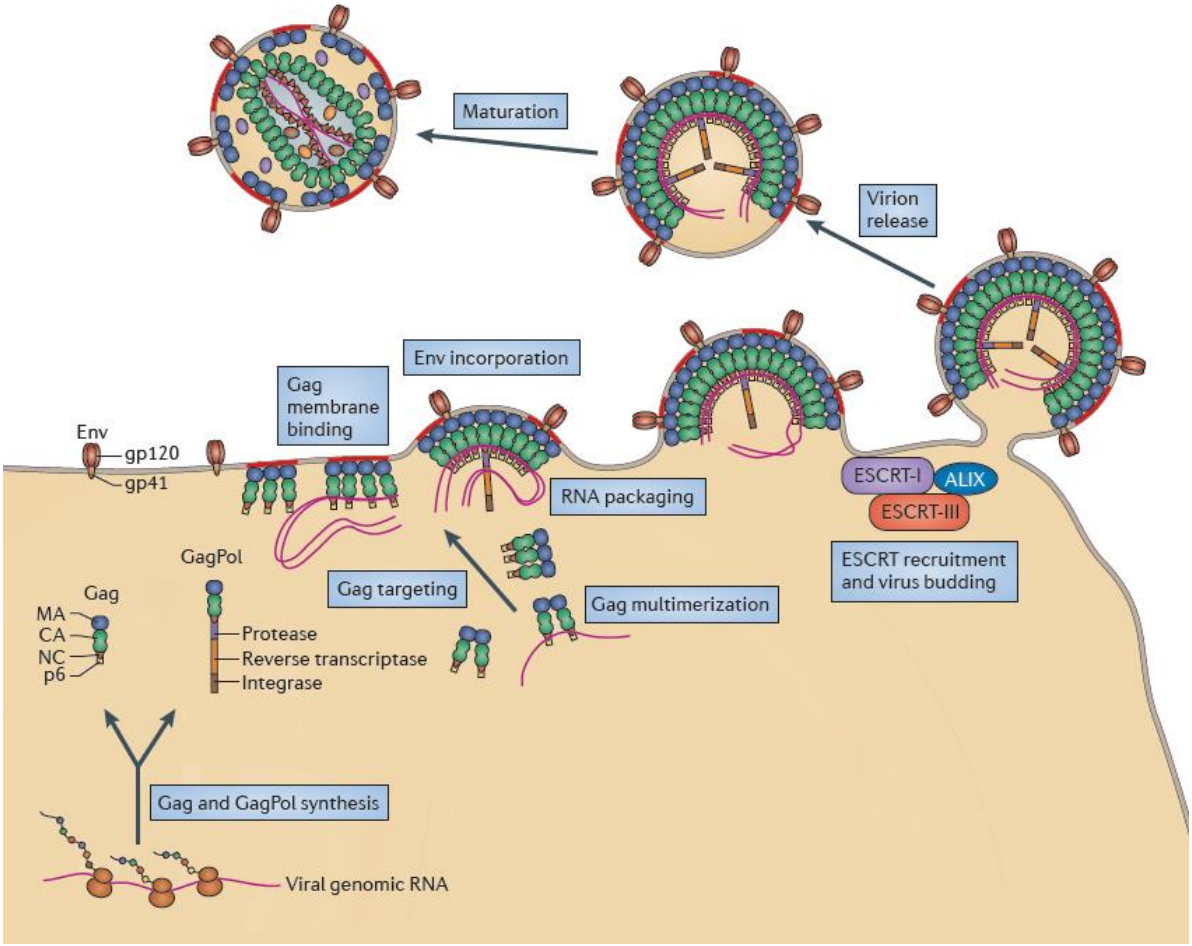

Figure 4 An illustration of the final stages of the HIV-1 replication process. Image was taken from Freed.[64]

The Gag precursor polyprotein ($Pr55^{Gag}$) is an essential component of the assembly process as it is responsible for targeting and binding the plasma membrane, encapsulating viral RNA and budding or pinching-off the immature virion from the host cell membrane.[38] The major Gag domains involved in these processes include the N-terminal MA domain, the central capsid (CA) domain, the basic NC domain and the C-terminal p6 domain.[65]

The MA domain targets and binds the host cell plasma membrane.[66] Post-translationally MA is myristoylated by N-myristoltransferase (NMT) which is essential for viral assembly as the myristic acid moiety, when exposed, interacts with phospholipids on the inner lipid bilayer of the plasma membrane

forming a lipid anchor to stabilize membrane binding in preparation for immature virion formation.[67-68] Additional interactions between a highly basic region of MA adjacent to the myristoylation site and anionic phospholipids on the lipid bilayer further promote membrane binding.[68] Viral Env glycoproteins also gather at the plasma membrane simultaneously to Gag and the MA domain is responsible for the incorporation of the Env glycoproteins into the forming virion.[64]

Upon reaching the plasma membrane, in addition to interactions between Gag and the lipid membrane, Gag-Gag and Gag-RNA interactions are required to initiate the assembly of the immature virions.[66] The former is mediated by the CA domain while the latter is mediated by the NC domain.[38]

It has been well established that HIV-1 virions carry two copies of the full RNA genome which dimerize in the cytoplasm prior to their encapsidation in the forming virion.[69] NC identifies a packaging signal located on the 5'-ends of the dimerized viral RNA known as the ψ-element. This packaging signal has a high affinity for NC and is recognized by two zinc finger motifs located in the NC domain.[70] The binding of NC to the RNA dimer is thought to aid in nucleating viral assembly. However, as mentioned previously the multimerization process, the formation of Gag-Gag interactions, is largely mediated by the CA domain.[38]

$Pr55^{Gag}$ then assembles into spherical immature particles with the membrane bound Gag molecules and the GagPol precursor projecting towards the interior of the forming virion while part of the cellular membrane makes up the viral membrane (**Figure 4**).[71] The subsequent budding of the newly formed immature particles is promoted by the p6 domain of $Pr55^{Gag}$ which recruits the cellular endosomal sorting complex required for transport (ESCRT) machinery, a series of cellular protein complexes and accessory proteins required for membrane scission.[64]

Finally, as budding of the immature virion is initiated, protease (PR) is activated and cleaves the Gag and GagPol polyprotein precursors into their mature constituent proteins.[38] These proteins include the MA, CA, NC and p6 proteins from Gag and RT, IN and PR from GagPol, although the mechanism by which PR is activated is not completely understood.[65] PR is a dimeric aspartic acid protease and cleaves the Gag and GagPol polyprotein precursors in an ordered step-wise manner by recognizing specific sites along the peptide chains.[65] Interestingly, studies suggest that PR does not recognize specific amino acid sequences but rather recognizes the overall shape of the cleavage site.[72]

After cleavage by PR the mature proteins rearrange within the virion. The most significant rearrangement involves the arrangement of CA into a conical shell surrounding the RNA-NC complex (**Figure 4**).[38] This

overall process, known as maturation, converts the immature virion into a mature virus able to infect the next host cell.[64]

During the acute or primary phase of infection, the levels of viremia are at their peak with approximately $10^6 – 10^7$ virion copies per mL of plasma.[8] Acutely infected individuals are therefore more likely to transmit the virus to others.[73] Initially, upon infection, HIV is held in the mucosal tissues but before long the virus is able to cross the mucosal barrier and spread through the bloodstream to various lymphoid organs such as the gut-associated lymphoid tissue, thymus, spleen and lymph nodes.[74] During this stage of infection the levels of CD4+ T cells, the major target for HIV infection, drastically decrease by 20 – 40% in the bloodstream.[75]

Following acute infection, a period known as clinical latency occurs. During this stage the host immune response gains some control over the viral levels in the bloodstream. By employing CD8+ T cells and antibodies the immune system is able to significantly decrease the levels of HIV in the blood allowing for the levels of CD4+ T cells to be restored almost back to normal.[75] This is known as the latent stage of infection because despite the immune response, HIV continues to replicate without detection in the lymphoid organs.[75] Normally upon infection, CD4+ T cells die quickly due to the immune response or cytopathic effects of HIV however, some infected cells are able to survive long enough to revert to a resting or latent state.[76] These latently infected cells have the HIV provirus integrated into their genome but are transcriptionally dormant and therefore do not express viral RNA and proteins. These cells can periodically reactivate to replenish the viral load in the bloodstream, albeit at low levels.[77]

Over time, left untreated, HIV again causes a slow decline in levels of CD4+ T cells, a process which can take up to 10 years. The resultant deterioration of an infected individual's immune system with CD4+ T cell levels less than 200 copies per mL^3 of blood eventually results in the onset of opportunistic infections, such as tuberculosis.[75] At this point HIV-infection has progressed to AIDS. Individuals with AIDS can survive for a time ranging from 3 months to over 2 years before death.[73]

1.5. Changing the outcome of HIV-infection: An overview of the different classes of HIV-1 ARVs

The very first ARV for HIV-1 was discovered in 1984 by Burroughs Wellcome Co. (BW). During a random screening of compounds, they found that azidothymidine (AZT) (**Figure 5**), later known as zidovudine, showed significant activity against murine retroviruses Friend Leukemia virus (FLV) and Harvey Sarcoma virus (HaSV). A few months later AZT was screened against HIV with the same positive outcome.[78-79]

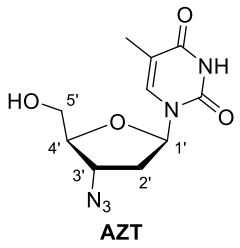

AZT

Figure 5 AZT (zidovudine) the first ARV licensed by the FDA.

AZT was first synthesized in 1964 as part of an effort to synthesize novel therapeutic agents able to combat the proliferation of cancer cells. When tested against leukemic cells in mice, AZT had no effect and was forgotten until it resurfaced in 1984.[78]

The FDA approved AZT (Retrovir®) for use in 1987, only 3 years after its identification as a potent anti-HIV therapeutic. At this time it was believed that AZT would be the 'wonder-drug' to completely eradicate AIDS.[75] Unfortunately, the success of AZT was short-lived due to issues pertaining to toxicity and the emergence of drug-resistance.[8, 80] The failure of AZT to eradicate the AIDS pandemic initiated a global effort to identify other more effective ARVs for HIV-1.

It was not until the mid-1990's, with the introduction of combination therapy, that the long-term outlook for infected individuals began to improve.[81] The introduction of combination therapy, also known as highly-active antiretroviral therapy (HAART) or triple therapy, made significant strides in reducing the morbidity and mortality of the infected global population.[82] Although not a cure for HIV, combination therapy has succeeded in transforming a 'death sentence' into a chronic but manageable disease. The motivation behind the development of HAART was to encumber the onset of drug resistance associated with monotherapeutic regimens. The poor proof-reading ability of HIV RT, combined with the high replication rate of HIV results in a high mutation rate of 3.4 X 10^{-5} mutations per base pair per replication

cycle resulting in significant variations in the HIV genome.[80] In the case of ARVs, the mutated genome codes for viral proteins that maintain their function despite the presence of the inhibitor.[82]

To overcome resistance HAART needs to drastically improve viral suppression.[8] This is achieved through the use of two or more ARVs from different classes targeting different stages of the HIV-1 life cycle. Currently HAART regimens are made up of two nucleoside reverse transcriptase inhibitors (NRTIs) and either a non-nucleoside reverse transcriptase inhibitor (NNRTI), integrase strand transfer inhibitor (INSTI) or a boosted protease inhibitor (BPI).[83]

1.5.1. Nucleoside and nucleotide reverse transcriptase inhibitors (NRTIs and NtRTIs)

The major component of HAART and the earliest class of ARVs are NRTIs. Like AZT these compounds are mimics of naturally occurring nucleosides but lack the 3'-hydroxyl group at the 2'-deoxyribosyl sugar moiety.[81] In the case of AZT, the 3'-hydroxyl moiety is replaced with a 3'-azido moiety (**Figure 5**). NRTIs competitively target the catalytic site of RT where they bind to and terminate the propagating vDNA chain. As NRTIs lack the 3'-hydroxyl group, 3',5'-phosphodiester bonds with incoming nucleotides cannot be formed.[81]

NRTIs are administered as prodrugs which means that in their dispensed forms they are inactive.[84] Therefore, in order for these NRTIs to be incorporated into the propagating chain they need to be metabolically converted into an active form.[85] This entails three consecutive phosphorylations by cellular kinases of the NRTI to the monophosphate, diphosphate and finally the active triphosphate form (**Figure 6**).[86]

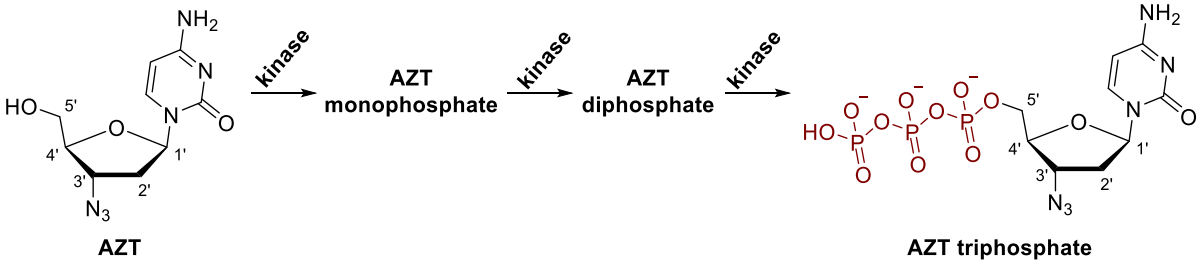

Figure 6 NRTIs have to be metabolically converted into the active triphosphate form. This activation process is carried out in three consecutive phosphorylation steps by cellular kinases.

Currently there are seven NRTIs approved by the FDA. In addition to AZT (**Figure 5**) these include didanosine (ddI, Videx®), zalcitabine (ddC, Hivid®), stavudine (d4T, Zerit®), abacavir (ABC, Ziagen®),

emtricitabine (FTC, Emtriva®) and lamivudine (3TC, Epivir®) (**Figure 7**). Of all the currently approved NRTIs, emtricitabine and lamivudine have the lowest propensity for causing mitochondrial toxicity in patients and exhibit the highest barrier to resistance.[87-88]

In some instances NRTIs are administered with the monophosphate already installed to overcome the activation barrier often encountered with the first phosphorylation step, and are referred to as nucleotide reverse transcriptase inhibitors (NtRTIs).[86] Currently two NtRTIs have been approved by the FDA for the treatment of HIV-1; tenofovir disoproxil fumarate (TDF, Viread®) and tenofovir alafenamide fumarate (TAF) (**Figure 7**). However, TAF has only been approved as a coformulation with FTC and an NNRTI or INSTI (Descovy®, Genvoya® and Odefsey®). Both tenofovir prodrugs contain lipophilic groups to mask the two negative charges on the phosphonate moiety, which otherwise would limit cellular permeability and prohibit oral administration.[89] Cleavage of these groups by various cellular hydrolases reveals the monophosphate which is subsequently converted into the active triphosphate.[89-90]

Based on WHO recommendations TDF in combination with emtricitabine or lamivudine is currently used for first-line treatment of infected individuals or for pre-exposure prophylaxis.[83, 88] However, TAF exhibits a lower propensity for renal and bone toxicity and delivers higher levels of tenofovir at lower doses than TDF and is therefore expected to replace TDF in future regimens.[8]

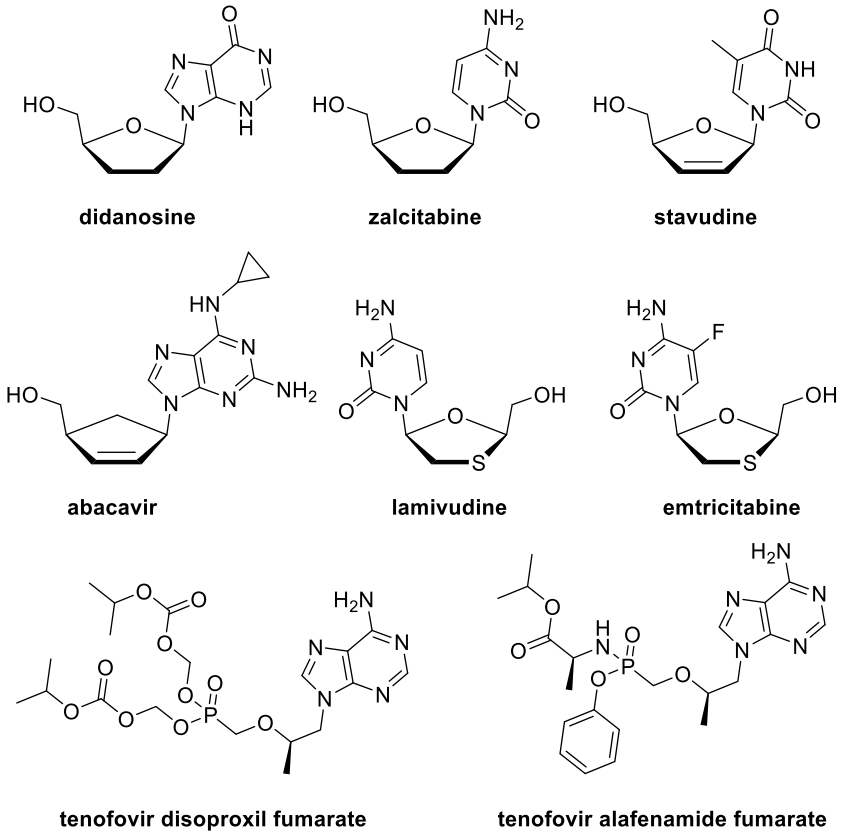

Figure 7 In addition to AZT 6 other NRTIs and 2 NtRTIs have been approved by the FDA for the treatment of HIV-1. All NRTIs lack the 3'-OH moiety required for DNA chian propagation. NtRTIs require only two phosphorylation steps to become active inhibitors of vDNA chain propagation.

1.5.2. Non-nucleoside reverse transcriptase inhibitors (NNRTIs)

Like NRTIs, NNRTIs target RT, but at a small hydrophobic allosteric pocket known as the non-nucleoside inhibitor binding pocket (NNIBP) situated approximately 10 Å from the catalytic site.[91] Under normal circumstances, in the apo-enzyme this NNIBP does not exist but opens only during the binding of an NNRTI.[50] Upon binding to the NNIBP, NNRTIs cause conformational changes to the enzyme as a result of torsional rotations of particular amino acids in the NNIBP.[92] This conformational change distorts the catalytic site and hinders propagation of the vDNA chain.[91-92] Unlike NRTIs, NNRTIs do not require metabolic activation to inhibit enzyme activity.[75] NNRTIs are small, non-competitive, hydrophobic molecules that are able to cross the blood-brain barrier (BBB) and exhibit high levels of structural and chemical diversity.[93]

It was only in the late 1980's that two series of compounds were discovered to inhibit RT at the NNIBP. These first NNRTIs belonged to a series of 1-(2-hydroxyethoxymethyl)-6-(phenylthiol)thymine (HEPT) and 4,5,6,7-tetrahydroimidazo[4,5,1-*jk*][1,4]benzodiazepine-2(1*H*)one (TIBO) derivatives.[94-95] HEPT derivatives were initially designed as NRTIs but it was discovered that these compounds inhibited RT through a completely different mechanism to other NRTIs.[94] Despite the structural differences between the HEPT and TIBO derivatives, both series of compounds adopted a butterfly-like conformation in the NNIBP.[96] The clinical candidates of both series, emivirine (HEPT) and tivirapine (TIBO), were found to be potent inhibitors of RT but were never developed for clinical use (**Figure 8**).[96]

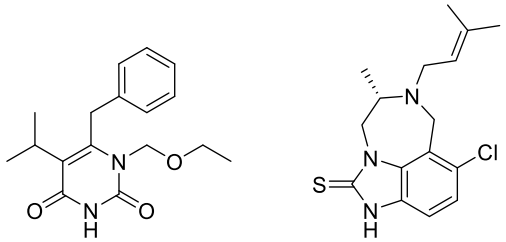

Figure 8 The very first NNRTI candidates were emivirine, a HEPT derivative and tivirapine, a TIBO derivative. Although both were potent inhibitors of RT neither made it past clinical trials.

Although the HEPT and TIBO compounds were never marketed, their development paved the way for the discovery of other more successful NNRTIs. The first NNRTI to be approved for clinical use in 1996 was nevirapine (Viramune®) (**Figure 9**) which like HEPT and TIBO adopted the rigid butterfly-like conformation in the NNIBP.[97] A year later another NNRTI, delavirdine (Rescriptor®), was also licensed by the FDA (**Figure 9**).[81] Nevirapine and delavirdine are today classified as first-generation NNRTIs. This classification is based on the observation that despite both NNRTIs' ability to reduce viral levels in infected individuals, they suffer from a low genetic barrier to resistance.[98] This means that after prolonged exposure to treatment single amino acid mutations will confer resistance and significantly reduce the potency of these NNRTIs.[98]

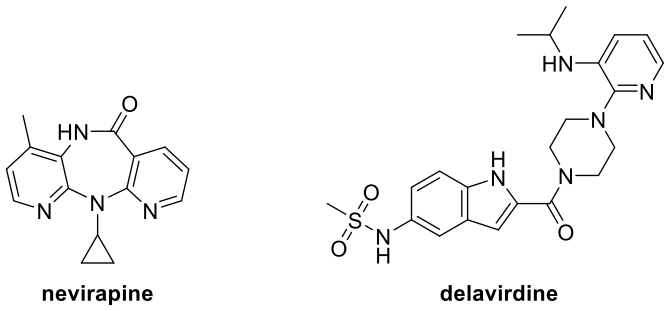

Figure 9 First-generation NNRTIs shown here are potent inhibitors of RT but suffer from a low genetic barrier to resistance.

Mutations that confer resistance to NNRTIs are situated in the immediate vicinity of the NNIBP and therefore, directly affect the binding of an NNRTI.[75] The most common clinically relevant mutations are K103N and Y181C. Other mutations include Y188C/L, V106A/M, G180A/S and A98G.[99] There are two methods by which these mutations can confer resistance to NNRTIs. The first is by decreasing the affinity of any NNRTI for the NNIBP by reducing Van der Waals interactions, π-π stacking interactions or changing the hydrogen bonding capabilities of the NNIBP.[100] The susceptibility of nevirapine to the Y181C mutation is an example of this. The affinity of nevirapine for the NNIBP relies heavily on π-π stacking interactions between the 4-methylpyridine present in nevirapine and Tyr181.[101] The Y181C mutation replaces the aromatic tyrosine residue with an aliphatic cysteine residue and as a result nevirapine loses that π-π stacking interaction and consequently suffers reduced efficacy.[102] The second method is by creating a steric conflict between any NNRTI and the NNIBP.[100] Interestingly, the prominent K103N mutation does not confer resistance by either of these methods. Instead, studies suggest that the K103N mutation stabilizes the closed form of the NNIBP by forming a hydrogen bond between the amide of the mutated N103 residue and the hydroxyl group of Y188.[103]

By understanding the mechanisms by which mutations confer resistance, successful strides were made in developing NNRTIs with improved resistance profiles. Efavirenz (Sustiva® or Stocrin®) was licensed only two years after nevirapine but is able to maintain activity in the presence of the Y181C mutation that renders nevirapine ineffective (**Figure 10**)[81, 102] This can be attributed to the presence of a cyclopropyl moiety present in efavirenz in place of the 4-methylpyridine found in nevirapine, which does not rely on π-π interactions with Tyr181.[102] Despite the improved resistance profile of efavirenz against the Y181C mutation, the overall genetic barrier to resistance is low.[104] Consequently, significant cross-resistance between efavirenz and nevirapine ensures that these two NNRTIs cannot be administered sequentially after virologic failure.[104] Nevertheless, efavirenz is currently the preferred NNRTI used in first-line treatment regimens for adults and adolescents.[83]

Etravirine (Intelence®) and rilpivirine (Edurant®) are the latest NNRTIs to be approved by the FDA and are considered to be second-generation NNRTIs (**Figure 10**). These NNRTIs fall into a new class of diarylpyrimidine (DAPY) NNRTIs that possess an element of structural flexibility not demonstrated by the first-generation NNRTIs, nevirapine and efavirenz.[105-106] This characteristic is believed to explain the superior resistance profile associated with these NNRTIs as conformational flexibility enables these compounds to cope with mutation associated structural changes in the NNIBP.[106] Despite their higher

barrier to resistance, etravirine and rilpivirine are only introduced as a salvage therapy after other NNRTIs have failed.[8]

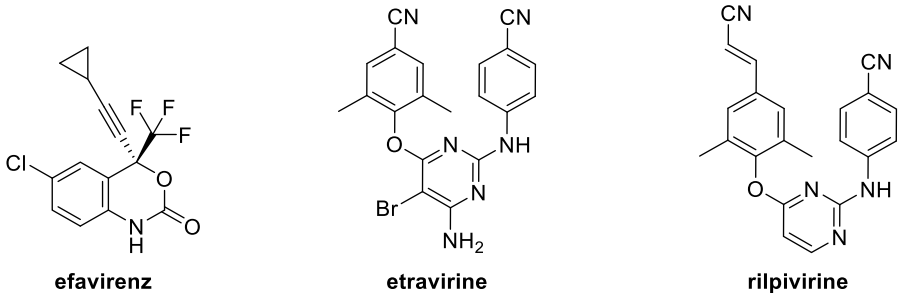

Figure 10 A depiction of efavirenz and second-generation NNRTs etravirine and rilpivirine. Second-generation NNRTIs are characterised by a higher genetic barrier to resistance.

Doravirine (**Figure 11**) is a next generation NNRTI currently in phase III clinical trials.[107] Doravirine has been shown to exhibit comparable efficacy to efavirenz, but with superior tolerability and a lower propensity for efavirenz associated side effects of the central nervous system (CNS).[108] Studies have also demonstrated that doravirine exhibits an even higher barrier to resistance than all currently licensed NNRTIs.[108-109]

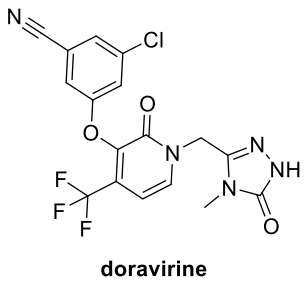

Figure 11 Doravirine, a new generation NNRTI with a superior resistance profile to currently licensed NNRTIs.

1.5.3. Protease Inhibitors (PIs)

Until recently PIs together with NRTIs and NNRTIs were recommended for use as a first-line treatment option for infected individuals. Today, however, the WHO recommends the use of PIs for second-line treatment regimens or as a salvage therapy.[83] Currently there are ten PIs licensed by the FDA and, all but one, are characterized by the presence of a hydroxyethylene core (**Figure 12**) as opposed to the normal peptidyl linkage found in polyprotein precursors.[93] This structural feature characterizes PIs as non-scissile peptidomimetic substrate analogues for HIV protease as the hydroxyethylene moiety cannot be

hydrolytically cleaved by the enzyme.[93] This results in the blockage of the enzyme active site preventing cleavage of GagPol polyprotein precursors and subsequent maturation of the HIV virion.[86] The first PI, saquinavir (Invirase®), was approved by the FDA in 1995. Over the next two years three more PIs were licensed by the FDA: ritonavir (Norvir®) and indinavir (Crixivan®) in 1996 and nelfinavir (Viracept®) in 1997 (**Figure 12**).[81] These PIs are identified as first-generation PIs as they suffered from poor bioavailability, a low genetic barrier to resistance and toxicity issues.[110]

Notably it was discovered that ritonavir, in addition to protease inhibition, was able to inhibit metabolic pathways of cytochrome P450 (CYP450) and could therefore be utilized as a booster for other PIs.[110-111] By co-administering ritonavir with another PI the bioavailability and potency of that PI would improve.[110] Unfortunately, in the case of first-generation inhibitors, this method only worked well with saquinavir. Ritonavir co-administered with indinavir led to greater nephrotoxicity or, with nelfinavir, had no notable effect on bioavailabilty.[110, 112]

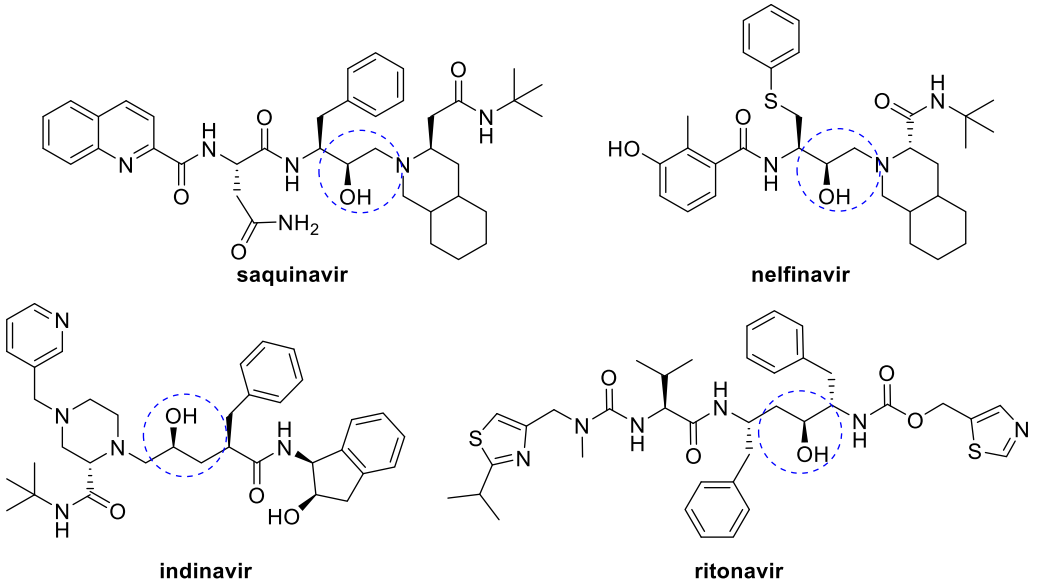

Figure 12 A depiction of the first-generation PIs with the characteristic hydroxyethylene core in blue.

Due to the limited success of first-generation PIs, second-generation PIs with improved pharmacokinetic and resistance profiles were developed. The first of these was amprenavir (Lexiva®) (**Figure 13**). Like the earlier PIs, amprenavir possessed the characteristic hydroxyethylene core however, unlike earlier PIs, amprenavir exhibited a unique resistance profile which resulted in a higher barrier to resistance with little cross-resistance to other PIs.[113] Unfortunately, the use of amprenavir was associated with low plasma levels and consequently a high pill burden of eight tablets, twice daily.[110] Fosamprenavir, a prodrug of

amprenavir, was developed to reduce the high pill burden linked with the administration of amprenavir.[113] The success of this endeavour led to the replacement of amprenavir with fosamprenavir. Following the approval of amprenavir and fosamprenavir, the FDA approved another four second-generation PIs, namely lopinavir (Kaletra®), atazanavir (Reyataz®), tipranavir (Aptivus®) and darunavir (Prezista®) (**Figure 13**). Lopinavir in combination with ritonavir is currently the preferred PI combination used in second-line treatment regimens.[83] The PI tipranavir falls into a new class of non-peptidomimetic inhibitors which differ structurally from other PIs. In the place of the common hydroxyethylene core, tipranavir is characterised by a dihydropyrone core (**Figure 13**). This structural diversity enables this class of PIs to maintain efficacy against various drug-resistant strains of HIV.[114] Unfortunately, harsh side-effects became associated with the administration of tipranavir.[115]

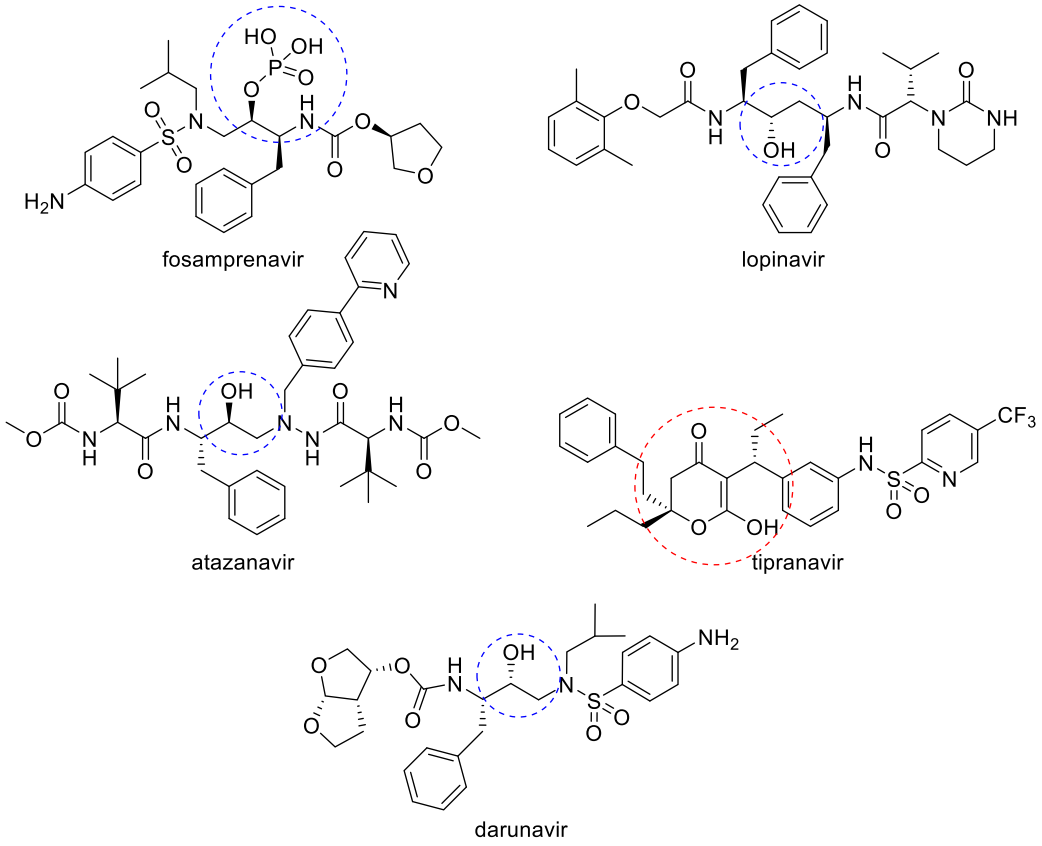

Figure 13 A depiction of the five FDA approved second-generation PIs. These PIs are characterized by a higher genetic barrier to resistance. Once again, the hydroxyethylene core is shown in blue with the exception of tiprananvir with its dihydropyrone core shown in red.

1.5.4. Integrase Strand Transfer Inhibitors (INSTIs)

The latest class of ARVs to be approved and recommended for first-line treatment in HAART are INSTIs. The discovery of INSTIs was made by pharmaceutical companies Merck and Shionogi in 2000. Through *in vitro* assays researchers from both companies discovered that aryl diketo acids (DKA) and derivatives thereof were effective inhibitors of IN.[116-117] Furthermore, as the name implies, these inhibitors specifically target the second step of the integration process, the strand transfer step (Refer to section **1.4.3**).[118] Examples of these include the pyrrole-containing compound L-731,988 (Merck) and indole-based compound 5-CITEP (Shionogi) shown below (**Figure 14**).

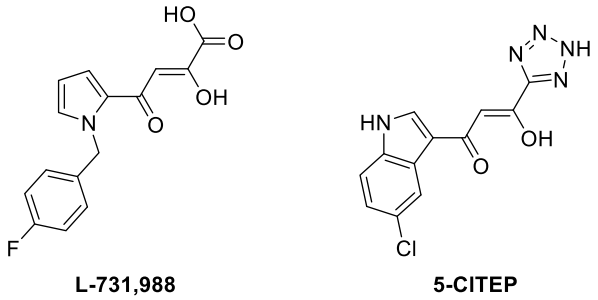

Figure 14 Merck and Shinonogi discovered that aryl diketo acids and related derivatives were effective inhibitors of HIV integrase.

INSTIs bind to the catalytic site of IN only in the presence of vDNA. It has been hypothesized that the presence of the vDNA stabilizes the formation of the active site hydrophobic binding pocket, which only exists following 3'-P, allowing for INSTI binding.[118-119] All effective INSTIs possess two important structural features: The first is the characteristic DKA moiety (in some cases monoketo acids are employed) which is particularly important to the mode of action of INTSIs as it chelates the divalent magnesium ions present at the catalytic triad in the active site. The second structural feature is a hydrophobic aromatic group able to form interactions with the binding pocket, as well as the penultimate deoxycytidine nucleobase located at the 3'-end of the vDNA (**Figure 15**).[119]

The first two INSTIs to be made commercially available for the treatment of HIV-1 encompass both these features. Raltegravir (Isenstress®) and elvitegravir (Vitekta®) were approved by the FDA in 2007 and 2014 respectively (**Figure 15**).[81, 120] Both raltegravir and elvitegravir were found to be potent inhibitors of IN, effectively reducing viral levels in treatment naïve and experienced individuals.[51] Unfortunately, despite their efficiency both INSTIs suffer from a moderate barrier to resistance as well as significant cross-resistance.[121-123] Single-point mutations that cause high levels of resistance to these first-generation INSTIs are not in the immediate vicinity of the INSTIs, but are believed to prompt conformational changes in the

catalytic site which decreases the affinity of the INSTIs for IN.[51] In addition to a moderate genetic barrier to resistance, elvitegravir is readily metabolized by liver enzymes and therefore, like many PIs, has to be administered with a booster.[108, 124] Cobicistat, a structural analogue of ritonavir lacking significant antiviral activity, is the recommended pharmacological booster for elvitegravir.[124]

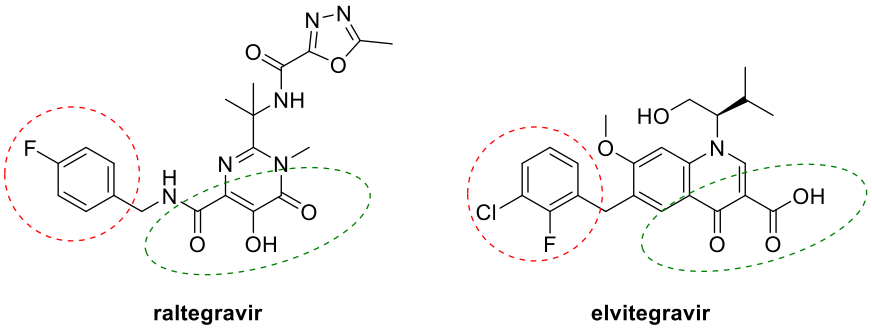

Figure 15 First-generation INSTIs raltegravir and elvitegravir possess two structural features important for binding to the active site of IN. The DKA moiety (green) to chelate to divalent magnesium ions and an aromatic ring (red) capable of forming interactions with residues in the pocket and the deoxycytidine nucleobase of the bound vDNA.

Following the observed trend with the ARVs discussed so far, a need for the development of second-generation INSTIs was required to deal with the resistance issues associated with raltegravir and elvitegravir. To this end the INSTI dolutegravir (Tivicay®) was developed and recently approved by the FDA (**Figure 16**).[125] Dolutegravir is a potent INSTI with a high genetic barrier to resistance, maintaining efficacy in the presence of mutations that confer resistance to raltegravir and elvitegravir.[51] Studies have suggested that dolutegravir adapts its conformation with the structural changes that occur within the mutated active site.[126] Due to a good pharmacokinetic profile with little to no evidence of any serious side effects, dolutegravir is also part of the preferred first line regimen with 3TC and TDF as an alternative to regimens containing efavirenz. [83, 127]

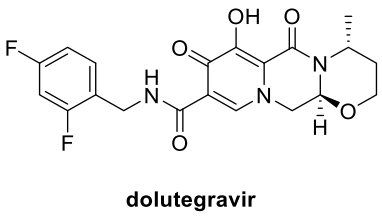

Figure 16 Dolutegravir is a second-generation INSTI with a high genetic barrier to resistance and is currently used as an alternative to efavirenz in first line treatment regimens.

1.5.5. Other classes of ARVs: Fusion and Entry Inhibitors

Maraviroc (Selzentry®) was the first ARV developed to target viral entry into the host cell (**Figure 17**). Maraviroc targets the chemokine receptor CCR5 preventing cellular fusion between the HIV viral envelope and the host cell plasma membrane. In binding to CCR5, maraviroc induces a conformational change in the chemokine receptor that prevents interactions with gp120.[81] Initially it was considered unusual to target CCR5 (a host receptor) due to the risks associated with the intervention of host cellular function especially at chronic doses.[128] However, studies have shown that CCR5 is a superfluous receptor and that chronic inhibition of this receptor does not alter the normal function of a host's immune system.[129] This observation is based on research around 1% of north European Caucasians who are resistant to HIV-1 infection as they lack the CCR5 receptor. Despite the lack of CCR5 these individuals suffered no health adversities.[130] A major drawback to maraviroc is that administration is limited to individuals who possess the CCR5 coreceptor, as maraviroc does not bind to and therefore has no activity against CXCR4, an issue affecting carriers of the R5/X4 virus as well.[131] As a result infected individuals have to be tested prior to taking maraviroc to establish whether the virus is R5 or X4 tropic.[130] Maraviroc is currently not on the list of recommended ARVs for HAART.

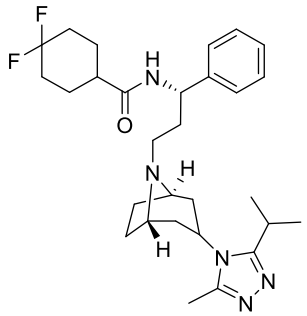

maraviroc

Figure 17 Maraviroc was the first ARV developed to target viral entry.

Enfuvirtide (Fuzeon®, **Figure 18**) is a complex 36 amino acid helical peptide developed by Roche and approved by the FDA in 2003 to inhibit viral fusion.[132-133] Enfuvirtide is derived from the C-terminal helical region of the gp41 ectodomain (Refer to section **1.4.1**) and is therefore a competitive inhibitor for the complementary N-terminal helical region of the gp41 ectodomain.[134-135] By binding to gp41, enfuvirtide prevents the formation of the 6HB fusion pore which would allow for delivery of the viral genome into the host cell.[136] Although a potent inhibitor of viral fusion, enfuvirtide has limited oral bioavailability and a half-life of only 3.5 to 4.5 hours.[135] As a result, administration of enfuvirtide is carried out intravenously twice daily, a regimen which can be challenging for chronic use.[85] Consequently, enfuvirtide is only

administered as a salvage therapy to treatment experienced patients with no remaining therapeutic options.[137]

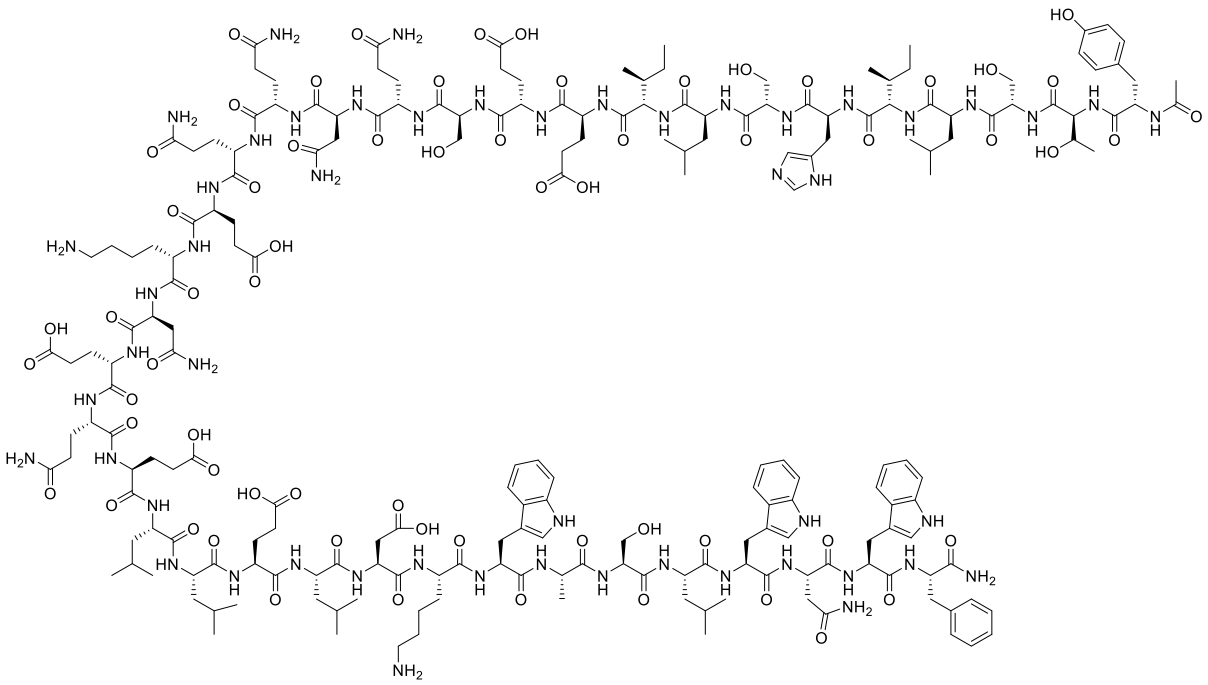

Figure 18 The first fusion inhibitor enfuvirtide is a synthetic peptide derived from gp41.

Interestingly an alternative to enfuvirtide has been in development for use in China. This alternative fusion inhibitor, albuvirtide is a 3-maleimimidopropionic acid peptide inhibitor.[138] Albuvirtide is related to enfuvirtide but has a superior half-life of approximately 11 days and requires once-weekly intravenous administration.[139] This is a consequence of albuvirtide's ability to conjugate to serum albumin, the most abundant protein found in human plasma.[140]

Fostemsavir (**Figure 19**) is the latest investigational ARV being developed as an entry inhibitor, more specifically an attachment inhibitor. Currently in Phase III clinical trials for treatment-experienced patients, fostemsavir acts by binding to gp120 preventing the conformational change that allows for binding to the host CD4 cell, although the exact mechanism is still under investigation.[141] Fostemsavir has been developed as a phosphonooxymethyl prodrug of the original azaindole compound to overcome adsorption issues of low solubility.[142]

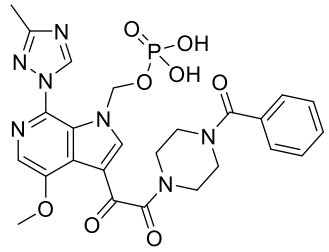

Figure 19 Fostemsavir is the latest entry inhibitor in clinical trials. In comparison to other licensed inhibitors, fostemsavir prevents viral entry by binding directly to gp120.

1.6. Conclusion

Over the past 30 years 25 ARVs targeting different stages of the HIV replication cycle have been licensed by the FDA. In addition, many new generation inhibitors that improve upon the profiles of currently licensed therapeutics, or are pursuing new targets altogether, are currently under investigation. These advances in combating HIV have drastically changed the outlook for sufferers of the disease. The introduction of combination therapy has successfully suppressed viremia in infected individuals to almost undetectable levels, improving quality of life and preventing the onset of AIDS. However, the use of combination therapy is not curative as difficulties related to drug resistance and adherence can lead to the re-occurrence of high plasma viral levels, AIDS and ultimately death. Until a cure for HIV is found there still exists a necessity for continued clinical development of novel superior ARVs that are efficacious against wild-type and mutated targets and that are inexpensive and well tolerated for chronic use.

Chapter 2: Optimization of a lead compound - a scaffold-hopping approach.

2.1. The discovery of a series of indole-based NNRTIs as potent inhibitors of RT

At the end of Chapter 1 it was concluded that despite the substantial number of anti-HIV agents on the market or in clinical development, the onset of resistance ensures that there remains a perpetual need for the development of new agents that can overcome this issue and effectively control the viral levels in the infected population.

In an effort to address this need our group has focused on the design and development of novel and potent NNRTIs with emphasis on the use of indoles as the core scaffold. Indoles are considered a "privileged scaffold"[†] in drug discovery and the development of indole-based NNRTIs as potent inhibitors of HIV RT has been well established in the literature.[143-146]

In 2014 our research group reported the development of a series of novel 3-alkyloxyindole derivatives (**1** – **3**, **Figure 20**) that exhibited low nanomolar activity against wild-type HIV.[147] Of this series, compound **3** was significantly more potent across a number of clinically relevant resistant strains. More importantly compound **3** was found to maintain potency in the presence of the most problematic and wide-spread K103N mutation.[147] The activity of these compounds can be attributed to a number of key structural features that enhance their affinity for the NNIBP. Using compound **3** as an example, **Figure 20** shows a schematic representation of the proposed binding mode of these indole analogues within the NNIBP. The 3,5-dimethylphenyl moiety located at the 3-position of the indole achieves π-π stacking interactions with Tyr181, while the methoxy moiety, located on the carbon linker joining the aryl ring to the indole core, occupies a small hydrophobic pocket in the vicinity of Val179. The indole NH and the ester carbonyl occupying position 2 on the indole core facilitate hydrogen bonding interactions with the backbone of Lys101. Prior structure-activity-relationship (SAR) studies have established the importance of these structural features towards the activity of these analogues. It was observed that the absence of any of these features would result in a significant loss in activity.[147-148]

[†] A term coined by Evans and co-workers in 1988 to describe modifiable molecular structures capable of providing novel ligands as agonists and antagonists for various receptors.[4]

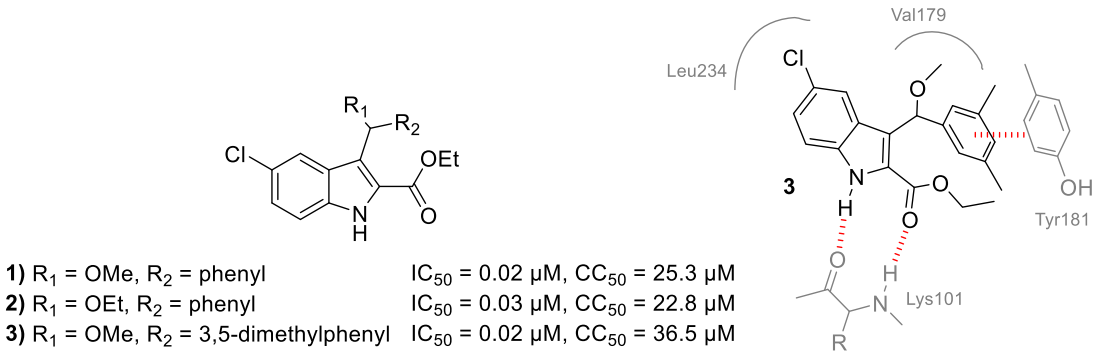

Figure 20. *(left)* Novel 3-alkyloxyindole derivatives were developed that exhibited low nanomolar activity against wild-type HIV RT. *(right)* A schematic representation of the binding mode of compound **3** in the NNIBP.

Despite the promising activity profile of these indole analogues against wild type HIV and K103N it was discovered that these compounds, when exposed to an acidic environment, were prone to degradation through hydrolysis of the alkoxy moiety.[149] Although this observation could be exploited in the synthesis of these compounds it did not bode well for the stability of these indole analogues *in vivo*. Using compound **1** as an example, **Scheme 1** depicts the proposed method by which acid-mediated hydrolysis occurs. In the presence of acid, the methoxy group is activated through protonation (**4**). The indole then facilitates the elimination of the activated methoxy group resulting in the formation of a reactive electrophilic intermediate **5** which is subsequently attacked by water to afford the (1*H*-indol-3-yl)methanol derivative **6**. The conversion of **1** to **6** was highly unfavourable as **6** was found to be a significantly poorer inhibitor of HIV RT when evaluated in a phenotypic assay.[149] Consequently, the acknowledgement of the alkoxy moiety as the indole analogue's 'Achille's heel' would hinder the possibility of advancing these compounds towards clinical development.

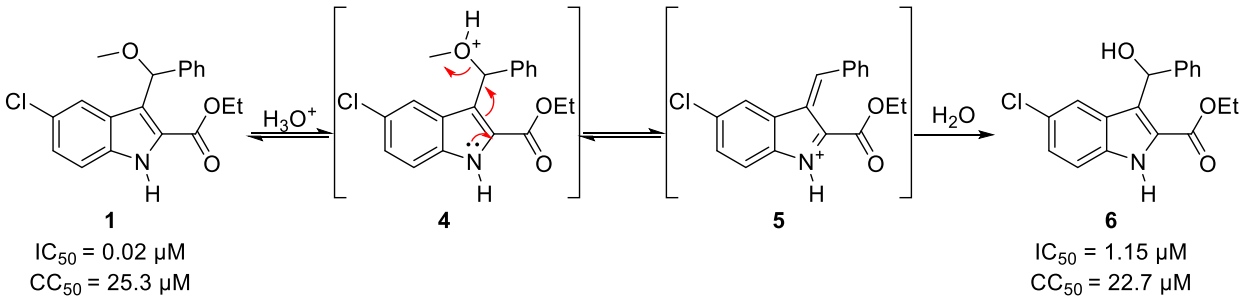

Scheme 1 A depiction of the manner in which indole analogues, such as compound **1**, are hydrolysed in the presence of acid to afford the hydroxyindole **6**, a poor inhibitor of HIV RT.

2.2. The exploration of a suitable bioisosteric replacement to improve upon the stability of a lead compound

In order to address this issue of acid lability a suitable bioisosteric replacement for the problematic alkyloxy moiety had to be discovered. It was crucial that the chosen bioisostere would occupy the Val179 pocket in a manner similar to the original alkyloxy moiety so as not to alter the binding orientation of the compound in the NNIBP. To this end three bioisosteric replacements, expected to be less susceptible to acid-promoted hydrolysis, were identified (**Figure 21**). These bioisosteres included a methyl sulfide group (**7**), a poorer Lewis base and therefore less likely to undergo acid-promoted hydrolysis, an ethyl group (**8**), lacking a protonatable heteroatom altogether and an N-ethylaniline moiety (**9**) for which acid promoted elimination would not be possible. Molecular modelling of compounds **7** – **9** suggested that all identified bioisosteres would be well accommodated in the NNIBP and that all the important interactions between ligand and NNIBP described for the indole analogues in **Figure 20** would be maintained.

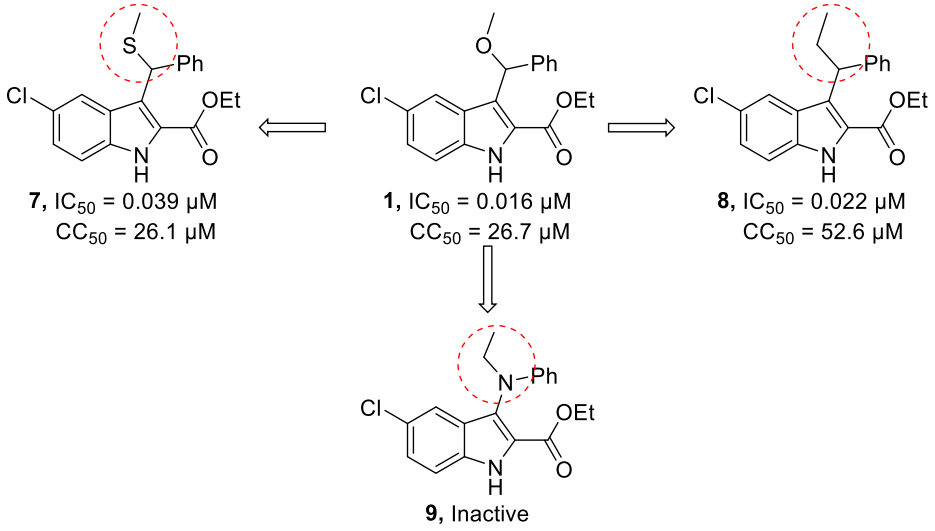

7, IC_{50} = 0.039 µM
CC_{50} = 26.1 µM

1, IC_{50} = 0.016 µM
CC_{50} = 26.7 µM

8, IC_{50} = 0.022 µM
CC_{50} = 52.6 µM

9, Inactive

Figure 21 Three possible bioisosteric replacements for the problematic alkyloxy moiety were identified.

The synthesis and evaluation of compounds **7** and **9** was published in 2016.[149] As with the original lead compound **1,** compound **7** and a few derivatives thereof exhibited low nanomolar activity against wild-type HIV (**Figure 21**). Stability testing of analogues of compounds **1** and **7** involved suspension of these analogues in solutions of concentrated sulfuric acid in ethanol and the periodic monitoring of degradation by HPLC. This study revealed that, unlike the methoxy indole compound which within 2 hours had been fully degraded, the corresponding methyl sulfide compound had remained unaffected after 72 hours.[149]

From this we could conclude that the methyl sulfide analogues were not only potent inhibitors of RT, but were stable under acidic conditions.

Unfortunately, compound **9** did not fare well as a replacement candidate, exhibiting poor activity against HIV and further study of this analogue was not pursued.[149]

Compound **8** was recently evaluated in a whole cell assay and was also found to exhibit low nanomolar activity against wild-type HIV. Although the stability of these compounds has not yet been evaluated we envisaged that derivatives of compound **8** would be unlikely to experience degradation through hydrolysis in acidic media due to the complete lack of a protonatable heteroatom.

Through the identification of indole analogues **7** and **8** our group had successfully optimized the stability of lead compound **1** while maintaining excellent activity against HIV. Nevertheless, these analogues were still not suitable for drug candidacy. We had recognized another lability issue in the form of the ester on the indole scaffold. We understood that, *in vivo*, the indole ester would likely be hydrolysed to the corresponding carboxylate by various cellular esterases which are ubiquitous in the human body.[150] This presented a serious problem as, in earlier studies, it had been established that the carboxylate was approximately 300 times less potent than its ester counterpart.[148]

Unfortunately, removing the ester entirely was not a suitable remedy to this issue. It had already been established that the presence of the ester was paramount to the activity of the indole series of compounds. In a previous study the synthesis and evaluation of the methoxy indole analogue with and without the ester present was reported (**Figure 22**).[147] It was observed that by removing the ester completely, the methoxy indole compound **10** suffered a greater than 100-fold loss in potency.

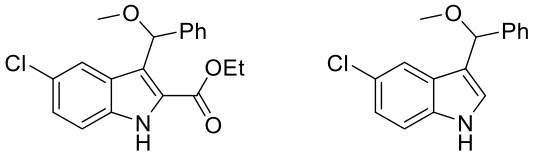

1
IC_{50} = 0.02 µM
CC_{50} = 25.3 µM

10
IC_{50} = 2.43 µM
CC_{50} = 67.0 µM

Figure 22

The contribution of the ester towards the activity of the indole compounds is thought to be two-fold. Firstly, the ester improves the affinity of the compound for the NNIBP by introducing additional electrostatic interactions with the backbone of Lys101 (**Figure 20**). Secondly, it was proposed that the

presence of the ester could be responsible for improving the hydrogen bonding capability of the adjacent indole NH. The presence of an electron withdrawing group such as the ester would pull electron density from the indole ring system, increasing the polarization of the indole N-H bond and thereby increasing its efficacy as a hydrogen bond donor.

2.3. A scaffold-hopping approach to overcome the metabolic instability of the labile indole ester

Although there exist a number of suitable bioisosteric replacements for the ester we decided to take a novel approach and address this issue by exchanging the indole scaffold altogether with a suitable replacement which we would identify through a scaffold hopping approach. The concept of 'scaffold hopping' was introduced by Schneider *et al*. in 1999 and has become increasingly popular in lead optimization.[151] This method, by definition, is a means to replace a known scaffold with one that is isofunctional but has altered certain properties that may have previously hindered drug development.[151-152]

Using this approach, and with the aid of molecular modelling, we identified the benzimidazolone heterocycle as a suitable bioisosteric replacement for the ethyl indole-2-carboxylate scaffold (**Figure 23**). Molecular modelling studies were undertaken using Schrödinger software, with extra-precision Glide as the main docking tool in order to compare the binding mode of the benzimidazolone scaffold against the indole series.[153] Schematic representations of indole compound **1** and corresponding benzimidazolone compound **11** bound to the NNIBP reveal that compound **11** maintains a similar binding orientation to the indole analogues by retaining interactions with Tyr181 and the backbone of Lys101 and by occupying the Val179 pocket (**Figure 23**). Although with this new scaffold the hydrogen bond acceptor in the form of the ester carbonyl was lost, it was hoped that the presence of the carbonyl directly adjacent to the benzimidazolone NH would be able to sufficiently strengthen the hydrogen bonding capability of the urea, thereby compensating for the loss of the second hydrogen bond.

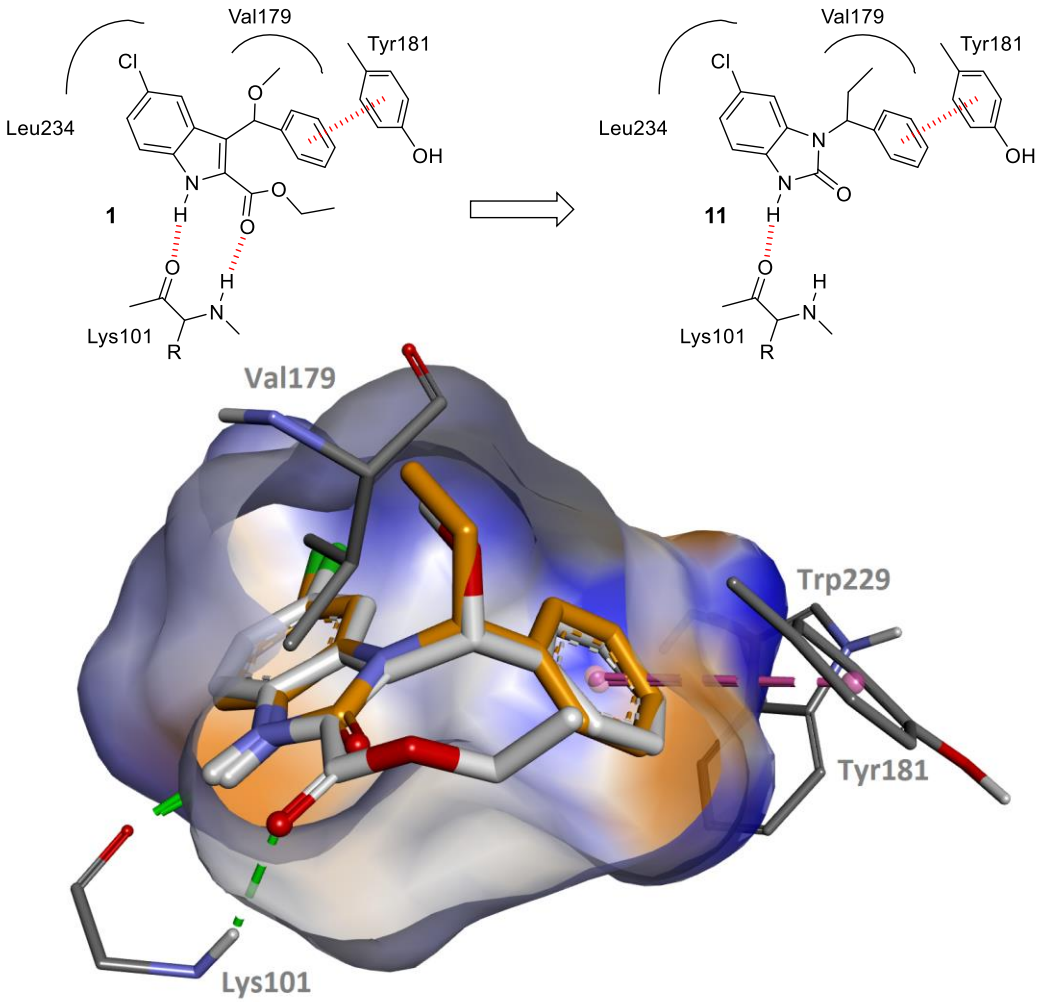

Figure 23 (top) schematic representations comparing the binding mode of compounds **1** and **11** in the NNIBP. (bottom) overlay of compounds **1** (white) and **11** (orange) in the NNIBP. Docking studies were conducted using the receptor PDB ID 2RF2.

Interestingly, a survey of the literature revealed that we were not the first to consider the benzimidazolone heterocycle as a potential NNRTI scaffold. In 2005 another group had designed and synthesized a series of similar compounds based on a 3D pharmacophore model built from efavirenz.[154-156] These benzimidazolone analogues exhibited moderate to excellent activity against HIV. Sulfonamide compound **12** in particular was the most potent of the series and displayed moderate activity against problematic mutant strains such as K103N (**Figure 24**).[155-156]

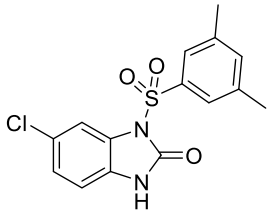

12

EC_{50} = 0.002 μM

Figure 24

These results provided confirmation that our choice of scaffold was not unfounded. Furthermore, in light of the fact that these benzimidazolone analogues exhibited excellent potency against HIV RT we were optimistic that the same exceptional results for our own benzimidazolone compounds would be obtained.

2.4. The strategy towards the synthesis of target compound 11

Having identified our target compound **11** we could embark upon its synthesis. We decided to base our synthetic strategy on the synthesis described for compound **12** due to the similarity with our target compound.[156] The reported synthetic strategy was fairly straightforward and comprised of three separate steps shown below in **Scheme 2**.

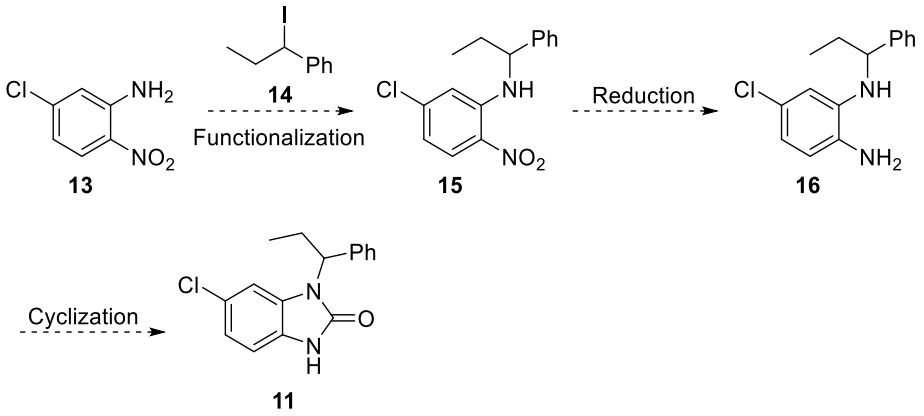

Scheme 2: Synthetic strategy of target compound **11** based on the synthetic procedure described by Barecca *et al.*[156]

The first step would involve the *N*-functionalization of 5-chloro-2-nitroaniline **13** with an appropriate aryl halide, which in our case would be (1-iodopropyl)benzene **14**, to yield the functionalized precursor **15**. Subsequent steps would involve the reduction of the nitro group to the diamine **16** and cyclization in the presence of CDI to yield the target compound **11** (**Scheme 2**).

As part of our strategy to synthesize **11**, the alkylating agent (1-iodopropyl)benzene **14**, which was not commercially available, had to be synthesized. Through retrosynthetic analysis it was anticipated that compound **14** could be synthesized from the corresponding alcohol **17** through a simple substitution reaction with an appropriate iodine source (**Scheme 3**). In turn, it was envisaged that the 2˚ alcohol **17** could be readily obtained through a Grignard reaction between commercially available ethyl iodide **18** and benzaldehyde **19** (**Scheme 3**). It is important to note that at this stage stereoselectivity was not important. As with the original series of indole compounds we acknowledged that the target compound **11** would be obtained as the racemate to establish a proof-of-concept and overall, to avoid synthetic complexity.

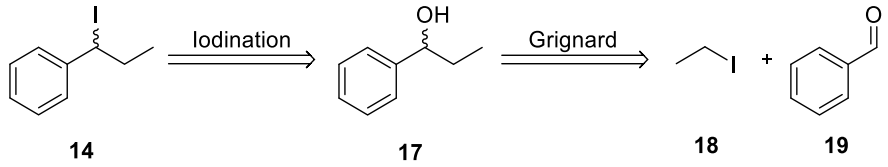

Scheme 3 A retrosynthetic approach to the synthesis of compound **14**

2.4.1. Synthesis of (±)-1-phenylpropan-1-ol (17)

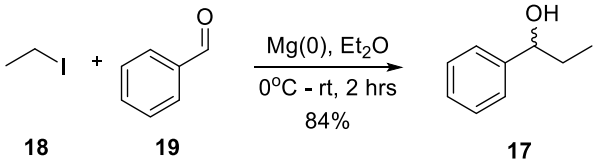

Scheme 4

For the Grignard reaction to form the precursor **17** we resolved to synthesize the Grignard reagent *in situ* despite the ready availability of solutions of ethylmagnesium bromide. This was achieved by the addition of ethyl iodide **18** to magnesium turnings in diethyl ether (**Scheme 4**). Notable consumption of the magnesium indicated that oxidative insertion of the magnesium to form the Grignard reagent had occurred. Subsequent addition of **19**, allowed for the nucleophilic addition of the Grignard reagent onto the aldehyde and an acid quench resulted in the formation of **17** in an 84% yield after purification.

At first glance, the presence of aromatic and aliphatic signals in the ^{1}H and ^{13}C NMR spectra gave a clear indication that the formation of **17** had occurred successfully. This observation was further justified by the complete lack of a singlet belonging to the aldehyde in the ^{1}H NMR spectrum and the appearance of

a broad singlet at 2.43 ppm which coincided with the presence of the hydroxyl group on **17**. As this was a known compound it was possible to compare the chemical shifts obtained experimentally with those reported in the literature and it was found that all spectroscopic data compared favourably.[157]

2.4.2. Synthesis of (±)-(1-iodopropyl)benzene (14)

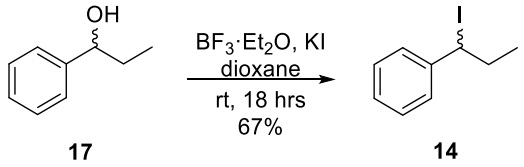

Scheme 5

With compound **17** in hand we could attempt the conversion of the alcohol to the corresponding iodine **14**. A survey of the literature revealed a large variety of methods to achieve this conversion. One publication in particular described the selective iodination of allylic and benzylic alcohols using KI in the presence of the Lewis acid $BF_3{\cdot}Et_2O$ as a mild and efficient method for the preparation of alkyl iodides.[158] Encouraged by the high yields reported in this publication, we resolved to employ this method for the conversion of **17** to the corresponding iodo-compound **14**. In our hands this Lewis acid assisted substitution of a benzylic hydroxyl group for an iodine produced **14** in a moderate yield of 67% (**Scheme 5**).

The notable absence of the OH signal in the ^{1}H NMR spectrum was the first indication that the conversion of **17** into **14** had occurred. In the ^{13}C NMR spectrum an upfield shift from 75.97 ppm to 36.74 ppm was observed for the sp^2 carbon directly attached to the iodine providing further evidence that the conversion had taken place. As with compound **17**, **14** was also a known compound and therefore the experimentally obtained chemical shifts could be compared to the chemical shifts reported in the literature. Again, all spectroscopic data was found to be in accordance with that in the literature.[159]

2.4.3. Synthesis of (±)-5-chloro-2-nitro-*N*-(1-phenylpropyl)aniline (15)

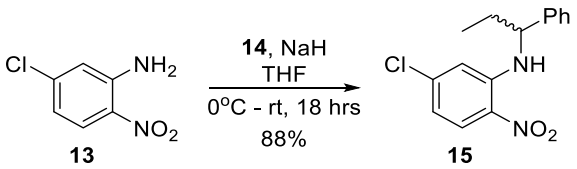

Scheme 6

Having successfully synthesized the precursor **14** we could proceed with the synthesis of target compound **11** using the strategy described in **Scheme 2**. The first step in this strategy was the *N*-functionalization of 5-chloro-2-nitroaniline **13**. This was readily achieved through the treatment of **13** with **14** in the presence of NaH in THF. The *N*-substituted aniline **15** was obtained in 88% yield (**Scheme 6**).

In the ^{1}H NMR spectrum all signals previously associated with compound **14** were observed in the spectrum for **15** in addition to four new signals. Of these new signals a broad doublet at 8.57 ppm was the most noteworthy. This signal which integrated for one proton corresponded to the amine and the multiplicity observed could be attributed to coupling of the amine to the adjacent benzylic proton. In the ^{13}C NMR spectrum 3 aliphatic and 10 aromatic signals were observed coinciding with the expected number of signals for compound **15**.

2.4.4. Synthesis of (±)-5-chloro-*N*1-(1-phenylpropyl)benzene-1,2-diamine (16)

For the reduction of the nitro group on **15** we decided to employ an alternative strategy to the classical catalytic hydrogenation method using Pd/C in the presence of hydrogen. This decision was based on the concern that under these conditions reductive dehalogenation of the chloride present on **15** could occur. While scrutinizing the literature we happened upon a publication which described the use of iron powder or stannous chloride under ultrasonic irradiation as an efficient method of reducing aryl nitro groups.[160] Not only did this method boast mild reaction conditions, short reaction times and high yields but it was also found to be selective for aryl nitro groups in the presence of various sensitive functional groups such as aryl halides, ketones and nitriles.[160] The use of ultrasonic irradiation is often associated with high reaction rates relative to reactions carried out under thermal conditions, an advantage most notable in reactions involving metals. This comes as a result of ultrasound cavitation and activation through the continuous cleaning of the metal surface to limit surface impurities such as oxides, hydroxides and carbonates which inhibit contact between reagents and the metal surface.[161]

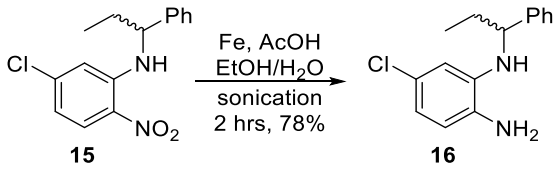

Scheme 7

Of the two reducing agents employed in this publication, iron powder in the presence of glacial acetic acid was reported to be superior to stannous chloride. With this in mind, iron powder was added to **15** in a 2:2:1 solution of glacial acetic acid, ethanol and water and the reaction was exposed to ultrasonic irradiation for 2 hours (**Scheme 7**). Interestingly, within this time the originally bright red reaction mixture had turned clear. As nitro-containing aryl compounds are often brightly coloured this became a clear visual indication that the nitro group had been reduced to the amine, an observation confirmed by TLC. After purification we were able to obtain the diamine **16** in a yield of 78%.

Inspection of the ^{1}H NMR spectrum of **16** revealed a broad singlet located at 5.08 ppm which integrated for 3 protons. Although the only real notable observation, it attested to the successful reduction of the nitro moiety to the amine. Unfortunately, due to degradation issues we were unable to characterize this compound using HRMS.

2.4.5. Synthesis of (±)-6-chloro-1-(1-phenylpropyl)-1,3-dihydro-2*H*-benzo[*d*]imidazol-2-one (11)

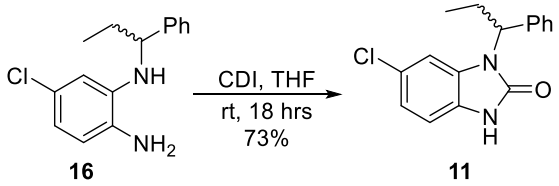

Scheme 8

With the diamine **16** in hand we could attempt the final stage in this synthetic procedure which involved the cyclization of **16** to the target compound **11**. For the synthetic procedure reported in the literature the final cyclization step was achieved through the use of phosgene.[156] We envisaged that the same reaction could be achieved by employing carbonyldiimidazole (CDI), a less toxic alternative. Through the use of CDI we were able to synthesize our target compound **11** in a yield of 73%.

The most distinguishing feature of the ^{1}H NMR spectrum was the presence of a highly deshielded broad singlet at 10.54 ppm. This singlet we could confidently assign to the benzimidazolone NH. All other expected proton signals were accounted for. A signal at 156.52 ppm was the only distinguishing feature in the ^{13}C NMR spectrum and attested to the presence of the benzimidazolone carbonyl group.

2.5. Synthesis of (±)-6-chloro-1-(1-phenylpropyl)-1,3-dihydro-2*H*-benzo[*d*]imidazole-2-thione (20), a sulfur-containing analogue of target compound 11

In addition to compound **11**, we decided that it would be worthwhile to synthesize the sulfur-containing analogue **20** (**Scheme 9**). Although sulfur is less electronegative than oxygen, it has a greater ability to accommodate and stabilize a negative charge due to its larger size, resulting in a much more polarized $S^{\delta-}=C^{\delta+}$ bond.[162-163] As a result, thioureas are more acidic than their urea counterparts and are, therefore, considered to be better hydrogen bond donors.[164] Despite its larger size, molecular modelling indicated that the sulfur analogue **20** would be well-accommodated in the NNIBP. Based on this information we would expect compound **20** to exhibit improved activity over the urea analogue **11**.

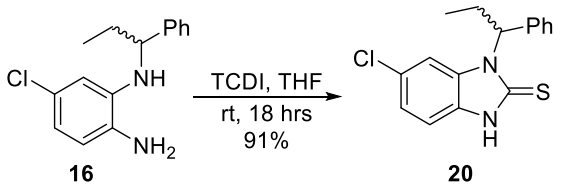

16 **20**

Scheme 9

As the ring-closing step is the final stage in the synthetic strategy, the synthesis of compound **20** would not deviate much from the synthesis described for compound **11**. In fact, the only deviation would be the use of thiocarbonyldiimidazole (TCDI) for the final cyclization step in place of CDI. As planned, the reaction of diamine **16** with TCDI afforded the sulfur compound **20** in a 91% yield.

As with compound **11**, a highly deshielded singlet was observed in the ^{1}H NMR spectrum. This singlet corresponding to the NH of compound **20** was located more downfield at 11.73 ppm, which gave credence to the fact that the thiourea is more acidic than its urea counterpart. The same trend was observed for the ^{13}C NMR spectrum with the thiocarbonyl signal being observed at 170.30 ppm.

2.6. Biological evaluation of compounds 11 and 20

Having arrived at our target compounds **11** and **20**, they could be evaluated for activity against HIV. To this end, the compounds were shipped to Johannesburg to be evaluated by our collaborator Dr Adriaan E. Basson at the HIV Pathogenesis Research Unit at WITS University. Here IC_{50} values were determined using an *in vitro* single-cycle, nonreplicating phenotypic assay and CC_{50} values were determined in a tetrazolium-based colorimetric assay. Both assays utilized HEK293T cell lines.[165-167]

Evaluation of these compounds revealed that **11** was a potent inhibitor of HIV with an IC_{50} value of 22 nM (**Figure 25**). This signified that compound **11** exhibited the same potency as the original lead indole compounds **1** – **3**, despite the lack of an additional hydrogen bond to the backbone of Lys101. This observation gave credence to our hypothesis that having an electron-withdrawing group directly adjacent to the hydrogen bond donor would compensate for the lack of the hydrogen bond acceptor in the form of the ester. Furthermore, not only was **11** potent against HIV, it also addressed the two lability issues exhibited by our indole analogues, namely the issue of acid stability and that of ester hydrolysis. Compound **20**, on the other hand, was found to be ten times less potent than compound **11**. This observation initially came as a surprise as we would have expected better, if not the same activity as for **11**. In an attempt to rationalize the poorer activity observed for **20**, we hypothesized that, perhaps, the introduction of the sulfur increases the lipophilicity of the compound which can negatively influence membrane penetration and solubility.[168] On the other hand, despite the results obtained by molecular modelling, perhaps the larger sulfur clashes sterically with the surrounding amino acid residues in the NNIBP.

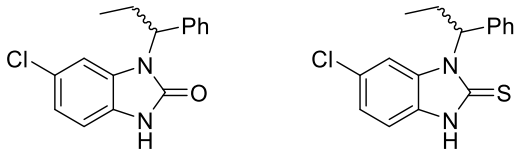

11
IC_{50} = 0.022 µM
CC_{50} = 55.0 µM

20
IC_{50} = 0.289 µM
CC_{50} = 31.2 µM

Figure 25

Due to the potency of compound **11** it was decided to further evaluate the compound's efficacy against the most problematic resistant strains in the clinic, namely K103N and Y181C.

Disappointingly, against K103N and Y181C compound **11** suffered a significant loss in activity. In the case of Y181C, this loss in activity could be attributed to the fact that benzimidazolone compound **11** relies

heavily on π-π stacking interactions between the aryl moiety situated at the *N*1 position and Tyr181 (**Figure 23**). The mutation of the aromatic tyrosine to the aliphatic cysteine residue results in a complete loss of this interaction and as a result, the binding affinity of these compounds for the NNIBP is reduced. The loss in activity against K103N was a little more difficult to rationalize as the manner in which this mutation confers resistance is still not fully understood.

2.7. Concluding Remarks – Can the loss in activity against resistant strains be overcome?

In conclusion, guided by molecular modelling we were able to significantly improve the acid stability and esterase lability of the lead indole compounds **1** – **3** by exchanging the indole scaffold for the benzimidazolone heterocycle. At the same time, we were able to maintain low nanomolar activity against wild-type HIV. Unfortunately, just like the indole series, lead compound **11** was susceptible to the Y181C resistant strain of HIV.

As a means to combat this issue we would need to eliminate any reliance on π-π stacking with Tyr181 altogether. To this end we envisaged designing a library of second-generation benzimidazolone compounds that would not rely on interactions with Tyr181 for their affinity to the NNIBP.

Chapter 3: The Design and Synthesis of a Series of Second-generation Benzimidazolone Compounds

3.1. Targeting Tyr181 and Trp229 as a strategy to overcome susceptibility to the Y181C resistance mutation

The strategy of reducing a therapeutic agent's reliance on interactions with a mutable amino acid residue in order to overcome resistance has found considerable success in the case of the licensed NNRTI efavirenz. In Chapter 1, we discussed and compared the susceptibility of first-generation NNRTIs nevirapine and efavirenz to the Y181C resistant strain. Efavirenz, unlike nevirapine, does not depend on π-stacking interactions with Tyr181 and as a result is able to maintain activity in the presence of the Y181C resistant strain of HIV.[169]

In an attempt to overcome the susceptibility of lead benzimidazolone compound **11** to the Y181C resistant strain we decided to employ a similar strategy. However, instead of removing the aryl functionality completely, which we knew from the indole analogues would result in a significant loss in potency, we envisaged transposing the aryl group from the 1-position to the 7-position on the benzimidazolone scaffold. According to molecular modelling, this shift would result in the occurrence of π-π interactions between the aryl ring and the conserved residue Trp299, as well as Tyr188, and the loss of π-π interactions with the mutable residue, Tyr181 (**Figure 26**).

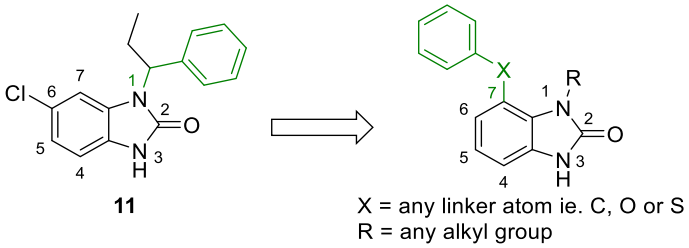

Figure 26 In an attempt to overcome susceptibility to the Y181C resistant strain we envisaged transposing the aryl group from position 1 to position 7 on the benzimidazolone scaffold.

This strategy presents a major advantage in light of the fact that Trp229 is a highly conserved residue in the NNIBP of RT.[170] Trp229 forms part of the primer grip region of the enzyme, and is thus responsible for maintaining the structural integrity of the primer terminus which enables propagation of the nascent DNA

chain at the active site.[171] It is therefore not surprising that site-directed mutagenesis at Trp229 severely compromises the viability of the enzyme.[170] As a result, it has been proposed that in designing NNRTIs that target immutable amino acid residues such as Trp229, the problematic susceptibility to resistant strains of HIV could be overcome.[172] In fact, the strategy of targeting Trp229 has already found considerable success in a number of other potent NNRTIs such as capravirine, lersivirine and doravirine (**Figure 27**).[173-175]

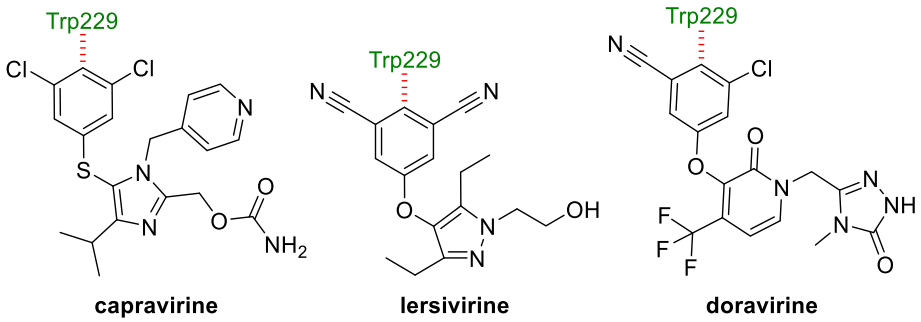

Figure 27 Capravirine, lersivirine and doravirine are known potent NNRTIs that bind to the NNIBP by forming π-π interactions with conserved residue Trp229 and Tyr188.

Docking studies, using extra-precision Glide, were employed to determine the binding mode of these second-generation benzimidazolone compounds within the NNIBP. Encouragingly, these studies revealed that despite the transposition of the aryl ring on the benzimidazolone scaffold we would be able to maintain a similar binding orientation to our lead compound **11**. This signified that, in addition to π-π interactions with Trp229 and Tyr188, these compounds would be able to retain the important hydrogen bonding interaction with the backbone of Lys101 (**Figure 28**). Furthermore, by maintaining the presence of an alkyl group at position 1 on the benzimidazolone scaffold we would still be able to occupy the small hydrophobic pocket in the vicinity of Val179.

It is also worth mentioning that by transposing the aryl ring from the 1 to 7-positon on the benzimidazolone scaffold, Tyr181 is able to adopt the energetically favoured “down” orientation as found in the apo form of the enzyme.[176-177] In the case of all licensed NNRTIs and our first-generation compound **11**, Tyr181 is forced to adopt an “up” orientation upon binding to the NNIBP (**Figure 28**).[178]

With the aid of molecular modelling we eventually decided upon compounds **21** and **22** as suitable proof-of-concept compounds for the second-generation benzimidazolone series (**Figure 28**). Compound **21,** which possesses the unsubstituted phenyl ring, came about as an obvious extension of lead compound **11**. The decision to synthesize compound **22**, on the other hand, which possesses the two methyl

substituents at *meta*-positions on the "upper" aryl ring, was based on observations made concerning the *m*-xylene-containing indole compound **3** discussed in Chapter 2. It was found that the presence of the methyl substituents on the aryl ring significantly improved the activity profile of **3** against the K103N resistant strain.[147]

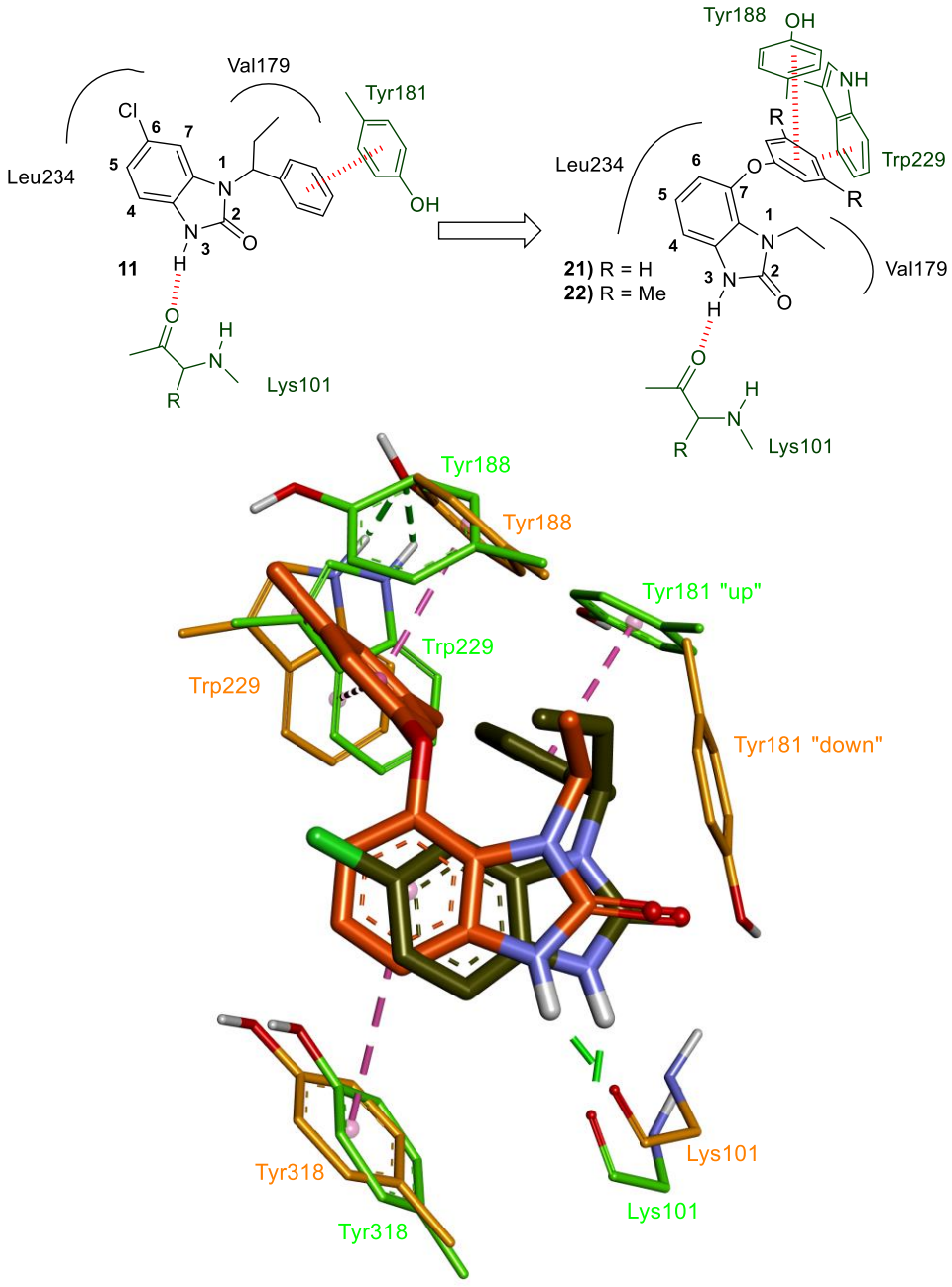

Figure 28 (top) By relying on π-π interactions with Tyr181 compound **11** is susceptible to the Y181C mutation (left). The strategy to overcome this involves transposing the aryl group to form π-π interactions with Tyr188 and conserved residue Trp229 (right).

(bottom) An overlay of compounds **11** (green) and **22** (orange) demonstrates how the orientation of Tyr181 moves from the "up" to the "down" position. Images were created using PDB files 2RF2 and 2JLE in Discovery Studio.

A similar observation was made for an earlier HEPT NNRTI, emivirine mentioned in Chapter 1. An analogue of emivirine, GCA-186 featuring two methyl substituents on the “upper” aryl ring in the vicinity of amino acid residue Trp229, was found to be a potent inhibitor of RT with an improved activity profile against the Y181C and K103N resistant strains (**Figure 29**).[179]

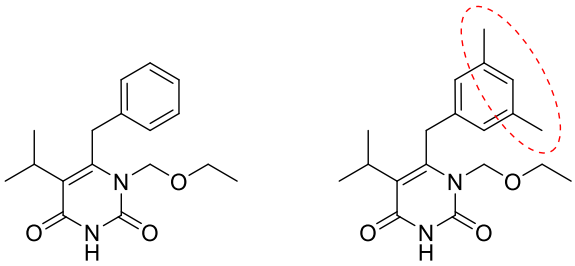

Figure 29 By introducing methyl groups on the "upper" ring of emivirine the activity profile against mutant strains Y181C and K103N was significantly improved.

It is important to note that docking studies indicated that the methyl groups on our benzimidazolone scaffold would be well-accommodated within the NNIBP and would not alter the binding orientation of **22**.

For ease of synthesis we decided to introduce an oxygen linker atom at the 7-positon on the benzimidazolone scaffold, as this would enable us to employ classical coupling techniques to install the “upper” aryl group at this position. From **Figure 27** it can be seen that the use of an oxygen linker is not without precedence. Moreover, we decided to functionalize position 1 on the benzimidazolone scaffold with an ethyl chain. Due to the fact that the ethyl groups of compounds **21** and **22** occupy the same region as the ethyl group on **11**, we were concerned that the installation of larger groups would not be tolerated (**Figure 28**).

Finally, in an attempt to reduce synthetic complexity, we decided not to introduce the chloride at position 6 on proof-of-concept compounds **21** and **22.** Although the loss of a halogen at this position might be expected to affect the efficacy of these compounds, the similarity of the docking scores obtained for compounds with (-13.141 kcal/mol) and without (-13.120 kcal/mol) the chloride present at this position implied that this would not be case.

3.2. Synthesis of proof-of-concept compounds 21 and 22

With a plausible strategy to overcome resistance to Y181C in mind we could embark upon the synthesis of our proof-of-concept compounds **21** and **22**. It was envisaged that target compounds **21** and **22** could be readily accessed by starting from commercially available 2-nitro-3-aminophenol **23** (**Scheme 10**). A coupling reaction between **23** and aryl iodides, iodobenezene **24** and 5-iodo-*m*-xylene **25** would yield the biaryl ether precursors **26** and **27**. From this point, the subsequent steps in the synthesis of compounds **21** and **22** would follow a similar route to that which was used to synthesize first-generation compound **11** described in Chapter 2. These steps would involve the *N*-alkylation of the biaryl ether precursor with ethyl iodide to obtain the functionalized biaryl ethers **28** and **29**, reduction of the nitro group to yield **30** and **31** and finally a ring-closing reaction with CDI to obtain the desired compounds **21** and **22**.

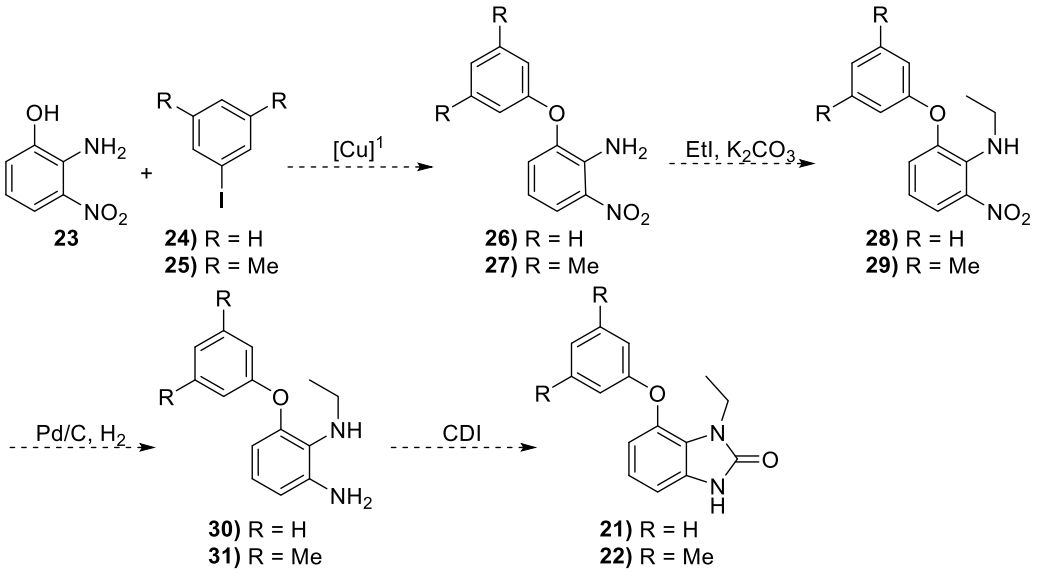

Scheme 10

3.2.1. Synthesis of biaryl ether precursors 26 and 27 by way of an Ullmann ether coupling reaction

For the coupling between **23** and aryl iodides **24** and **25**, it was imperative that coupling conditions were chosen that would allow for the chemoselective arylation of the phenol without competitive coupling to the aniline. Such conditions were described in a publication by Maiti and Buchwald.[180] Herein they

reported the discovery of a copper catalyst derived from CuI and picolinic acid which, in the presence of K_3PO_4 and DMSO, could selectively catalyze the arylation of phenols in the presence of amines. It appeared that the chemoselectivity reported was based on the large differences in pKa between phenols (pKa ≈ 18) and anilines (pKa ≈ 31) in DMSO.[181]

For the synthesis of biaryl ether **27**, a mixture of **23** and **25** in DMSO was treated with picolinic acid and K_3PO_4. The DMSO was then thoroughly degassed under vacuum for approximately 15 minutes to ensure a completely oxygen-free atmosphere prior to the introduction of the copper catalyst, CuI. Following the addition of CuI, the reaction was heated to 90 ˚C and left for 18 hours (**Scheme 11**).

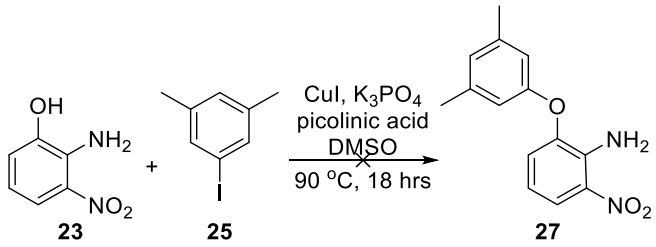

Scheme 11

After this time TLC revealed that all of **23** had been consumed and only one product had formed and following purification by column chromatography we were able to isolate this product in 89% yield.

At first glance, in the ^1H and ^{13}C NMR spectra of this product all signals expected for the biaryl ether compound **27** were accounted for. However, in the ^1H NMR spectrum two broad singlets at 5.67 and 7.33 ppm, each integrating for one proton, were observed as opposed to just one broad singlet integrating for two protons which would be expected for the aniline. In order to absolutely confirm the chemoselectivity of the reaction we obtained FTIR data for the product. Analysis of the FTIR spectrum revealed a broad signal at 3429 cm^{-1}, a characteristic absorption typically associated with an alcohol or phenol OH stretch. Unfortunately, these observations indicated that the coupling had occurred exclusively on to the aniline to yield **32** as the product (**Scheme 12**).

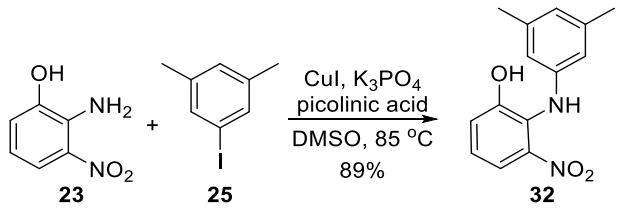

Scheme 12

3.3. A new synthetic strategy to overcome the problem of chemoselectivity

Having run into chemoselectivity issues with our current synthetic strategy, we decided to introduce the aryl group only at the end of the synthesis, following the formation of the benzimidazolone core (**Scheme 13**). Installing the aryl ring at the end of the synthesis would necessitate the introduction of a suitable protecting group for the phenol **23**, thereby increasing the number of steps in the synthesis. However, this new route would allow for divergence of the synthesis to occur at the final step in that a range of variously substituted aryl groups could be introduced at the end of the synthesis.

The first step in the revised synthetic strategy would involve the introduction of a benzyl protecting group onto the phenol **23**, which could be readily installed and removed under mild reaction conditions (**Scheme 13**). The subsequent steps in the revised strategy would follow the route described in **Scheme 10**, which would involve the *N*- alkylation of the amine **33**, reduction of the nitro compound **34** and a ring-closing of the diamine **35** with CDI to afford the precursor **36**. Due to the chemoselectivity issues faced previously, we decided that the introduction of a suitable protecting group onto the benzimidazolone scaffold **36** prior to debenzylation would also be a necessity. Although Boc protecting groups are often utilized for the protection of amines, we did not believe that a Boc group would survive the subsequent coupling conditions due to the utilization of K_3PO_4 and high temperatures (In the synthesis of indole analogues **1** – **3**, described in Chapter 2, we were able to readily remove the Boc protecting group with K_3PO_4 at 70 ˚C).[149] As a result we had to find an alternative protecting group that would survive the Ullmann coupling conditions. To this end we came upon the 2-(trimethylsilyl)ethoxy methyl (SEM) protecting group as an appropriate alternative due to its stability under a variety of reaction conditions.[182] SEM protection of **36** would afford **37** which could subsequently undergo a debenzylation reaction to yield precursor **38.** Penultimately, the Ullmann ether coupling reaction with aryl iodides **24** and **25** would afford the desired precursors **39** and **40**. From the literature we were able to ascertain that the SEM protecting group could then be readily removed by introducing a fluoride source by way of BF_3.OEt or TBAF to afford the proof-of-concept compounds **21** and **22**.[182-186]

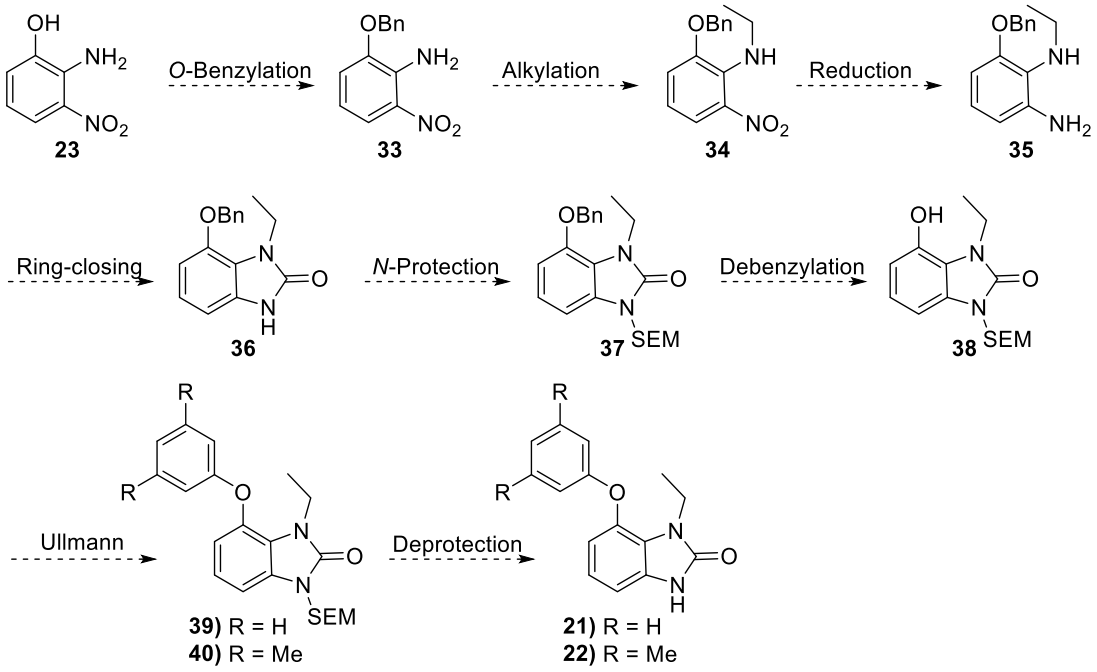

Scheme 13

3.3.1. Synthesis of 2-(benzyloxy)-6-nitroaniline (33)

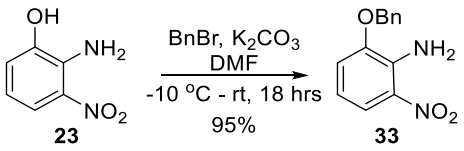

Scheme 14

The first reaction in the altered synthetic route between **23** and benzyl bromide in the presence of potassium carbonate proceeded readily to afford **33** (**Scheme 14**). Interestingly, we found that if the benzyl bromide was added at room temperature or even at 0 ˚C we would form some of the doubly benzylated product (*O*- and *N*-benzylated) which, due to the similarity in R_f value, would be challenging to separate from the desired product **33**. However, by running the reaction at a lower temperature of -10 ˚C (acetone/ice) the amount of doubly benzylated product was almost negligible, enabling the isolation of **33** in a yield of 95%.

The identification of a singlet at 5.12 ppm integrating for 2 protons and a multiplet at 7.40 ppm integrating for 5 protons gave a clear indication that the benzyl group had been installed onto **23** successfully. A broad singlet at 6.46 ppm integrating for 2 protons suggested that the primary amine was unaffected and that

only the phenol had been benzylated. This was confirmed by the absence of a phenolic stretch in the corresponding FTIR spectrum.

3.3.2. Synthesis of 2-(benzyloxy)-*N*-ethyl-6-nitroaniline (34)

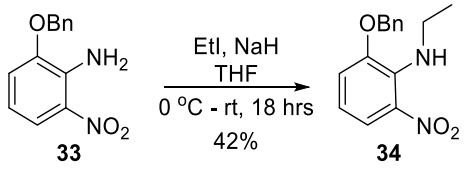

Scheme 15

The subsequent *N*-alkylation of compound **33** which involved the use of ethyl iodide and sodium hydride in THF provided the alkylated product **34** in a disappointingly low yield of 42% (**Scheme 15**). Inexplicably, when we attempted to improve the yield by increasing the amount of reagent added, the yield was found to decrease further. Monitoring the reaction by TLC revealed the formation of a significantly more polar by-product which become more prominent upon the addition of more reagent. Fortunately, it was possible to isolate and characterize this unknown by-product. Study of the ^{1}H NMR spectrum revealed the presence of a triplet and quartet which was indicative that alkylation did occur. However, these aliphatic signals were accompanied by the presence of a singlet at 2.59 ppm which integrated for 3 protons. Furthermore, in the ^{1}H NMR spectrum, although there was a notable absence of any proton signal belonging to the aniline, all signals belonging to the benzyl and aromatic portion of the compound were still present. In the ^{13}C NMR spectrum two additional signals not expected for the alkylated product **34** were observed. Finally, HRMS of the unknown product provided a mass of 283.1441 amu, which was 10 units higher than the mass obtained for the alkylated product **34**.

At first, this characterization data compiled for the unknown compound was confusing. However, while attempting to make sense of it all, we came upon a paper by Gardiner and Loyns who described the one-pot synthesis of a series of *O*-alkylated-*N*-hydroxybenzimidazoles (**Scheme 16**).[187] Their discovery of this one-pot synthesis towards these heterocycles appeared to have been a serendipitous one. In an attempt to alkylate 6-methyl-2-nitroaniline **41** with propyl iodide in the presence of sodium hydride, they found that the *O*-alkylated-*N*-hydroxybenzimidazole **43** was being formed as a major product. The desired *N*-alkylated product **42**, on the other hand, they were never able to isolate in greater than 5% yield.

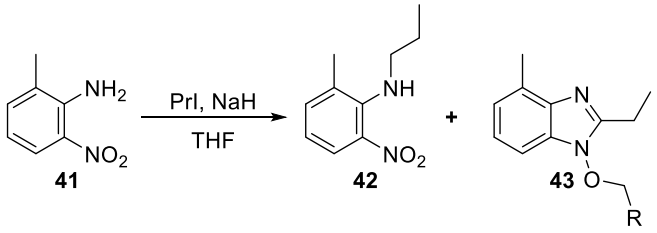

Scheme 16

The almost exclusive formation of **43** came as a surprise as prior to this discovery, base-mediated cyclization of *N*-substituted 2-nitroaniline derivatives were limited to *N*-alkyl groups that possessed a relatively acidic or benzylic proton α to the nitrogen. Furthermore, *in situ O*-alkylation under these circumstances did not occur.[188-190] Although the mechanism for the cyclization of *N*-substituted 2-nitroanilines without an acidic or benzylic α-proton is not fully understood, it has been generally accepted that the formation of the *O*-alkylated-*N*-hydroxybenzimidazole product occurs as a three-step process which involves *N*-alkylation, cyclization and *O*-alkylation. Nevertheless, in a related publication Gardiner *et al.* proposed two possible mechanisms for the formation of these heterocycles (**Scheme 17** and **Scheme 18**).[191] These proposed mechanisms take into account the fact that no *N*-dialkylated products and no unalkylated 1-hydroxybenzimidazoles were ever obtained.

Mechanism A proposes that, following *N*-alkylation to afford **42**, the *N*-anion **42A** tautomerizes to the α-carboanion **42B** which promptly cascades through to benzimidazole-*N*-oxide **44**. Rapid alkylation with excess alkyl halide (propyl iodide in the case of **43**) then affords the *O*-alkylated-*N*-hydrobenzimidazole product (**Scheme 17**).[191]

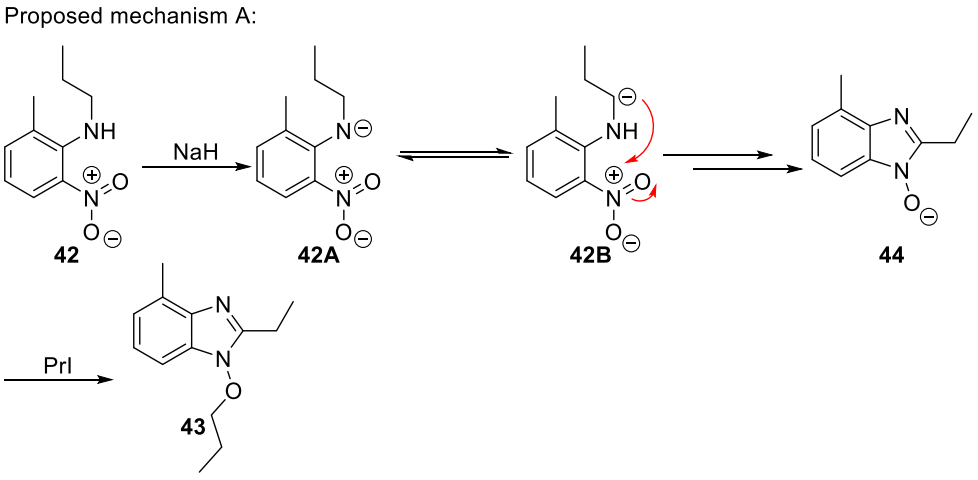

Scheme 17

For the alternative mechanism B, it was postulated that an intramolecular deprotonation by the nitro oxygen occurs by way of the mesomeric form **42C** of **42A**. Cyclization onto the resulting imine **42D** regenerates the aminoanion **45**, which then undergoes a dehydration and subsequent tautomerization to afford **44**. As with mechanism A, **44** is then alkylated *in situ* to afford **43** (**Scheme 18**).[191]

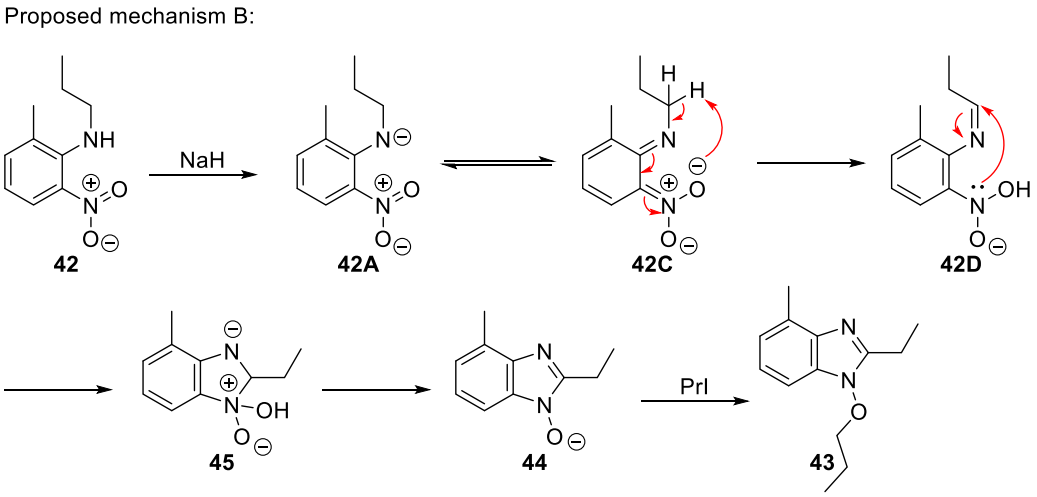

Scheme 18

Having established precedence for the formation of the *O*-alkylated-*N*-hydroxybenzimidazole heterocycle, we revisited the characterization data obtained for our unknown by-product and came to the realization that we had also formed the *O*-alkylated-*N*-hydroxybenzimidazole **46** (**Scheme 19**).

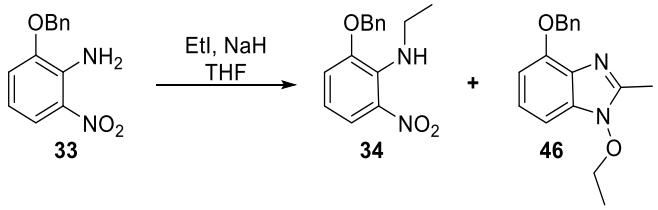

Scheme 19

We knew that in order to avoid the formation of **46** only one equivalent of ethyl iodide and one equivalent of NaH could be added to the reaction mixture. Although this provided us with **34** in a low yield, never greater than 45%, we were always able to recover the starting material **33**. In an attempt to improve upon the yield of the alkylation reaction we decided to introduce a much better electrophile in the form of diethyl sulfate (DES) (**Table 1**). By carrying out the alkylation reaction with DES in presence of NaH we were able to improve the yield of **34** to a moderate 64%. Encouraged by this result, we were tempted to try and improve this yield further by changing the solvent from THF to DMF. DMF, unlike THF, poorly

solvates anionic species thereby enhancing nucleophilic reactivity.[192] To our delight, the alkylation reaction with DES and with DMF as the solvent afforded the product **34** in a much improved yield of 81%.

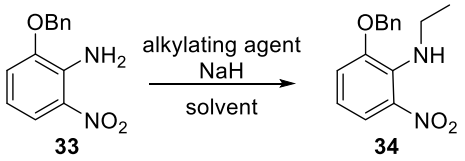

33 **34**

Conditions	Alkylating Agent	Solvent	Yield
A	EtI	THF	42%
B	DES	THF	64%
C	DES	DMF	81%

Table 1

In the ^{1}H NMR spectrum of **34** the presence of a multiplet and triplet at 3.57 and 1.18 ppm, integrating for two and three protons respectively, attested to the presence of the ethyl group. This observation was supported by the presence of two additional aliphatic signals in the corresponding ^{13}C NMR spectrum. Furthermore, a broad singlet observed at 7.54 ppm, which integrated for only one proton, was indicative that *N*-alkylation had occurred only once.

3.3.3. Synthesis of 3-(benzyloxy)-*N*2-ethylbenzene-1,2-diamine (35)

Having successfully optimized the *N*-alkylation reaction we could endeavour to perform the subsequent nitro reduction step to afford **35**. In Chapter 2 we described the use of iron powder in the presence of glacial acetic acid with ultrasonic irradiation as an alternative means to reduce a nitro group in the presence of sensitive functional groups. As classical dehydration methods using palladium on activated carbon would result in the removal of the benzyl protecting group, we decided to employ these alternative conditions for the nitro reduction of **34**. Under these conditions we were able to obtain the reduced product **35** in high yields up to 79% (Conditions A, **Scheme 20**). However, when we attempted to scale-up this reaction we found that yields decreased significantly. In fact, we were only able to obtain product **35** in yields up to 40%.

In a publication by Gamble *et al.*, the use of a large excess of stannous chloride dihydrate with ultrasonic irradiation was reported as an effective alternative to the iron powder/acetic acid route (Conditions B, **Scheme 20**).[160] We decided to attempt the reduction under these conditions in the hope that this would provide an improvement on the yields obtained on a larger scale. Fortunately, when we utilized these conditions we were able to obtain the reduced product **35** in high yields regardless of the scale of the

reaction. Furthermore, while conditions A required approximately 2 hours for the reaction to reach completion (as determined by the obvious colour change described in Chapter 2 and TLC), under conditions B the reaction reached completion within 15 minutes.

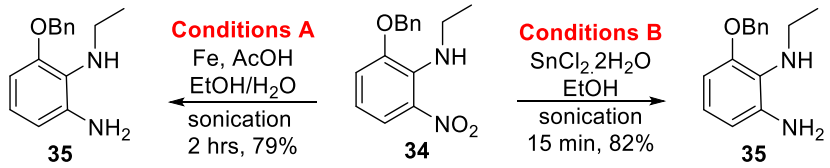

Scheme 20

It is worth noting that the diamine **35** had a tendency to degrade, a process which appeared to be accelerated following purification by column chromatography. As a result, we decided to utilize **35** crude in the subsequent ring-closing step with CDI.

The most distinguishing feature in the ^{1}H NMR spectrum of **35** was a broad singlet located at 5.41 ppm which integrated for three protons. This could be attributed to the presence of the three exchangeable protons of the phenylenediamine **35**. This observation was further corroborated by the HRMS obtained for **35** which gave a mass of 243.1504 amu, coinciding with the calculated mass of 243.1497 amu.

3.3.4. Synthesis of 7-(benzyloxy)-1-ethyl-1,3-dihydro-2*H*-benzo[*d*]imidazol-2-one (36)

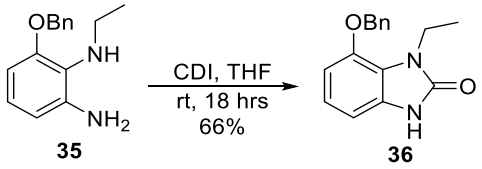

Scheme 21

The subsequent ring-closing reaction between phenylenediamine **35** and CDI in THF was carried out at room temperature for 18 hours to afford the cyclized product **36** in a moderate yield of 66% (**Scheme 21**). Unfortunately, purification by column chromatography proved to be problematic as the product tended to stick to the column resulting in significant band broadening and consequently, tailing on the column. This often led to inconsistent yields or the acquisition of impure product.

By surveying the literature it was found that, in some instances, through the use of acetonitrile the benzimidazolone product would precipitate out of solution which removed the need for further purification by column chromatography.[193-194] We decided to attempt this in the hope that our compounds

would also precipitate from solution. Fortunately, while both **35** and CDI were soluble in acetonitrile, the resulting benzimidazolone product **36** was not. As a result, we were able to obtain **36** in relatively high yields by filtration (**Scheme 22**). Moreover, the product obtained was pure enough that no further purification was necessary.

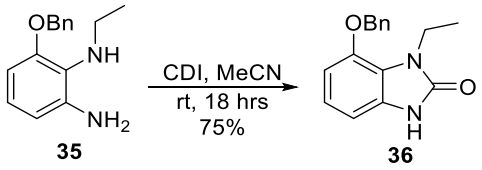

Scheme 22

In the ^{1}H NMR spectrum of **36** the presence of a singlet at 10.38 ppm, which integrated for one proton, attested to the presence of the urea N*H* proton. Additionally, the absence of the broad singlet observed for the exchangeable protons for **35** confirmed that the cyclization with CDI had occurred. In the ^{13}C NMR spectrum all the expected carbon signals for **36** were observed.

3.3.5. Synthesis of 4-(benzyloxy)-3-ethyl-1-(((2-(trimethylsilyl)ethoxy)methyl)-1,3-dihydro-2*H*-benzo[*d*]imidazol-2-one (37)

Having successfully optimized all the steps in the synthetic sequence leading up to the formation of the benzimidazolone precursor **36** we could introduce the SEM-protecting group in preparation for the subsequent debenzylation and biaryl ether coupling reactions.

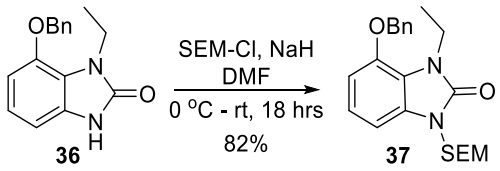

Scheme 23

To this end, 2-(trimethylsilyl)ethoxymethyl chloride (SEM-Cl) was added to a solution of **36** and NaH in DMF at 0 ˚C (**Scheme 23**). After 18 hours the reaction was quenched and purified by column chromatography to afford **37** in a very good yield of 82%.

In the ^{1}H NMR spectrum of **37**, the absence of the characteristic urea N*H* signal at 10.38 ppm observed for **36** provided a clear indication that a group had been installed onto the benzimidazolone scaffold. This observation was accompanied by the presence of four additional aliphatic signals belonging to the SEM

group. These included a singlet at 5.30 ppm integrating for two protons belonging to the methylene, two multiplets at 3.61 and 0.93 ppm each integrating for two protons belonging to the ethyl portion and a large singlet at -0.03 ppm integrating for nine protons attributed to the trimethylsilyl group. The corresponding additional aliphatic signals were observed in the ^{13}C NMR spectrum.

3.3.6. Synthesis of 3-ethyl-4-hydroxy-1-((2-(trimethylsilyl)ethoxy)methyl)-1,3-dihydro-2*H*-benzo[*d*]imidazol-2-one (38)

With compound **37** in hand we could attempt to remove the benzyl protecting group in preparation for the subsequent Ullmann coupling step. The debenzylation of **37** took place readily with palladium on carbon under an atmosphere of hydrogen to afford **38** in 85% yield (**Scheme 24**).

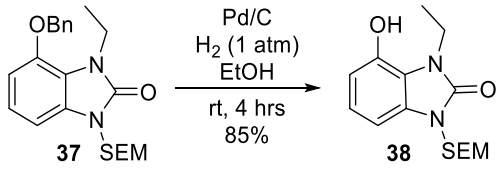

Scheme 24

In the ^{1}H and the ^{13}C NMR spectra of **38** the absence of the benzylic methylene signal and five aromatic proton signals attested to the fact that the benzyl group had been removed. In addition to a broad singlet at 6.99 ppm integrating for one proton in the ^{1}H NMR spectrum which could be attributed to the phenol, the success of the debenzylation was further validated by FTIR which exhibited the characteristic phenol absorbance stretch at 3144 cm^{-1}.

3.3.7. Synthesis of 3-ethyl-4-phenoxy-1-((2-(trimethylsilyl)ethoxy)methyl)-1,3-dihydro-2*H*-benzo[*d*]imidazol-2-one (39) and 4-(3,5-dimethylphenoxy)-3-ethyl-1-((2-(trimethylsilyl)ethoxy)methyl)-1,3-dihydro-2*H*-benzo[*d*]imidazol-2-one (40) by way of an Ullmann ether coupling reaction

With **38** in hand and confident that the unprotected phenol was the only available nucleophile on the scaffold we could attempt to carry out the penultimate step in the reaction sequence which involved an Ullmann ether coupling reaction between **38** and aryl iodides **24** and **25**.

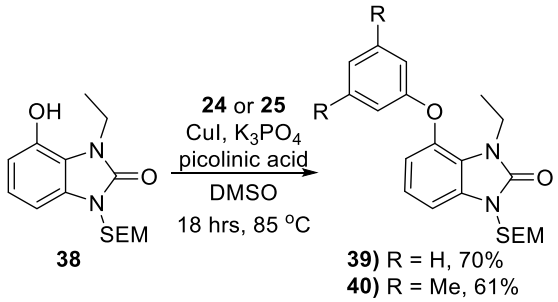

Scheme 25

For the coupling between **38** and **24** or **25** we decided to employ the same conditions described for the attempted synthesis of **27** in section **3.2.1**. To this end, **38** and aryl iodide **24** or **25** were treated with K_3PO_4, picolinic acid and CuI at 85 °C. After 18 hours, TLC revealed full consumption of the starting material and, following purification by column chromatography, we were able to obtain the desired products **39** and **40** in moderate yields of 70% and 61% respectively (**Scheme 25**).

The absence of the broad phenol signal in the ^{1}H NMR spectra of compounds **39** and **40** and the observance of additional aromatic signals in the ^{1}H and ^{13}C NMR spectra gave testimony to the success of the Ullmann ether coupling reaction. Furthermore, all signals attributed to the SEM protecting group were observed in the ^{1}H and ^{13}C NMR spectra of **39** and **40** indicative that, as expected, the SEM group had survived these reaction conditions.

3.3.8. SEM-deprotection to obtain target compounds 1-ethyl-7-phenoxy-1,3-dihydro-2*H*-benzo[*d*]imidazol-2-one (21) and 7-(3,5-dimethylphenoxy)-1-ethyl-1,3-dihydro-2*H*-benzo[*d*]imidazol-2-one (22)

Finally, having successfully obtained the precursors **39** and **40** in satisfactory yields, we could attempt to remove the SEM protecting group to afford the final proof-of-concept compounds **21** and **22**.

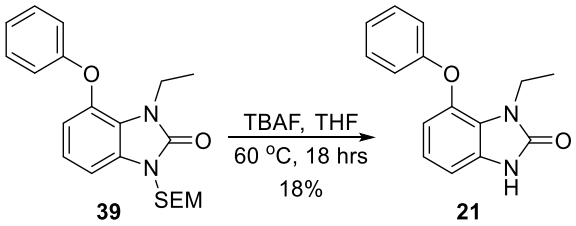

Scheme 26

A survey of the literature suggested that the use of TBAF was the most popular SEM *N*-deprotection method.[195-198] Therefore, for the removal of the SEM group, an excess solution of 1.0M TBAF in THF was added to a solution of the precursor **39** in THF and the reaction was heated to 60 ˚C (**Scheme 26**). However, after approximately 18 hours monitoring the reaction by TLC revealed that the reaction had not reached completion. This situation did not appear to change even with the addition of additional equivalents of TBAF. Unfortunately, subsequent workup and attempted purification by column chromatography afforded the desired compound **21**, albeit impure, in an unacceptably low yield of 18%. Due to the poor yield obtained we did not possess enough of **21** to attempt a second purification, obtain full characterization and evaluate for activity against HIV RT.

In an attempt to optimize this reaction, we decided to employ boron trifluoride diethyl etherate (BF_3OEt_2) as an alternative means to remove the SEM protecting group.[185-186] To this end, BF_3OEt_2 was added to **39** in DCM at 0 ˚C (**Scheme 27**). The reaction was warmed to room temperature and encouragingly, after 30 minutes TLC revealed that all of **39** had been consumed. As the product formed shared the same R_f value as the product obtained from the deprotection reaction with TBAF we were fairly surprised when analysis of the ^{1}H NMR spectrum for the resulting product indicated that the desired compound **21** was not the product that had been isolated.

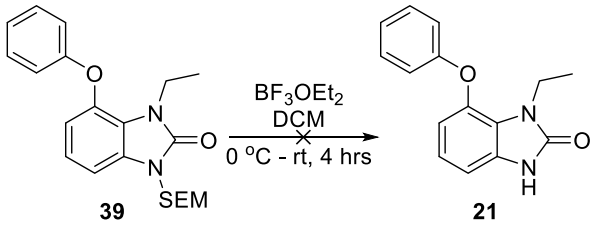

Scheme 27

At first glance the signals associated with the SEM group appeared to be absent from the ^{1}H NMR spectrum, yet the expected urea signal normally observed between 10 and 11 ppm was also absent. On closer inspection, however, we realized that the signal for the methylene protons at 5.45 ppm of the aminomethanol portion of the SEM group was still present. This was also observed in the corresponding ^{13}C NMR spectrum. This implied that BF_3OEt_2 had removed only the ethyltrimethylsilyl portion of the SEM group and that the resulting product was, in fact, the hemiaminal **47** (**Scheme 28**).

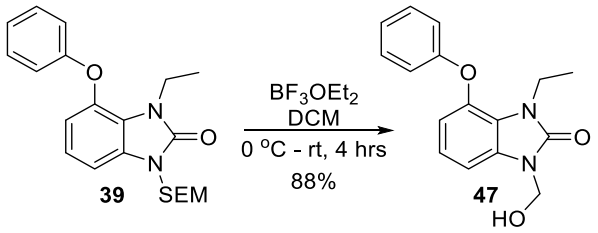

Scheme 28

In a publication by Muchowski and Solas the same phenomenon was described for the *N*-SEM deprotection of pyrroles and indoles.[199] Herein, they reported that *N*-SEM deprotection with BF_3OEt_2 would lead exclusively to the formation of the hemiaminal product. However, the hemiaminal could be readily cleaved through the introduction of base. In the paper by Muchowski and Solas, the hemiaminal was cleaved through the introduction of benzyltrimethylammonium hydroxide or Triton B.[199] Nevertheless, a review of the literature revealed that the hemiaminal could just as readily be cleaved with more common benchtop reagents such as sodium hydroxide (NaOH).[200-201] To this end, NaOH was added to the hemiaminal **47** in a solution of THF and water and the reaction was carried out for 18 hours at room temperature (**Scheme 29**).

It is worth mentioning that in the publication by Muchowski and Solas it was reported that *N*-SEM deprotection by way of BF_3OEt_2 and base, although a two-step process, was overall found to be superior to TBAF with regards to yield and purity.[199] This observation was reflected in the deprotection of **39**. After purification by column chromatography the desired product **21** was afforded in a yield of 44% over 2 steps.

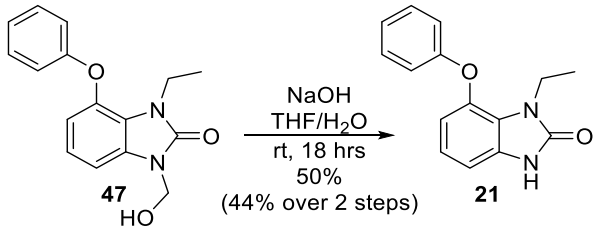

Scheme 29

In the ^{1}H NMR spectrum of **21**, the expected urea proton signal was detected at 11.07 ppm which attested to the successful cleavage of the hemiaminal **47**. This conclusion was made in conjunction with the notable disappearance of the hemiaminal methylene signal in the ^{1}H and ^{13}C NMR spectra. Finally, HRMS which provided a mass of 255.1128 amu confirmed that **21** had been successfully synthesized.

Despite the additional step required to obtain the desired *N*-deprotected product, the overall yield obtained for **21** using BF_3OEt_2 and NaOH was notably superior to the yield obtained for the single-step SEM-deprotection method with TBAF. Therefore, we decided to employ these SEM deprotection conditions for the *N*-deprotection of the dimethyl analogue **40** (**Scheme 30**). In this instance we decided not to isolate and purify the hemiaminal but rather take it crude to the subsequent cleavage step with NaOH. Under these conditions, compound **22** was afforded in a moderate yield of 48% over two steps.

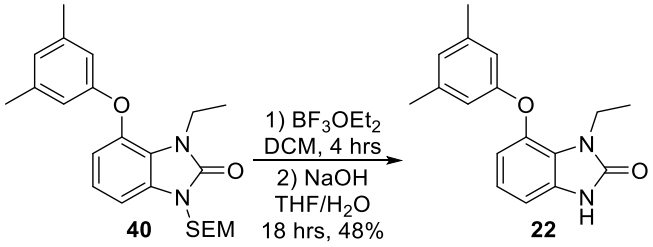

Scheme 30

3.4. Evaluation of target compounds 21 and 22

Having arrived at our proof-of-concept compounds **21** and **22** we could evaluate whether our strategy to target Tyr188 and Trp229 by transposing the aryl group from position 1 to 7 on the benzimidazolone scaffold was a feasible one.

Unfortunately, the activity results obtained in the phenotypic HIV assay for compounds **21** and **22** were disappointingly poor compared with the results for the lead compound **11**.

Compound **21**, in particular, exhibited very poor activity against HIV with an IC_{50} value of 4 µM (**Figure 30**). Interestingly, with the introduction of the two methyl groups on the "upper" aryl ring the potency of compound **22** was salvaged by almost 13-fold.

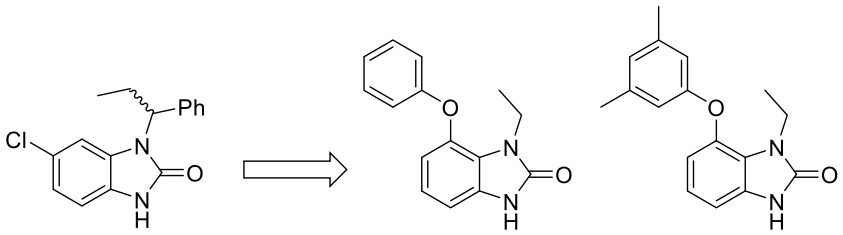

11
IC_{50} = 0.022 µM
CC_{50} = 55.0 µM

21
IC_{50} = 3.88 µM
CC_{50} = 55.0 µM

22
IC_{50} = 0.303 µM
CC_{50} = 7.16 µM

Figure 30

Although still significantly less potent than lead compound **11**, the gain in potency due to the introduction of the methyl groups on **22** indicated that our aim to target Tyr188 and Trp229 was still viable. In fact, we were optimistic that by altering the substituents on the "upper" aryl ring of our second-generation compounds we would be able to further salvage their activity.

This optimism was based on a series of publications by Mowbray *et al.* which demonstrated that by manipulating the substituents on an aryl ring the pharmacokinetic properties, and consequently the efficacy of a compound, could be altered.[202-204] The best example of this was reported for pyrazole NNRTIs **48** and **49** for which the 3,5-dimethyl aryl group of compound **48** was replaced by a 3-chloro-5-benzonitrile ring to afford **49** resulting in a 15-fold improvement in potency against wild-type HIV RT (**Figure 31**).

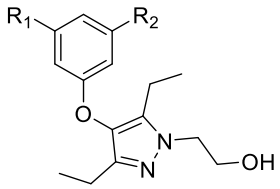

48) $R_1 = R_2$ = Me, IC_{50} = 0.51 µM
49) R_1 = Cl, R_2 = CN, IC_{50} = 0.034 µM

Figure 31

As a proof-of-concept we decided to employ the same substitution pattern exhibited by pyrazole compound **49** on our own benzimidazolone compounds in the hope that we would observe a similar improvement in potency (**Figure 32**).

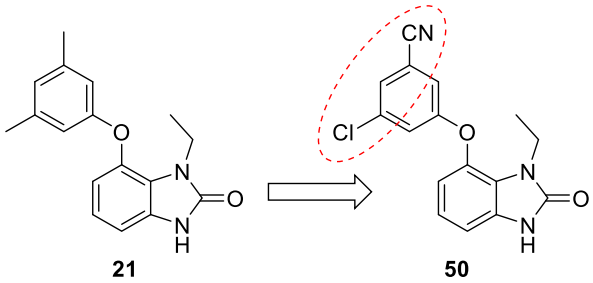

Figure 32

3.5. Altering the substituents on the "upper" aryl ring in an attempt to improve potency

For compound **50** we envisaged being able to employ a similar synthetic strategy to what was used in the synthesis of compounds **21** and **22** (**Scheme 13**). Unfortunately for the coupling step, as we were unable to obtain the 3-chloro-5-cyano-substituted aryl iodide or bromide, we could not utilize the Ullmann coupling conditions described for the synthesis of **39** and **40**. However, we were able to obtain 3-chloro-5-fluorobenzonitrile **51** and therefore, envisaged that the coupling reaction could be achieved by way of an aromatic nucleophilic substitution (S_NAr) reaction between compounds **38** and **51** (**Scheme 31**).

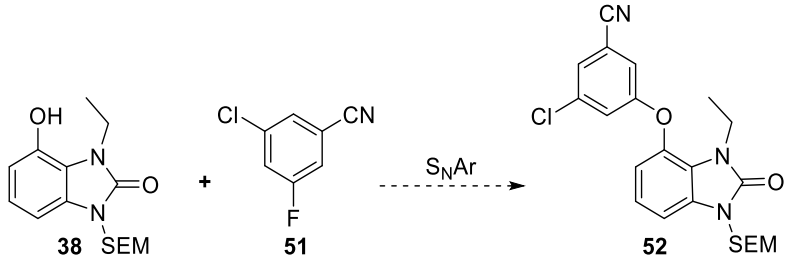

Scheme 31

The nucleophilic displacement of fluorine on an aromatic ring is made possible by the strong electron-withdrawing inductive effect which polarizes the $C_{Ar}^{\delta+} - F^{\delta-}$ bond on the aryl ring and increases the susceptibility of the δ^+ C_{Ar} atom to nucleophilic attack.[205-206] Typically, this reaction is facilitated by the presence of an electron-withdrawing group (EWG), such as a nitro group, situated *ortho* or *para* to the fluoride on the aryl ring.[207-208] However, on our system the EWG, the nitrile, is situated *meta* to the fluoride and, therefore, cannot facilitate the S_NAr reaction to the same extent. Despite this, in the literature there exist a number of examples where S_NAr reactions are carried out with similar aryl fluorides with the

electron-withdrawing group situated *meta* as opposed to *ortho* or *para* to the fluoride.[209-210] These reactions are typically carried out in the presence of K_2CO_3 or Cs_2CO_3 in DMF or NMP at high temperatures.

3.5.1. Synthesis of 3-chloro-5-((3-ethyl-2-oxo-1-((2-trimethylsilyl)ethoxy)methyl-2,3-dihydro-1*H*-benzo[*d*]imidazol-4-yl)oxy)benzonitrile (52)

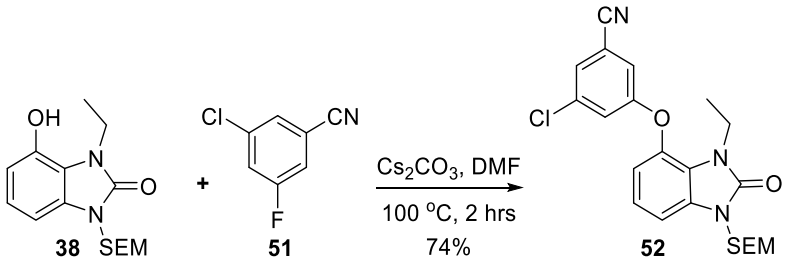

Scheme 32

For the synthesis of **52**, Cs_2CO_3 was added to **38** and **51** in DMF and the reaction was heated to 100 ˚C (**Scheme 32**). The reaction was closely monitored by TLC and after two hours it was observed that all of the starting material **38** had been consumed. Subsequent quenching and purification by column chromatography provided **52** in a 74% yield.

As with compounds **39** and **40**, the most notable feature in the ^{1}H NMR spectrum of **52** was the absence of the proton signal attributed to the phenol of **38**. In addition, three additional proton signals in the aromatic region of the ^{1}H NMR spectrum and seven additional signals in the aromatic region of the ^{13}C NMR spectrum of **52** attested to the successful coupling of **51** and **38**.

3.5.2. Synthesis of 3-chloro-5-((3-ethyl-2-oxo-2,3-dihydro-1*H*-benzo[*d*]imidazol-4-yl)oxy)benzonitrile (50)

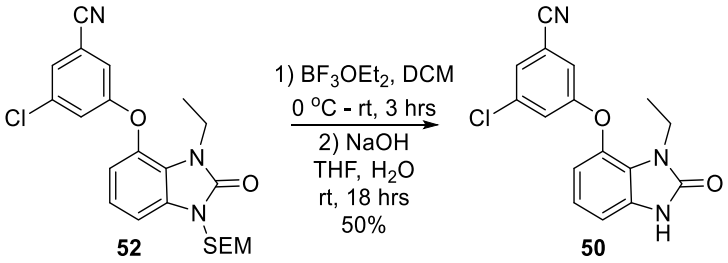

Scheme 33

With **52** in hand, we could carry out the subsequent *N*-SEM deprotection using the two-step method described for compounds **21** and **22**. To this end, **52** was treated with BF_3OEt_2. After 3 hours TLC revealed that all of **52** had been consumed and the reaction was subsequently stopped by quenching with $NaHCO_3$. The resulting hemiaminal was then treated with NaOH to afford the desired product **50** in a moderate yield of 50% over two steps (**Scheme 33**).

A singlet observed at 10.04 ppm in the ^{1}H NMR spectrum of **50** could be attributed to the urea N*H* which gave testimony to the success of the *N*-SEM deprotection. This was supported by HRMS which gave a mass of 314.0711 amu, which correlated well with the theoretical mass of 314.0696 amu.

3.6. Evaluation of compound 50

Having successfully synthesized compound **50** we could evaluate the effectiveness of our strategy to introduce alternative substituents onto the "upper" aryl ring in an attempt to improve the potency of our second-generation benzimidazolone compounds.

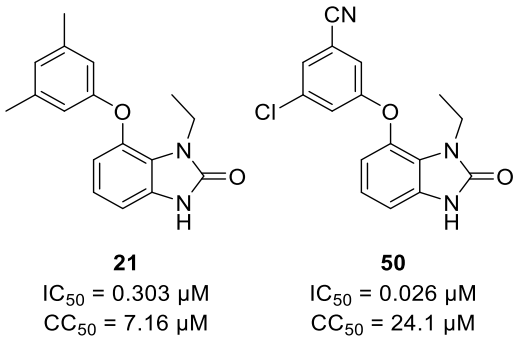

21
IC_{50} = 0.303 µM
CC_{50} = 7.16 µM

50
IC_{50} = 0.026 µM
CC_{50} = 24.1 µM

Figure 33

To our delight, evaluation of **50** in a phenotypic assay revealed that by altering the substituents we were able to significantly improve the potency of our second-generation benzimidazolone compounds from 300 nM to 26 nM (**Figure 33**)! We hypothesized that the significant improvement in potency could somehow be attributed to the idea that the introduction of an EWG such as the nitrile optimizes the edge-to-face π- interactions with Trp229.[211] Nevertheless, although we had succeeded in obtaining another lead compound with low nanomolar activity we still had to verify the feasibility of our strategy to target Trp229 and Tyr188 in an attempt to overcome resistance to the Y181C resistant strain. To this end, compound **50**

was evaluated against Y181C as well as a panel of other clinically relevant resistant strains of HIV (**Figure 34**).

	IC_{50} (μM)
WT	0.026
K103N	0.111
Y181C	0.018
V106M	0.293
G190A	0.126
Y188C	0.007
Y188H	0.415
K103N/Y181C	0.052

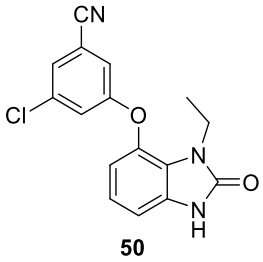

50

Figure 34

Remarkably, from these results it was clear that compound **50** was able to maintain complete potency against the Y181C resistant strain. This result was particularly significant when compared to the currently licensed first-generation NNRTI nevirapine, which is highly susceptible to the Y181C resistant strain (**Figure 35**).[104] Furthermore, compound **50** was found to maintain potency against the Y188C resistant strain, despite the fact that it forms π-π stacking interactions with this amino acid residue when bound to the NNIBP (**Figure 34**). Against the most problematic K103N resistant strain, compound **50** experienced only low levels of resistance with a 4-fold loss in potency. This result is considerable when compared to the susceptibility of first-generation NNRTIs nevirapine and efavirenz to the K103N mutant. Nevertheless, as **Figure 35** demonstrates, second-generation NNRTIs etravirine and rilpivirine still exhibit the best performance against K103N as they are able to maintain efficacy against this resistant strain.[104] Remarkably, against the K103N/Y181C double mutant which causes high levels of resistance to first-generation NNRTIs efavirenz and nevirapine, compound **50** was found to perform similarly to second-generation NNRTIs etravirine and rilpivirine, exhibiting only a 2-fold loss in potency (**Figure 35**).

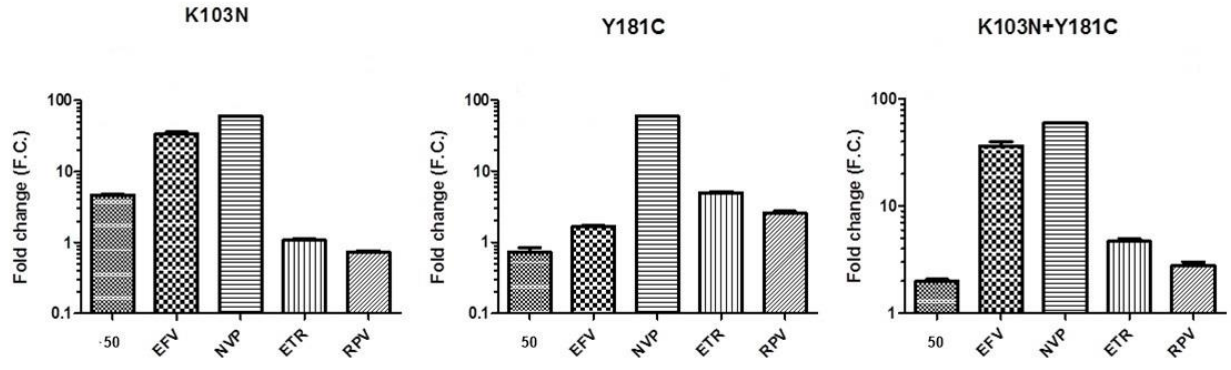

Figure 35 A series of charts comparing the fold change ($IC_{50(mutant)}/IC_{50(WT)}$) observed for all currently licensed NNRTIs and lead compound **50** in the presence of the K103N, Y181C and K103N/Y181C resistant strains of HIV RT.

3.7. The generation of a small library of second-generation benzimidazolone compounds

Having successfully designed and synthesized a second-generation benzimidazolone compound with low nanomolar activity against wild-type RT and the clinically relevant Y181C and K103N/Y181C resistant strains, we could embark upon the synthesis of a small library of second-generation compounds. For this library we would endeavour to derivatize the alkyl and aryl substituents at positions 1 and 7 on the benzimidazolone scaffold respectively and subsequently explore the effects that these derivations have on the potency of the new lead compound **50**.

3.7.1. Derivatizations at position 1 on the benzimidazolone scaffold: Testing the limits of the Val179 pocket

At the start of Chapter 2 we mentioned that the occupation of the small hydrophobic pocket in the vicinity of Val179 was highly influential towards the activity of a compound against HIV RT. As a result, we wished to explore the effect that exchanging the ethyl for a methyl or propyl substituent at position 1 would have on the activity of our lead compound **50** (**Figure 36**).

In section **3.1.** we expressed the concern that the propyl group would not be well-tolerated in the Val179 pocket due to a possible clash with surrounding amino acid residues. However, subsequent docking studies suggested that the propyl chain would be able to occupy the Val179 pocket despite its length. This observation was substantiated by comparing the binding energies calculated for compounds **50**, **53** and **54** (**Figure 36**). The binding energies calculated for all three compounds were found to be very similar which implied that all three compounds would be effective inhibitors of RT regardless of the length of the alkyl chain at position 1.

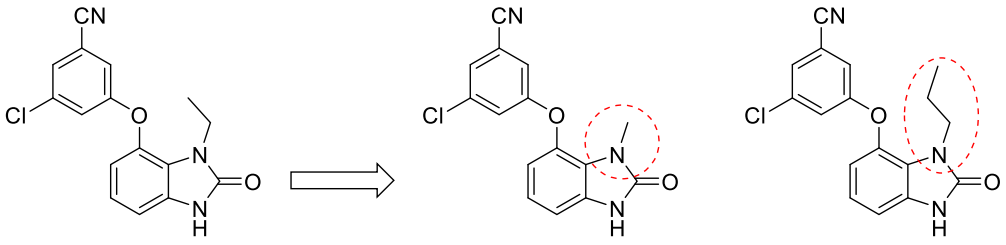

Figure 36 The similarity of the binding energies calculated for compounds **50**, **53** and **54** suggested that compounds **53** and **54** would be as effective in inhibiting HIV RT as lead compound **50**.

For the synthesis of compounds **53** and **54** we could begin with the *N*-alkylation of benzyl protected 2-amino-3-nitrophenol **33**, synthesized previously in section **3.6**. The *N*-propylation of **33** with propyl bromide and sodium hydride in DMF proceeded readily affording the alkylated product **55** in a moderate yield of 68% (**Table 2**). However, the corresponding methylation of **33** with methyl iodide in DMF afforded exclusively the di-alkylated product. Surprisingly, it was only by returning to the use of THF as the solvent that we were able to obtain solely the mono-alkylated product **56** in a yield of 97% (**Table 2**).

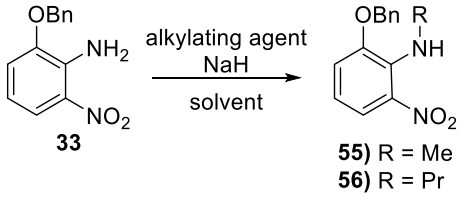

33

55) R = Me
56) R = Pr

N-alkylated Product	R	Alkylating Agent	Solvent	Yield*
55	Me	MeI	DMF	0%
	Me	MeI	THF	97%
56	Pr	PrBr	DMF	68%

* Refers to the yield of monoalkylated product obtained

Table 2

The presence of a singlet at 3.15 ppm in the ^{1}H NMR spectrum of **55** which integrated for three protons attested to the successful methylation of **33**. Furthermore, the presence of a broad singlet at 7.56 ppm which integrated for one proton could be attributed to the amine, indicating that the methylation had occurred only once. For **56**, the presence of a triplet at 3.49 ppm, a multiplet at 1.56 ppm and a triplet at 0.85 ppm which integrated for two, two and three protons respectively attested to the success of the propylation of **33**.

Fortunately, all subsequent steps in the synthesis of compounds **53** and **54**, which followed the route described for lead compound **50** in section **3.6**, were carried out without incident (**Scheme 34**). Reduction of the nitro groups on compounds **55** and **56**, followed by a ring-closing reaction with CDI afforded benzimidazolones **57** and **58** in yields of 79% and 89% respectively over two steps. High yields were also obtained for the *N*-SEM protection affording **59** and **60** and for the subsequent debenzylation with palladium on carbon under an atmosphere of hydrogen affording the compounds **61** and **62**. The penultimate S_NAr reaction between **61** or **62** and 3-chloro-5-fluorobenzonitrile **51** provided the biaryl ether compounds **63** and **64** in moderate yields of 64% and 74% respectively. Finally, the two-step *N*-SEM deprotection with BF_3OEt_2 and NaOH afforded the desired compounds **53** and **54** in yields of 62% and 29% respectively over two steps.

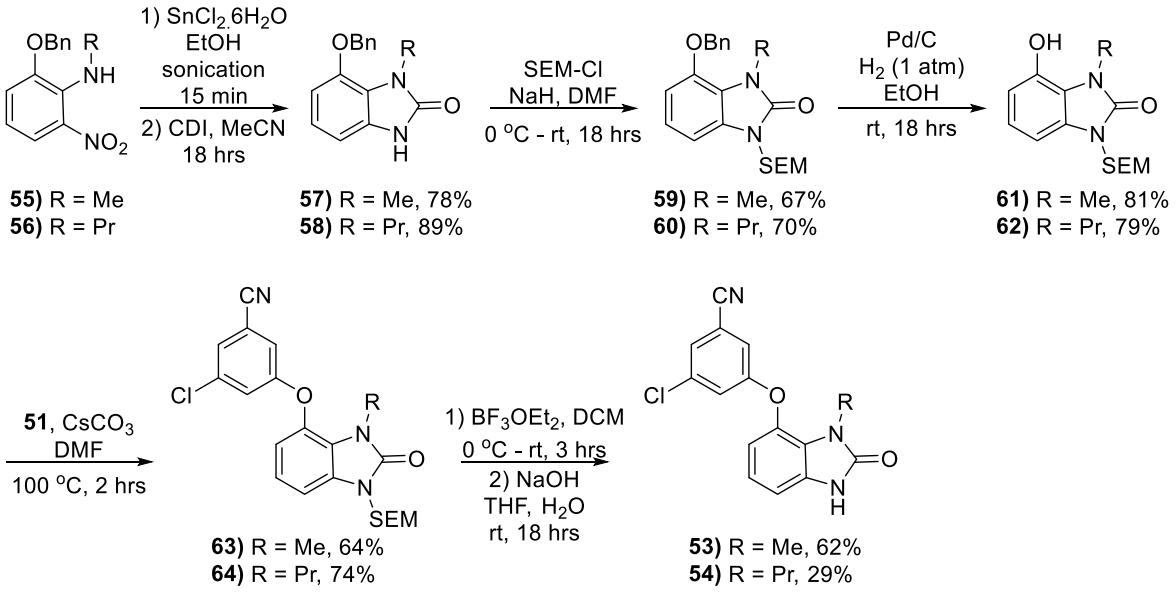

Scheme 34

3.7.2. Derivatizing the "upper" aryl ring

In addition to varying the alkyl group at position 1, we decided to explore the effect that various aryl and heteroaryl groups at position 7 on the benzimidazolone scaffold would have on the efficacy of our compounds. To this end, we chose to synthesize compounds **65** to **69** (**Figure 37**). Although the binding energies calculated for these compounds were notably lower than the binding energy obtained for our lead compound **50**, which implied that they would be less effective, we decided to pursue the synthesis of these compounds as a proof-of-concept and as a means to establish the accuracy and dependability of our docking studies.

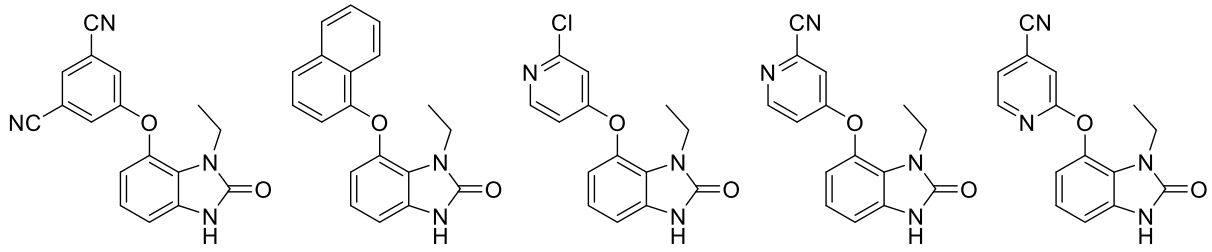

Figure 37

The synthesis of compounds **65** – **69** could be readily achieved by the coupling of commercially available aryl and heteroaryl halides with the benzimidazolone precursor **38**, the synthesis for which was described previously in this chapter.

3.7.2.1. Synthesis of 5-((3-ethyl-2-oxo-2,3-dihydro-1*H*-benzo[*d*]imidazol-4-yl)oxy)isophthalonitrile (65)

For the synthesis of **65**, **38** and **70** were heated to 100 °C for 2 hours in the presence of Cs_2CO_3. Once TLC had indicated that the reaction had reached completion, a workup and subsequent purification by column chromatography afforded the precursor **71** in a 94% yield (**Scheme 35**).

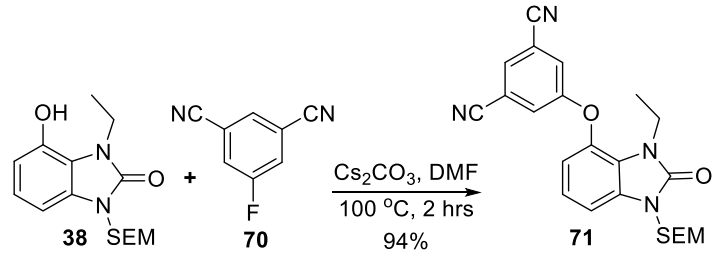

Scheme 35

In the ^{1}H NMR spectrum of **71** the notable absence of the phenolic proton signal, in conjunction with the appearance of a doublet integrating for two protons at 7.47 ppm and a triplet integrating for one proton at 7.64 ppm attested to the successful coupling of **70** to **38**. These additional aromatic signals could be attributed to the isophthalonitrile portion of **71**. Furthermore, in the ^{13}C NMR spectrum of **71** all expected carbon signals were accounted for.

With **71** in hand we could carry out the subsequent SEM deprotection with BF_3OEt_2 and NaOH (**Scheme 36**). This two-step process afforded the product **65** in a satisfactory yield of 54% over two steps.

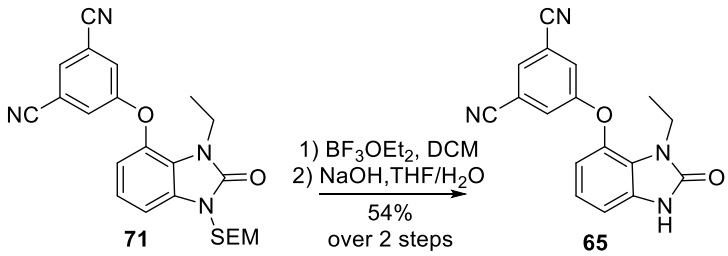

Scheme 36

The presence of the highly deshielded urea signal at 11.14 ppm in the ^{1}H NMR spectrum of **65** provided the most conclusive evidence that the removal of the SEM protecting group and subsequent cleavage of the resulting hemiaminal had occurred. This conclusion was further supported by the notable absence of the hemiaminal methylene carbon signal in the ^{13}C NMR spectrum of **65**. Finally, HRMS analysis provided a mass of 305.10302 amu which coincided with the theoretical mass for **65**.

3.7.2.2. Synthesis of 1-ethyl-7-(naphthalen-1-yloxy)-1,3-dihydro-2*H*-benzo[*d*]imidazol-2-one (66)

For the Ullmann ether coupling, benzimidazolone precursor **38** and iodonaphthalene were treated with K_3PO_4, picolinic acid and CuI in DMSO which had been thoroughly degassed under a positive pressure of argon to ensure an oxygen-free environment. After 18 hours, full consumption of **38** was observed by way of TLC. Therefore, following workup and purification we were able to obtain compound **72** in an excellent yield of 91% (**Scheme 37**).

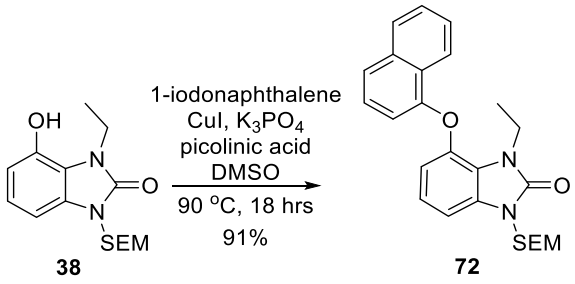

Scheme 37

In the ^{1}H NMR spectrum of **72** we observed the presence of seven additional aromatic protons signals. This observation, in conjunction with the absence of the phenolic proton signal in the ^{1}H NMR spectrum and the addition of ten additional carbon signals in the ^{13}C NMR spectrum of **72** offered clear evidence that the Ullmann coupling between **38** and iodonaphthalene had transpired.

For the subsequent SEM deprotection with BF_3OEt_2 and NaOH, the desired product **66** was obtained impure despite attempted purification by column chromatography. However, from a recrystallization from EtOH we were able to obtain pure **66**, albeit in an inexplicably poor yield of 16% (**Scheme 38**). However, we were fortunate that, despite the yield, we had isolated enough product to proceed with full characterization and evaluation in a phenotypic assay.

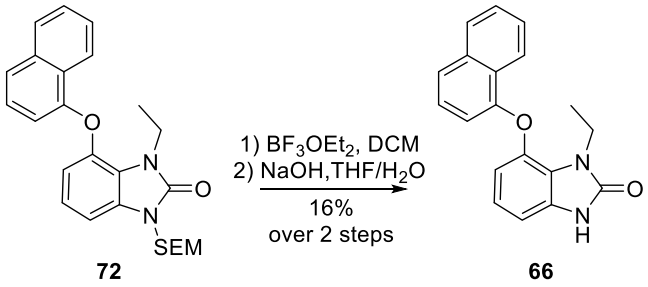

Scheme 38

The characteristic urea proton signal observed at 10.31 ppm in the ^{1}H NMR spectrum of **66**, in conjunction with HRMS analysis which provided the desired mass of 305.1281 amu attested to the successful, albeit low yielding, removal of the SEM group to afford the desired product **66**.

3.7.2.3. Synthesis of the substituted pyridine-containing analogues 76 - 78

For the synthesis of pyridine-containing precursors **76** – **78** (**Scheme 39**) we envisaged employing simple S_NAr reaction conditions due to the fact that nucleophilic substitution on pyridine rings occurs readily at the 2, 4 and 6 positions.[212] The S_NAr reactions between **38** and pyridine analogues **73** – **75** were carried out with K_2CO_3 in DMF at 90 ˚C (**Scheme 39**). When all the starting material had been consumed (as determined by TLC after 18 hours), purification with column chromatography afforded compounds **76** – **78** in yields ranging from 62 – 90%. It is worth noting that for the S_NAr reaction with the dichloro-pyridine analogue **75**, although two potential substitution sites exist, a survey of the literature revealed that in these instances there was precedence for substitution to occur at the position *para* to the pyridine nitrogen.[213-215]

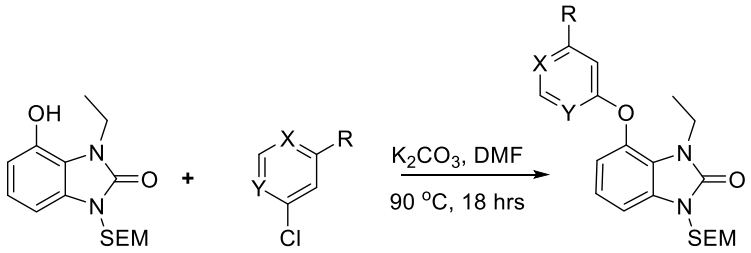

Scheme 39

For precursors **76** – **78** the absence of the phenolic proton signal in the ^{1}H NMR spectra and the observance of the expected number of additional proton and carbon aromatic signals belonging to the substituted pyridine portion of compounds **76** – **78** in the ^{1}H and ^{13}C NMR spectra indicated that all S_NAr couplings between **38** and pyridine analogues **73** – **75** had occurred successfully.

Finally, the subsequent *N*-SEM deprotection reaction on compounds **76** – **78** was carried out in the presence of BF_3OEt_2 and subsequently NaOH to afford compounds **67** – **69** in acceptable yields (**Scheme 40**).

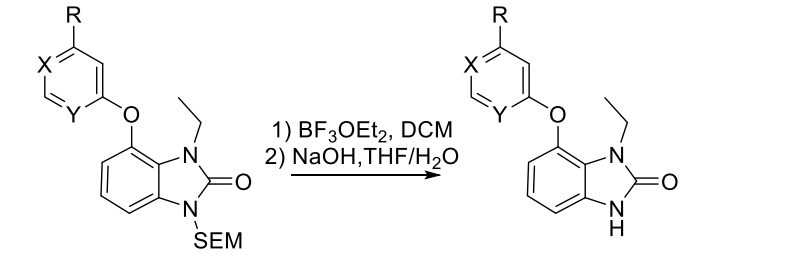

76) X = N, Y = CH, R = CN
77) X = CH, Y = N, R = CN
78) X = N, Y = CH, R = Cl

67) X = N, Y = CH, R = CN, 74%
68) X = CH, Y = N, R = CN, 90%
69) X = N, Y = CH, R = Cl, 66%

Scheme 40

In the ^{1}H NMR spectra of compounds **67** – **69**, the absence of all signals attributed to the SEM protecting group, including the methyl alcohol portion, and the appearance of the characteristic urea proton signal attested to the successful removal of the SEM. This was further validated by analysis of the corresponding ^{13}C NMR spectra and HRMS.

3.7.3. Biological evaluation of our small library of benzimidazolone analogues

Having successfully generated a small library of second-generation benzimidazolone compounds we could evaluate their efficacy in a phenotypic assay.

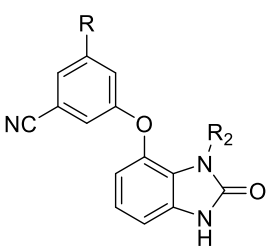

50) R = Cl, R_2 = Et
53) R = Cl, R_2 = Me
54) R = Cl, R_2 = Pr
65) R = CN, R_2 = Et

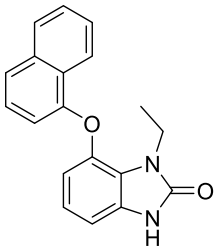

66

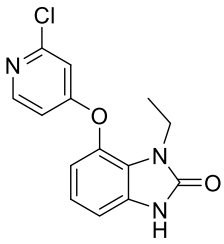

67

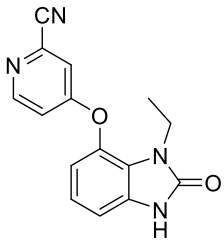

68

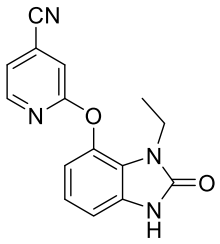

69

Product	IC_{50} (μM)	CC_{50} (μM)	Binding Energies (kcal/mol)
50	0.026	24.1	-91.922
53	0.029	53.4	-90.416
54	0.050	24.8	-90.441
65	0.063	96.6	-87.900
66	2.267	31.3	-73.776
67	>44.1	95.1	-67.412
68	13.340	>100	-66.688
69	1.364	>100	-79.495

Table 3

Of this library of compounds, only compounds **53**, **54** and **65**, which most closely resembled lead compound **50**, were found to be potent inhibitors of HIV RT (**Table 3**). For compound **54** this indicated that, despite our concerns, the larger propyl chain could be accommodated in the hydrophobic pocket in the vicinity of Val179. Compound **53** in particular, performed very similarly to lead compound **50** against wild-type HIV RT, but also exhibited a slightly improved selectivity index. As a result, we were interested in comparing the activities of **53** and **50** against a panel of resistant strains in the hope that we might observe an improvement in the overall resistance profile (**Table 4**).

	IC_{50} (μM)	
	50	**53**
WT	0.026	0.029
K103N	0.111	0.126
Y181C	0.018	0.055
V106M	0.293	0.494
G190A	0.126	0.107
Y188C	0.007	0.236
Y188H	0.415	0.074
K103N/Y181C	0.052	ND

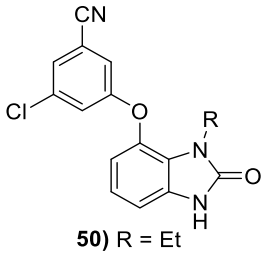

50) R = Et
53) R = Me

Table 4

Against the most problematic clinical resistant strain K103N, compounds **53** and **50** performed similarly, exhibiting only low levels of resistance (<10 fold). However, for the Y181C and Y188C resistant strains against which compound **50** was able maintain full potency, compound **53** experienced low to high levels of resistance. Unfortunately, we were unable to obtain activity data against the K103N/Y181C double mutant. Nevertheless, due to the susceptibility of **53** to both single-point mutations we would expect a

similar susceptibility to the double-mutant. Overall, we concluded that lead compound **50** generally performed better against the resistant strains of HIV and, therefore, remained our most promising second-generation benzimidazolone compound.

Interestingly, with the introduction of the naphthalene and pyridine analogues we observed a significant drop in potency. More specifically, compounds **66** and **69** exhibited only low micromolar activity while compounds **67** and **68** were inactive. The inactivity of compounds **67** and **68** can be explained by taking into account the position of the pyridine nitrogen and the fact that the lone pair of electrons on the pyridine nitrogen occupy an sp^2 orbital which is situated in the plane of the pyridine ring (**Figure 38**). For compounds **67** and **68**, this orbital is pointed directly towards Trp229. We postulated that this would result in an electronic repulsion between these compounds and Trp229 which would, consequently, remove the ability to form the edge-to-face π stacking interactions normally achieved by the "upper" aryl ring of the benzimidazolone scaffold without the nitrogen present. This hypothesis is somewhat substantiated by the fact that when the pyridine nitrogen is not in the vicinity of Trp229, the activity is to some extent restored, as observed for compound **69**.

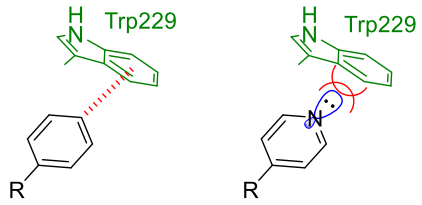

Figure 38 For compounds **67** and **68** the complete lack of activity against HIV RT is thought to be a consequence of the position of the pyridine nitrogen which causes an electronic clash with Trp229.

Although, from this library lead compound **50** remains the most potent compound with the best resistance profile, it is worth noting that there appears to be a direct correlation between the binding energies calculated and the IC_{50} values obtained (**Table 3**). This observation provides testimony to the fact that for this series of compounds, molecular modelling could be relied upon for the design of other benzimidazolone analogues.

3.8. A short SAR study to corroborate the proposed binding mode of lead compound 50

In order to confirm our proposed binding orientation, we decided to carry out SAR studies for the second-generation benzimidazolones within the NNIBP which were discussed earlier in this chapter. According to molecular modelling, the key binding interactions for these compounds are the hydrogen-bonding with the backbone of Lys101 and π-π stacking interactions with Tyr188 and Trp229 (**Figure 28**). We postulated that if compound **50** binds in the manner predicted, then by removing the possibility for these key interactions between the ligand and the NNIBP to form, consequently, we would observe a notable decrease in the potency of our compound. To this end, we envisaged carrying out two separate SAR studies. The first SAR study would focus on eliminating the possibility to attain hydrogen bonding with the backbone of Lys101 (**Figure 39**). The second SAR study would focus on removing the ability to form π-interactions with Trp229 and Tyr188.

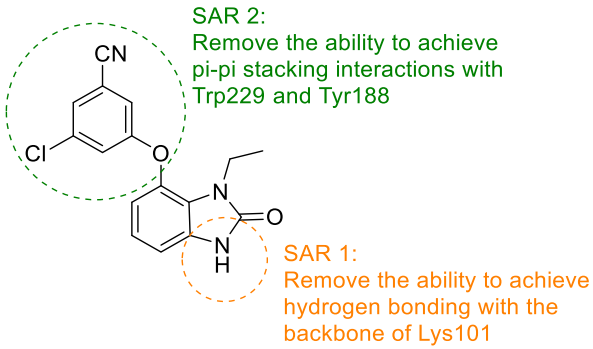

Figure 39 By carrying out two series of SAR studies we hoped to validate the binding mode of our second-generation benzimidazolone compounds within the NNIBP.

3.8.1. SAR 1: Removing the possibility of hydrogen bonding between the core scaffold and Lys101

For our first SAR study to corroborate the predicted binding mode of lead compound **50** in the NNBIP we aimed to eliminate the possibility for hydrogen bonding to the backbone of Lys101. We envisaged that this could be achieved by replacing the hydrogen bond donor, the urea portion of the benzimidazolone scaffold, with a suitable hydrogen bond acceptor. To this end, we decided to replace the benzimidazolone core (**50**) with the corresponding benzoxazolone **79** (**Figure 40**).

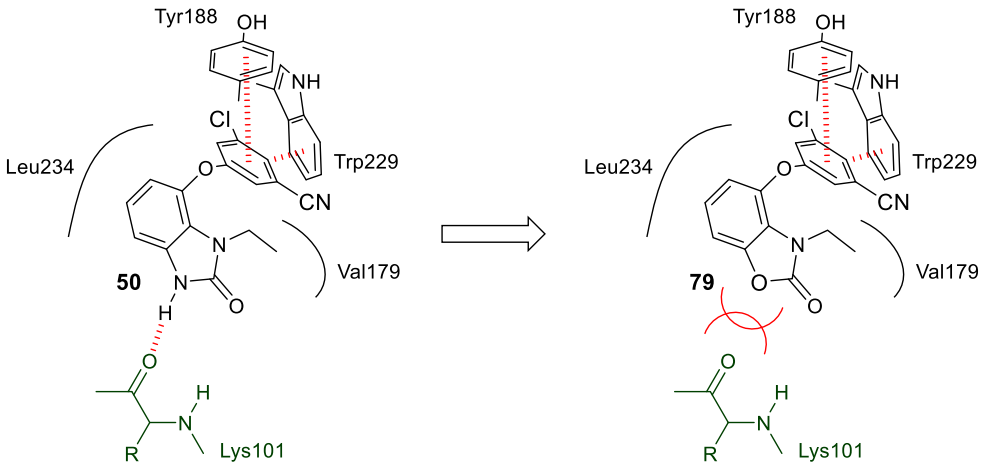

Figure 40

For the synthesis of **79** we envisaged starting from commercially available 2-nitroresorcinol **80** which could be reduced to 2-aminoresorcinol **81** (**Scheme 41**). Previous research within our department demonstrated that the amine of 2-aminoresorcinol could be chemoselectively acylated to afford **82** without the need for protecting groups to be introduced onto the phenols.[216] The resulting secondary amide could then be reduced to the amine with $LiAlH_4$ and $AlCl_3$ to afford the N-alkylated product **83**.[217] Penultimately a ring closing reaction with CDI would afford the benzoxazolone precursor **84** which could then undergo an S_NAr reaction with **51** to afford the desired product **79**.

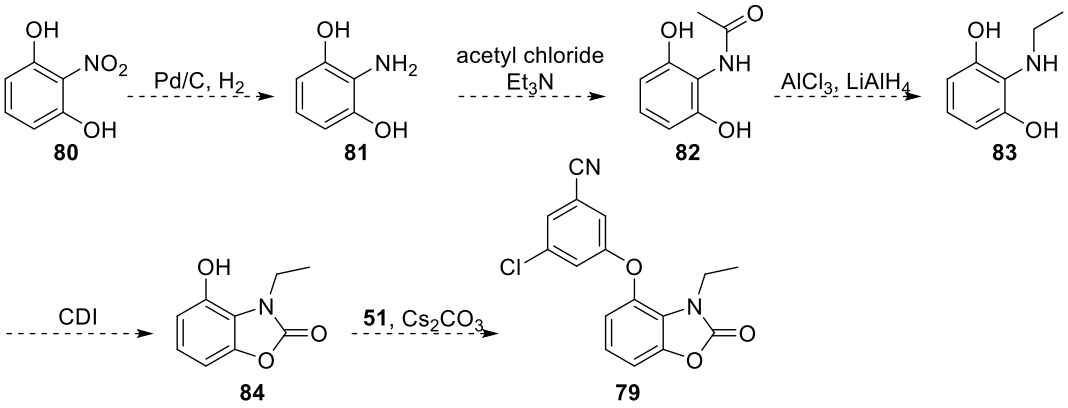

Scheme 41

3.8.1.1. Synthesis of *N*-(2,6-dihydroxyphenyl)acetamide (82) following the reduction of 2-nitroresorcinol (80) to 2-aminoresorcinol (81)

The reduction of **80** by employing palladium on carbon under an atmosphere of hydrogen occurred readily to afford the corresponding amine **81** in a yield of 96% (**Scheme 42**). As **81** is a known compound in the literature we were able to compare the spectral data obtained experimentally with that reported in the literature and found that the data correlated favourably.[218]

For the subsequent chemoselective acylation reaction, **81** was treated with acetyl chloride and triethylamine in THF. After 18 hours the reaction was purified by column chromatography to afford the product **82** in 80% yield.

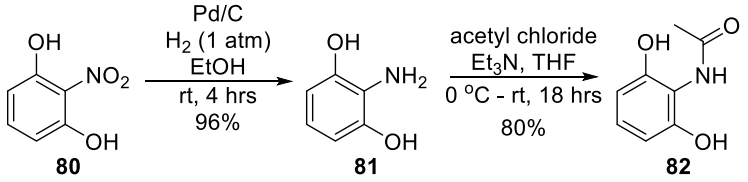

Scheme 42

The most notable feature in the ^{1}H NMR spectrum of **82** was the presence of a singlet at 2.11 ppm which integrated for three protons and could be attributed to the methyl group on the acetyl of **82**. The chemoselectivity of this reaction was validated due to the presence of a triplet and doublet observed at 6.87 ppm and 6.35 ppm which integrated for one and two protons respectively, which attested to there being symmetry in the molecule.

3.8.1.2. Synthesis of 2-(ethylamino)benzene-1,3-diol (83)

For the reduction of the secondary amide we decided to employ conditions reported by Chiellini *et al.*[217, 219] To this end **82** was added to a suspension of $LiAlH_4$ and $AlCl_3$ in THF and the reaction was carried out under reflux for 18 hours (**Scheme 43**). Subsequent quenching with aqueous HCl and purification by column chromatography afforded the reduced product **83** in a moderate yield of 61%.

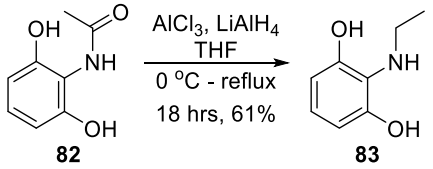

Scheme 43

Analysis of the ^{1}H NMR spectrum of **83** revealed the presence of a quartet and triplet at 3.12 ppm and 1.02 ppm which integrated for two and three protons respectively and could be attributed to the *N*-ethyl group on **83**. These signals, in addition to the notable absence of the methyl signal observed for **82**, indicated that the reduction of the secondary amide had occurred successfully. In the ^{13}C NMR spectrum the carbon signals belonging to the ethyl group were observed at 41.6 ppm and 17.0 ppm.

3.8.1.3. Ring-closing with CDI to afford 3-ethyl-4-hydroxybenzo[*d*]oxazol-2(3*H*)-one (84)

With **83** in hand, we could attempt the subsequent ring-closing reaction with CDI. To this end **83** was treated with CDI. After 18 hours, the formation of a white precipitate indicated that the reaction had transpired. In fact, following filtration we were able to isolate benzoxazolone precursor **84** in an 83% yield (**Scheme 44**).

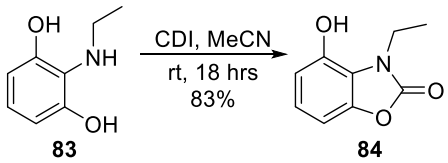

Scheme 44

In this instance there was no characteristic urea proton signal to indicate that the ring-closing reaction had occurred successfully. Furthermore, due to the use of deuterated methanol as a co-solvent in order to fully dissolve **84** for NMR analysis, we were unable to visualize the unreacted phenolic proton signal. However, all expected carbon signals for **84** were observed in the ^{13}C NMR spectrum and HRMS which provided a mass of 180.0654 amu (theoretical mass was 180.0661 amu) attested to the fact that **84** had been obtained successfully.

3.8.1.4. Synthesis of target compound 3-chloro-5-((3-ethyl-2-oxo-2,3-dihydrobenzo[*d*]oxazol-4-yl)oxy)benzonitrile (79)

The final S_NAr reaction between **51** and **84** was carried out in the presence of Cs_2CO_3 at 100 °C for 2 hours. Surprisingly, following workup and purification by column chromatography, this reaction provided the desired compound **79** in a disappointing yield of 42% (**Scheme 45**). Nevertheless, enough material was obtained to carry out full characterization and evaluate for activity in a whole cell phenotypic assay.

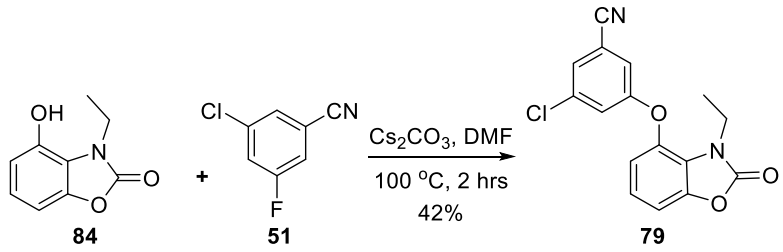

Scheme 45

For compound **79** the presence of three additional aromatic proton signals in the ^1H NMR spectrum and the presence of seven additional aromatic carbon signals in the ^{13}C NMR spectrum attested to the successful coupling of **51** to **84**. This was validated by HRMS which provided a mass of 315.0536 amu which correlated with the theoretical mass of 315.0536 amu.

3.8.2. SAR 2: Removing the potential for π-π stacking to Tyr188 and Trp229

With compound **79** in hand we could turn our focus to our second SAR study in which we aimed to replace the substituted aryl group at position 7 with substituents that could not effectively achieve π-stacking interactions with Tyr188 and Trp229. One example of this would be to install a simple methoxy group (**85**) onto position 7 of the benzimidazolone scaffold (**Figure 41**). In addition, we decided to install a slightly larger group that could, at least, occupy the region in the vicinity of Tyr188 and Trp229. To this end, we chose to introduce a prenyl substituent (**86**) at the 7-position on the benzimidazolone scaffold. It is worth mentioning that the prenyl substituent was originally introduced on the TIBO NNRTI tivirapine, which was briefly mentioned in Chapter 1. On tivirapine the prenyl reportedly occupies the region in the vicinity of Tyr188 and Trp229 and forms weak hydrophobic interactions with the surrounding residues.[220]

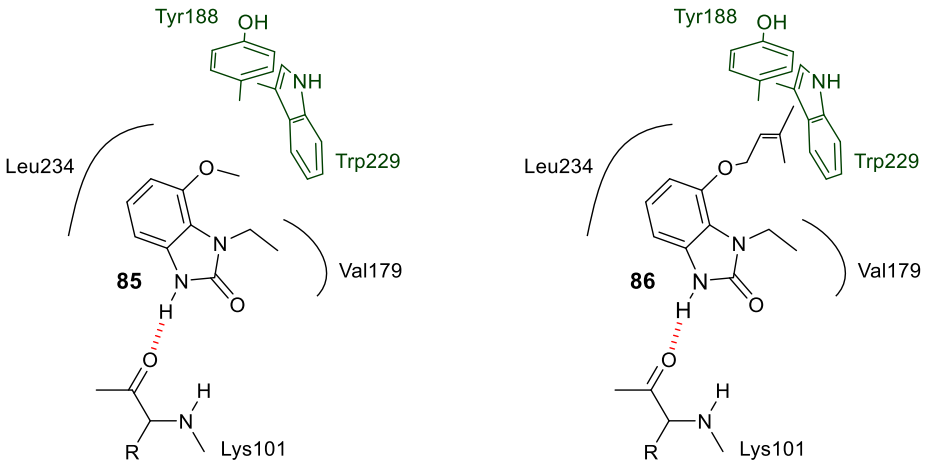

Figure 41

For the synthesis of compounds **85** and **86** we envisaged following the same synthetic route described for all previously synthesized benzimidazolones by introducing the methyl and prenyl substituents onto the *N*-SEM protected benzimidazolone precursor **38** and subsequently removing the SEM group with BF_3OEt_2 and NaOH (**Scheme 46**).

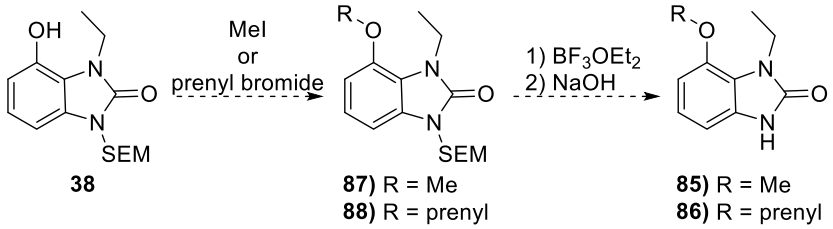

Scheme 46

3.8.2.1. Attempted synthesis of 85 and 86 starting from benzimidazolone precursor 38

For the synthesis of compounds **87** and **88**, **38** was reacted with methyl iodide or prenyl bromide in the presence of NaH and K_2CO_3 respectively (**Scheme 47**). Compound **87** was obtained in an excellent yield of 92%, while **88** was obtained in a moderate yield of 65%.

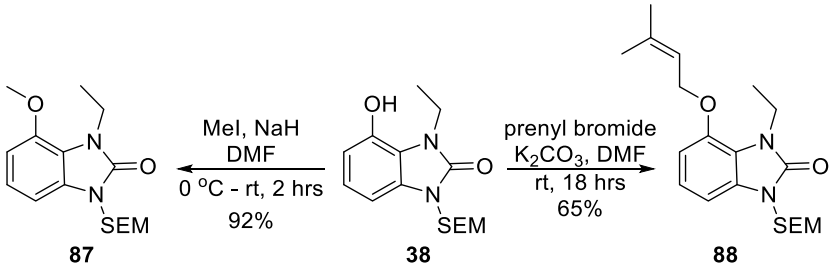

Scheme 47

In the ^{1}H NMR spectrum for compound **87**, the most notable feature was the presence of a singlet at 3.90 ppm which integrated for three protons, and could therefore be attributed to the methoxy group at position 7. In the ^{1}H NMR spectrum for compound **88**, three additional protons were observed that could be attributed to the prenyl substituent. These included a multiplet integrating for one proton at 5.49 ppm, a doublet integrating for two protons at 4.61 ppm and, finally, two singlets integrating for three protons each at 1.77 ppm. Carbon signals for the methyl and prenyl substituents were also observed in the respective ^{13}C NMR spectra for compounds **87** and **88**.

Unfortunately, when we attempted the subsequent SEM deprotection of **87** and **88** with BF_3OEt_2 and NaOH, we were unable to isolate any significant amount of product (**Scheme 48**).

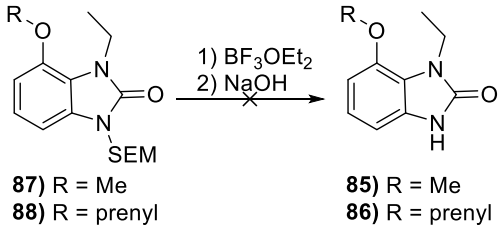

Scheme 48

As all the starting material had been consumed (as determined by TLC) we were concerned that the BF_3OEt_2 may have removed the methyl and prenyl substituents in addition to the SEM protecting group.

3.8.2.2. Attempted synthesis of 85 and 86 starting from benzimidazolone precursor 89

In an attempt to overcome this issue, we decided to try and install the prenyl and methyl substituents onto the unprotected benzimidazolone precursor **90** which was obtained by carrying out a debenzylation of **36** with palladium on carbon under an atmosphere of hydrogen (**Scheme 49**).

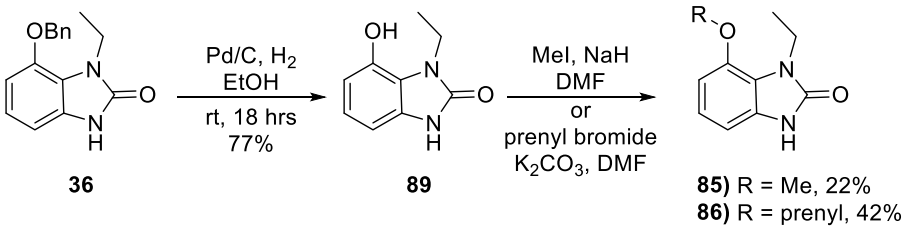

Scheme 49

Fortunately, by employing the same reaction conditions reported in **Scheme 47**, we were able to obtain the desired compounds **85** and **86**, albeit in low yields. However, for both compounds we were able to obtain full characterization data with enough compound left over to evaluate in a phenotypic assay.

In the ^{1}H NMR spectrum of compound **85** the presence of a singlet which integrated for three protons at 3.91 ppm attested to the successful introduction of a methyl group onto benzimidazolone **89**. In the case of compound **86**, the identification of the characteristic prenyl signals at 5.50, 4.61 and 1.78 ppm in the ^{1}H NMR spectrum gave testimony to the success of the alkylation reaction with prenyl bromide. Moreover, the characteristic urea signal observed at 10.10 ppm and 10.41 ppm in the ^{1}H NMR spectra of **85** and **86** repectively was indicative that alkylation had occurred exclusively at the phenol.

3.8.3. Evaluation of compounds 79, 85 and 86 in a whole cell phenotypic assay

With compounds **79**, **85** and **86** in hand we could evaluate their efficacies in a whole cell assay and, from the results, determine whether we could validate the proposed binding mode of our second-generation benzimidazolone compounds, such as lead compound **50**, in the NNIBP.

For our first SAR study we set out to investigate the effect of removing the hydrogen bond donor responsible for forming a hydrogen bond with the backbone of Lys101. To this end, compound **79**, for which the hydrogen bond donating urea was exchanged with a hydrogen bond accepting carbamate, was synthesized. As expected, evaluation of **79** revealed a significant loss in potency (>300 fold), indicative that the hydrogen bond with the backbone of Lys101 was beneficial to the binding of the inhibitor in the NNIBP (**Figure 42**).

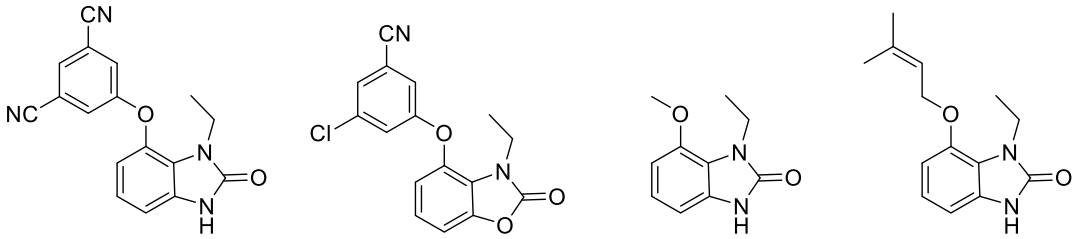

50
IC_{50} = 0.022 μM
CC_{50} = 29.3 μM

79
IC_{50} = 7.529 μM
CC_{50} = 72.3 μM

85
IC_{50} = 29.38 μM
CC_{50} > 100 μM

86
IC_{50} = 0.733 μM
CC_{50} = 68.06 μM

Figure 42

Our second SAR study focused on the removal of the aryl group at position 7 which contributed to the binding of the inhibitor within the NNIBP by achieving π-π interactions with nearby amino acid residues Trp229 and Tyr188. To this end compounds **85** and **86**, for which the aryl functionality was replaced with a methyl and prenyl substituent respectively, were synthesized. For compound **85**, the complete removal of the aryl functionality had a substantially detrimental effect on the potency. Interestingly, although compound **86** suffered a greater than 30-fold loss in potency compared to lead compound **50**, it was still able to maintain submicromolar activity against HIV RT. The ability of **86** to retain some activity could be attributed to the fact that, although unable to form π-interactions with Trp229 and Tyr188, the prenyl could facilitate weak hydrophobic interactions with the surrounding amino acid residues.

As expected, by disrupting key interactions between the ligand and NNIBP, a detrimental effect on the potency of these compounds was observed. Fortunately, by carrying out these SAR studies, we were able to lend testimony to the predicted binding mode of our second-generation benzimidazolone compounds.

3.9. Metabolic stability testing of lead compound 50 against human and mouse liver microsomes

Of all the compounds synthesized in our small series of second-generation benzimidazolone compounds, compound **50** remained the most potent compound against wild-type and resistant strains of HIV RT. As a result, we decided to evaluate how compound **50** might perform *in vivo* by testing its metabolic stability towards human and mouse liver microsomes. To this end, compound **50** was incubated with human and mouse liver microsomes and subsequently analysed by LC-MS over 5-minute intervals for a total of 30 minutes. Pleasingly, in the presence of both human and mouse liver microsomes, compound **50** remained

relatively unaffected. From **Table 5** it can be seen that after 30 minutes, approximately 90% of compound **50** still remained in both liver microsome assays. These results are highly encouraging for the advancement of these compounds towards drug candidacy.

	% Remaining after 30 minutes	
	Mouse liver microsomes	**Human liver microsomes**
Compound **50**	89	93
Verapamil (positive control)	-	7.0
Diphenhydramine (positive control)	51	-

Table 5

3.10. Concluding remarks

In an attempt to overcome susceptibility to the Y181C resistant strain experienced by our first-generation benzimidazolone compounds, we decided to transpose the aryl functionality from position 1 to position 7 on the benzimidazolone scaffold. In doing so these compounds would no longer rely on π-π stacking interactions with Tyr181 but would form π-π interactions with Tyr188 and immutable Trp229. To this end a small library of second-generation benzimidazolone compounds was synthesized. Of these compounds, compound **50** was found to be the most potent with an IC_{50} value of 22 nM against wild-type HIV RT. Furthermore, compound **50** was able to maintain potency in the presence of the Y181C, Y188C and K103N/Y181C resistant strains. Unfortunately, compound **50** showed a 4-fold decrease in potency to the globally prevalent K103N resistant strain. Finally, compound **50** was found to be highly stable towards human and mouse liver microsomes.

As a means to optimize the activity of our second-generation benzimidazolone compounds against wild-type and resistant strains of HIV, we envisaged designing compounds that would be able to introduce additional interactions within the NNIBP. This will be discussed in the following two chapters.

Chapter 4: Lead Optimization Through the Introduction of Additional Electrostatic Interactions within the NNIBP – Part 1

4.1. Targeting Lys223 in an attempt to improve the potency of 50

From the library of compounds discussed in Chapter 3, compound **50** was found to be the most potent compound of the series with an IC_{50} value of 22 nM. In addition, **50** exhibited the best resistance profile, maintaining potency against the Y181C resistant strain as well as the double mutant K103N/Y181C. Nevertheless, we envisaged that we could further boost the potency of **50** against wild-type and resistant strains of HIV through the introduction of additional electrostatic interactions within the NNIBP.

To this end, we considered targeting a lysine residue (Lys223) located at the top of a small hydrophobic chimney towards the back of the NNIBP formed by amino acid residues Trp229, Tyr188 and Phe227 (**Figure 43**). In order to achieve hydrogen bonding with Lys223 it was necessary to identify an appropriate substituent to install onto the "upper" aryl ring of the benzimidazolone scaffold that would be long enough to introduce a hydrogen bond acceptor at an approximate distance of 2.2 Å from the lysine residue. Although a few NNRTIs in the literature have been described as being able to occupy this chimney region, as of yet none have been able to protrude deep enough to attain satisfactory hydrogen bonding with Lys223.[221-222]

With the aid of molecular modelling we were able to identify the cyanoacetylene group (compound **90**) as a suitable substituent to achieve hydrogen bonding interactions with the targeted residue Lys223 (**Figure 43**). The cyanoacetylene group was postulated to be sufficiently narrow and rigid to fit readily into the narrow chimney region and would be long enough to bring the nitrile into close enough proximity with Lys223. Encouragingly, docking studies and binding energy calculations using Schrodinger's Prime MM/GBSA (molecular mechanics energies combined with generalized Born and surface area continuum solvation) revealed that the cyanoacetylene substituent would be able to achieve hydrogen bonding with Lys223 at a calculated distance of 2.3 Å and, at the same time, the rest of the molecule would maintain the crucial electrostatic interactions with residues Trp229, Tyr188 and Lys101.

Furthermore, the binding energies of compounds **50** and **90** were compared and found to be similar for both compounds at -89.657 and -91.481 kcal/mol respectively, which implied that **90** would be as effective an inhibitor as **50**.

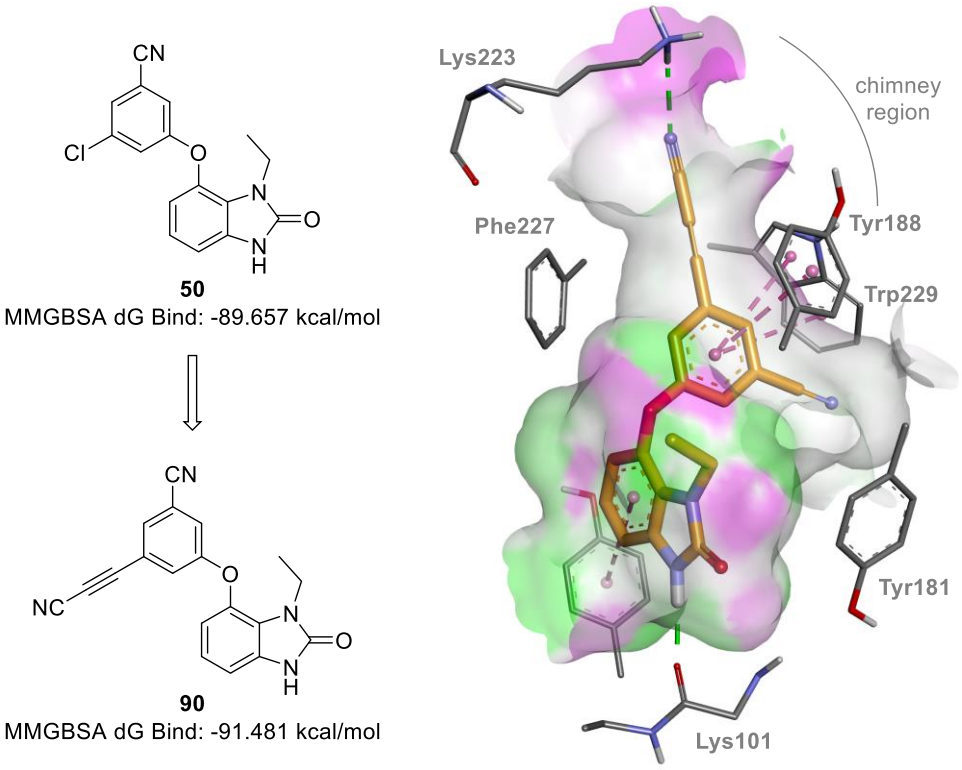

Figure 43 The introduction of a cyanoacetylene substituent would enable the formation of a hydrogen bond to Lys223 situated at the top of a narrow hydrophobic chimney. The similar binding energies of compounds **50** and **90** indicated that the cyanoacetylene substituent would be well accommodated in the NNIBP. Images were created using PDB file 2JLE in Discovery Studio.

4.2. Envisaged approach to the synthesis of target compound 90

For the synthesis of compound **90**, we envisaged starting from commercially available 3-bromo-5-fluorobenzonitrile **91** (**Scheme 50**). Unfortunately, the preferred iodo-analogue of this reagent was not available. However, we envisaged that the presence of the electron-withdrawing nitrile situated *meta* to the bromide would activate the aryl system enough to compensate for the presence of the slightly less reactive halogen.[223]

We envisaged that the first step in the synthetic sequence (**Scheme 50**) would involve a Sonogashira coupling between **91** and propiolamide to afford the amide acetylene precursor **93**. Subsequent

dehydration of the amide with phosphorous oxychloride would provide cyanoacetylene **94** which could then undergo an S_NAr reaction with the benzimidazolone precursor described in Chapter 3 to afford the target compound **90**.

Unfortunately, there existed a slight drawback to this approach in that the starting reagent **91** was expensive. Consequently, we decided to first synthesize an analogue of compound **90** without the nitrile present. Not only would this route provide us with a proof-of-concept compound, but would also allow us to optimize all steps within the synthetic scheme prior to the use of the more costly material.

To this end, we envisaged that the proof-of-concept analogue **97** could be synthesized starting from cheaply and readily available 3-fluoroiodobenzene **92**. Subsequent steps for the synthesis of **97** would once again follow the route of a Sonogashira reaction between **92** and propiolamide to afford **94**, subsequent dehydration of the amide to the nitrile **96** and an S_NAr reaction with the benzimidazolone precursor **38** (from Chapter 3) to afford **97** (**Scheme 50**).

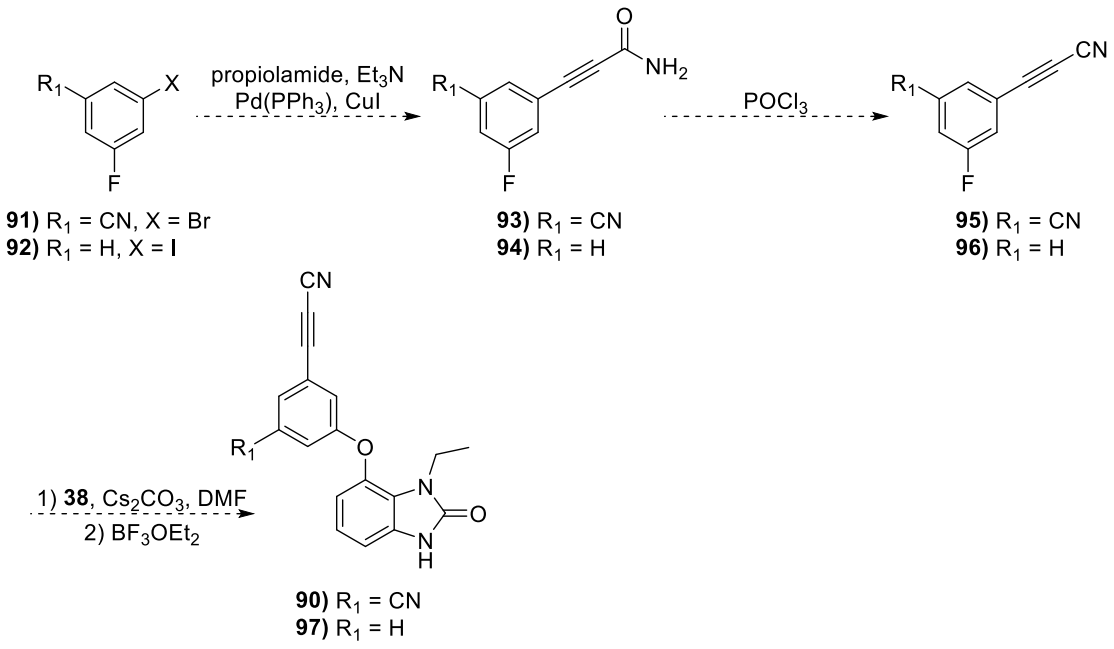

Scheme 50

4.3. Alkynylation through the use of the Sonogashira reaction

The Sonogashira reaction, discovered in 1975 by Sonogashira, Tohda and Hagihara as an extension of the Heck reaction, is considered to be one of the most prevalent and reliable methods for the coupling of an sp hybridized carbon from a terminal acetylene and an sp^2 hybridized carbon from a vinyl or aryl halide.[224-225] Generally the Sonogashira reaction is carried out at room temperature using a palladium catalyst with co-catalytic copper. The introduction of co-catalytic copper was a means to increase the reactivity of the system which allowed for it to be carried out under mild reaction conditions.[225]

Although the exact mechanism of the copper co-catalysed Sonogashira reaction is not yet fully understood, it has been generally accepted that the mechanism occurs through two independent catalytic cycles.[226] The first cycle (Cycle A, **Figure 44**), which is a classical example of a palladium catalysed C-C cross-coupling formation, is initiated by oxidative addition of an aryl or vinyl halide **II** to a catalytically active $Pd(0)L_2$ species **I**, such as $Pd(PPh_3)_4$[224, 227] This stage is generally accepted as the rate-limiting step of the Sonogashira reaction and is largely dependent on the nature of the aryl halide **II**. In this instance the order of increasing reactivity of aryl halides is as follows: ArCl < ArBr < ArI. The resulting palladium adduct **III** then undergoes transmetallation with copper acetylide **XI**, formed from the copper cycle (Cycle B, **Figure 44**), to form the palladium-acetylide adduct **IV**. Subsequent *cis*/*trans* isomerization of adduct **IV** to **V** and reductive elimination of adduct **V** yields the desired alkyne **VI** and regenerates the palladium catalyst **I**.[224] The copper-cycle is less well-understood. It has been hypothesized that the copper salt **VII** (usually copper iodide) and terminal acetylene **VIII** associate to generate the π-alkyne copper complex **IX**. This association supposedly increases the acidity of the alkyne proton enabling it to be extracted by the amine base **X** (typically triethylamine) and subsequently form the copper acetylide **XI**.[224]

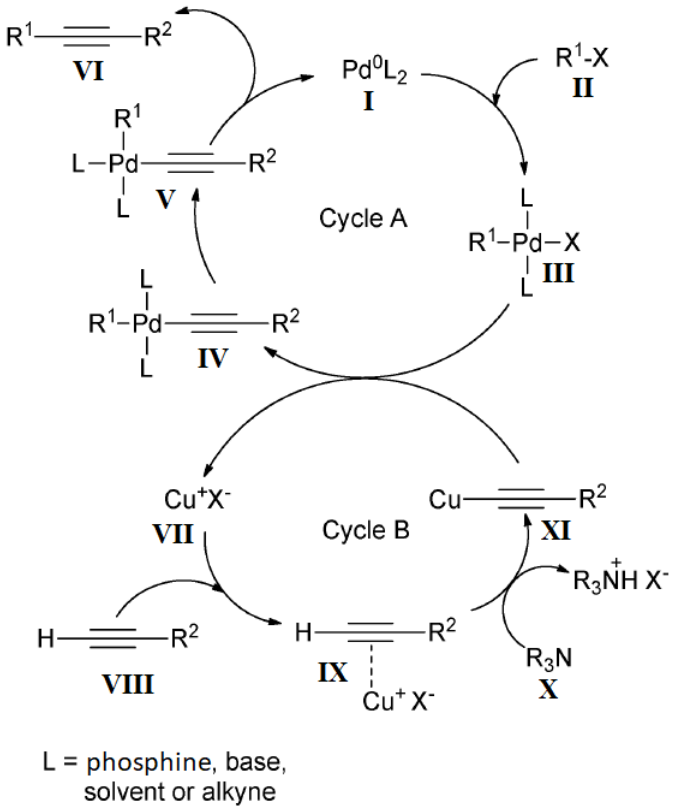

Figure 44 It has been generally accepted that the copper co-catalysed Sonogashira reaction mechanism is comprised of two independent catalytic cycles. These include the palladium catalysed cycle (A) and the copper cycle (B). This image was adapted from Chinchilla *et al*.[226]

4.3.1. Attempted synthesis of 3-(3-fluorophenyl)propiolamide (94)

For the Sonogashira reaction between **92** and propiolamide we were careful to ensure that the reaction was kept under inert conditions. Due to the employment of copper iodide, the presence of oxygen in the reaction could lead to the occurrence of the Hay/Glaser reaction which would result in the homocoupling of terminal acetylenes to form a dimer.[224] This undesired side reaction would encumber the formation of the Sonogashira product **94**.

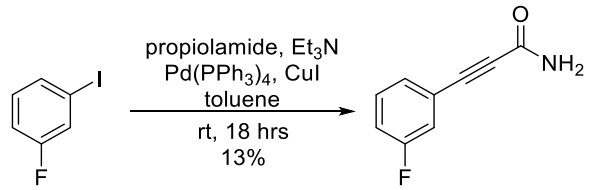

92 **94**

Scheme 51

The Sonogashira alkynylation reaction between **92** and propiolamide was carried out in the presence of $Pd(PPh_3)_4$, co-catalyst CuI and triethylamine in toluene (**Scheme 51**). Monitoring the reaction by TLC revealed that, after 18 hours at room temperature, all the starting material had been consumed. Despite this, following the workup of the reaction and purification by column chromatography, the Sonogashira product **94** was obtained in a disappointingly low yield of 13%.

For **94** the main distinguishing feature in the ^{1}H NMR spectrum were two broad singlets at 5.98 ppm which could be attributed to the amide and the restricted rotation about the amide bond. The ^{13}C NMR spectrum gave a clearer indication that the desired product had been formed. A doublet and singlet located at 84.5 and 82.9 ppm respectively could be attributed to the presence of the acetylene. The doublet observed at 84.5 ppm is a result of the ^{13}C-^{19}F coupling effect which extends to the acetylene carbon directly attached to the aryl ring. In addition, a signal at 154.7 ppm could be attributed to the amide carbonyl carbon atom.

Regrettably, the low yield obtained for the Sonogashira product **94** hampered our ability to continue on to the dehydration step described in **Scheme 50**. We feared that despite our efforts to ensure an oxygen-free environment, the low yield was a result of the dimerization of the propiolamide. Unfortunately, we struggled to isolate and identify any by-product that may have formed. We were concerned that due to the polarity of the propiolamide, any by-product formed had been lost during the aqueous workup of the Sonogashira reaction.

4.3.2. Attempted synthesis of ethyl 3-(3-fluorophenyl)propiolate (98)

In an attempt to identify the formation of any by-product we decided to carry out the Sonogashira reaction again, but this time using the less polar ethyl propiolate (**Scheme 52**). If dimerization occurred in this instance we hypothesized that it would be easier to isolate and characterize the ethyl propiolate dimer, thereby allowing us to optimize reaction conditions in order to prevent dimer formation.

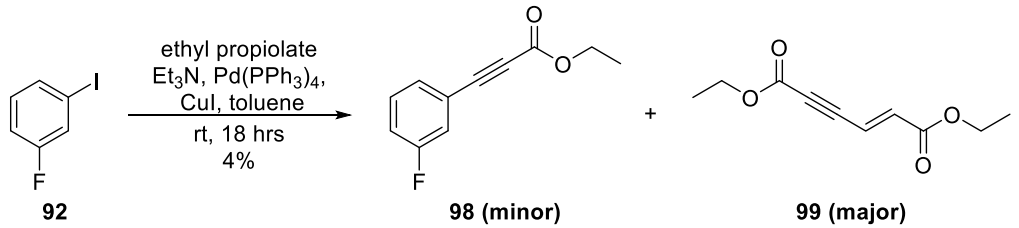

92 **98 (minor)** **99 (major)**

Scheme 52

The Sonogashira reaction between **92** and ethyl propiolate afforded **98** in an even lower yield of 4% (**Scheme 52**). However, as we had hoped, the major by-product formed in this instance was readily isolated and characterized by NMR spectroscopy. Surprisingly, the ethyl propiolate had not undergone a homocoupling as expected but had reacted with itself in a Michael addition reaction to afford the product **99**.

For the ^{1}H NMR spectrum of **98** the presence of aromatic signals, in addition to a quartet and triplet at 4.31 and 1.36 ppm respectively, was indicative that the Sonogashira coupling between **92** and ethyl propiolate had occurred, albeit in a low yield. This observation was further justified by the identification of the alkyne signals in the ^{13}C NMR spectrum at 84.6 and 81.5 ppm. The ^{13}C-^{19}F coupling observed for compound **94** was also observed for **98**. Fortunately, as this was a known compound in the literature we were able to compare the chemical shifts obtained in the ^{1}H and ^{13}C NMR spectra and found them to compare favourably.[228]

In the ^{1}H NMR spectrum for **99**, no aromatic signals were observed. Instead the presence of two doublets, one at 6.74 ppm and one at 6.42 ppm integrating for one proton each was indicative of the formation of an alkene. Furthermore, the coupling constants for both doublets was 16 Hz which suggested that the alkene possessed a *trans* configuration. Two multiplets located at 4.23 and 1.29 ppm were found to integrate for four and six protons respectively which could be attributed to the presence of two non-equivalent ethyl esters. As with **98**, **99** was known in the literature and the chemicals shifts obtained were found to correlate well with the chemical shifts reported in the literature.[229]

Interestingly, a review of the literature revealed that poor yields are often associated with alkynes substituted with electron-withdrawing substituents.[230] This occurs as a result of the fact that electron-withdrawing substituents can significantly polarize the alkynyl π-bond. Consequently, alkynes such as ethyl propiolate and propiolamide are generally poor nucleophiles in the Sonogashira reaction but act as better electrophiles which enables them to readily undergo a Michael addition reaction.[231]

However, in the literature it has been suggested that this issue could be overcome by carrying out the alkynylation under Negishi conditions (**Scheme 53**).[230, 232] Generally, in the case of electron-deficient alkynes, the use of zinc has been found to exhibit superior reactivity and product yield when compared to copper and other metals such as tin, magnesium and aluminium.[233] The Negishi reaction typically employs zinc salts, such as zinc bromide or chloride, to form the alkynylmetal **II** from **I** which can then, in a similar fashion to the Sonogashira reaction, couple with an appropriate aryl halide to form the acetylene product **III**.[231]

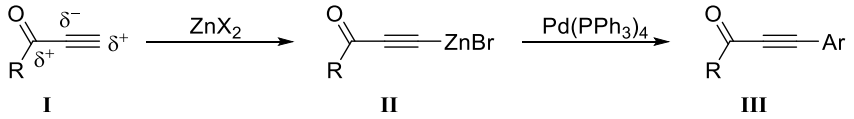

Scheme 53

To this end, we attempted the coupling of **92** with ethyl propiolate under the conditions reported by Anastasia and Negishi in 2003 (**Scheme 54**).[230] Herein, they reported the use of LDA and $ZnBr_2$ to generate the alkynylzinc *in situ*, followed by the addition of an aryl halide and $Pd(PPh_3)_4$ to produce the respective cross-coupled product.[230]

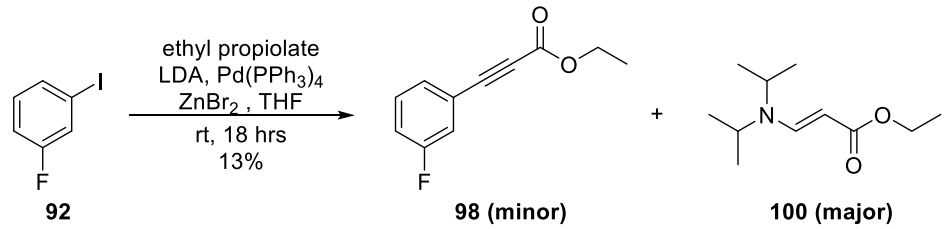

Scheme 54

Unfortunately, in our hands and under these conditions we were only able to slightly improve the yield of **98**. Despite the reported advantage of using zinc in place of copper, we observed that the major product of this reaction (**100**) was a result of another Michael addition onto the alkyne. Astonishingly, the nucleophile in this instance appeared to be diisopropylamide.

As with **99**, two doublets attributed to the alkene were observed in the ^1H NMR spectrum for **100**. Furthermore, in addition to a quartet and triplet integrating for two and three protons respectively which were associated with the ethyl ester, a singlet and doublet integrating for two and twelve protons at 3.61 and 1.17 ppm respectively were identified as belonging to the diisopropylamide. Fortunately, **100** was also a known compound in the literature and the chemical shifts reported were found to compare favourably with those obtained experimentally.[234]

In the paper by Anastasia and Negishi, the use of triethylamine as an alternative to LDA was also reported.[230] Although we re-attempted the Negishi reaction with triethylamine, we were unable to obtain any of the desired product **98**.

4.4. Alternative methods towards the synthesis of the cyanoacetylene precursor 96

In the meantime, while struggling to find optimal conditions for the introduction of an electron-deficient acetylene onto **92**, we decided to turn our attention to the possibility of altering our synthetic strategy by introducing more electron rich acetylenes.

4.4.1. Strategy 1: Alkynylation with TMS-acetylene

One such alternative strategy involved the attempted synthesis of cyanoacetylene **96** by coupling **92** with trimethylsilylacetylene (TMS-acetylene) (**Scheme 55**).

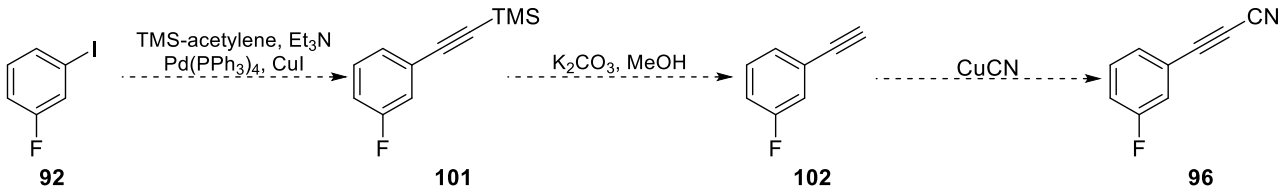

Scheme 55

The first step in this synthetic scheme would involve the coupling of TMS-acetylene to **92** under Sonogashira reaction conditions. The resulting coupled product **101** would then undergo a deprotection of the TMS group with potassium carbonate in MeOH to afford the terminal acetylene **102**. Following deprotection, precursor **102** could then be cross-coupled with copper cyanide to yield the desired cyanoacetylene precursor **96**.[235-236]

With a synthetic strategy in mind, we could embark upon the first step which involved the Sonogashira cross-coupling between **92** and TMS-acetylene under conditions described for the synthesis of **94** and **98** (**Scheme 56**).

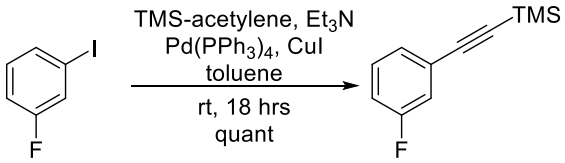

92 **101**

Scheme 56

Encouragingly, the coupling of **92** to TMS-acetylene was carried out successfully and the Sonogashira product **101** was obtained in quantitative yield.

The most distinguishing feature in the ^{1}H NMR spectrum of **101**, in addition to the expected aromatic signals, was the presence of a large singlet located at 0.24 ppm which integrated for 9 protons. This was attributed to the presence of the TMS group. In the ^{13}C NMR spectrum a doublet at 103.8 ppm, a singlet at 95.5 ppm and another singlet at 0.0 ppm attested to the presence of the TMS-acetylene. As this was a known compound in the literature we were able to correlate the chemical shifts observed experimentally with those obtained from the literature which assured us that we had obtained the desired product **101**.[228]

Unfortunately, despite the precedence for this reaction in the literature, in our hands the subsequent deprotection of the TMS-acetylene with potassium carbonate was unsuccessful (**Scheme 57**).[237-238] Although monitoring the reaction by TLC indicated that all of **101** had been consumed, upon workup we were unable to isolate any product at all. Another attempt at the deprotection using tetrabutylammonium fluoride was equally unsuccessful.

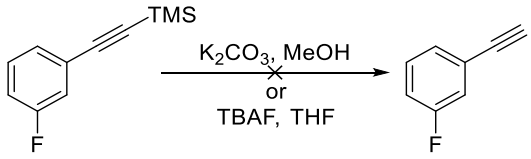

101 **102**

Scheme 57

4.4.2. Strategy 2: Alkynylation with propargyl alcohol

Another approach to the synthesis of the desired cyanoacetylene compound **96**, which was described prominently in the literature, involved a one-pot conversion of an activated alcohol to the corresponding nitrile.[239-243] This direct conversion of an alcohol to a nitrile was originally introduced by Lai *et al*. in 2000

but was described only for benzylic alcohols.[239] Inspired by this method, McAllister *et al.* extended this methodology further by applying it to various propargyl alcohols.[240] This transformation is initiated by the oxidation of propargyl alcohol **103** to the corresponding aldehyde **104** (**Scheme 58**). It has been postulated that the aldehyde **104** then reacts with ammonia affording the analogous imine **105**, which is subsequently oxidized *in situ* to afford the desired nitrile **106**.[240]

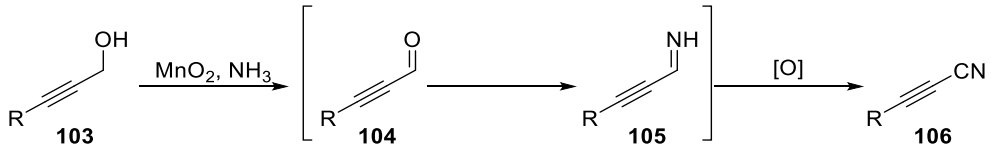

Scheme 58

In order to employ these conditions for our purposes we would have to first install propargyl alcohol onto **92** (**Scheme 59**). Once again, we envisaged that this could be achieved under Sonogashira coupling conditions.

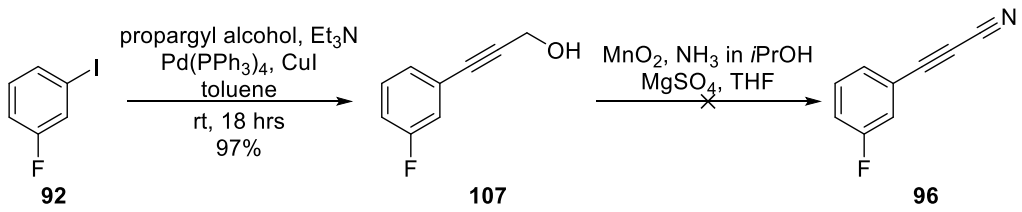

Scheme 59

To this end, **92** was treated with propargyl alcohol in the presence of Et_3N, $Pd(PPh_3)_4$ and CuI under inert conditions and after 18 hours at room temperature TLC determined that the reaction had reached completion. Subsequent workup and purification by column chromatography afforded the desired compound **107** in 97% yield (**Scheme 59**).

Distinguishing features in the ^1H NMR spectrum of **107** included a doublet and triplet located at 4.50 and 2.43 ppm which integrated for two and one proton respectively. These observed signals could be attributed to the presence of the methyl alcohol portion of propargyl alcohol. In the ^{13}C NMR spectrum signals at 88.3, 84.5 and 51.5 ppm provided further testament that the Sonogashira coupling had occurred successfully.

With the propargyl alcohol precursor **107** in hand we could attempt to carry out the conversion of **107** to **96** by utilizing the one-pot reaction conditions described by McAllister *et al*.[240] To this end, treatment of **107** with a solution of ammonia in *iso*-propanol in the presence of anhydrous magnesium sulfate was

followed by the addition of manganese dioxide. The reaction was closely monitored by TLC, but unfortunately after 18 hours revealed that no reaction had taken place. Seemingly, the desired cyanoacetylene **96** could not be obtained using this methodology.

4.5. Alkynylation using "copper-free" Sonogashira conditions

Although we had so far been unsuccessful in our endeavour to synthesize the cyanoacetylene **96** we decided to persevere and revisit the coupling of propiolamide and **92**. Although the by-products that were isolated from the Sonogashira and subsequent Negishi couplings did not appear to be a result of copper-catalysed homocoupling of the terminal alkynes, we thought it could be worthwhile to attempt a "copper-free" Sonogashira reaction, also known as the Sonogashira-Heck-Cassar reaction or Heck alkynylation reaction.[224]

As with the copper co-catalysed Sonogashira reaction mechanism, the mechanism for the "copper-free" reaction is not well known.[226] It is generally accepted that this mechanism, like the mechanism described in **Figure 44** begins with the oxidative addition of the aryl halide **II** to the catalytic [Pd(0)L_2] species **I** to form **III** (**Figure 45**).[226] It has been proposed that the subsequent step involves the displacement of a ligand through reversible π-coordination of the alkyne **IV** to form the intermediary complex **V**.[244] This complex is thought to serve a similar purpose to the copper acetylide complex formed in Cycle B in **Figure 44**, in that the acetylene proton is acidified which facilitates its removal by an amine base **VI** to give the complex **VII**.[226] Once again, *cis*/trans isomerization to afford **VIII**, is followed by reductive elimination of the complex **VIII** which releases the cross-coupled product **IX** and reforms the catalytic palladium species **I**.[224]

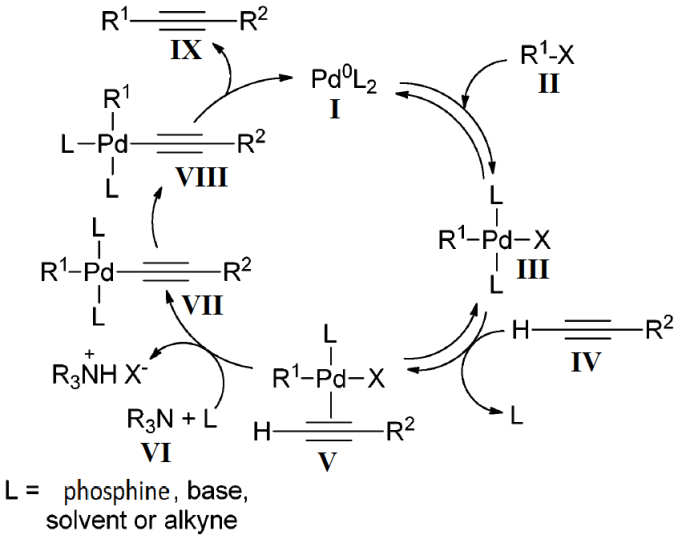

Figure 45 The proposed mechanism for the copper-free Sonogashira reaction is shown here.[226]

The "copper-free" Sonogashira coupling between **92** and propiolamide was performed in the presence of $Pd(OAc)_2$, triphenylphosphine and triethylamine which could facilitate the *in situ* reduction of the Pd(II) species to the catalytically active Pd(0) species (**Scheme 60**).[245] Unlike the copper co-catalysed Sonogashira reaction which was carried out at room temperature, this coupling had to be carried out at an elevated temperature of 70 ˚C.

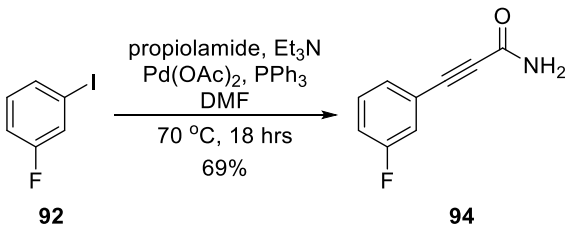

92 **94**

Scheme 60

To our astonishment, under these conditions we were able to obtain the desired compound **94** in a significantly improved yield of 69% which enabled us to continue with the synthesis of compound **96** as described in **Scheme 50**. Unfortunately, at the time we did not have access to $POCl_3$ which was required for the dehydration of amide **94** to the corresponding nitrile **96**. As a result, an alternative dehydration method had to be identified. To this end, we came upon a paper by Nakajima and Ubukata which described the use of Swern oxidation conditions for the dehydration of amides to the corresponding nitriles.[246] In general, the Swern reaction is used for the oxidation of various alcohols to the corresponding

carbonyls; however it has found application in the dehydration of oximes, hydroxylamines and amides.[246-249]

The mechanism for the dehydration of amides begins with the formation of the chlorosulfonium species **111** (**Scheme 61**).

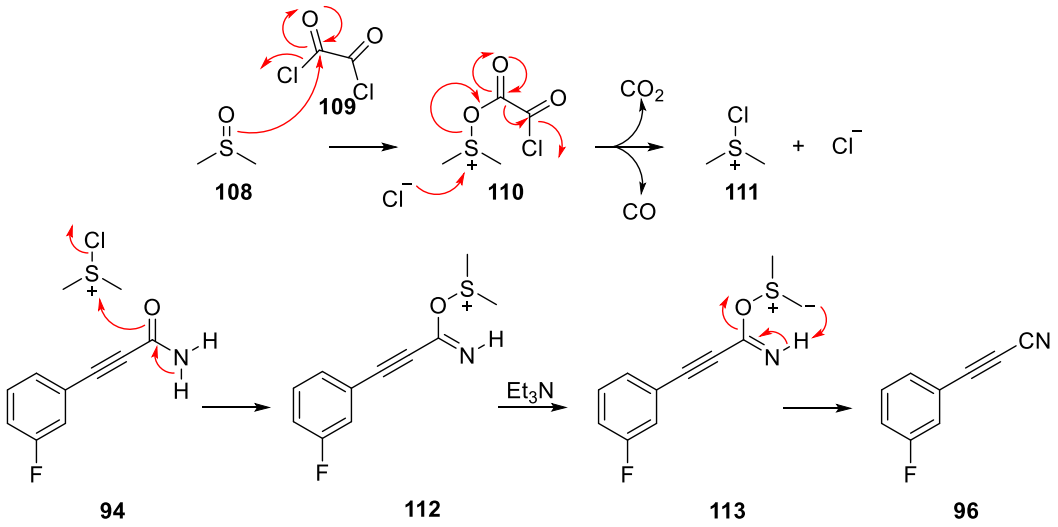

Scheme 61 The proposed mechanism for the dehydration of amide under Swern oxidation conditions.[246-247]

For this to occur DMSO (**108**) reacts with oxalyl chloride (**109**) to form the intermediate **110** which readily decomposes, giving off carbon dioxide and carbon monoxide, to afford the chlorosulfonium species **111**.[250] The chlorosulfonium species **111** then reacts with the amide carbonyl of **94** to form the sulfonium salt **112**. In the presence of triethylamine the sulfonium salt **112** is converted into the ylide **113**.[247] Intramolecular proton-abstraction from the ylide **113** then results in the formation of the desired nitrile **96** and the regeneration of DMSO.[247]

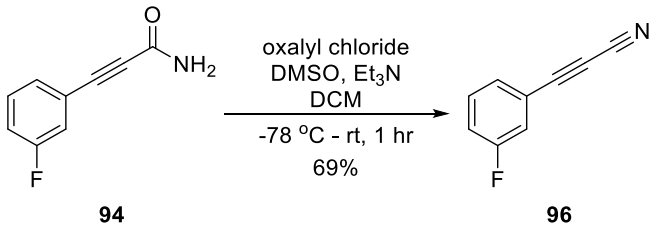

Scheme 62

In preparation for the dehydration of **94** to **96** using Swern oxidation conditions, oxalyl chloride was treated with DMSO at -78 °C to form the active chlorosulfonium species (**111** in **Scheme 61**). This was followed by the addition of **94** and, after approximately 20 minutes, the addition of triethylamine to

facilitate dehydration to the nitrile. The reaction was closely monitored by TLC and after 1 hour the reaction had reached completion. After purification we were finally able to obtain the elusive cyanoacetylene compound **96** in a satisfactory yield of 69% (**Scheme 62**).

In the ^{1}H NMR spectrum of **96** the absence of the broad doublet belonging to the amide was the only clear indication that the dehydration reaction had occurred. This observation was further supported by the loss of the carbonyl carbon signal in the ^{13}C NMR spectrum and the occurrence of an additional more shielded carbon signal in the aromatic region. Unfortunately, attempted analysis through HRMS did not provide an accurate mass. As a means of determining with certainty that **96** had been synthesized, we decided to obtain and compare the FTIR spectra of **94** and **96**. The 2 bands at 3164 and 3378 cm^{-1} that correspond to an amide stretch for **94** were not observed in the IR spectrum for **96**. Instead, a clear band at 2259 cm^{-1} could be attributed to the nitrile expected for **96**.

4.6. The attempted synthesis of target compound 97

Finally, with the desired cyanoacetylene **96** in hand we could attempt the much anticipated S_NAr reaction, using the reaction conditions described in Chapter 3, with the benzimidazolone precursor **38** to obtain the penultimate product **114** (**Scheme 63**).

Surprisingly, upon addition of **96** to a mixture of **38** and Cs_2CO_3 at room temperature, an immediate colour change was observed. This was an unusual observation as these reactions have required elevated temperatures to occur at all in the past. Nonetheless, analysis of the reaction by TLC revealed that all the starting material had been consumed and that a single product had formed.

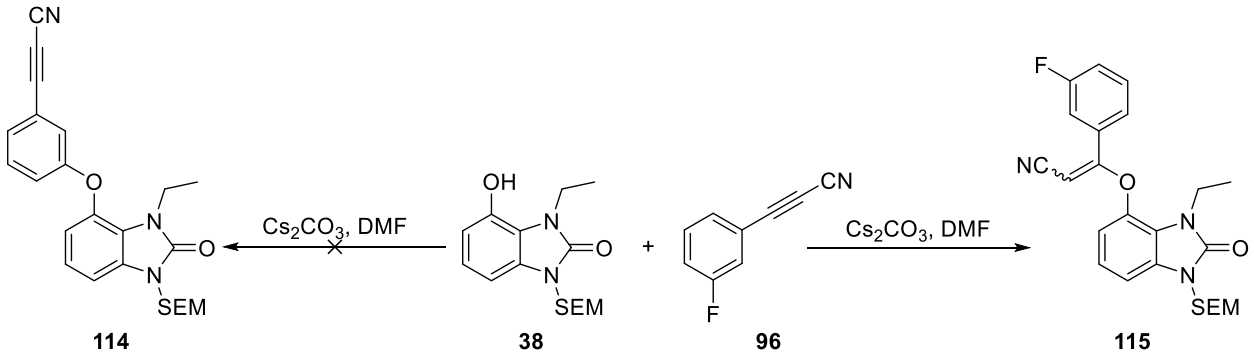

Scheme 63

Unfortunately, the spectral data for the compound obtained were not consistent with those of the desired product **114**. Analysis of the ^{1}H and ^{13}C NMR spectra, in addition to HRMS, revealed that the product obtained was in fact **115**, a result of a Michael addition of **38** onto the cyanoacetylene substituent of **96** (**Scheme 63**).

The clearest indication that the desired S_NAr did not occur was observed in the ^{13}C NMR spectrum of **115**. The fact that we still observed the doubling up on carbon signals as a result of ^{13}C-^{19}F coupling indicated that the fluorine was still present on the compound. Furthermore, in the ^{1}H NMR spectrum of **115** the presence of an unexpected singlet at 4.72 ppm which integrated for one proton was indicative that a vinyl proton was present. The presence of a single vinyl proton signal implied that only a single stereoisomer had been formed; however, with the information we had we were unable to conclusively assign the resulting alkene as *cis* or *trans*. HRMS analysis of **115** provided a mass of 454.1948 amu which coincided with the expected mass of 454.1962 amu.

The formation of **115** confirmed the suspicions we had with regards to the reactivity of the cyanoacetylene group as a Michael acceptor. Unfortunately, this observation implied that target compounds **90** and **97** could be involved in off-target effects due to their ability to act as Michael acceptors and, therefore, would be toxic in a whole cell assay. However, we were not ready to abandon the idea of targeting Lys223 altogether and, as a result, decided to change tactics by introducing a less reactive substituent onto the "upper" aryl ring of the benzimidazolone scaffold.

4.7. A change in tactics: Introducing a cyanovinyl group as an alternative for the cyanoacetylene group

In our search for a suitable bioisostere to replace the reactive cyanoacetylene substituent, we identified the cyanovinyl group (compound **116**) (**Figure 46**). At first glance the cyanovinyl group, another unsaturated nitrile, does appear to be a potential Michael acceptor. However, in a publication by Fleming and Wan, the cyanovinyl group is described as recalcitrant in that reactive organometallic nucleophiles are required for conjugate addition to occur.[251]

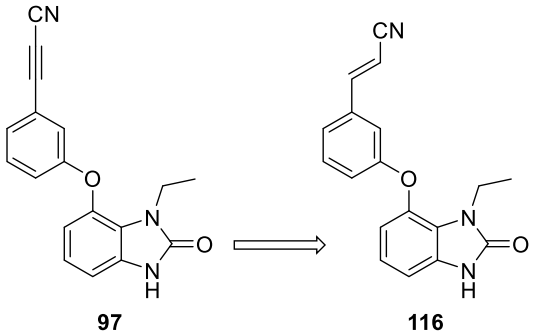

Figure 46

We were further encouraged by the fact that rilpivirine, a potent FDA-approved NNRTI which possesses a cyanovinyl group on one of its terminal aryl rings, has a selectivity index of >8000 *in vitro* indicative of its selectivity for HIV RT (**Figure 47**).[252] The cyanovinyl group has also found precedence in other NNRTIs such as compounds **117** and **118**. In both instances, the introduction of the cyanovinyl group was found to considerably improve potency.[221, 253] In the case of **117** this improvement was particularly significant as the introduction of the cyanovinyl group led to picomolar activity.[221]

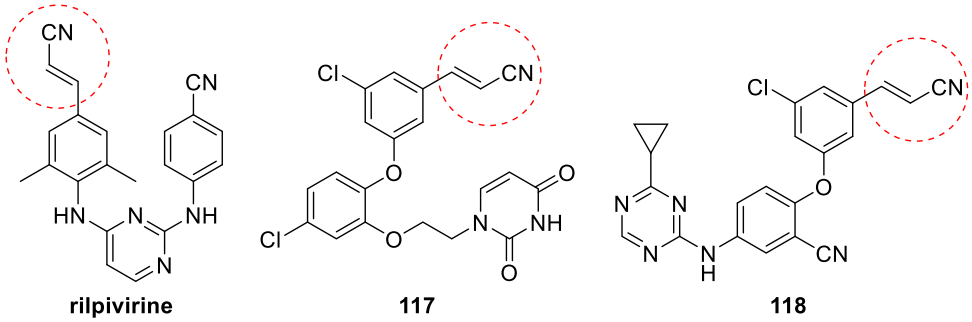

Figure 47 The introduction of the cyanovinyl group considerably improved the potency of a number of NNRTIs.

In order for compound **116** to be an effective inhibitor of RT it was imperative that the cyanovinyl substituent, as with the cyanoacetylene, be able to extend into the chimney region deep enough to facilitate a strong enough hydrogen bond with Lys223 and, at the same time, maintain the binding orientation of lead second-generation benzimidazolone **50** within the NNIBP. To this end, with the purpose of validating the incorporation of the cyanovinyl group on our benzimidazolone scaffold, docking studies were conducted on compound **116**. These studies revealed that, in the *trans* configuration, the cyanovinyl group was able to comfortably occupy the chimney region formed by Trp229, Tyr188 and Phe227 and achieve hydrogen bonding with the target Lys223 residue at an acceptable calculated distance of 2.3 Å (**Figure 48**). Furthermore, compound **116** was able to maintain other important electrostatic

interactions such as π-interactions with Tyr188 and conserved residue Trp229, as well as hydrogen bonding with the backbone of Lys101. Encouragingly, when the binding energies calculated for compounds **116** and **97** were compared, the difference in binding energies between the two compounds was found to be negligible. This result provided further testimony to the fact that the cyanovinyl substituent was a suitable replacement for the cyanoacetylene group.

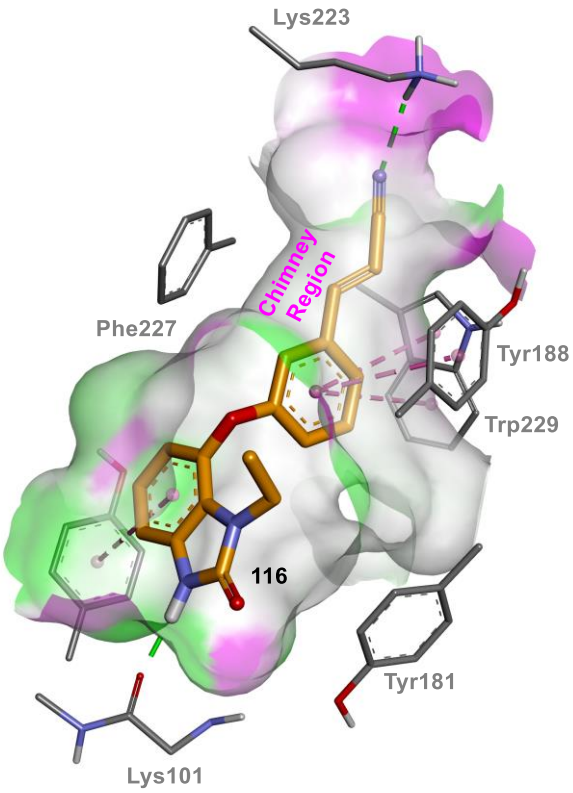

Figure 48 Docking studies of target compound **116** in the NNIBP revealed that the cyanovinyl substituent of **116** would be able to occupy the chimney region formed by Trp229, Tyr188 and Phe227. Furthermore, **116** would be able to achieve hydrogen bonding with the target lysine residue and, at the same time, maintain the important interactions to Trp229, Tyr188 and Lys101. Images were created using PDB file 2JLE in Discovery Studio.

For the synthesis of compound **116** we envisaged that we could follow the same procedure described for the synthesis of **97** in **Scheme 50**. However, in place of the Sonogashira coupling reaction the first step in the reaction sequence would involve the cross-coupling of **92** with acrylamide by way of a Heck reaction to obtain **119** (**Scheme 64**). As with **97**, subsequent steps would involve dehydration of **119** under Swern conditions to afford **120** which could then undergo an S_NAr reaction with benzimidazolone precursor **38** and a subsequent SEM deprotection to yield the desired product **116**.

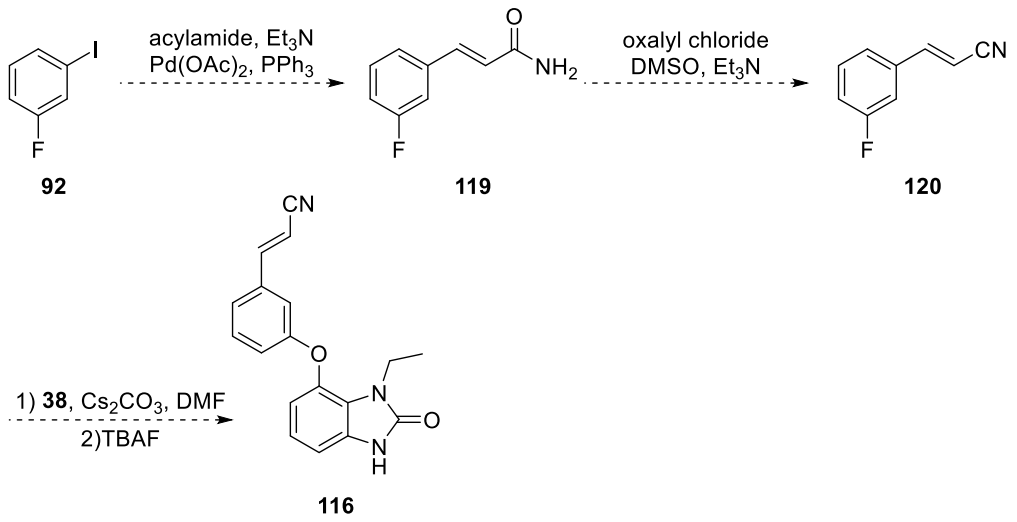

Scheme 64

4.7.1. Synthesis of (*E*)-3-(3-fluorophenyl)acrylamide (119) by way of a Heck cross-coupling reaction

The Heck or Mizoroki-Heck reaction is an efficient, versatile and popular method for the cross-coupling of aryl halides and alkenes.[254] We have already described the mechanism for the Heck coupling reaction between alkynes and aryl halides in Section **4.5** and for the first few steps (**I** - **V**) this mechanism is much the same for the coupling between aryl halides and alkenes (**Figure 49**).[254-255] However, following the carbopalladation step leading to **V**, an internal C-C bond rotation occurs which brings the β-hydrogen into a *syn* position relative to the palladium (**VI**). This allows for a *syn* β-hydride elimination to occur which affords the ligated complex **VII**.[255] Finally, after dissociation of the alkene **VIII** from the complex, reductive elimination of **IX** regenerates the active palladium species **I**.[255]

One of the major benefits of the Heck reaction is the propensity for delivering predominantly the *trans* product due to the occurrence of the *syn* β-hydride elimination step in the mechanism.[254] In our case, this was incredibly important as only the *trans* configuration of the cyanovinyl group would be able to occupy the narrow hydrophobic chimney.

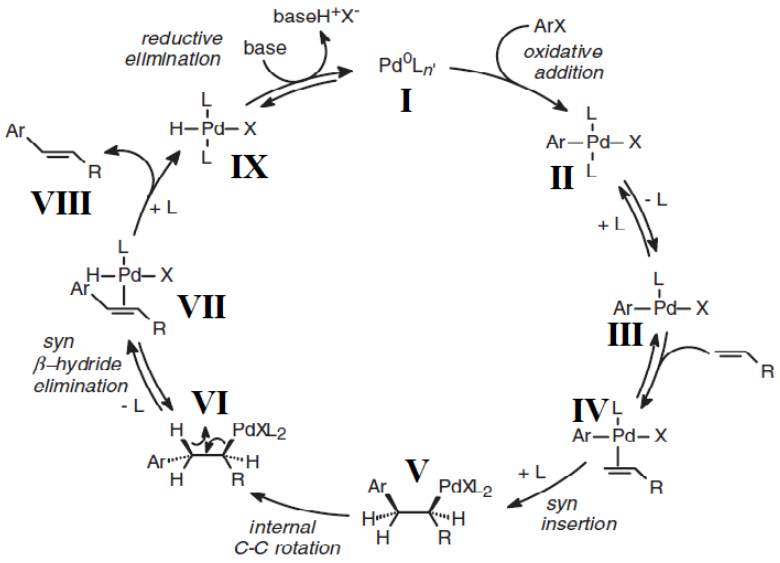

Figure 49 Proposed mechanism of the Heck reaction.[255]

For the Heck reaction we decided to employ the conditions used to synthesize compound **94**. To this end, **92** and acrylamide were treated with $Pd(OAc)_2$, PPh_3 and Et_3N and then heated to 70 °C (**Scheme 65**). After 18 hours TLC indicated that all of **92** had been consumed and that a single, significantly more polar, product had formed. This product was purified by column chromatography to afford the desired product **119** in a quantitative yield.

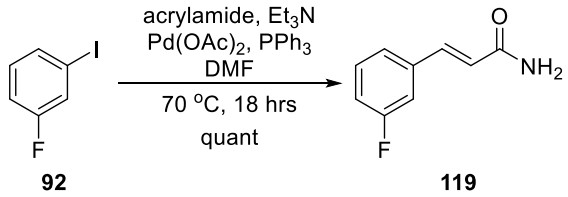

Scheme 65

Analysis of the ^1H NMR spectrum of **119** confirmed that only the desired *trans* isomer had been synthesized. Two doublets observed at 7.62 and 6.49 ppm, both integrating for one proton, could be attributed to the two vicinal vinyl protons and the *J*-coupling constants of both doublets were found to be 16 Hz which indicated that the stereochemistry of the alkene was in the *trans* configuration. It is well known that the *J*-coupling constants for vinyl protons in the *trans* configuration are often within the range of 12 – 18 Hz, while *cis* protons are in the range of 6 – 12 Hz.[256] In addition, two broad singlets at 5.99 ppm integrating for 2 protons altogether, provided a further indication that the Heck reaction had successfully introduced propiolamide onto **92**. Although we were unable to unambiguously assign the signals in the

^{13}C NMR spectrum, all expected carbon signals for **119** were observed. Furthermore, HRMS analysis of **119** provided a mass of 166.0667 amu which coincided with the expected mass of 166.0668 amu.

4.7.2. Synthesis of (*E*)-3-(3-fluorophenyl)acrylonitrile (120)

With **119** in hand, we could carry out the subsequent dehydration using the same Swern conditions employed for the synthesis of **96**. To this end, the active chlorosulfonium species, formed *in situ* with DMSO and oxalyl chloride, was treated with **119** and triethylamine to afford the cyanovinyl product **120** in a rather disappointing yield of 45% (**Scheme 66**). Nevertheless, we had enough material in hand to attempt the subsequent S_NAr reaction.

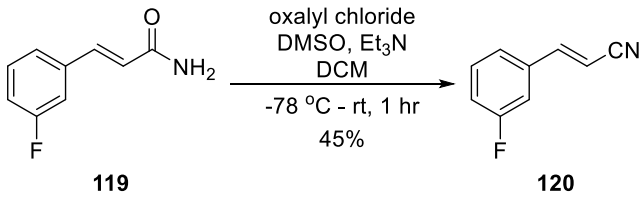

119 **120**

Scheme 66

As with **96**, analysis of the ^{1}H NMR spectrum for **120** revealed an absence of the two broad singlets attributed to the presence of the amide. This observation in conjunction with the loss of the amide carbonyl signal in the ^{13}C NMR spectrum verified that the dehydration of **119** had occurred. Additional confirmation came from HRMS which gave a mass of 148.0557 amu, coinciding with the calculated mass of 148.0563 amu.

4.7.3. Attempted synthesis of (*E*)-3-(3-((3-ethyl-2-oxo-1-((2-(trimethylsilyl)ethoxy)methyl)-2,3-dihydro-1*H*-benzo[*d*]imidazol-4-yl)oxy)phenyl)acrylonitrile (121)

For the S_NAr reaction the benzimidazolone precursor **38** and **120** were treated with Cs_2CO_3 in DMF (**Scheme 67**). Encouragingly in this instance, no evident reaction had occurred prior to the introduction of heat which seemed to verify the claim, discussed in section **4.7**, that the cyanovinyl group was less reactive than the corresponding cyanoacetylene group and therefore, not prone to Michael addition. However, after 2 hours at 100 °C still no reaction had taken place, a situation which did not change even after 18 hours at 100 °C.

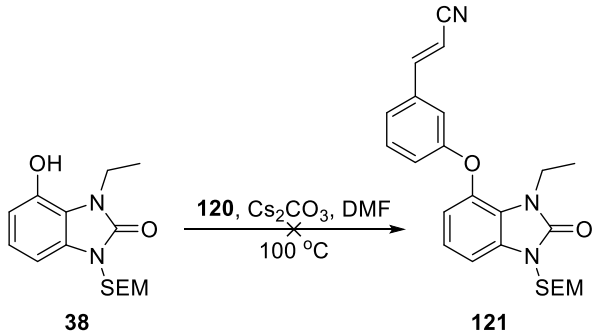

Scheme 67

In an attempt to explain the lack of product formation, we considered the possibility that the cyanovinyl aryl group **120** was not activated enough for the S_NAr reaction to occur. We knew from Chapter 3 that the presence of an electron-withdrawing group such as a nitrile would activate the fluoro-containing aryl ring sufficiently for the S_NAr to occur albeit at high temperatures. As a result, we realized that we would have to employ the starting reagent **91** described earlier in the chapter which contained the additional nitrile functionality (Section **4.2**). Fortunately, we knew that we could readily install the cyanovinyl group onto **91** using the conditions described for the synthesis of precursors **119**.

4.7.4. Attempted synthesis of (*E*)-3-(3-cyano-5-fluorophenyl)acrylamide (122).

As with 3-iodo-fluorobenzene **92**, **91** with acrylamide was treated with $Pd(OAc)_2$, PPh_3 and Et_3N and heated to 70 °C for 18 hours (**Scheme 68**). However, following purification the desired cyanovinyl compound **122** was obtained in a frustratingly poor yield of 17%, in contrast to the quantitative yield obtained for **119**.

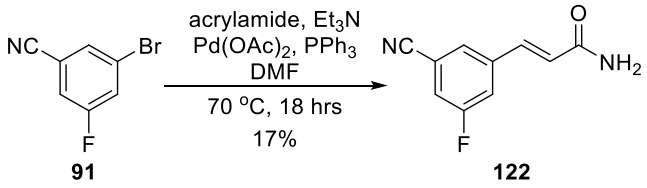

Scheme 68

In order to optimise this reaction, we had to consider the possibility that the bromide, in comparison to the iodide, was considerably less amenable to the initial oxidative addition step with the palladium catalyst, despite the presence of the nitrile on the ring. Therefore, in an attempt to increase the yield of

122 we re-attempted the Heck coupling of **91** and acrylamide using P(o-tolyl)$_3$ as the ligand in place of PPh_3. In 1978 it was discovered that the utilization of substituted triarylphosphines such as P(o-tolyl)$_3$ in conjunction with $Pd(OAc)_2$ was superior to the use of PPh_3 when the reaction involved the use of aryl bromides.[255, 257]

To this end, P(o-tolyl)$_3$ and $Pd(OAc)_2$ were introduced to a mixture of **91**, acrylamide and Et_3N under inert conditions (**Scheme 69**). Unfortunately, after 18 hours a poor yield of impure **122** was obtained despite attempted purification by column chromatography.

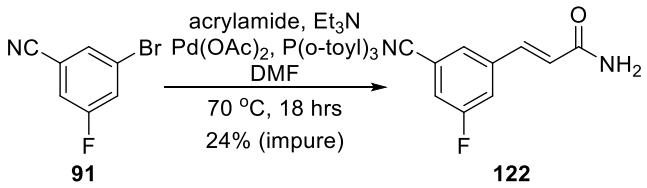

Scheme 69

In the ^{1}H NMR spectrum of **122**, two doublets observed at 7.58 and 6.77 ppm, each integrating for one proton could be attributed to the presence of the vicinal vinyl protons from the acrylamide portion of **122**. Moreover, the coupling constants for both doublets was reported as 16 Hz, indicative that the vinyl protons were arranged in the desired *trans* configuration. The coupling of **91** to acrylamide was further validated by HRMS analysis which gave a mass of 191.0615 amu coinciding with the theoretical mass of **122** which was 191.0615 amu.

4.7.5. The use of a phosphine-free Heck cross-coupling reaction

For the past several years researchers have explored the use of phosphine-free Heck reactions in an attempt to overcome the various challenges faced when using phosphine-based ligands which include toxicity, air sensitivity and degradation at high temperatures.[258-260] A paper by Cui *et al.* described the use of *N*-phenylurea as an inexpensive and highly efficient ligand for palladium catalysed Heck and Suzuki reactions.[258] Herein they reported high yields for Heck reactions between electron-rich or deficient aryl halides, featuring a bromide or iodide, and styrene or butyl acrylate. We decided to employ the reaction conditions described by Cui *et al.* in the hope that we would be able to obtain compound **122** in similarly high yields.

To this end, a mixture of **91**, acrylamide and *N*-phenylurea in DMF was treated with $Pd(OAc)_2$ and K_2CO_3 (**Scheme 70**). Astonishingly, after just 2 hours at 130 ˚C, TLC analysis revealed that all of **91** had been consumed. A subsequent aqueous workup and purification by column chromatography afforded **122** in a more acceptable yield of 88%.

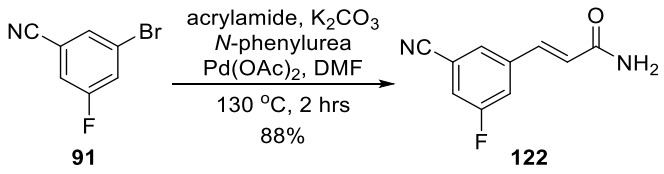

Scheme 70

4.7.6. Synthesis of (*E*)-3-(2-cyanovinyl)-5-fluorobenzonitrile (123)

Finally, with compound **122** in hand, we could carry out the dehydration of the amide to the corresponding nitrile **123** using the Swern conditions reported for the synthesis of compound **96**. Therefore, compound **122** and Et_3N were introduced to a mixture of DMSO and oxalyl chloride in DCM. After 1 hour, TLC indicated that all of **122** had been consumed to produce a single product. Nevertheless, following purification the dehydration of **122** afforded compound **123** in a disappointingly poor yield of 29% (**Scheme 71**).

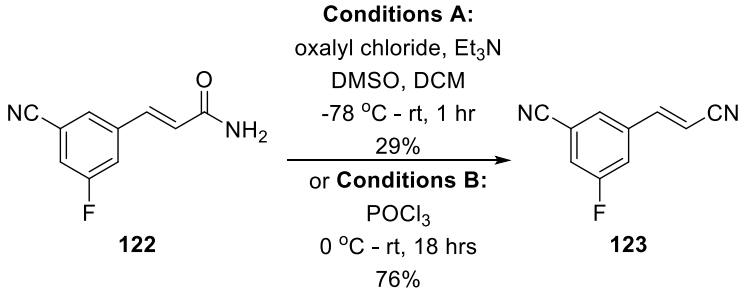

Scheme 71

Fortunately, by this stage we had access to $POCl_3$ and could, therefore, re-attempt the transformation of **122** to **123** using the more classical dehydration method. To this end, compound **122** was suspended in neat $POCl_3$ at 0 °C and then warmed to room temperature (**Scheme 71**). After several hours the suspension had completely cleared and subsequent monitoring by TLC revealed that **122** had been consumed. Fortunately this time, under these conditions the desired cyanovinyl compound **123** was obtained in 76% yield.

In the ^{1}H NMR spectrum of **123** the most obvious confirmation that the dehydration had occurred successfully was the absence of signals belonging to the exchangeable amide protons. In the ^{13}C NMR spectrum this observation was corroborated by the absence of the amide carbonyl carbon signal. HRMS analysis further confirmed the successful synthesis of **123** by providing a mass of 173.0509 amu which corresponded with the expected mass of 173.0506 amu.

Finally, with **123** in hand we could attempt the greatly anticipated S_NAr reaction with the benzimidazolone precursor **38** (**Scheme 72**). We were confident that, with the nitrile functionality present, the S_NAr reaction would occur readily. To our dismay however, when **38** and **123** were heated to 100 °C in the presence of Cs_2CO_3, once again after the usual two hours the desired reaction had not occurred.

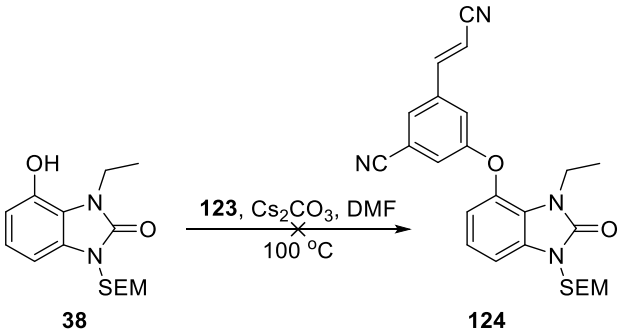

Scheme 72

4.8. A final attempt

Although the synthesis of the target cyanovinyl product was proving to be more problematic than originally anticipated, through perseverance we decided to introduce the cyanovinyl group only after **91** had been installed onto benzimidazolone scaffold **38**, in a final effort to obtain the desired cyanovinyl containing benzimidazolone compound **116**. We reasoned that due to the success of the S_NAr reaction between **38** and the 3-chloro-5-fluorobenzonitrile compound **51** described in Chapter 3, the same reaction between **38** and **91**, essentially a bromide-containing analogue of **51**, should occur just as readily to afford the coupled product **125** (**Scheme 73**). Furthermore, we hoped that, having optimized the conditions for the Heck and subsequent dehydration reactions, the desired acrylamide (**126**) and cyanovinyl (**124**) could be readily obtained and we could, finally, carry out the ultimate *N*-SEM deprotection step to afford the elusive target product **127**.

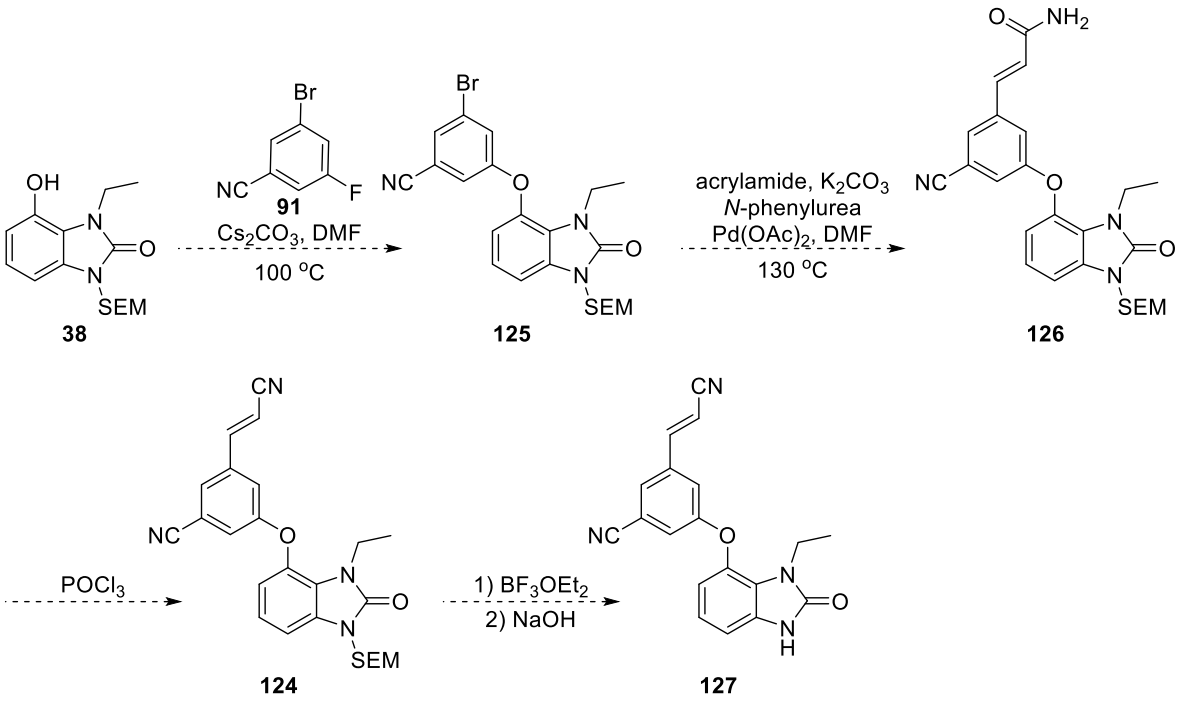

Scheme 73

4.8.1. Synthesis of 3-bromo-5-((3-ethyl-2-oxo-1-((2-(trimethylsilyl)ethoxy)methyl)-2,3-dihydro-1*H*-benzo[*d*]imidazol-4-yl)oxy)benzonitrile (125)

For the S_NAr reaction to afford **125**, benzimidazolone precursor **38** and **91** were heated to 100 °C in the presence Cs_2CO_3 (**Scheme 74**). Reassuringly, monitoring the reaction by TLC after 2 hours revealed complete consumption of **38**. To our delight subsequent workup and purification by column chromatography afforded the coupled product **125** in an excellent yield of 96%.

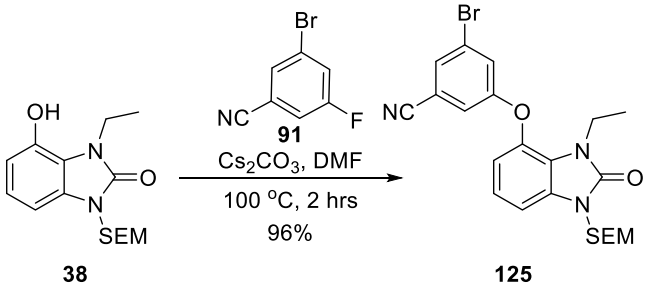

Scheme 74

In the ^{1}H NMR spectrum of **125**, the absence of the broad singlet belonging to the OH of **38**, in conjunction with the presence of three new aromatic, protons provided the clearest indication that the S_NAr reaction had occurred. The occurrence of 7 additional carbon signals in the ^{13}C NMR spectrum of **125** gave further testament to the success of the reaction.

4.8.2. Synthesis of (*E*)-3-(3-cyano-5-((3-ethyl-2-oxo-1-((2-(trimethylsilyl)ethoxy)methyl)-2,3-dihydro-1*H*-benzo[*d*]imidazol-4-yl)oxy)phenyl)acrylamide (126)

For the Heck cross-coupling reaction we employed the phosphine-free conditions described for the synthesis of **122**, which involved treatment of **125** and acrylamide with $Pd(OAc)_2$, *N*-phenylurea and K_2CO_3 (**Scheme 75**). As we had hoped, under these optimized conditions, we were able to obtain the coupled product **126** in a very good 89% yield.

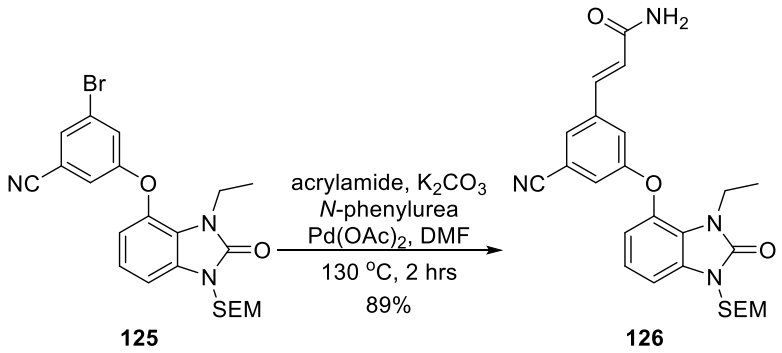

Scheme 75

In the ^{1}H NMR spectrum of **126** two doublets, each integrating for one proton, at 7.54 and 6.50 ppm and a broad singlet integrating for two protons at 5.94 ppm attested to the presence of the acrylamide. The desired *trans* configuration of the acrylamide was confirmed by the fact that both doublets expressed coupling constants of 16 Hz. In addition to these signals, all other proton signals expected for **126** were observed. This observation was mirrored in the ^{13}C NMR spectrum of **126**.

4.8.3. Attempted synthesis of (*E*)-3-(2-cyanovinyl)-5-((3-ethyl-2-oxo-1-((2-(trimethylsilyl)ethoxy)methyl)-2,3-dihydro-1*H*-benzo[d]imidazol-4-yl)oxy)benzonitrile (124)

With compound **126** in hand we could attempt to carry out the subsequent transformation of amide **126** to **124** using $POCl_3$ (**Scheme 76**). Interestingly, after 18 hours in $POCl_3$ we still observed by TLC the presence of unreacted **126** and, contrary to what we anticipated, the presence of a more polar product relative to **126**. This observation indicated that the dehydration reaction had not proceeded as expected.

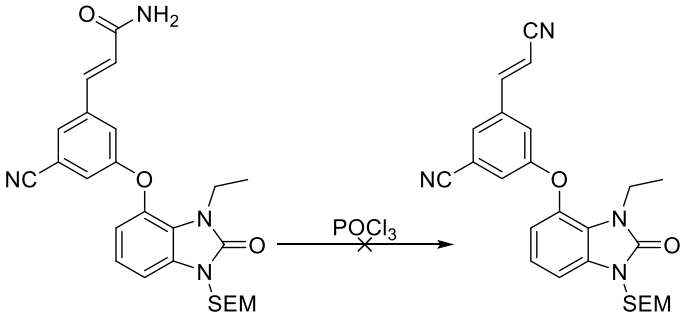

Scheme 76

Unfortunately, analysis of the ^1H NMR spectrum of the unexpected product revealed that, despite attempted purification by column chromatography, we had obtained an impure and inseparable mixture of products.

Due to the challenges faced with the dehydration of **126** in the presence of the SEM protecting group, we decided to purposefully carry out the deprotection of the SEM group prior to the dehydration of the amide. Furthermore, as the *N*-SEM deprotection was not the final step in this strategy we decided to utilize the single-step deprotection method with TBAF described in Chapter 3. To this end **126** was stirred in TBAF for 18 hours which afforded compound **128** in a relatively low yield of 32% after purification (**Scheme 77**). Nevertheless, we had obtained enough of **128** to continue with the subsequent dehydration with $POCl_3$.

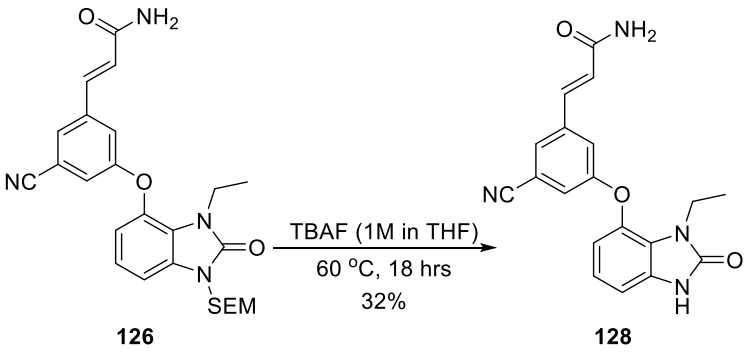

126 **128**

Scheme 77

In the ^{1}H and ^{13}C NMR spectra of **128** the notable absence of all signals pertaining to the SEM protecting group attested to the successful removal of the SEM group from **126**. Unfortunately, due to the fact that deuterated methanol was utilized for the NMR sample of **128**, the characteristic urea signal was not observed. However, HRMS analysis of **128** delivered a mass of 349.12955 amu which coincided with the calculated mass 349.12952 amu and thereby validated the observation that **128** had been successfully synthesized.

4.8.4. The final step towards the synthesis of the elusive cyanovinyl product 127

Having successfully synthesized precursor **128** we could embark upon the final step in our strategy towards the synthesis of target compound **127**. Having attempted countless methods to synthesize this compound we were eager and, at the same time, apprehensive about setting up the conversion of the amide **128** to the cyanovinyl compound **127** using $POCl_3$. Nevertheless, necessity dictated our actions and **128** was suspended in neat $POCl_3$ (**Scheme 78**). The reaction was closely monitored by TLC and after 2 hours we observed that **128** had been completely consumed. Gratifyingly, following purification by column chromatography we were able to isolate the desired product in a yield of 41%.

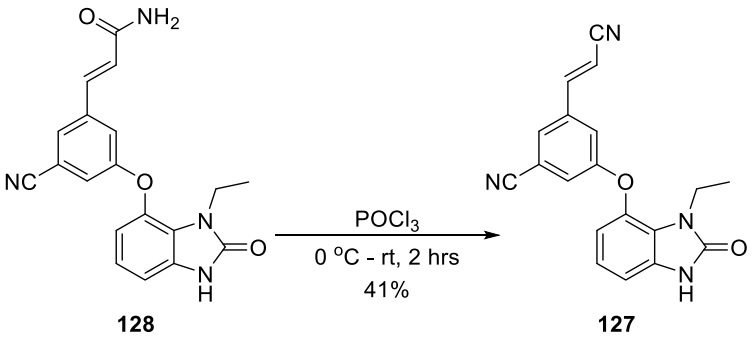

Scheme 78

Analysis of the ^{1}H NMR spectrum of **127** revealed that all expected proton signals were present. Of these, the most distinguishing signals included a broad singlet integrating for one proton at 10.01 ppm belonging to the urea and two doublets at 5.94 and 6.68 ppm each integrating for one proton which attested to the vinyl protons on the cyanovinyl group. In the ^{13}C NMR spectrum of **127** the presence of only one carbonyl carbon signal indicated that only the urea carbonyl was present, and that the amide had been successfully dehydrated to the corresponding nitrile. Finally, HRMS gave a mass of 331.1188 amu which coincided with the theoretical mass of 331.1190 amu.

4.9. Evaluation of target compound 127 against wild-type and resistant strains of HIV

Having successfully synthesized the desired cyanovinyl compound **127**, we could finally evaluate its efficacy against wild-type HIV RT in the hope that we would observe a marked improvement in potency.

Disappointingly, although compound **127** was found to be a potent inhibitor of HIV with an IC_{50} value of 49 nM, we were not able to achieve the desired improvement on the potency exhibited by our lead benzimidazolone compound **50** (IC_{50} = 26 nM). Nevertheless, we decided to evaluate this compound against a panel of clinically relevant resistant strains in the hope that compound **127** might exhibit an improved resistance profile in comparison to **50** (**Figure 50**). However unremarkably, analysis of the activity results against a panel of resistant strains revealed that overall, compound **127** was found to exhibit a very similar resistance profile to compound **50**. For example, against the most problematic K103N resistant strain which exhibits high-levels of resistance to NNRTIs nevirapine and efavirenz, compound **127** suffered only a 3-fold loss in potency while against Y181C, Y188C and the K103N/Y181C resistant strains, **127** was able to maintain potency. From **Figure 50** it can be seen that these results closely mirror the activity results reported for lead compound **50**.

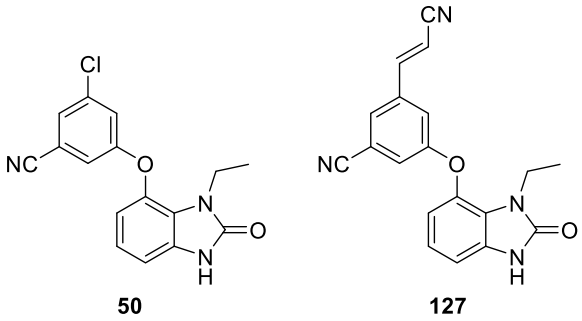

50 **127**

	IC_{50} (μM)	
	50	**127**
WT	0.026	0.049
K103N	0.111	0.166
Y181C	0.018	0.073
Y188C	0.007	0.014
K103N/Y181C	0.052	0.051

Figure 50 Compound **127** was found to be a potent inhibitor of HIV RT. Furthermore, the potency of **127** dropped only 3-fold against the K103N resistant strain and was maintained against Y181C, Y188C and the double mutant K103N/Y181C.

4.10. Concluding remarks

In an attempt to optimize the potency of lead compound **50** against wild-type and resistant strains of HIV, we envisaged introducing substituents onto the "upper" aryl ring that would be able to occupy a narrow hydrophobic chimney formed by Trp229, Tyr188 and Phe227 and form an additional hydrogen bond with the lysine residue located at the top of this chimney. To this end we were eventually able to synthesize the cyanovinyl containing compound **127**. However, evaluation of **127** in a phenotypic assay revealed that, using this design approach, we were unable to achieve any improvement on the potency exhibited by lead compound **50** against wild-type or resistant strains of HIV.

Chapter 5: Lead Optimization Through the Introduction of Additional Electrostatic Interactions within the NNIBP – Part 2

5.1. A molecular hybridization approach to re-introduce additional hydrogen bonding to the backbone of Lys101

In our continued effort to improve the potency of lead compound **50**, we decided to focus on modifying our structure to re-introduce the double hydrogen bonds to the backbone of Lys101, a feature imperative to the potency of the indole compounds discussed in Chapter 2. We envisaged that, by way of a molecular hybridization approach facilitated by molecular modelling, a hybrid of lead compound **50** and licensed NNRTI efavirenz would furnish a new scaffold **129** capable of forming the desired double hydrogen bond to the backbone of Lys101. Moreover, this new hybrid compound would be able to maintain the important interactions with Tyr188 and conserved residue Trp229 (**Figure 51**). This approach was based on the observation that the benzoxazin-2-one scaffold of efavirenz repositions the carbonyl at position 2 in a manner that favours hydrogen bonding with Lys101.[102]

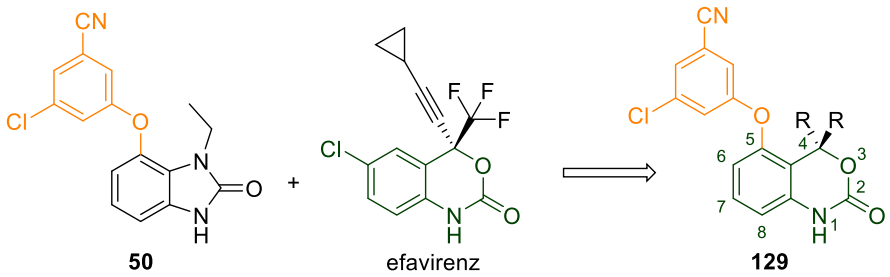

Figure 51 Generic compound **129** was designed using a molecular hybridization approach between lead compound **50** and efavirenz as a means to reintroduce additional hydrogen bonding to the backbone of Lys101.

Fortunately, molecular modelling was able to validate this approach. Docking studies of the new hybrid compound within the NNIBP revealed that this new scaffold was able to accomplish the desired double hydrogen bonding interaction with the backbone of Lys101, while maintaining the crucial π-interactions between the substituted aryl ring and Trp229 and Tyr188 (**Figure 52**).

In order to establish a proof-of-concept compound to synthesize, we had to decide on appropriate substituents to occupy position 4 on the new benzoxazin-2-one template (**Figure 51**). These substituents would have to occupy the small hydrophobic pocket in the vicinity of Val179 without altering the binding

orientation of the compound in the NNIBP and, for the sake of avoiding synthetic complexity, would have to be non-chiral. To this end, we decided to introduce the dimethyl substituents shown in **Figure 52**. Docking studies revealed that the benzoxazin-2-one scaffold with the dimethyl substituent at position 4 (**130**) would be well-tolerated in the NNIBP. Moreover, the difference in binding energies calculated for **50** (-96.51 kcal/mol) and **130** (-96.44 kcal/mol) was found to be negligible which implied that the efficacy of **130** would be comparable with that of **50**.

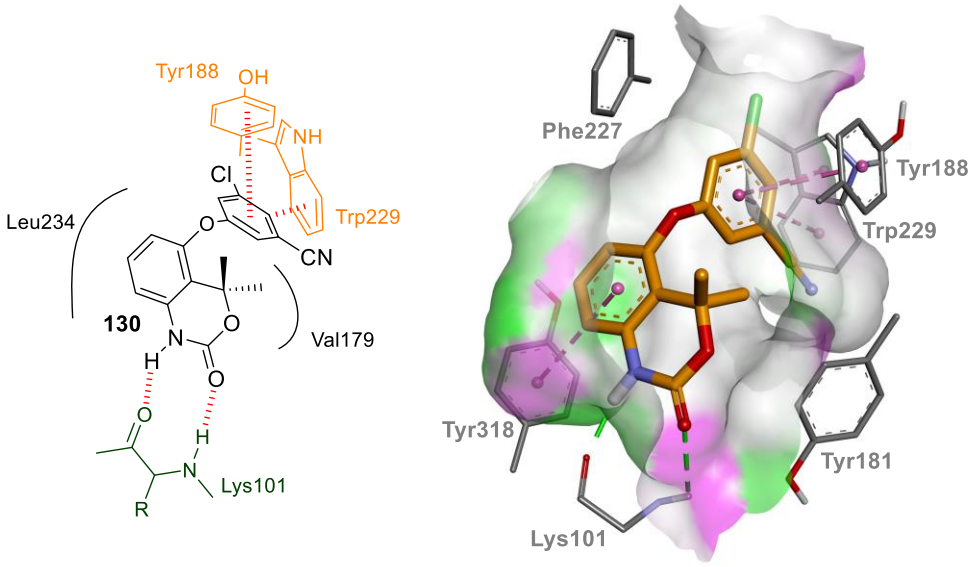

Figure 52 Docking studies revealed that the new benzoxazin-2-one scaffold would be able to facilitate double hydrogen bonding to the backbone of Lys101 while maintaining the important π-interactions with Tyr188 and Trp229.

5.2. Proposed synthesis of the proof-of-concept compound 130

For the synthesis of compound **130**, we envisaged starting from 1-(benzyloxy)-2-iodo-3-nitrobenzene **131**, which in turn, could be synthesized by way of a Sandmeyer reaction from the benzylated 2-amino-3-nitrophenol **33** synthesized in Chapter 3 (**Scheme 79**). We decided to introduce the halogen as a means of directing the subsequent acylation to the desired position between the phenol and nitro group. With the halogen in place we envisaged that lithium-halogen exchange with *n*-BuLi and quenching with an appropriate acyl group would afford the desired acylated product **132**. Subsequent reduction of the nitro group to the amine **133** and a Grignard reaction with methyl magnesium bromide would provide the tertiary alcohol **134**. A ring-closing reaction with CDI would then afford the precursor **135**, which could subsequently be protected with a SEM group to provide **136** in preparation for debenzylation to the

benzoxazin-2-one precursor **137**. Penultimately, **137** would be coupled to 3-chloro-5-fluorobenzonitrile **51** to afford **138**. Finally, removal of the SEM group using the deprotection methods described in Chapter 3 would provide the desired proof-of-concept compound **130**.

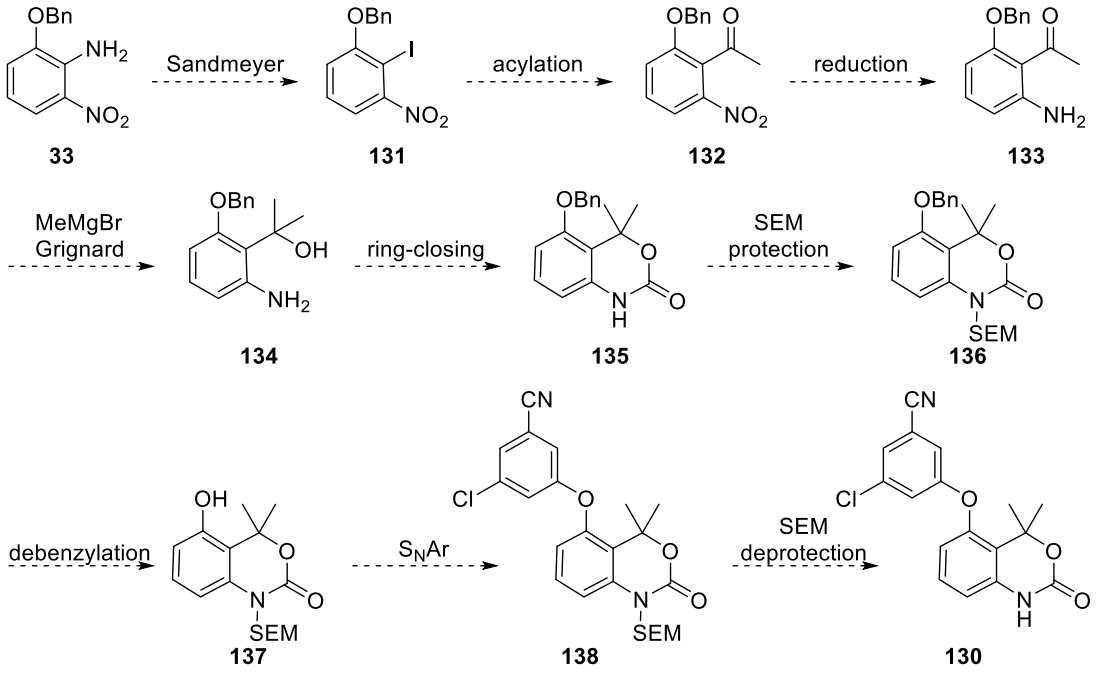

Scheme 79

5.2.1. Synthesis of 1-(benzyloxy)-2-iodo-3-nitrobenzene (131) by way of a Sandmeyer reaction

For the Sandmeyer reaction we decided to utilize conditions reported by Dai *et al.*[261] Under these conditions the amine **33** was activated to the corresponding diazonium salt in the presence of sodium nitrite ($NaNO_2$) and H_2SO_4 (**Scheme 80**). Subsequent quenching of the diazonium salt with potassium iodide afforded the iodo compound **131** in a moderate yield of 60%.

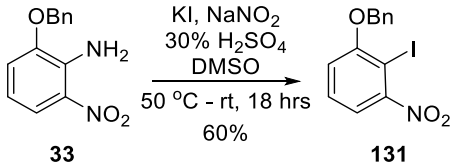

Scheme 80

The notable absence of the amine proton signals in the ^{1}H NMR spectrum of **131** gave testimony to the conversion of **33** to the corresponding iodo-compound **131**. A survey of the literature revealed that the carbon signal for the aromatic carbon directly attached to the iodine on very similar systems is often located between 79 and 82 ppm.[262-264] As a result, we were confident that the signal observed at 80.86 ppm in the ^{13}C NMR spectrum for **131** could be attributed to the iodo-bound carbon. Finally, the mass obtained by HRMS analysis coincided well with the calculated mass for **131**.

5.2.2. Attempted synthesis of the acylated compound 132

As we were confident that the iodo-compound **131** had been successfully synthesized, we could attempt the conversion to the desired ketone **132** by way of lithium-halogen exchange with *n*-BuLi and subsequent quenching with the Weinreb amide **139** (**Scheme 81**).

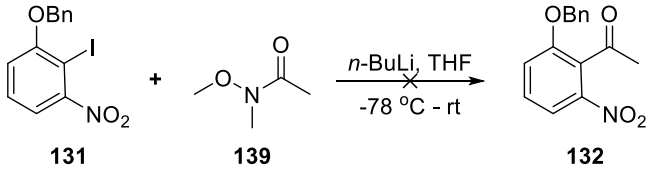

131 **139** **132**

Scheme 81

To this end, freshly titrated *n*-BuLi was added to **131** in dry THF at -78 ˚C. A notable colour change from yellow to red implied that lithium-halogen exchange had occurred and **139** was introduced into the reaction. The reaction was closely monitored by TLC which revealed the formation of two products. The reaction was subsequently quenched and the two products were isolated and purified by column chromatography. Unfortunately, analysis by ^{1}H and ^{13}C NMR spectroscopy indicated that neither product was the desired acylated product **132** as no signals attributed to the ketone were observed.

For the one product, only an additional aromatic proton signal was observed in the ^{1}H NMR spectrum. This observation, in addition to the absence of the C_{Ar}-I signal in the ^{13}C NMR spectrum, indicated that although lithium-halogen exchange had occurred, the lithiated product had been quenched to afford **140** (**Scheme 82**).

In the ^{1}H NMR spectrum of the second product, four additional aliphatic signals were observed indicative that a butyl group had been added onto the aromatic ring. These additional signals included two triplets at 2.73 and 0.92 ppm which integrated for two and three protons respectively and two multiplets at 1.60 and 1.37 ppm both integrating for two protons. Moreover, the multiplicity observed for the aromatic

protons in the ^{1}H NMR spectrum of this product suggested that the butyl group had been introduced at positions *para* or *ortho* to the phenol as indicated by compounds **141** and **142** in **Scheme 82**. A doublet of doublets at 7.79 ppm which could be attributed to the proton at position 6 on **141** or 4 on **142** had coupling constants of 8.2 Hz and 2.1 Hz. This proton was clearly partnered with a small doublet at 7.75 ppm with a coupling constant of 2.1 Hz which could be attributed to the proton at position 2. Finally, a doublet with a coupling constant of 8.2 Hz and no observable long-range coupling was observed at 7.27 ppm which could be attributed to the proton at position 5 on **141** and **142**.

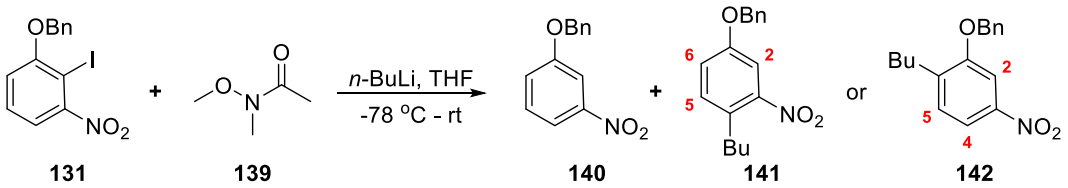

Scheme 82

When we attempted the reaction for a second time, monitoring the reaction by TLC prior to the addition of the Weinreb amide, revealed that the by-products isolated previously had already formed.

As a result, we decided to change tactic and carry out the acylation by way of a transmetallation reaction with *iso*propylmagnesium chloride to form the aryl Grignard reagent *in situ* and subsequently quench with **139** (**Scheme 83**). Unfortunately, under these conditions no reaction occurred.

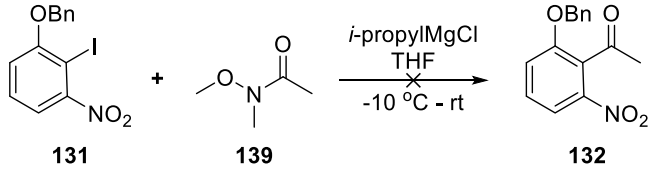

Scheme 83

At this point, we considered the possibility that the nitro-group might be incompatible with the organometallic reagents introduced in **Scheme 81** and **Scheme 83**. In fact, in validation of this concern while surveying the literature we came across papers by Bartoli *et al.* which describe the 1,4 or 1,6-conjugate addition of alkyl magnesium halides onto nitroarenes, a phenomenon which later led to the identification of the Bartoli indole synthesis.[265-267] A generic representation of the conjugate addition of Grignard reagents onto nitroarenes is given in **Scheme 84**. According to Bartoli this reaction proceeds through two steps. The first involves the formation of nitronate compounds **144** and **145** from the 1,4 and 1,6 conjugate addition of an akyl magnesium halide (RMgX) onto nitroarene **143**. Subsequent

decomposition of **144** and **145** then leads to the formation of products **146** and **147**.[265] Although this reaction is specific to the conjugate addition of RMgX onto nitroarenes we envisaged that, with regards to the reaction of **131** with *n*-BuLi, that a similar phenomenon had occurred leading to the unexpected formation of butylated compound **141** or **142** (**Scheme 82**).

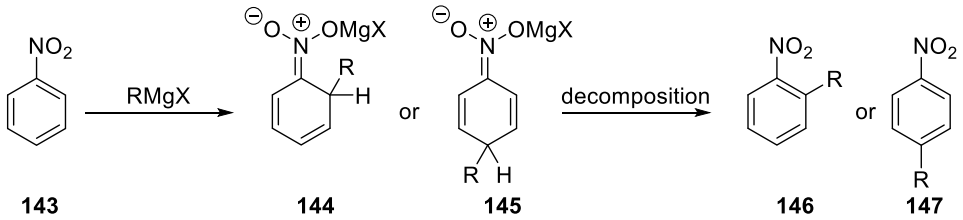

Scheme 84

In an attempt to circumvent the issue of possible interference from the nitro group, we decided to reduce the nitro to the corresponding amine prior to acylation using the reaction conditions reported in **Scheme 81**. To this end **131** was exposed to ultrasonic irradiation in the presence of $SnCl_2.2H_2O$ (**Scheme 85**). The reaction was monitored closely by TLC and after two hours the reaction appeared to have gone to completion, affording only a single product.

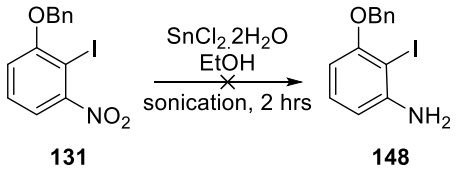

Scheme 85

At first glance, a broad singlet at 3.60 ppm in the ^{1}H NMR spectrum which integrated for two protons implied that the reduction of the nitro group had been successful. However, analysis of the aromatic region in the ^{1}H NMR spectrum revealed an additional proton than would have been expected for **148**. This observation in conjunction with the absence of a carbon signal around 80 ppm in the ^{13}C NMR spectrum indicated that, although the reduction of the nitro had been successful, the iodine had been removed to afford the product **149** (**Scheme 86**). As this is a known compound we were able to confirm this by comparing our spectroscopic data with the data reported in the literature.[268]

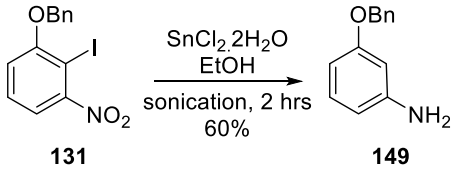

131 **149**

Scheme 86

Nevertheless, although we were unable to synthesize the desired compound **148** with the iodine in place, we desired to press on with **149** and direct *ortho* acylation by introducing a Boc protecting group onto the amine. We understood that, under these circumstances, we could end up with competitive acylation at the *ortho* and *para* positions relative to the phenol. However, we reasoned that this route could provide a means to determine whether the acylation would occur without the nitro present and that we could optimize regioselectivity at a later stage.

The installation of the Boc protecting group onto the amine **149** was carried out readily in the presence of DMAP affording **150** in a high yield of 90% (**Scheme 87**). In the ^{1}H NMR spectrum of **150**, the presence of a singlet integrating for nine protons at 1.36 ppm and a broad singlet integrating for one proton at 10.96 ppm could be attributed to the introduction of only a single Boc group onto the amine.

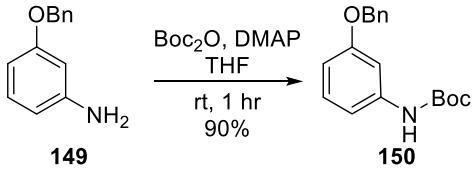

149 **150**

Scheme 87

With **150** in hand we could attempt to carry out the acylation using conditions reported in **Scheme 81**. Only, in this instance we expected to obtain a mixture of products, namely **151** and **152** as shown in **Scheme 88**. When monitored by TLC, although the reaction had not gone to completion, only a single product appeared to have formed. However, when this product was analysed by ^{1}H and ^{13}C NMR spectroscopy we realized that the Boc group had simply been removed and that we had regenerated the unprotected amine **149**.

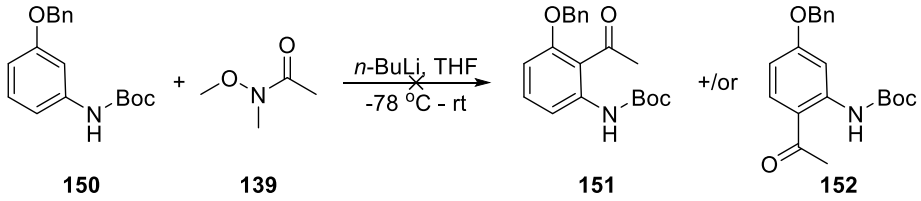

Scheme 88

5.3. Changing tactics: The introduction of an acyl group onto the aryl ring through the oxidation of an activated toluene

While struggling to introduce the acyl group onto our aryl ring using organometallic methods we decided to turn our attention to alternative methods, namely the oxidation of an activated toluene to the corresponding aldehyde or carboxylic acid. A review of the literature revealed a vast number of methods whereby this could be achieved when the aromatic methyl group was situated *ortho* to a nitro group.[269-273]

For our purposes we envisaged starting from commercially available 2-methyl-3-nitrophenol **153** (**Scheme 89**). After the introduction of a suitable protecting group, we decided that we would attempt the oxidation of **154** to the corresponding aldehyde **155** and the carboxylic acid **156** as we knew that both functional groups could be directly and readily converted into the corresponding ester **157**.[274-275] We envisaged that, following the reduction of the nitro group to the corresponding amine **158**, the ester could be reacted with an excess of methylmagnesium bromide to afford the desired tertiary alcohol precursor **159**, which could then undergo a ring-closing reaction with CDI providing the benzoxazin-2-one precursor **160**.

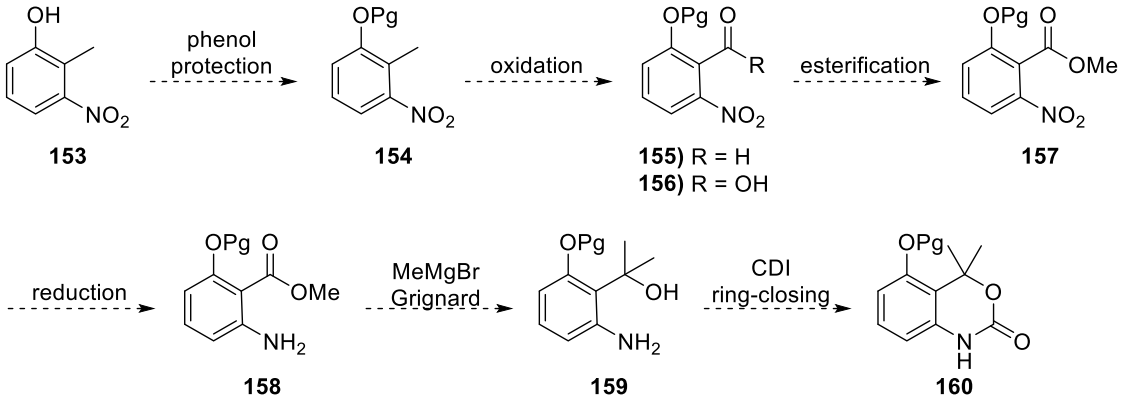

Scheme 89

5.3.1. Oxidation of the activated toluene to the corresponding aldehyde 167

For the oxidation of **153** to the corresponding aldehyde **155** we decided to employ conditions reported by Caron and Vazquez in 2003.[270] Herein, Caron and Vazquez described the preparation of *o*-nitrobenzaldehyde **164** from the activated aryl methyl group **161** by way of a one-pot reaction which involved the formation of an enamine intermediate **163** using *N*,*N*-dimethylformamide dimethyl acetal (DMF·DMA) **162** and subsequent oxidative cleavage to the aldehyde **164** with sodium periodate ($NaIO_4$) (**Scheme 90**). This procedure came about as a slight modification of a two-step process originally reported by Vetelino and Coe from Pfizer in 1994.[269] Interestingly, in the original 1994 publication it was reported that, although the oxidative cleavage of an alkene to the aldehyde typically requires catalytic amounts of osmium tetroxide to hinder over-oxidation to the carboxylic acid, in this instance the utilization of osmium tetroxide was found to be superfluous.[269, 276]

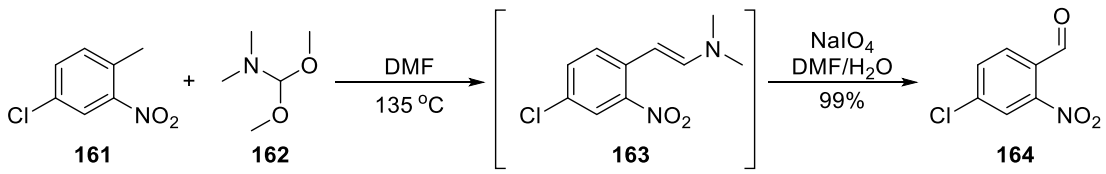

Scheme 90

In **Scheme 89** it is shown that the phenol of **153** required the introduction of a suitable protecting group prior to carrying out the oxidation of the activated methyl to the aldehyde. This was to ensure that **162**, which can also act as a methylating agent, would not be competitively targeted by the phenol.[277] To this end we decided to introduce a benzyl protecting group on the phenol of **153**. This was readily achieved with benzyl bromide and K_2CO_3 to afford **165** (**Scheme 91**).

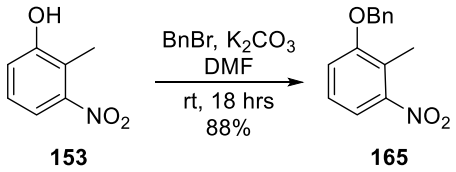

Scheme 91

The identification of five additional aromatic proton signals in the ^{1}H NMR spectrum of **165**, in addition to a singlet at 5.11 ppm which integrated for two protons, were indicative that the benzyl protecting group had been successfully installed. This observation was mirrored by the identification of four additional aromatic and one additional aliphatic carbon signal in the ^{13}C NMR spectrum of **165**.

With **165** in hand we could attempt the conversion of the activated methyl into the corresponding aldehyde using the one-pot reaction conditions described by Caron and Vazquez.[270] To this end, **165** and **162** in DMF were heated at 135 ˚C for 18 hours, after which the reaction was monitored by TLC to reveal that all starting material had been consumed and a single product, assumed to be the enamine **166**, had formed. The reaction was subsequently cooled and $NaIO_4$ was added. After an additional 18 hours, the product assumed to be **166** had disappeared and two new products had formed. However, following workup and purification by column chromatography we were only able to isolate a single product. Fortunately, analysis of the ^{1}H and ^{13}C spectroscopic data obtained for the uknown product, revealed that we had in fact isolated the desired aldehyde **167**, albeit in a very poor yield of 15% (**Scheme 92**).

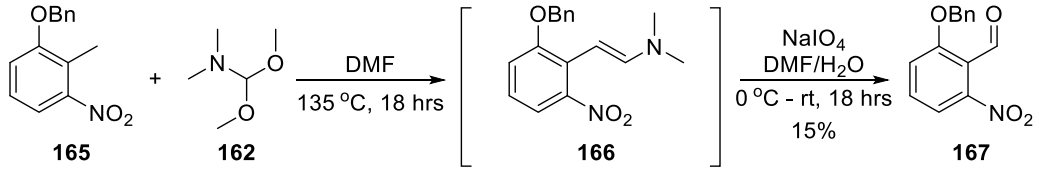

Scheme 92

The most distinguishing feature observed in the ^{1}H NMR spectrum of **167** was a highly deshielded singlet at 10.43 ppm which could be attributed to the proton of the aldehyde. In the ^{13}C NMR spectrum of **167** a carbon signal located at 187.7 ppm could be attributed to the aldehyde carbonyl carbon. Moreover, this spectroscopic data was compared to the spectroscopic data available in the literature and was found to compare favourably, confirming that **167** had been synthesized.[278]

Although we were able to obtain the desired aldehyde **167** using the conditions reported by Caron and Vazquez, the yield was unfortunately very low and, therefore, we were not able to isolate enough material to proceed to the subsequent esterification step. As a result, we decided to attempt oxidation of the activated methyl of **165** to the corresponding carboxylic acid.

5.3.2. Oxidation of the activated toluene to the corresponding carboxylic acid 169

For the oxidation of the activated methyl to the corresponding carboxylic acid we opted to employ the procedure reported by Yoakim *et al.* which described the use of potassium permanganate ($KMnO_4$) as the oxidizing agent under refluxing conditions.[279] Once again it was imperative that a protecting group be introduced onto the phenol **153** to avoid oxidation of the phenol to the corresponding quinone. However, in this instance, we decided not to utilize a benzyl protecting group for fear that the benzylic position

would also be susceptible to oxidation under the conditions reported.[280] Instead we decided to employ a methyl group as the 'protecting group' for the phenol **153**.

For the methylation reaction **153** was treated with methyl iodide in the presence of sodium hydride. This reaction proceeded readily to afford **168** in a high yield of 92% after 18 hours (**Scheme 93**).

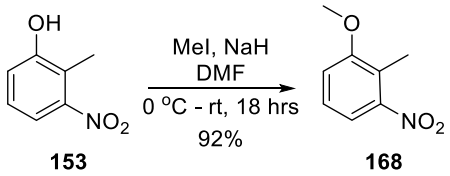

153 **168**

Scheme 93

From the spectroscopic data of **168**, a singlet which integrated for three protons at 3.89 ppm in the ^{1}H NMR spectrum and carbon signal at 56.4 ppm in the ^{13}C NMR spectrum provided the clearest evidence that the methylation of phenol **153** had occurred successfully.

Assured that competitive oxidation of the phenol to the quinone would not occur, we could now attempt the desired oxidation of the activated methyl **168** to the carboxylic acid **169** using the conditions reported by Yoakim *et al.* (**Scheme 94**).[279] To this end, an excess of $KMnO_4$ was added to **168** in *t*-BuOH and H_2O and the reaction was heated under reflux. However, after 18 hours TLC indicated that the reaction had not gone to completion. Nevertheless, the reaction was cooled in preparation for workup. Under the impression that **169** was the only product formed under these conditions we reasoned that **168** and **169** could be separated and isolated as pure product by simple acid-base extraction techniques. As expected, we were able to recover unreacted **168** and isolate the desired carboxylic acid **169** without the need for further purification. Unfortunately, we were only able to obtain **169** in a low yield of 34%.

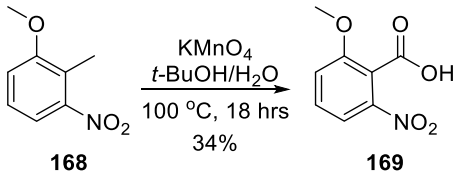

168 **169**

Scheme 94

In the ^{1}H NMR spectrum of **169** the absence of the singlet belonging to the aromatic methyl group was the most notable indication that oxidation of the methyl group had occurred. In the ^{13}C NMR spectrum of **169** the absence of the aromatic methyl carbon signal in conjunction with the appearance of an additional signal at 165.0 ppm provided further testimony to the success of the oxidation reaction. Finally, HRMS

provided a mass of 198.03974 amu which coincided well with the calculated mass of **169** which was 198.03970 amu.

Of the two oxidation reactions carried out, the oxidation with $KMnO_4$ to the carboxylic acid was only marginally superior to the oxidation with DMF-DMA and $NaIO_4$ to the corresponding aldehyde. Nevertheless, despite the low yields, we were able to obtain enough of the carboxylic acid **169** to proceed to the subsequent esterification step in the synthetic route shown in **Scheme 89**.

5.3.3. Synthesis of methyl 2-methoxy-6-nitrobenzoate (170)

For the esterification reaction we envisaged that methyl ester **170** could be obtained by a simple methylation of the carboxylic acid **169**. To this end, **169** was treated with methyl iodide in the presence of K_2CO_3 (**Scheme 95**). After 2 hours at room temperature TLC indicated that the reaction had reached completion. Subsequent workup and purification by column chromatography afforded the methyl ester **170** in an excellent yield of 96%.

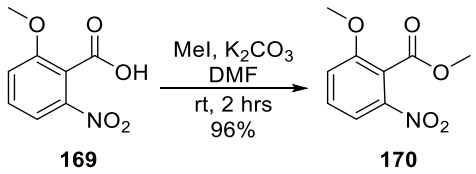

169 **170**

Scheme 95

The presence of two singlets each integrating for three protons at 3.95 and 3.90 ppm in the ^1H NMR spectrum of **170** could be attributed to the presence of the methoxy group and methyl ester. Similarly, two aliphatic carbon signals observed at 56.9 and 53.3 ppm in the ^{13}C NMR spectrum of **170** attested to the presence of two methyl groups on the compound. These observations, in addition to the presence of the ester carbonyl carbon signal at 166 ppm was indicative that the esterification reaction had occurred successfully.

5.3.4. Synthesis of methyl 2-amino-6-methoxybenzoate (171)

With the methyl ester **170** in hand we could endeavour to reduce the nitro group to the corresponding amine **171** (**Scheme 96**). The decision to reduce the nitro group prior to performing a Grignard reaction onto the ester was based on our desire to avoid complications that may arise due to the phenomena

reported by Bartoli *et al*. which we described in section **5.2.2**. For the reduction compound **170** was taken up in ethanol and treated with palladium on carbon under an atmosphere of hydrogen. After 18 hours the reaction was filtered over Celite and purified by column chromatography to afford the reduced product **171** in 93% yield.

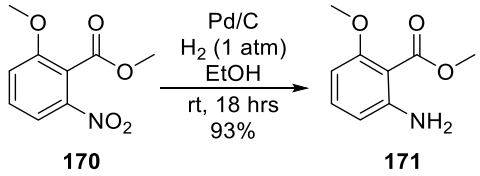

Scheme 96

In the ^{1}H NMR spectrum of **171** the presence of a broad singlet at 4.93 ppm provided the clearest indication that the reduction of the nitro group had transpired. Furthermore the presence of two singlets at 3.87 and 3.79 ppm, each integrating for three protons testified to the fact that the ester had remained unaffected. This was corroborated by the presence of two aliphatic carbon signals at 56.1 and 51.8 ppm in the ^{13}C NMR spectrum and a signal at 168.6 ppm which could be attributed to the ester carbonyl carbon.

5.3.5. Synthesis of 2-(2-amino-6-methoxyphenyl)propan-2-ol (172) by way of a Grignard reaction with methylmagnesium bromide

For the Grignard reaction between **171** and methylmagnesium bromide it was imperative that a large excess of the Grignard reagent be introduced into the reaction to ensure double addition of MeMgBr onto the ester to afford the desired tertiary alcohol **172**. This was due to the presence of the amine and the fact that Grignard reagents can competitively act as a strong base. To this end, **171** was treated with five equivalents of MeMgBr in THF at 0 °C (**Scheme 97**). The reaction was closely monitored by TLC and revealed that, after 4 hours, the ester **171** had been completely consumed. Subsequent quenching with H_2O and extraction afforded **172** in 91% yield without the need for further purification.

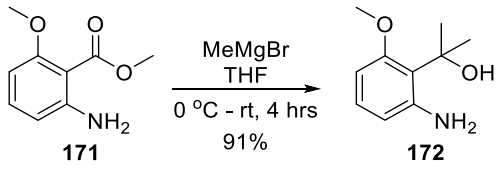

Scheme 97

The presence of a singlet at 1.71 ppm which integrated for six protons in the ^{1}H NMR spectrum of **172** offered the first indication that a double addition of the Grignard reagent MeMgBr onto the ester had occurred successfully. This was substantiated by the presence of an additional aliphatic carbon signal in the ^{13}C NMR spectrum of **172** and the absence of the carbon signal attributed to the ester carbonyl carbon. Finally, HRMS provided a mass of 182.11766 amu which coincided with the calculated mass of 182.11756 amu.

5.3.6. Synthesis of 5-methoxy-4,4-dimethyl-1,4-dihydro-2*H*-benzo[*d*][1,3]oxazin-2-one (173)

For the synthesis of **173** we envisaged that we could employ the same ring-closing reaction conditions with CDI that were used for the formation of our first and second-generation benzimidazolone compounds described in Chapters 2 and 3. Therefore, treatment of **172** with CDI in MeCN resulted in the formation of benzoxazin-2-one compound **173** after 30 minutes at room temperature (**Scheme 98**).

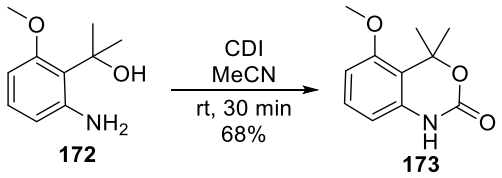

Scheme 98

In the ^{1}H NMR spectrum of **173** the presence of a highly deshielded singlet at 9.47 ppm integrating for one proton and the absence of the broad singlet attributed to the amine gave testimony to the successful formation of **173**. The presence of an additional carbon signal in the aromatic region of the ^{13}C NMR spectrum of **173** and HRMS which provided a mass of 208.09682 amu, which was in accord with the calculated mass, provided further validation that **173** had been formed.

5.3.7. Synthesis of 5-hydroxy-4,4-dimethyl-1,4-dihydro-2*H*-benzo[*d*][1,3]oxazin-2-one (174)

In the original proposed synthetic route for target compound **130** (**Scheme 79**) it was stated that following the formation of the benzoxazin-2-one precursor **135** we would introduce a SEM protecting group onto the carbamate in preparation for the removal of the phenol protecting group and subsequent coupling to 3-chloro-5-fluorobenzonitrile (**51**). However, with the methoxy as the 'protecting group' for compound **173** we were concerned that a SEM protecting group would not survive a demethylation reaction requiring

the use of boron tribromide. We doubted that any other *N*-protecting group would survive these conditions and, as a result, we realized that we would have to attempt the S_NAr reaction without any protecting group on the carbamate. However empirical pK_a calculations using Epik, a feature of Schrödinger, on the demethylated benzoxazin2-one precursor **174** (**Scheme 99**) predicted that the phenol was slightly more acidic than the carbamate. Therefore, we hoped that by controlling the amount of **51** and base introduced into the S_NAr reaction that we might be able to selectively couple **51** to the phenol without additional coupling to the carbamate.

For the demethylation reaction compound **173** was treated with boron tribromide at 0 °C (**Scheme 99**). The reaction was monitored closely by TLC and after 4 hours it was observed that the starting material had been consumed. Unfortunately, when we attempted to purify the resulting product by column chromatography we observed that the product was degrading on silica gel. To overcome this problem, in a second experiment we decided not to purify the product following the workup. Fortunately, spectral analysis revealed that further purification was unnecessary and that we had successfully synthesized and isolated pure demethylated product **174** in 90% yield.

Scheme 99

Two highly deshielded singlets, each integrating for one proton, were observed at 9.98 and 9.85 ppm in the ^1H NMR spectrum of **174**. These singlets we attributed to the carbamate proton and the deprotected phenolic proton. This observation in conjunction with the absence of the methoxy proton signal in the ^1H and ^{13}C NMR spectra of **174** indicated that the methoxy group had been successfully removed with BBr_3.

5.3.8. The final step towards the synthesis of 3-chloro-5-((4,4-dimethyl-2-oxo-1,4-dihydro-2*H*-benzo[*d*](1,3)oxazin-5-yl)oxy)benzonitrile (130)

Having successfully demethylated compound **173** to afford the precursor **174** we could finally endeavour to carry out the final S_NAr step towards the synthesis of target compound **130**. To this end, **174** was treated with a single equivalent of **51** and Cs_2CO_3 and the reaction was heated to 100 °C. Nevertheless, monitoring the reaction by TLC revealed the formation of multiple products, none of which appeared to be the desired

product **130**. We decided to re-attempt the S_NAr reaction at room temperature but observed no reaction. We then tentatively raised the temperature to 70 °C and monitored the reaction closely. To our delight, after several hours we observed the formation of only a single product. Spectral analysis of the resulting product, following workup and attempted purification by column chromatography, revealed that we had successfully synthesized the final product **130**, albeit impure. However, subsequent recrystallization from ethanol afforded pure **130** in a 13% yield (**Scheme 100**). Although the yield obtained was disappointingly low, we thankfully had enough product for full characterization and evaluation in our HIV whole cell phenotypic assay.

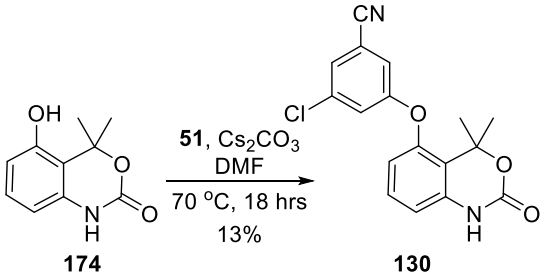

Scheme 100

In the ^1H NMR spectrum of **130** the absence of a highly deshielded proton which we attributed to the phenol and the presence of three additional aromatic protons indicated that an S_NAr reaction with **51** had transpired. This observation was further substantiated by the presence of seven additional carbon signals in the ^{13}C NMR spectrum and analysis of HRMS which gave a mass of 329.06869 amu which concurred with the calculated mass of 329.06875 amu. Although all the spectral data confirmed that an S_NAr reaction had occurred we still had to verify that **51** had been coupled to the phenol and not the carbamate. To this end, we decided to obtain a crystal structure of **130**. To our delight, X-ray crystallography confirmed that the S_NAr reaction had occurred between **51** and the phenol of **174** to afford our desired proof-of-concept compound **130** (**Figure 53**).

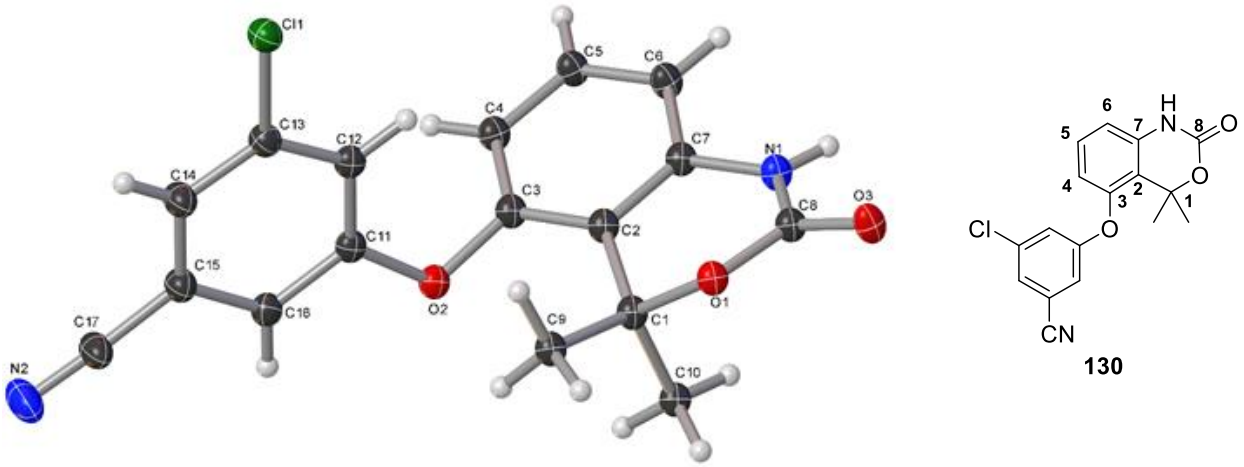

Figure 53 Crystal structure obtained for compound **130** (left) with a diagram of **130** rotated and numbered to correlate with the crystal structure for clarity (right).

5.4. Evaluation of compound 130 in a whole-cell phenotypic assay

In the evaluation of compound **130** we were overjoyed to discover that our proof-of-concept compound was not only slightly more potent than our lead compound **50** with an IC_{50} value of 17 nM but also exhibited a significantly higher selectivity index (> 4000) (**Figure 54**). Although we had not significantly improved upon the potency of compound **50**, we believed that this might be achieved by derivatizing the dimethyl substituents located at position 4 on the benzoxazin-2-one scaffold. Unfortunately, we have not yet been able to evaluate **130** against a panel of resistant strains; however, we were encouraged by the results obtained against the wild-type virus which we believed would open the door to the generation of a whole new library of compounds.

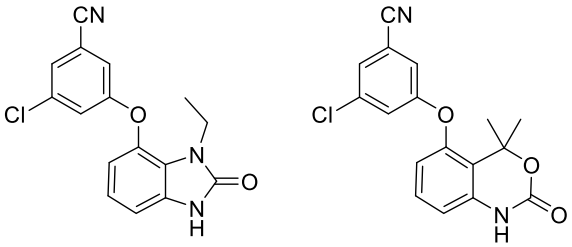

Figure 54

5.5. Metabolic stability testing of compound 130 against human and mouse liver microsomes

Having established compound **130** as another lead compound, we were curious as to how this compound would fare in mouse and human liver microsome assays. To this end, as with compound **50**, compound **130** was incubated with mouse and human liver microsomes and then analysed by LCMS over 5-minute intervals over a total of 30 minutes. We were pleased to see that compound **130** was highly stable in both liver microsome assays, which bodes well for this compound's performance *in vivo* (**Table 6**).

	% Remaining after 30 minutes	
	Mouse liver microsomes	**Human liver microsomes**
Compound **130**	94	90
Verapamil (positive control)	-	7.0
Diphenhydramine (positive control)	51	-

Table 6

5.6. Concluding remarks

In conclusion, guided by molecular modelling we employed a molecular hybridization approach between our most potent second-generation benzimidazolone compound **50** and efavirenz to generate a new hybrid compound capable of achieving double hydrogen bonding interactions with the backbone of Lys101. By re-introducing the double hydrogen bond originally expressed by the indole compounds described in Chapter2, we had hoped to improve upon the potency of compound **50** against the wild-type virus and a variety of resistant strains. To this end, we synthesized the benzoxazin-2-one compound **130**. Evaluation of **130** in a whole-cell phenotypic assay revealed that **130** was an equally potent inhibitor of RT, compared to **50**, but with a much-improved selectivity index.

Chapter 6: Conclusion

At the start of this project, we endeavoured to tackle the lability issues faced by a series of lead indole-based compounds previously synthesized within our research group. These indole-based compounds (**1**), although potent inhibitors of HIV RT, were not suitable for drug candidacy. This was due to the presence of an acid-labile methoxy group situated at the 3-position on the indole scaffold and an ester at the 2-position which, inevitably, would be susceptible to hydrolysis by cellular esterases (**Figure 55**). To address these issues, we employed a scaffold-hopping approach with the aid of molecular modelling to replace the indole scaffold with the bioisosteric benzimidazolone scaffold (**11**) (**Figure 55**). With this approach we lost the hydrogen bond acceptor in the form of the ester carbonyl and, therefore, the additional hydrogen bond to the backbone of Lys101. However, we envisaged that the urea carbonyl on the benzimidazolone scaffold would be able to compensate for the loss of this interaction by strengthening the hydrogen bonding capability of the urea N*H*.

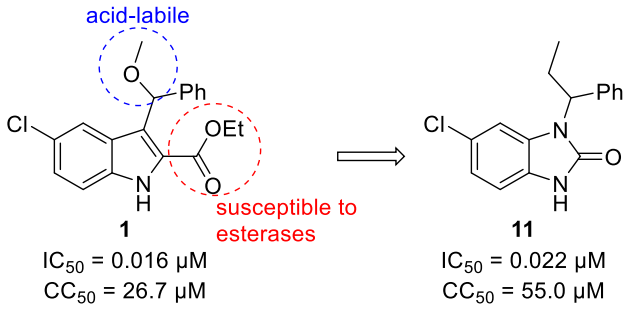

Figure 55

In the evaluation of **11** in a whole cell HIV phenotypic assay we found that **11** was an equally potent inhibitor of HIV RT when compared with the lead indole compound **1**, an observation which validated our hypothesis that the carbonyl directly adjacent to the N*H* would compensate for the loss of the additional hydrogen bond with the backbone of Lys101. However, compound **11** was found to be a poor inhibitor against the common K103N and Y181C resistant strains of HIV. The susceptibility of **11** to the Y181C mutant we attributed to the fact that the binding of this compound to the NNIBP of RT relies heavily on π-interactions between the aryl group, situated at the *N*1 position on the benzimidazolone scaffold, and Tyr181. In an effort to overcome the susceptibility of **11** to the Y181C resistant strain we designed a series of second-generation benzimidazolone compounds whereby the aryl group at the *N*1 position was transposed to the 7-position on the benzimidazolone scaffold (**Figure 56**). This eliminated the dependency

on π-interactions with the mutable amino acid residue Tyr181, while introducing π-interactions with Tyr188 and conserved residue Trp229.

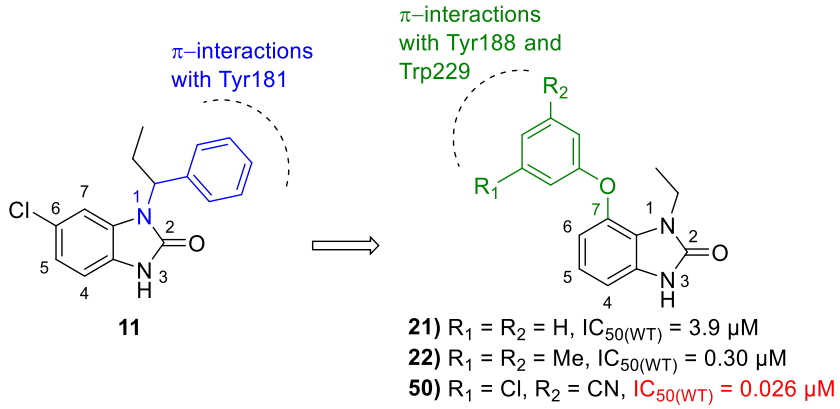

Figure 56

The first compounds synthesized in this series, compounds **21** and **22**, were unfortunately found to be poor inhibitors of HIV RT with micromolar activity. However, by introducing a chloride and nitrile substituent onto the scaffold, we were able to significantly improve the potency from 300 nM for compound **22** to 26 nM for compound **50** (**Figure 56**). Furthermore, when evaluated against a panel of clinically relevant resistant strains of HIV, compound **50** was found to exhibit a superior resistance profile compared to the first-generation compound **11**. Not only was **50** able to maintain potency against the Y181C resistant strain, it was also found to maintain potency against the Y188C resistant strain and the double mutant K103N/Y181C which renders licensed NNRTIs nevirapine and efavirenz ineffective. Moreover, against the most prevalent and problematic K103N resistant strain, compound **50** exhibited only a 4-fold drop in potency.

Having obtained a potent lead compound for our second-generation series of compounds we embarked upon the synthesis of a small library of compounds by derivatizing the alkyl group at position *N*1 and the aryl group at position 7. Although some of these compounds were found to be similarly potent inhibitors of HIV RT, compound **50** maintained superior potency against wild-type RT and, more importantly, against resistant strains of HIV!

In an attempt to further optimize the potency of lead compound **50** we next endeavoured to introduce additional electrostatic interactions between **50** and the NNIBP. Two different approaches were undertaken to achieve this.

The first approach focused on targeting a lysine residue (Lys223) situated at the top of a narrow hydrophobic chimney, formed by amino acid residues Trp229, Tyr188 and Phe227, towards the back of the NNIBP. We envisaged that, by introducing a hydrogen bond acceptor by way of a suitably long substituent on the "upper" aryl ring of **50**, we would be able to achieve an additional hydrogen bond with this residue. To this end we designed, with the aid of molecular modelling, the cyanoacetylene-containing compound **90** (**Figure 57**). However, during the synthesis of this compound it was discovered that the cyanoacetylene substituent, being a good Michael acceptor, was a significant liability. As a result, we changed tactics and synthesized compound **127** which possessed the less reactive, but bioisosteric, cyanovinyl substituent. Evaluation of **127** in a phenotypic assay revealed that we had synthesized another compound with low nanomolar activity. However, using this design approach, we were unable to meet our aim in improving upon the potency of lead compound **50**.

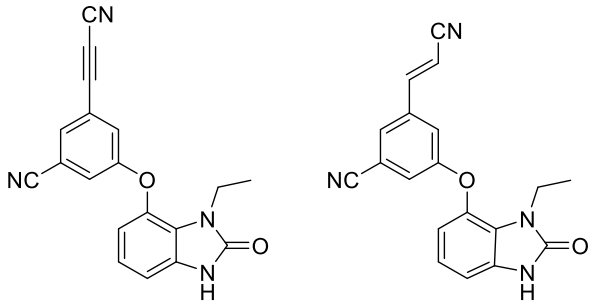

Figure 57

For the second approach to improve upon the potency of lead compound **50**, we focused on modifying our structure to re-introduce the double hydrogen bond, exhibited by the indole compounds, to the backbone of Lys101. To this end, compound **130** was designed using a molecular hybridization approach between our compound **50** and licensed NNRTI efavirenz (**Figure 58**). This novel hybrid compound would be able to achieve additional hydrogen bonding to the backbone of Lys101 due to the repositioning of the carbonyl on the benzoxazin-2-one scaffold of efavirenz, while maintaining the important π-stacking interactions with conserved residue Trp229 through the chloro-cyano-substituted aryl ring of **50**. As this was a proof-of-concept compound, the dimethyl substituent at position 4 on the scaffold was introduced in order to reduce synthetic complexity. Evaluation of **130** in a HIV phenotypic assay revealed that **130** was an equally potent inhibitor when compared to lead compound **50**. Moreover, compound **130** exhibited a significantly higher selectivity index. Unfortunately, we have not yet been able to evaluate this compound against a panel of resistant strains of HIV. As our first simplified proof-of-concept compound

was a potent inhibitor of HIV RT we envisaged that, through optimization of the substituents at position 4 on this scaffold with the aid of molecular modelling, we would be able to further improve upon the potency of these compounds.

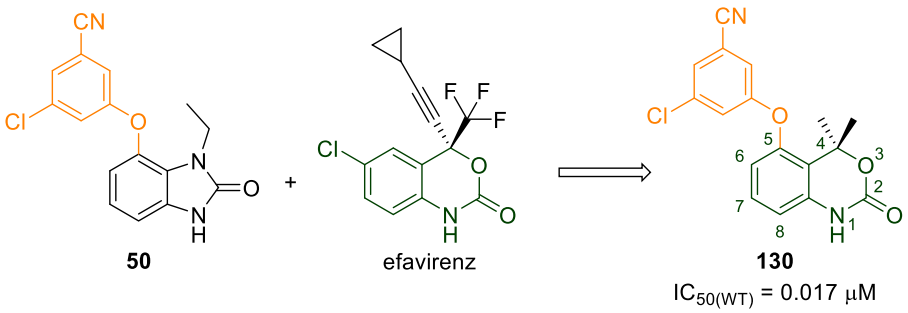

Figure 58

In conclusion, through various stages of optimization, we have successfully designed and synthesized three generations of potent (low nanomolar) inhibitors of HIV RT. Moreover, as compounds **50** and **130** fared well against human and mouse liver microsomes, both scaffolds are promising for drug candidacy.

Chapter 7: Future Work

7.1. Optimizing the potency of compound 130

Future endeavours in this project will focus on optimizing the activity of the benzoxazin-2-one compound **130** against wild-type and resistant strains of HIV. This we envisage, could be achieved by derivatizing the alkyl substituents located at position 4 on the scaffold and by introducing a halogen at position 6.

7.1.1. The 4-position: Exploring various alkyl substituents to occupy the Val179 pocket

Occupation of the small hydrophobic pocket in the vicinity of Val179 has been shown to have a significant influence on the activity of a compound against HIV RT.[147] As a result, we will explore various alkyl substituents at position 4 on the benzoxazin-2-one scaffold to occupy the Val179 pocket. Preliminary molecular modelling has identified a few promising substituents which are represented by compounds **175** – **177** (**Figure 59**). Docking studies have shown that these substituents are able to occupy the small Val179 pocket without altering the binding orientation of the compound within the NNIBP, and binding energy calculations indicate that these compounds are indeed more favourable than our first benzoxazin-2-one lead compound **130**.

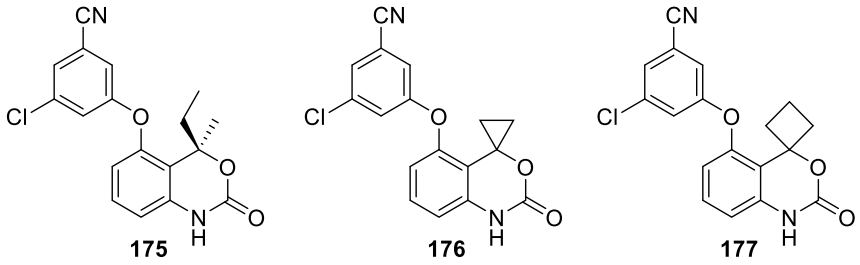

Figure 59

However, of these compounds, **176** and **177** cannot be synthesized using the same synthetic procedure described for compound **130** in chapter 5. Instead, we would have to revisit our original strategy whereby we attempted to acylate an aryl halide using transmetallation reaction conditions. Although in our hands acylation of our 2-iodo-nitrobenze analogue **131** had been unsuccessful, it recently came to our attention

that this could be achieved if we employ phenylmagnesium chloride as our magnesium source (**Figure 60**).[281-282]

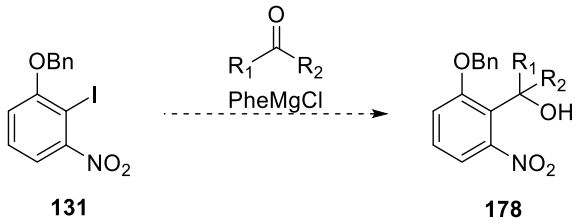

131 **178**

Figure 60 General depiction of the proposed strategy to acylate 2-iodo-nitrobenzene **131** using phenylmagnesium chloride as the magnesium source to obtain the desired tertiary alcohol **178**.

7.1.2. The 6-position: Introduction of a halogen

Generally, inhibitors that possess a suitable halogen to occupy a small hydrophobic pocket at the back of the non-nucleoside inhibitor binding pocket (NNIBP) are found to exhibit improved potency.[209] It has been proposed that the link between improved potency and the introduction of a halogen at this position is a result of halogen bonding between the ligand and the NNIBP.[168] We envisaged that this trend could be translated over to our hybrid compounds by introducing a halogen, such as a fluorine, at position 6 (**179**, **Figure 61**). In chapter 3 it was mentioned that, according to docking studies, the introduction of chlorine appeared to have no significant effect on the binding energy of our benzimidazolone compounds. A similar observation was made for our benzoxazin-2-one compound **130**. However, preliminary docking studies and binding energy calculations have indicated that the introduction of a fluorine is considerably more favourable.

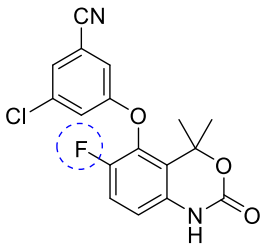

179

Figure 61

Fortunately, a survey of the literature has revealed that the synthesis of compound **179** can be achieved through late stage functionalization of **130** through electrophilic fluorination of **130** with selectfluor (**Figure 62**).[209]

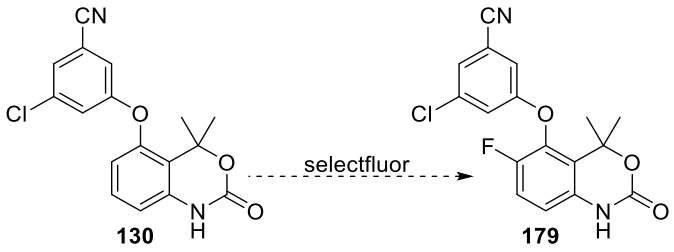

Figure 62 We have proposed that the introduction of the fluorine can be achieved through late stage functionalization of lead compound **130**.

Chapter 8: Experimental

8.1. General procedures pertaining to synthesis and characterization.

8.1.1. Purification of Reagents and Solvents

All chemicals used in the following experiments were purchased from Sigma Aldrich or Apollo Scientific. Solvents used for chromatographic purposes were distilled by means of conventional distillation procedures. All anhydrous solvents used for reaction purposes were dried over the appropriate drying agents and then distilled under an atmosphere of nitrogen or obtained from anhydrous septum-sealed DriSolv® bottles. Tetrahydrofuran (THF) was distilled over sodium metal, using benzophenone as an indicator. Dichloromethane and acetonitrile were distilled from calcium hydride. Other solvents were purchased with a ≥98% purity grade from Sigma Aldrich and then dried on activated 3Å molecular sieves.

8.1.2. Chromatography

Thin layer chromatography was performed using Merck silica gel 60 F254 coated on aluminium sheets. Visualization was performed with a UV lamp or using common stains such as *p*-anisaldehyde, ninhydrin (NIN) or a potassium permanganate (KMnO4) solution followed by gentle heating. Column chromatography was performed using a Teledyne Isco Combiflash® Rf+ automated column machine with Redisep® silica gel-packed columns or performed manually using Merck silica gel 60 (particle size 0.040-0.063 mm) with one of or combinations of hexane, EtOAc, DCM or MeOH as the mobile phase.

8.1.3. Spectroscopic and physical data

NMR spectra (^{1}H, ^{13}C) were recorded on a 300 MHz Varian VNMRS (75 MHz for ^{13}C), a 400 MHz Varian INOVA (101 MHz for ^{13}C), a 400 MHz Varian VNMRS, a 500 MHz Varian INOVA (126 MHz for ^{13}C) or a 600 MHz Varian INOVA (150 MHz for ^{13}C). Chemical shifts (δ) are reported in ppm and *J* - values are given in Hz. Multiplicities are reported as a singlet (s), doublet (d), triplet (t), quartet (q), multiplet (m) or doublet of doublet (dd). Chemical shifts were recorded using the residual solvent peak or external reference. All spectra were obtained at 25 °C unless otherwise reported. Spectroscopic data were processed using

MestReNova v6.0.2. Mass spectrometry was performed by the Central Analytical Facilities (CAF) of Stellenbosch University on a Waters SYNAPT G2 instrument, using a diode array as the detection method, or by the Emory University Mass Spectroscopy Center. Infrared spectra were recorded on a Thermo Nicolet Nexus 470 by means of Attenuated Total Reflectance (ATR) mode. Melting points were obtained using a Gallenkamp Melting Point Apparatus. Melting points are reported as an average. Purity was determined by LC-MS analysis performed on an Agilent 1200 HPLC equipped with a 6120 Quadrupole mass spectrometer (ESI-API) using mixtures of HPLC grade MeOH/H_2O (spiked with 0.1% formic acid). The purity of all final compounds was found to be >95%.

8.1.4. Other general procedures

The molarity of *n*-BuLi was determined by titration with *N*-benzylbenzamide, as described in the literature.[283] All reactions requiring inert conditions were carried out under a positive atmosphere of argon. All glassware was flame-dried while under vacuum or oven dried overnight before purging with argon. Standard Schlenk techniques were employed when necessary. Solvents were removed using a rotary evaporator followed by the removal of trace amounts of solvent using a high vacuum pump at ca. 0.08 mm Hg.

8.2. General procedures pertaining to metabolic stability tests

8.2.1. Human Liver Microsomes

Pooled mixed gender human liver microsomes at a concentration of 20 mg/mL were purchased from XenoTech (Kansas City, KS). The vials of microsomes were stored at -80 °C and thawed on ice before each experiment. The microsomes were diluted to 1 mg/mL with 100 mM potassium phosphate buffer (pH 7.4).

8.2.2. Mouse Liver Microsomes

Pooled CD-1 mouse liver microsomes at a concentration of 20 mg/mL were purchased from XenoTech (Kansas City, KS). The vials of microsomes were stored at -80 °C and thawed on ice before each experiment. The microsomes were diluted to 1 mg/mL with 100 mM potassium phosphate buffer (pH 7.4).

8.2.3. Experimental Conditions

Test compounds were weighed and dissolved in 100% acetonitrile to make 2 mM stock solutions. Verapamil (human, Sigma Aldrich) and diphenhydramine (mouse, Sigma Aldrich) served as positive controls and were dissolved in 100% acetonitrile to make 2 mM stock solutions. The 2 mM stock solution of test and control compounds were further diluted in sodium phosphate buffer (100 mM, pH 7.4) to 50 µM to ensure the acetonitrile content was < 0.2%.

The liver microsome assay was prepared in a 1.5 mL Eppendorf tube (Fisher Scientific) with a final volume of 1100 µL. Each reaction contained sodium phosphate buffer, liver microsomes (1 mg/mL), and test compound resulting in a final concentration of 3 µM. Following a 5 min preincubation of drug and microsomes in a 37 °C shaking incubator, the reaction was initiated with NADPH (110 µL). Aliquots (100 µL) were removed in duplicate at 0, 5, 10, 15, and 30 min time intervals and quenched in cold acetonitrile (200 µL). The aliquots were centrifuged at 12,000 *g* for 5 min and the supernatant removed and placed in an LCMS vial. Positive controls were conducted at a final volume of 600 µL to give each time point in a singlet run. A no NADPH negative control with test and control compound was conducted in singlet (150 µL) at the longest time point. Controls were processed and analysed like test compounds.

8.2.4. LC/MS Analysis

Analysis was performed on an Agilent Technologies LCMS system consisting of an Agilent 6120 quadrupole mass spectrometer equipped with an Agilent 1200 binary pump, degasser, and auto sampler (Santa Clara, CA). The analytical column used for analysis was an Ascentis column (5 cm x 2.1 mm, 2.7 µm particle size; Sigma Aldrich). The mobile phase for the HPLC was 25 mM ammonium formate buffer, pH 3.5 (A) and

acetonitrile (B). The samples were analysed using the following 8-minute method: A linear gradient from 10% B to 95% B for 5 minutes, with a 3 min hold at 95%. An equilibration at 10% B for 5 min was conducted after each run. Sample injection volume was 15 µL and the flow rate was 0.35 µL/min. Single ion monitoring of the mass in negative mode was conducted for the samples at 312 and 327 m/z. Each time point was assessed on the LCMS and the area, based on the extracted ion in negative ion mode, was manually integrated. The relative percent remaining was calculated using: Relative % remaining = $Area_{Time}/Area_{Time=0}$ *100.

8.3. Experimental pertaining to Chapter 2

8.3.1. Synthesis of (±)-1-(phenyl)propanol (17)

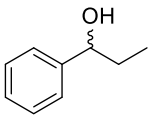

Ethyl iodide (0.75 mL, 9.4 mmol) was added dropwise to a suspension of magnesium turnings (229 mg, 9.42 mmol) in Et_2O (5 mL). Once all the magnesium turnings had been consumed, benzaldehyde (0.96 mL, 9.4 mmol) in Et_2O (5 mL) was added to the mixture dropwise at 0 °C. The reaction was then carried out at room temperature for 2 hours after which the reaction was quenched with a 2M solution of HCl (20 mL) and extracted twice with Et_2O (2 × 50 mL). The organic phase was washed with brine, dried over $MgSO_4$ and concentrated *in vacuo*. The crude product was then purified by column chromatography (5% – 20% EtAOc/hexane) to yield the product **17** as a colourless oil (1.08 g, 7.90 mmol, 84%).

Rf, 0.35 (20% EtOAc/Hexane) **^{1}H NMR (300 MHz, $CDCl_3$) δ** 7.41 – 7.26 (m, 5H, Ar*H*), 4.58 (t, *J* = 6.6 Hz, 1H, C*H*), 2.43 (s, 1H, O*H*), 1.92 – 1.68 (m, 2H, CH_2), 0.94 (t, *J* = 7.4 Hz, 3H, CH_3). **^{13}C NMR (75 MHz, $CDCl_3$) δ** 144.7, 128.4, 127.5, 126.1, 76.0, 31.9, 10.2.

This spectroscopic data compares favourably with that in the literature.[157]

8.3.2. Synthesis of (±)-(1-iodopropyl)benzene (14)[158]

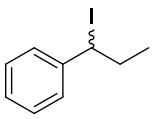

$BF_3{\cdot}Et_2O$ (0.70 mL, 5.7 mmol) and KI (949 mg, 5.72 mmol) were added to **17** (773 mg, 5.72 mmol) in dioxane (10 mL) and the reaction was carried out at room temperature for 18 hours. The reaction mixture was quenched with ice cold H_2O (20 mL) and extracted twice with Et_2O (2 × 50 mL). The organic phases were combined, washed with brine (100 mL), dried over $MgSO_4$ and then concentrated *in vacuo*. The product was then purified by column chromatography (5% EtOAc/hexane – 20% EtAOc/hexane) to yield **14** as a red oil (938 mg, 3.83 mmol, 67%).

Rf, 0.68 (20% EtOAc/Hexane) **^{1}H NMR (300 MHz, $CDCl_3$) δ** 7.42 – 7.19 (m, 5H, Ar*H*), 5.04 (t, *J* = 7.6 Hz, 1H, C*H*), 2.44 – 2.25 (m, 1H, CH_2), 2.15 – 1.98 (m, 1H, CH_2), 0.96 (t, *J* = 7.2 Hz, 3H, CH_3). **^{13}C NMR (75 MHz, $CDCl_3$) δ** 144.1, 128.8, 128.0, 127.2, 36.7, 34.9, 14.9.

This spectroscopic data is in accordance with that in the literature.[159]

8.3.3. Synthesis of (±)-5-chloro-2-nitro-N-(1-phenylpropyl)aniline (15)

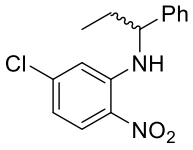

NaH (60% in mineral oil, 46 mg, 1.2 mmol) was added to 5-chloro-2-nitroaniline (**13**) (100 mg, 575 µmol) in THF (3 mL) at 0 °C. The reaction was carried out for 30 minutes before (1-iodopropyl)benzene (**14**) (169 mg, 690 µmol) was added. The reaction was then carried out at room temperature for 18 hours after which NH_4Cl (50 mL) was added to quench the reaction mixture. The crude product was extracted twice with EtOAc (2 × 50 mL), the organic phases were then combined and washed with brine (100 mL), dried over $MgSO_4$ and the solvent was removed *in vacuo*. Purification was carried out by column chromatography (5% – 20% EtOAc/hexane) to yield **15** as a yellow wax (147 mg, 506 µmol, 88%).

Rf, 0.51 (20% EtOAc/Hexane) **^{1}H NMR (400 MHz, $CDCl_3$) δ** 8.57 (d, *J* = 5.4 Hz, 1H, N*H*), 8.10 (d, *J* = 9.1 Hz, 1H, Ar*H*), 7.40 – 7.24 (m, 5H, Ar*H*), 6.64 (d, *J* = 2.1 Hz, 1H, Ar*H*), 6.55 (dd, *J* = 9.1, 2.1 Hz, 1H, Ar*H*), 4.44 – 4.34 (m, 1H, C*H*), 2.05 – 1.86 (m, 2H, CH_2), 1.01 (t, *J* = 7.4 Hz, 3H, CH_3). **^{13}C NMR (101 MHz, $CDCl_3$) δ** 145.4, 142.7, 141.7, 130.9, 129.1, 128.3, 127.8, 126.3, 116.3, 114.6, 59.6, 31.7, 10.8. **HRMS** calc. for $C_{15}H_{16}ClN_2O_2$ $[M+H]^+$, 291.0900 found, 291.0901. **IR ATR (cm^{-1}):** 3366, 2924, 1522, 1487, 1330, 1021, 699.

8.3.4. Synthesis of (±)-5-chloro-N1-(1-phenylpropyl)benzene-1,2-diamine (16)[160]

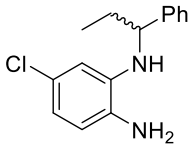

Iron powder (138 mg, 2.47 mmol) was added to **15** (144 mg, 495 µmol) in a mixture of glacial acetic acid (2 mL), ethanol (2 mL) and water (1 mL). The reaction mixture was then exposed to ultrasonic irradiation for 2 hours at 30 °C and monitored by TLC. When all starting material had been consumed, the reaction mixture was filtered through celite and the filtrate was neutralized with a 1 M KOH solution (20 mL). The filtrate was then extracted thrice with EtOAc (3 × 50 mL) and the combined organic phases were washed with brine (200 mL), dried over $MgSO_4$ and concentrated *in vacuo*. The crude product was then purified by column chromatography (5 – 40% EtOAc/Hexane) to yield the diamine product **16** as a dark brown solid (100 mg, 384 µmol, 78%).

Rf, 0.30 (20% EtOAc/Hexane) **^{1}H NMR (400 MHz, $CDCl_3$) δ** 7.40 – 7.19 (m, 5H, Ar*H*), 6.66 – 6.51 (m, 2H, Ar*H*), 6.39 (d, *J* = 2.0 Hz, 1H, Ar*H*), 5.08 (s, 3H, N*H*), 4.19 (t, *J* = 6.6 Hz, 1H, C*H*), 1.95 – 1.77 (m, 2H, CH_2), 0.95 (t, *J* = 7.3 Hz, 3H, CH_3). **^{13}C NMR (101 MHz, $CDCl_3$) δ** 143.2, 138.7, 132.0, 128.7, 127.3, 126.6, 126.2, 117.8, 117.6, 112.8, 59.9, 31.7, 10.9.

*Unable to obtain HRMS of this compound due to degradation.

8.3.5. Synthesis of (±)-6-chloro-1-(1-phenylpropyl)-1,3-dihydro-2*H*-benzo[*d*]imidazol-2-one (11)

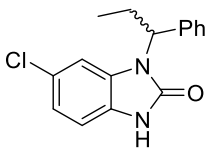

CDI (47 mg, 0.29 mmol) was added to **16** (50 mg, 0.19 mmol) in THF (2 mL). The reaction was carried out at room temperature for 18 hours after which the reaction was quenched with H_2O (20 mL) and the product was extracted twice with EtOAc (2 × 20 mL). The organic phase was then washed with brine (50 mL), dried over $MgSO_4$ and concentrated *in vacuo*. Purification of the crude material by column chromatography (10% – 40% EtOAc/hexane) yielded the product **11** as a white solid (40 mg, 0.14 mmol, 73%).

Rf, 0.29 (40% EtOAc/Hexane) **^{1}H NMR (300 MHz, $CDCl_3$) δ** 10.54 (s, 1H, N*H*), 7.46 – 7.27 (m, 5H, Ar*H*), 7.08 – 6.99 (m, 2H), 6.84 (d, *J* = 1.5 Hz, 1H, Ar*H*), 5.57 (dd, *J* = 9.9, 6.3 Hz, 1H, C*H*), 2.53 – 2.39 (m, 2H, CH_2), 1.01 (t, *J* = 7.3 Hz, 3H, CH_3). **^{13}C NMR (75 MHz, $CDCl_3$) δ** 156.5, 139.0, 130.0, 128.9, 127.9, 127.2, 126.9, 126.7, 121.6, 110.5, 110.2, 57.4, 24.1, 11.4. **HRMS** calc. for $C_{16}H_{16}ClN_2O$ $[M+H]^+$, 287.0951 found, 287.0951. **IR ATR (cm^{-1}):** 3135, 2964, 2837, 1684, 1479, 1059. **Mp:** 190 °C

8.3.6. Synthesis of (±)-6-chloro-1-(1-phenylpropyl)-1,3-dihydro-2*H*-benzo[*d*]imidazole-2-thione (20)

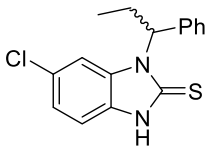

TCDI (51 mg, 0.29 mmol) was added to **16** (50 mg, 0.19 mmol) in THF (5 mL). The reaction was carried out at room temperature for 18 hours after which the reaction mixture was concentrated *in vacuo*. The crude mixture was purified by silica gel column chromatography (5% – 20% EtOAc/Hexane) to yield the product **20** as an off-white solid (53 mg, 0.18 mmol, 91%).

Rf, 0.58 (40% EtOAc/Hexane) **^{1}H NMR (300 MHz, $CDCl_3$) δ** 11.73 (s, 1H, N*H*), 7.48 – 7.06 (m, 7H, Ar*H*), 6.96 – 6.91 (m, 1H, Ar*H*), 6.60 – 6.51 (m, 1H, C*H*), 2.67 – 2.35 (m, 2H, CH_2), 1.01 (t, *J* = 7.2 Hz, 3H, CH_3). **^{13}C NMR (75 MHz, $CDCl_3$) δ** 170.4, 138.0, 131.8, 129.5, 129.0, 128.5, 128.2, 127.2, 123.6, 111.3, 110.9, 59.6, 23.8, 11.1. **HRMS** calc. for $C_{16}H_{16}ClN_2S$ $[M+H]^+$, 303.0723 found, 303.0721.

8.4. Experimental pertaining to Chapter 3

8.4.1. Synthesis of 2-((3,5-dimethylphenyl)amino)-3-nitrophenol (32)[180]

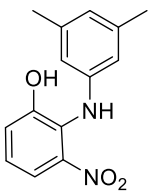

DMSO (3 mL) was added to a Schlenk tube charged with 2-amino-3-nitrophenol (**23**) (1.00 g, 6.49 mmol), K_3PO_4 (2.75 g, 13.0 mmol), 2-picolinic acid (160 mg, 1.30 mmol) and 5-iodo-*m*-xylene (**25**) (2.80 mL, 19.5 mmol). The reaction mixture was then degassed for approximately 15 minutes under a positive flow of argon before the addition of CuI (124 mg, 649 µmol). The reaction was then heated to 85 °C and run for 18 hours after which the reaction was cooled to room temperature, diluted with EtOAc (50 ml) and quenched with H_2O (50 mL). The aqueous layer was separated and twice extracted with EtOAc (2 × 100 mL). The organic phases were then combined, washed with brine (200 mL) and dried over $MgSO_4$. The organic phase was then concentrated *in vacuo* and purified by silica gel column chromatography (5% – 30% EtOAc/Hexane) to give the undesired product **32** as a purple solid (1.51 g, 5.85 mmol, 89%).

Rf, 0.35 (20% EtOAc/Hexane) **^{1}H NMR (300 MHz, $CDCl_3$) δ** 7.70 (dd, *J* = 8.2, 1.5 Hz, 1H, Ar*H*), 7.33 (s, 1H, N*H* or O*H*), 7.29 (d, *J* = 1.3 Hz, 1H, Ar*H*), 7.22 – 7.15 (m, 1H, Ar*H*), 6.64 (s, 1H, Ar*H*), 6.39 (s, 2H, Ar*H*), 5.67 (s, 1H, N*H* or O*H*), 2.24 (s, 6H, CH_3). **^{13}C NMR (75 MHz, $CDCl_3$) δ** 152.2, 141.9, 139.8, 125.7, 125.6, 124.7, 124.5, 121.5, 119.3, 117.8, 21.5. **HRMS** calc. for $C_{14}H_{15}N_2O_3$ $[M+H]^+$, 259.1083 found, 259.1071. **IR ATR (cm^{-1}):** 3429, 2913, 1598, 1518, 1247, 1137. **Mp:** 100 °C.

8.4.2. Synthesis of 2-(benzyloxy)-6-nitroaniline (33)

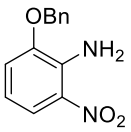

Benzyl bromide (1.85 mL, 15.6 mmol) was added to a mixture of 2-amino-3-nitrophenol (**23**) (2.00 g, 13.0 mmol) and K_2CO_3 (3.59 g, 26.0 mmol) in DMF (40 mL) at -10 ˚C (acetone/ice bath). The reaction was then warmed to room temperature and carried out for 18 hours after which the reaction mixture was quenched with NH_4Cl (50 mL) and then extracted three times with EtOAc (3 × 100 mL). The organic phases were combined, washed with brine (300 mL) and dried over $MgSO_4$. The organic phases were then concentrated *in vacuo* and the product was purified by silica gel column chromatography (5% – 20% EtOAc/Hexane) to yield the benzylated product **33** as an orange solid (3.01 g, 12.3 mmol, 95%).

Rf, 0.31 (20% EtOAc/Hexane) **^{1}H NMR (300 MHz, $CDCl_3$) δ** 7.73 (dd, *J* = 8.9, 1.2 Hz, 1H, Ar*H*), 7.48 – 7.33 (m, 5H, Ar*H*), 6.96 (dd, *J* = 7.7, 0.8 Hz, 1H, Ar*H*), 6.61 – 6.54 (m, 1H, Ar*H*), 6.46 (s, 2H, NH_2), 5.12 (s, 2H, CH_2). **^{13}C NMR (75 MHz, $CDCl_3$) δ** 147.3, 137.3, 135.9, 131.8, 128.8, 128.6, 127.8, 117.7, 115.0, 114.6, 71.3. **HRMS** calc. for $C_{13}H_{13}N_2O_3$ $[M+H]^+$, 245.0926 found, 245.0918. **IR ATR (cm^{-1}):** 3506, 3391, 3031, 1621, 1519, 1202. **Mp:** 55 °C.

8.4.3. Synthesis of 2-(benzyloxy)-*N*-ethyl-6-nitroaniline (34)

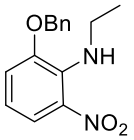

Conditions A: NaH (60% in mineral oil, 197 mg, 4.91 mmol) was added to **33** (1.00 g, 4.09 mmol) in THF (10 mL). After approximately 30 minutes ethyl iodide (0.40 mL, 4.9 mmol) was added to the reaction mixture and the reaction was carried out at room temperature for 18 hours after which the reaction mixture was quenched with NH_4Cl (100 mL) and extracted twice with EtOAc (2 × 100 mL). The organic phase was dried over $MgSO_4$ and then concentrated *in vacuo*. The crude material was then purified by silica gel column chromatography (5% EtOAc/Hexane) to yield the product **34** as a red solid (472 mg, 1.73 mmol, 42%).

Conditions B: NaH (291 mg, 7.27 mmol) was added to **33** (1.48 g, 6.06 mmol) in THF (15 mL). After approximately 30 minutes diethyl sulfate (0.95 mL, 7.3 mmol) was added to the reaction mixture. After 18 hours the reaction mixture was quenched with aqueous NH_4OH solution (100 mL) and then extracted twice with EtOAc (2 × 150 mL). The organic phase was dried over $MgSO_4$ and then concentrated *in vacuo*. The crude material was purified by silica gel column chromatography (5% – 40% EtOAc/Hexane) to afford **34** (1.06 g, 3.89 mmol, 64%).

Conditions C: Using the reaction conditions described for conditions B, but with DMF as the solvent, the product **34** was obtained in 81% yield.

Rf, 0.40 (20% EtOAc/Hexane) **^{1}H NMR (400 MHz, $CDCl_3$) δ** 7.73 (dd, *J* = 8.8, 1.4 Hz, 1H, Ar*H*), 7.54 (s, 1H, N*H*), 7.45 – 7.33 (m, 5H, Ar*H*), 6.98 (dd, *J* = 7.8, 1.4 Hz, 1H, Ar*H*), 6.59 (dd, *J* = 8.7, 7.9 Hz, 1H, Ar*H*), 5.07 (s, 2H, CH_2), 3.57 (q, 2H, *J* = 7.1 Hz, CH_2), 1.18 (t, *J* = 7.2 Hz, 3H, CH_3). **^{13}C NMR (75 MHz, $CDCl_3$) δ** 150.0, 139.0, 136.2, 135.5, 128.9, 128.5, 127.9, 119.2, 117.8, 115.7, 72.0, 41.9, 16.7, 0.2. **HRMS** calc. for $C_{15}H_{17}N_2O_3$ $[M+H]^+$, 273.1239 found, 273.1229. **IR ATR (cm^{-1}):** 3323, 2978, 2361, 1609, 1510, 1345, 1241, 1169. **Mp:** 49 °C.

8.4.4. Synthesis of 4-(benzyloxy)-1-ethoxy-2-methyl-1*H*-benzo[*d*]imidazole (46)

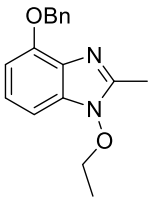

NaH (60% in mineral oil, 146 mg, 3.64 mmol) was added to **33** (222 mg, 9.09 µmol) in THF (5 mL). After approximately 30 minutes ethyl iodide (0.29 mL, 3.6 mmol) was added to the reaction mixture and the reaction was carried out at room temperature for 18 hours after which the reaction mixture was quenched with NH_4Cl (50 mL) and extracted twice with EtOAc (2 × 50 mL). The organic phase was dried over $MgSO_4$ and then concentrated *in vacuo*. The crude material was then purified by silica gel column chromatography (5% EtOAc/Hexane) to yield the product **46** as a brown oil (109 mg, 386 µmol, 42%).

Rf, 0.22 (40% EtOAc/Hexane) **^{1}H NMR (300 MHz, $CDCl_3$) δ** 7.53 – 7.45 (m, 2H, Ar*H*), 7.36 – 7.24 (m, 2H, Ar*H*), 7.10 – 7.04 (m, 1H, Ar*H*), 6.96 (d, *J* = 8.1 Hz, 1H, Ar*H*), 6.65 (d, *J* = 7.9 Hz, 1H, Ar*H*), 5.33 (s, 2H, CH_2), 4.26 (q, *J* = 7.1 Hz, 2H, CH_2), 2.59 (s, 3H, CH_3), 1.40 (t, *J* = 7.1 Hz, 3H, CH_3). **^{13}C NMR (75 MHz, $CDCl_3$) δ** 150.2, 146.5, 137.2, 132.4, 128.6, 128.4, 127.7, 127.4, 123.2, 104.8, 101.3, 74.1, 70.6, 13.7, 12.4. **HRMS** calc. for $C_{17}H_{19}N_2O_2$ $[M+H]^+$, 283.1447 found, 283.1441. **IR ATR (cm^{-1}):** 2977, 1593, 1330, 1238, 733.

8.4.5. Synthesis of 3-(benzyloxy)-*N*^{2}-ethylbenzene-1,2-diamine (35)

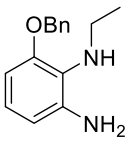

Conditions A: Iron powder (555 mg, 9.93 mmol) was added to **34** (541 mg, 1.99 mmol) in a mixture of glacial acetic acid (4 mL), ethanol (4 mL) and water (2 mL). The reaction mixture was then exposed to ultrasonic irradiation for 2 hours at 30 °C and monitored by TLC. When all starting material had been consumed, the reaction mixture was filtered through celite and the filtrate neutralized with 1 M KOH solution (20 mL). The filtrate was extracted thrice with EtOAc (3 × 100 mL). The combined organic phases were washed with brine (300 mL), dried over $MgSO_4$ and concentrated *in vacuo*. The crude product was purified by column chromatography (10% – 40% EtOAc/Hexane) to yield the reduced product **35** as an orange oil (382 mg, 1.58 mmol, 79%).

Conditions B: Tin(II) chloride dihydrate (10.5 g, 46.6 mmol) was added to **34** (1.27 g, 4.66 mmol) dissolved in EtOH (20 mL). The reaction mixture was then exposed to ultrasonic radiation for approximately 15 minutes after which TLC confirmed that all starting material had been consumed. The reaction mixture was then basified with 1 M KOH solution (200 mL) and extracted three times with DCM (3 × 200 mL). The organic phases were combined, washed with brine (500 mL), dried over $MgSO_4$ and concentrated *in vacuo*. The crude product was purified by column chromatography (10% – 40% EtOAc/hexane) to yield the reduced product **35** as an orange oil (924 mg, 3.81 mmol, 82%).

Rf, 0.44 (40% EtOAc/Hexane) **^{1}H NMR (300 MHz, $CDCl_3$) δ** 7.47 – 7.31 (m, 5H, Ar*H*), 6.90 – 6.83 (m, 1H, Ar*H*), 6.45 – 6.39 (m, 2H, Ar*H*), 5.41 (s, 3H, N*H*), 5.08 (s, 2H, CH_2), 3.06 (q, *J* = 7.2 Hz, 2H, CH_2), 1.19 (t, *J* = 7.2 Hz, 3H, CH_3). **^{13}C NMR (75 MHz, $CDCl_3$) δ** 152.7, 142.1, 137.3, 128.6, 128.0, 127.4, 124.3, 122.8, 109.6, 102.4, 70.6, 42.0, 15.5. **HRMS** calc. for $C_{15}H_{19}N_2O$ $[M+H]^+$, 243.1497 found, 243.1506. **IR ATR (cm^{-1}):** 3425, 3341, 2965, 1615, 1591, 1450, 1254, 728.

8.4.6. Synthesis of 4-(benzyloxy)-3-ethyl-1*H*-benzo[*d*]imidazol-2-one (36)

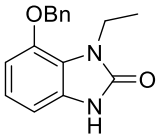

Conditions A: Carbonyldiimidazole (243 mg, 1.44 mmol) was added to **35** (175 mg, 722 µmol) in THF (10 mL) at 0°C. The reaction was allowed to warm to room temperature and was carried out for 18 hours. The reaction was monitored by TLC and upon completion the reaction mixture was concentrated *in vacuo* and then purified by silica gel column chromatography (10% – 80% EtOAc/Hexane) to yield the desired benzimidazolone product **36** as a pale pink solid (128 mg, 477 µmol, 66%).

Conditions B: CDI (583 mg, 3.59 mmol) was added to **35** (871 mg, 3.59 mmol) in MeCN (15 mL) at room temperature. After 18 hours the resulting white precipitate was filtered off and dried under vacuum. No additional purification was required and **36** was obtained as a white solid (649 mg, 2.70 mmol, 75%).

Rf, 0.11 (40% EtOAc/Hexane) **^{1}H NMR (300 MHz, $CDCl_3$) δ** 10.38 (s, 1H, N*H*), 7.48 – 7.32 (m, 5H, Ar*H*), 7.01 – 6.94 (m, 1H, Ar*H*), 6.81 (dd, *J* = 7.9, 0.8 Hz, 1H, Ar*H*), 6.71 (dd, *J* = 8.3, 0.6 Hz, 1H, Ar*H*), 5.17 (s, 2H, CH_2), 4.16 (q, *J* = 7.1 Hz, 2H, CH_2), 1.31 (t, *J* = 7.1 Hz, 3H, CH_3). **^{13}C NMR (75 MHz, $CDCl_3$) δ** 155.6, 144.3, 136.8, 129.7, 128.8, 128.3, 127.5, 121.9, 118.7, 105.5, 103.7, 70.9, 37.8, 15.8. **HRMS** calc. for $C_{16}H_{17}N_2O_2$ $[M+H]^+$, 269.1290 found, 269.1293. **IR ATR (cm^{-1}):** 2969, 1681, 1626, 1470, 1237, 1117. **Mp:** 213 °C.

8.4.7. Synthesis of 4-(benzyloxy)-3-ethyl-1-((2-(trimethylsilyl)ethoxy)methyl)-1*H*-benzo[*d*]imidazol-2(3*H*)-one (37)

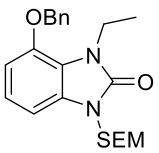

NaH (76 mg, 1.6 mmol) was added to **36** (213 mg, 0.794 mol) in DMF (5 mL) at 0 °C. The reaction was stirred for approximately 1 hour before 2-(trimethylsilyl)ethoxymethyl chloride (0.28 mL, 1.6 mmol) was added to the reaction mixture dropwise. The reaction was carried out at room temperature for 18 hours. The reaction was quenched with H_2O (20 mL) and extracted twice with EtOAc (2 × 50 mL). The organic phases were combined, washed with brine (100 mL),

dried over $MgSO_4$ and concentrated *in vacuo*. The crude product was purified on silica gel by column chromatography (5% – 30% EtOAc/Hexane) to yield the product as a clear oil (258 mg, 0.647 mmol, 82%).

Rf, 0.53 (40% EtOAc/Hexane) **^{1}H NMR (400 MHz, $CDCl_3$) δ** 7.47 – 7.33 (m, 5H, Ar*H*), 7.03 – 6.98 (m, 1H, Ar*H*), 6.85 (dd, *J* = 7.9, 0.8 Hz, 1H, Ar*H*), 6.76 (dd, *J* = 8.4, 0.7 Hz, 1H, Ar*H*), 5.30 (s, 2H, CH_2), 5.17 (s, 2H, CH_2), 4.14 (q, *J* = 7.0 Hz, 2H, CH_2), 3.63 – 3.58 (m, 2H, CH_2), 1.28 (t, *J* = 7.1 Hz, 3H, CH_3), 0.96 – 0.88 (m, 2H, CH_2), -0.03 (s, 9H, Si(CH_3)$_3$). **^{13}C NMR (101 MHz, $CDCl_3$) δ** 154.1, 144.2, 136.7, 130.5, 128.8, 128.3, 127.5, 121.8, 117.9, 106.3, 102.7, 70.9, 70.9, 66.2, 38.1, 17.9, 15.6, -1.3. **HRMS** calc. for $C_{22}H_{31}N_2O_3Si$ $[M+H]^+$, 399.2104 found, 399.2104. **IR ATR (cm^{-1}):** 2951, 2894, 1702, 1477, 1245, 1078, 833.

8.4.8. Synthesis of 3-ethyl-4-hydroxy-1-((2-(trimethylsilyl)ethoxy)methyl)-1*H*-benzo[*d*]imidazol-2(3*H*)-one (38)

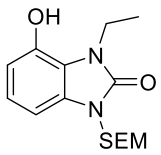

A catalytic amount of Pd/C was added to **37** (250 mg, 627 µmol) in EtOH (5 mL). The reaction was then carried out for 18 hours under an atmosphere of hydrogen after which the reaction mixture was run through celite and concentrated *in vacuo*. The crude mixture was purified on silica gel by column chromatography (5% – 30% EtOAc/Hexane) to yield the product **38** as a pink solid (140 mg, 454 µmol, 73%).

Rf, 0.44 (40% EtOAc/Hexane) **^{1}H NMR (300 MHz, $CDCl_3$) δ** 6.99 (br s, 1H, O*H*), 6.96 – 6.89 (m, 1H, Ar*H*), 6.78 (dd, *J* = 7.9, 0.9 Hz, 1H, Ar*H*), 6.66 (dd, *J* = 8.1, 0.9 Hz, 1H, Ar*H*), 5.32 (s, 2H, CH_2), 4.21 (q, *J* = 7.1 Hz, 2H, CH_2), 3.67 – 3.57 (m, 2H, CH_2), 1.37 (t, *J* = 7.1 Hz, 3H, CH_3), 0.98 – 0.87 (m, 2H, CH_2), -0.05 (s, 9H, Si(CH_3)$_3$). **^{13}C NMR (75 MHz, $CDCl_3$) δ** 154.4, 141.7, 130.8, 122.1, 116.8, 110.1, 101.8, 70.9, 66.3, 38.2, 18.0, 15.7, -1.3. **HRMS** calc. for $C_{15}H_{25}N_2O_3Si$ $[M+H]^+$, 309.1634 found, 309.1631. **IR ATR (cm^{-1}):** 3144, 2953, 1673, 1075. **IR ATR (cm^{-1}):** 3176, 2953, 1664, 1483, 1071, 777. **Mp:** 116 °C.

8.4.9. Synthesis of 3-ethyl-4-phenoxy-1-((2-(trimethylsilyl)ethoxy)methyl)-1,3-dihydro-2*H*-benzo[*d*]imidazol-2-one (39)

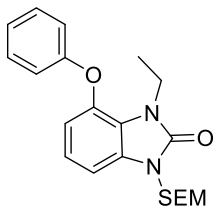

DMSO (2 mL) was added to a Schlenk tube charged with **38** (200 mg, 648 µmol), K_3PO_4 (275 mg, 1.30 mmol), 2-picolinic acid (16 mg, 0.13 mmol) and iodobenzene (**24**) (0.20 mL, 1.8 mmol) and the reaction mixture was degassed under a positive flow of argon for approximately 15 minutes prior to the addition of CuI (12 mg, 63 µmol). The

reaction mixture was then heated to 90 °C and run for 18 hours after which the reaction was cooled to room temperature, diluted with EtOAc (50 mL) and quenched with H_2O (100 mL). The aqueous layer was separated and extracted twice with EtOAc (2 × 100 mL). The organic phases were then combined, washed with brine (200 mL) and dried over $MgSO_4$. The organic phase was then concentrated *in vacuo* and purified by silica gel column chromatography (5% – 30% EtOAc/Hexane) to give the product **39** as a clear oil (174 mg, 453 µmol, 70%).

Rf, 0.41 (20% EtOAc/Hexane) **^{1}H NMR (500 MHz, $CDCl_3$) δ** 7.37 – 7.32 (m, 2H, Ar*H*), 7.13 – 7.09 (m, 1H, Ar*H*), 7.03 – 6.96 (m, 4H, Ar*H*), 6.69 (dd, *J* = 8.0, 1.2 Hz, 1H, Ar*H*), 5.33 (s, 2H, CH_2), 4.03 (q, *J* = 7.1 Hz, 2H, CH_2), 3.66 – 3.60 (m, 2H, CH_2), 1.27 (t, *J* = 7.1 Hz, 3H, CH_3), 0.98 – 0.90 (m, 2H, CH_2), -0.02 (s, 9H, Si(CH_3)$_3$). **^{13}C NMR (126 MHz, $CDCl_3$) δ** 157.7, 154.2, 140.4, 131.3, 130.1, 123.4, 121.9, 120.6, 117.8, 113.8, 104.8, 71.0, 66.3, 38.0, 18.0, 15.3, -1.3. **HRMS** calc. for $C_{21}H_{29}O_3N_2Si$ $[M+H]^+$, 385.19420 found, 385.19413.

8.4.10. Synthesis of 4-(3,5-dimethylphenoxy)-3-ethyl-1-((2-(trimethylsilyl)ethoxy)methyl)-1,3-dihydro-2*H*-benzo[*d*]imidazol-2-one (40)

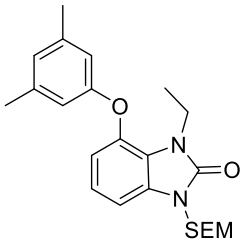

This reaction was carried out according to the procedure described for **39** using the following: **38** (200 mg, 648 µmol), K_3PO_4 (275 mg, 1.30 mmol), 2-picolinic acid (16 mg, 0.13 mmol), 5-iodo-*m*-xylene (**25**) (0.30 mL, 2.1 mmol) and CuI (12 mg, 63 µmol). The reaction yielded **40** as a clear oil (163 mg, 395 µmol, 61%).

Rf, 0.46 (20% EtOAc/Hexane) **^{1}H NMR (500 MHz, $CDCl_3$) δ** 7.02 – 6.99 (m, *J* = 8.0 Hz, 1H, Ar*H*), 6.96 (dd, *J* = 7.8, 1.1 Hz, 1H, Ar*H*), 6.76 – 6.74 (m, 1H, Ar*H*), 6.68 (dd, *J* = 8.1, 1.1 Hz, 1H, Ar*H*), 6.63 – 6.61 (m, 2H, Ar*H*), 5.33 (s, 2H, CH_2), 4.03 (q, *J* = 7.1 Hz, 2H, CH_2), 3.67 – 3.61 (m, *J* = 10.9, 5.5 Hz, 2H, CH_2), 2.29 (s, 6H, (CH_3)$_2$), 1.28 (t, *J* = 7.1 Hz, 3H, CH_3), 0.97 – 0.91 (m, 2H, CH_2), -0.02 (s, 9H, Si(CH_3)$_3$). **^{13}C NMR (126 MHz, $CDCl_3$) δ** 157.6, 154.2, 140.6, 139.9, 131.2, 125.2, 121.9, 120.5, 115.5, 113.8, 104.6, 71.0, 66.3, 38.0, 21.5, 18.0, 15.3, -1.3. **HRMS** calc. for $C_{23}H_{33}O_3N_2Si$ $[M+H]^+$, 413.22550 found, 413.22535.

8.4.11. Synthesis of 1-ethyl-7-phenoxy-1,3-dihydro-2*H*-benzo[*d*]imidazol-2-one (21)

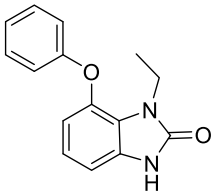

A solution of tetrabutylammonium fluoride (TBAF) (1.0 M in THF, 0.60 mL, 2.1 mmol) was added dropwise to a solution of **39** (68 mg, 0.18 mmol) in THF (0.5 mL) and the reaction was heated to 60 °C. After 18 hours the reaction was cooled to room temperature, diluted with EtOAc (50 mL) and washed with brine (50 mL). The organic phase was then dried over $MgSO_4$, concentrated *in vacuo* and then purified by column chromatography (40% – 100% EtOAc/Hexane) to afford compound **21** as a white solid (8.0 mg, 0.021 mmol, 18%).

Rf, 0.43 (100% EtOAc/Hexane) **^{1}H NMR (500 MHz, $CDCl_3$) δ** 11.07 (s, 1H, N*H*), 7.37 – 7.32 (m, 2H, Ar*H*), 7.14 – 7.09 (m, 1H, Ar*H*), 7.04 – 6.96 (m, 4H, Ar*H*), 6.69 – 6.64 (m, 1H, Ar*H*), 4.07 (q, *J* = 7.1 Hz, 2H, CH_2), 1.33 (t, *J* = 7.1 Hz, 3H, CH_3). **^{13}C NMR (126 MHz, CDCl3) δ** 157.7, 155.9, 140.4, 130.6, 130.0, 123.3, 121.9, 121.3, 117.7, 113.0, 105.9, 37.7, 15.4. **HRMS** calc. for $C_{15}H_{15}O_2N_2$ $[M+H]^+$, 255.11280 found, 255.11283. **IR ATR (cm^{-1}):** 3162, 2978, 1692, 1501, 1230, 744. **Mp:** 137 °C.

8.4.12. Synthesis of 3-ethyl-1-(hydroxymethyl)-4-phenoxy-1,3-dihydro-2*H*-benzo[*d*]imidazol-2-one (47)

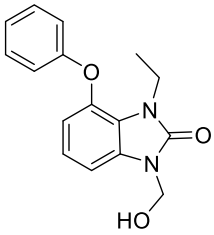

Boron trifluoride diethyl etherate (BF_3OEt_2) (0.60 mL, 4.9 mmol) was added dropwise to **39** (163 mg, 424 µmol) in DCM (2 mL) at 0 °C after which the reaction was allowed to warm to room temperature. After 4 hours TLC revealed that all **39** had been consumed, therefore the reaction was once more cooled to 0 °C, quenched with a saturated solution of $NaHCO_3$ (40 mL) and subsequently extracted twice with DCM (2 × 50 mL). The organic phases were then combined, dried over $MgSO_4$ and concentrated *in vacuo*. The resulting crude product was then purified by column chromatography (40% – 100% EtOAc/Hexane) to afford the hemiaminal **47** as a white waxy solid (107 mg, 376 µmol, 88%).

Rf, 0.43 (100% EtOAc/Hexane)**^{1}H NMR (500 MHz, $CDCl_3$) δ** 7.38 – 7.30 (m, 2H, Ar*H*), 7.14 – 6.95 (m, 5H, Ar*H*), 6.72 – 6.66 (m, 1H, Ar*H*), 5.45 (s, 2H, CH_2), 3.96 (q, *J* = 7.0 Hz, 2H, CH_2), 1.21 (t, *J* = 7.0 Hz, 3H, CH_3). **^{13}C NMR (126 MHz, $CDCl_3$) δ** 157.5, 153.8, 140.6, 130.9, 130.0, 123.4, 122.2, 120.3, 117.8, 113.7, 104.6, 65.3, 37.9, 15.2. **HRMS** calc. for $C_{16}H_{17}O_3N_2$ $[M+H]^+$, 285.12337 found, 285.12359. **IR ATR (cm^{-1}):** 3230, 2982, 2947, 1679, 1477, 1035, 694.

8.4.13. Cleavage of the hemiaminal to afford 1-ethyl-7-phenoxy-1,3-dihydro-2*H*-benzo[*d*]imidazol-2-one (21)

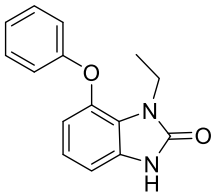

For the cleavage of the hemiaminal **47**, NaOH (30 mg, 0.75 mmol) was added to **47** (107 mg, 0.376 mmol) in THF (7 mL) and H_2O (1 mL). After 18 hours the reaction was quenched with a saturated solution of NH_4Cl (50 mL) and extracted twice with DCM (2 × 50 mL). The organic phases were combined, dried over $MgSO_4$ and concentrated *in vacuo*. The crude product was then purified by column chromatography to afford compound **21** as a white solid (48 mg, 0.19 mmol, 50%).

*Spectral data described in **8.4.11.**

8.4.14. Synthesis of 7-(3,5-dimethylphenoxy)-1-ethyl-1,3-dihydro-2*H*-benzo[*d*]imidazol-2-one (22)

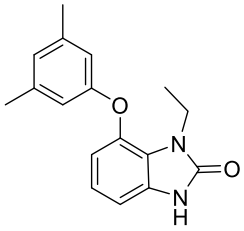

BF_3OEt_2 (0.50 mL, 4.1 mmol) was added dropwise to **40** (154 mg, 0.373 mmol) in DCM (2 mL) at 0 °C after which the reaction was allowed to warm to room temperature. After 4 hours TLC revealed that all **40** had been consumed, therefore the reaction was once more cooled to 0 °C, quenched with a saturated solution of $NaHCO_3$ (40 mL) and subsequently extracted twice with DCM (2 × 50 mL). The organic phases were then combined, dried over $MgSO_4$ and concentrated *in vacuo*. The crude product was then taken up in THF (7 mL) and H_2O (1 mL) and treated with NaOH (30 mg, 0.75 mmol). After 18 hours the reaction was quenched with a saturated solution of NH_4Cl (40 mL) and extracted twice with DCM (2 × 50 mL). The organic phases were combined, dried over $MgSO_4$ and concentrated *in vacuo*. The crude product was then purified by column chromatography to afford compound **22** as a white solid (50 mg, 0.18 mmol, 48% over two steps).

Rf, 0.43 (100% EtOAc/Hexane) **^{1}H NMR (500 MHz, $CDCl_3$) δ** 11.05 (s, 1H, N*H*), 7.01 – 6.95 (m, 2H, Ar*H*), 6.77 – 6.74 (m, 1H, Ar*H*), 6.68 – 6.64 (m, 3H, Ar*H*), 4.08 (q, *J* = 7.1 Hz, 2H, CH_2), 2.30 (s, 6H, (CH_3)$_3$), 1.35 (t, *J* = 7.1 Hz, 3H, CH_2). **^{13}C NMR (126 MHz, $CDCl_3$) δ** 157.67, 155.9, 140.6, 139.9, 130.5, 125.1, 121.9, 121.3, 115.4, 113.0, 105.7, 37.7, 21.4, 15.4. **HRMS** calc. for $C_{17}H_{19}O_2N_2$ $[M+H]^+$, 283.14410 found, 283.14395. **IR ATR (cm^{-1}):** 3150, 2915, 1703, 1591, 1229, 772. **Mp:** 173 °C.

8.4.15. Synthesis of 3-chloro-5-((3-ethyl-2-oxo-1-((2-(trimethylsilyl)ethoxy)methyl)-2,3-dihydro-1*H*-benzo[*d*]imidazol-4-yl)oxy)benzonitrile (52)

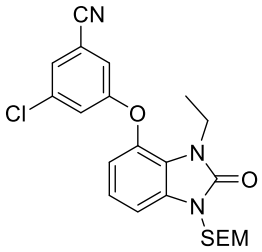

3-chloro-5-fluorobenzonitrile (**51**) (101 mg, 649 µmol) was added to **38** (100 mg, 324 µmol) and Cs_2CO_3 (211 mg, 648 µmol) in DMF (2 mL) and the reaction was heated to 100 °C. After 2 hours TLC revealed that all of **38** had been consumed. As a result, the reaction was cooled to room temperature, diluted with EtOAc (50 mL) and quenched with water (50 mL). The organic phase was subsequently washed with brine (50 mL), dried over $MgSO_4$ and then concentrated *in vacuo*. Purification of the crude material by silica gel column chromatography (5% – 40% EtOAc/Hexane) yielded the desired product **52** as a clear oil (107 mg, 241 µmol, 74%).

Rf, 0.52 (40% EtOAc/Hexane) **^{1}H NMR (500 MHz, $CDCl_3$) δ** 7.37 – 7.36 (m, 1H, Ar*H*), 7.23 – 7.22 (m, 1H, Ar*H*), 7.14 (dd, *J* = 2.4, 1.3 Hz, 1H, Ar*H*), 7.11 – 7.07 (m, 2H, Ar*H*), 6.72 (dd, *J* = 6.7, 2.5 Hz, 1H, Ar*H*), 5.33 (s, 2H, CH_2), 3.93 (q, *J* = 7.1 Hz, 2H, CH_2), 3.66 – 3.61 (m, 2H, CH_2), 1.24 (t, *J* = 7.1 Hz, 3H, CH_3), 0.97 – 0.92 (m, 2H, CH_2), -0.03 (s, 9H, Si(CH_3)$_3$). **^{13}C NMR (126 MHz, $CDCl_3$) δ** 159.1, 154.0, 137.7, 136.9, 131.8, 126.6, 122.4, 122.0, 120.9, 118.5, 117.0, 115.0, 114.4, 106.5, 71.0, 66.5, 37.9, 17.9, 15.2, -1.3. **HRMS** calc. for $C_{22}H_{26}O_3N_3ClSi$ $[M+]^+$, 444.15047 found, 444.15102. **IR ATR (cm^{-1}):** 3075, 2952, 2235, 1710, 1573, 1212, 1079.

8.4.16. Synthesis of 3-chloro-5-((3-ethyl-2-oxo-1-((2-trimethylsilyl)ethoxy)methyl)-2,3-dihydro-1*H*-benzo[*d*]imidazol-4-yl)oxy)benzonitrile (50)

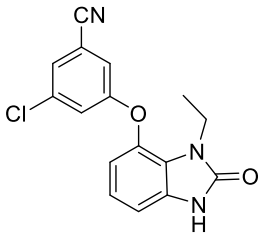

This reaction was carried out according to the procedure described for **22** using the following: **52** (107 mg, 0.241 mmol), BF_3OEt_2 (0.30 mL, 2.4 mmol) and NaOH (20 mg, 0.48 mmol). The reaction yielded **50** as a white solid (38 mg, 0.12 mmol, 50% over two steps).

Rf, 0.15 (40% EtOAc/Hexane) **^{1}H NMR (300 MHz, $CDCl_3$) δ** 10.04 (s, 1H, N*H*), 7.38 – 7.36 (m, 1H, Ar*H*), 7.25 – 7.23 (m, 1H, Ar*H*), 7.17 – 7.14 (m, 1H, Ar*H*), 7.10 – 7.00 (m, 2H, Ar*H*), 6.69 (dd, *J* = 7.6, 1.7 Hz, 1H, Ar*H*), 3.95 (q, *J* = 7.1 Hz, 2H, CH_2), 1.28 (t, *J* = 7.1 Hz, 3H, CH_3). **^{13}C NMR (75 MHz, $CDCl_3$) δ** 159.2, 155.3, 137.8, 136.9, 130.9, 126.6, 122.5, 122.0, 121.7, 118.5, 117.0, 115.1, 113.8, 107.4, 37.7, 15.3. **HRMS** calc. for $C_{16}H_{13}ClO_2N_3$ $[M+H]^+$, 314.0696 found, 314.0711. **IR ATR (cm^{-1}):** 3130, 2236, 1693, 1573, 959, 848. **Mp:** 206 °C.

8.4.17. Synthesis of 2-(benzyloxy)-*N*-methyl-6-nitroaniline (55)

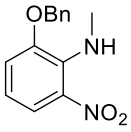

This reaction was carried out according to the procedure (conditions A) described for **34** using the following: **33** (300 mg, 1.23 mmol), methyl iodide (0.12 mL, 1.8 mmol) and NaH (114 mg, 4.75 mmol). This reaction yielded **55** as a red solid (307 mg, 1.19 mmol, 97%).

Rf, 0.39 (20% EtOAc/Hexane) **^{1}H NMR (300 MHz, $CDCl_3$) δ** 7.72 (dd, *J* = 8.7, 1.4 Hz, 1H, Ar*H*), 7.56 (s, 1H, N*H*), 7.46 – 7.34 (m, 5H, Ar*H*), 6.99 (dd, *J* = 7.8, 1.3 Hz, 1H, Ar*H*), 6.63 – 6.54 (m, 1H, Ar*H*), 5.07 (s, 2H, CH_2), 3.15 (d, *J* = 4.5 Hz, 3H, CH_3). **^{13}C NMR (75 MHz, $CDCl_3$) δ** 149.9, 139.9, 136.1, 128.9, 128.5, 127.9, 127.4, 119.2, 117.8, 115.5, 72.1, 34.3. **HRMS** calc. for $C_{14}H_{15}N_2O_3$ $[M+H]^+$, 259.1083 found, 259.1076. **IR ATR (cm^{-1}):** 3310, 2939, 1745, 1521, 1247, 1191. **Mp:** 74 °C.

8.4.18. Synthesis of 2-(benzyloxy)-*N*-propyl-6-nitroaniline (56)

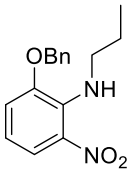

This reaction was carried out according to the procedure (conditions C) described for **34** using the following: **33** (500 mg, 2.05 mmol), propyl bromide (0.19 mL, 2.1 mmol) and NaH (82 mg, 3.4 mmol). This reaction yielded **56** as a red solid (399 mg, 1.39 mmol, 68%).

Rf, 0.44 (20% EtOAc/Hexane) **^{1}H NMR (400 MHz, $CDCl_3$) δ** 7.76 – 7.71 (m, 1H, Ar*H*), 7.46 – 7.32 (m, 5H, Ar*H*), 7.00 – 6.95 (m, 1H, Ar*H*), 6.64 – 6.58 (m, 1H, Ar*H*), 5.06 (s, 2H, CH_2), 3.49 (t, *J* = 7.1 Hz, 2H, CH_2), 1.62 – 1.51 (m, 2H, CH_2), 0.85 (t, *J* = 7.4 Hz, 3H, CH_3). **^{13}C NMR (101 MHz, $CDCl_3$) δ** 150.0, 138.8, 136.1, 128.8, 128.5, 127.9, 119.2, 117.7, 115.8, 72.0, 48.9, 24.4, 11.3. **HRMS** calc. for $C_{16}H_{19}O_3N_2$ $[M+H]^+$, 287.13902 found, 287.13884. **IR ATR (cm^{-1}):** 3330, 2960, 2872, 1517, 1260, 1028. **Mp:** 50 °C.

8.4.19. Synthesis of 4-(benzyloxy)-3-methyl-1*H*-benzo[*d*]imidazol-2-one (57)

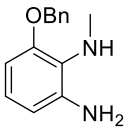

The reduction of **55** was carried out according to the procedure (conditions B) described for **35** using the following: **55** (504 mg, 1.95 mmol) and $SnCl_2.2H_2O$ (4.4g, 19 mmol). However, in this instance the reduced product was taken crude to the following ring-closing step with CDI.

Rf, 0.30 (40% EtOAc/Hexane) **^{1}H NMR (300 MHz, $CDCl_3$) δ** 7.48 – 7.32 (m, 5H, Ar*H*), 6.90 – 6.80 (m, 1H, Ar*H*), 6.46 – 6.39 (m, 2H, Ar*H*), 5.07 (s, 2H, CH_2), 4.51 (s, 3H, N*H*), 2.70 (s, 3H, CH_3). **^{13}C NMR (75 MHz, $CDCl_3$) δ** 152.5, 142.0, 137.3, 128.7, 128.1, 127.6, 125.4, 124.0, 109.4, 102.7, 70.6, 34.4. **HRMS** calc. for $C_{14}H_{17}N_2O$ $[M+H]^+$, 229.1341 found, 229.1345. **IR ATR (cm^{-1}):** 3433, 3352, 1613, 1486, 1431, 1144.

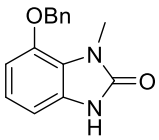

The subsequent ring-closing reaction was carried out according to the procedure (conditions B) described for **36** using the following: the crude *N*-methylated phenylene diamine and CDI (519 mg, 3.20 mmol). The reaction yielded **59** as a white solid (387 mg, 1.52 mmol, 78% over two steps).

Rf, 0.38 (40% EtOAc/Hexane) **^{1}H NMR (300 MHz, DMSO-*d*) δ** 10.83 (s, 1H, N*H*), 7.51 – 7.31 (m, 5H, Ar*H*), 6.93 – 6.86 (m, 1H, Ar*H*), 6.81 – 6.76 (m, 1H, Ar*H*), 6.63 (dd, *J* = 7.7, 0.7 Hz, 1H, Ar*H*), 5.18 (s, 2H, CH_2), 3.46 (s, 3H, CH_3). **^{13}C NMR (75 MHz, DMSO-*d*) δ** 154.3, 143.5, 137.0, 129.5, 128.5, 127.9, 127.6, 121.4, 119.1, 105.9, 102.8, 70.2, 29.1. **HRMS** calc. for $C_{15}H_{15}N_2O_2$ $[M+H]^+$, 255.1134 found, 255.1133. **IR ATR (cm^{-1}):** 3006, 1682, 1474, 1246, 1104. **Mp:** 238 °C.

8.4.20. Synthesis of 4-(benzyloxy)-3-propyl-1*H*-benzo[*d*]imidazol-2-one (58)

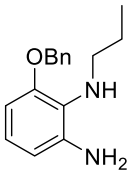

The reduction of **56** was carried out according to the procedure (conditions B) described for **35** using the following: **56** (350 mg, 1.22 mmol) and $SnCl_2.2H_2O$ (2.8 g, 12 mmol). However, in this instance the reduced product was taken crude to the following ring-closing step with CDI.

Rf, 0.18 (40% EtOAc/Hexane) **^{1}H NMR (500 MHz, CDCl3) δ** 7.51 – 7.36 (m, 5H, Ar*H*), 6.91 – 6.85 (m, 1H, Ar*H*), 6.49 – 6.43 (m, 2H, Ar*H*), 5.10 (s, 2H, CH_2), 3.82 (s, 3H, N*H*), 2.95 (t, *J* = 7.1 Hz, 2H, CH_2), 1.69 – 1.57 (m, 2H, CH_2), 1.01 (t, *J* = 7.4 Hz, 3H, CH_3). **^{13}C NMR (101 MHz, CDCl3) δ** 146.9, 137.5, 128.7, 128.1, 127.6, 126.5, 116.9, 106.1, 70.9, 35.7, 9.4, 0.2. **IR ATR (cm^{-1}):** 3345, 2957, 1612, 1440, 1243, 694.

*Unable to obtain HRMS of this compound due to degradation

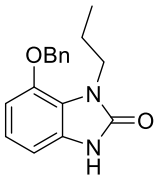

The subsequent ring-closing reaction was carried out according to the procedure (conditions B) described for **36** using the following: the crude *N*-propylated phenylene diamine and CDI (316 mg, 1.95 mmol). The reaction yielded **60** as a white solid (306 mg, 1.08 mmol, 89% over two steps).

Rf, 0.11 (40% EtOAc/Hexane) **^{1}H NMR (500 MHz, DMSO-*d*) δ** 10.82 (s, 1H, N*H*), 7.51 – 7.47 (m, 2H, Ar*H*), 7.44 – 7.40 (m, 2H, Ar*H*), 7.38 – 7.34 (m, 1H, Ar*H*), 6.94 – 6.90 (m, 1H, Ar*H*), 6.83 – 6.79 (m, 1H, Ar*H*), 6.65 – 6.62 (m, 1H, Ar*H*), 5.16 (s, 2H, CH_2), 3.84 – 3.77 (m, 2H, CH_2), 1.60 – 1.51 (m, 2H, CH_2), 0.67 (d, *J* = 7.4 Hz, 3H, CH_3). **^{13}C NMR (126 MHz, DMSO-*d*) δ** 154.1, 143.3, 136.8, 129.6, 128.5, 128.0, 127.8, 121.3, 105.4,

70.1, 43.2, 23.2, 10.6. **HRMS** calc. for $C_{17}H_{19}O_2N_2$ $[M+H]^+$, 283.14410 found, 283.14380. **IR ATR (cm^{-1}):** 3110, 2955, 2872, 1677, 1375, 1124, 749. **Mp:** 236 °C.

8.4.21. Synthesis of 4-(benzyloxy)-3-methyl-1-((2-(trimethylsilyl)ethoxy)methyl)-1*H*-benzo[*d*]imidazol-2(3*H*)-one (59)

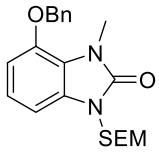

This reaction was carried out according to the procedure described for **37** using the following: **57** (380 mg, 1.49 mmol), SEM-Cl (0.40 mL, 2.3 mmol) and NaH (60 mg, 2.5 mmol). The reaction yielded **59** as a clear oil (382 mg, 0.993 mmol, 67%).

Rf, 0.75 (60% EtOAc/Hexane) **^{1}H NMR (300 MHz, $CDCl_3$) δ** 7.47 – 7.31 (m, 5H, Ar*H*), 7.00 (m, 1H, Ar*H*), 6.84 (dd, *J* = 7.9, 0.8 Hz, 1H, Ar*H*), 6.75 (dd, *J* = 8.4, 0.7 Hz, 1H, Ar*H*), 5.29 (s, 2H, CH_2), 5.15 (s, 2H, CH_2), 3.63 (s, 3H, CH_3), 3.62 – 3.57 (m, 2H, CH_2), 0.97 – 0.87 (m, 2H, CH_2), -0.03 (s, 9H, Si(CH_3)$_3$). **^{13}C NMR (75 MHz, $CDCl_3$) δ** 154.6, 144.5, 136.7, 130.3, 128.8, 128.3, 127.6, 122.0, 118.8, 106.6, 102.8, 71.09, 71.05, 66.2, 30.2, 18.0, -1.3. **HRMS** calc. for $C_{21}H_{29}N_2O_3Si$ $[M+H]^+$, 385.1947 found, 385.1952. **IR ATR (cm^{-1}):** 2951, 2894, 1704, 1481, 1247, 833.

8.4.22. Synthesis of 4-(benzyloxy)-3-propyl-1-((2-(trimethylsilyl)ethoxy)methyl)-1*H*-benzo[*d*]imidazol-2(3*H*)-one (60)

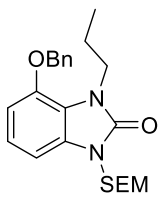

This reaction was carried out according to the procedure described for **37** using the following: **57** (380 mg, 1.49 mmol), SEM-Cl (0.40 mL, 2.3 mmol) and NaH (60 mg, 2.5 mmol). The reaction yielded **60** as a clear oil (306 mg, 0.742 mmol, 70%)

Rf, 0.52 (40% EtOAc/Hexane) **^{1}H NMR (500 MHz, $CDCl_3$) δ** 7.47 – 7.33 (m, 5H, Ar*H*), 7.05 – 6.98 (m, 1H, Ar*H*), 6.85 (dd, *J* = 7.9, 0.7 Hz, 1H, Ar*H*), 6.76 (d, *J* = 8.3 Hz, 1H, Ar*H*), 5.30 (s, 2H, CH_2), 5.14 (s, 2H, CH_2), 4.02 – 3.97 (m, 2H, CH_2), 3.62 – 3.57 (m, 2H, CH_2), 1.75 – 1.66 (m, 2H, CH_2), 0.94 – 0.90 (m, 2H, CH_2), 0.77 (t, *J* = 7.4 Hz, 3H, CH_3), -0.04 (s, 9H, Si(CH_3)$_3$). **^{13}C NMR (126 MHz, $CDCl_3$) δ** 154.4, 144.3, 143.8, 136.6, 130.5, 128.8, 128.4, 127.8, 118.1, 106.2, 102.7, 70.98, 70.86, 66.1, 44.6, 23.7, 18.0, 10.9, -1.3. **HRMS** calc. for $C_{23}H_{33}O_3N_2Si$ $[M+H]^+$, 413.2250 found, 413.22563.

8.4.23. Synthesis of 4-hydroxy-3-methyl-1-((2-(trimethylsilyl)ethoxy)methyl)-1*H*-benzo[*d*]imidazol-2(3*H*)-one (61)

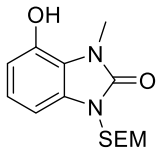

This reaction was carried out according to the procedure described for **38** using the following: **59** (382 mg, 993 µmol) and catalytic palladium on carbon. The reaction yielded **61** as a white solid (236 mg, 961 µmol, 81%).

Rf, 0.47 (50% EtOAc/Hexane) **^{1}H NMR (300 MHz, $CDCl_3$) δ** 7.17 (s, 1H, O*H*), 6.98 – 6.86 (m, 1H, Ar*H*), 6.77 (dd, *J* = 7.9, 0.8 Hz, 1H, Ar*H*), 6.66 (dd, *J* = 8.1, 0.8 Hz, 1H, Ar*H*), 5.31 (s, 2H, CH_2), 3.71 (s, 3H, CH_3), 3.67 – 3.58 (m, 2H, CH_2), 0.97 – 0.88 (m, 2H, CH_2), -0.05 (s, 9H, Si(CH_3)$_3$). **^{13}C NMR (75 MHz, $CDCl_3$) δ** 154.8, 142.1, 130.6, 122.2, 117.5, 110.2, 101.8, 71.1, 66.4, 30.0, 18.0, -1.3. **HRMS** calc. for $C_{14}H_{23}N_2O_3Si$ $[M+H]^+$, 295.1478 found, 295.1481. **IR ATR (cm^{-1}):** 3244, 2952, 2926, 1674, 1266, 1092. **Mp:** 123 °C.

8.4.24. Synthesis of 4-hydroxy-3-propyl-1-((2-(trimethylsilyl)ethoxy)methyl)-1*H*-benzo[*d*]imidazol-2(3*H*)-one (62)

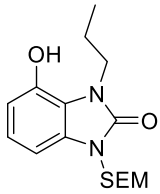

This reaction was carried out according to the procedure described for **38** using the following: **60** (296 mg, 717 µmol) and catalytic palladium on carbon. The reaction yielded **62** as a white solid (183 mg, 568 µmol, 79%).

Rf, 0.36 (20% EtOAc/Hexane) **^{1}H NMR (500 MHz, $CDCl_3$) δ** 7.03 (s, 1H, O*H*), 6.95 – 6.90 (m, 1H, Ar*H*), 6.79 – 6.77 (m, 1H, Ar*H*), 6.68 – 6.65 (m, 1H, Ar*H*), 5.33 (s, 2H, CH_2), 4.13 – 4.09 (m, 2H, CH_2), 3.64 – 3.59 (m, 2H, CH_2), 1.87 – 1.78 (m, 2H, CH_2), 0.93 (t, *J* = 7.5 Hz, 3H, CH_3), -0.06 (s, 9H, Si(CH_3)$_3$). **^{13}C NMR (126 MHz, $CDCl_3$) δ** 154.7, 141.7, 130.7, 122.1, 117.1, 110.1, 101.8, 70.9, 66.4, 44.6, 23.7, 18.0, 11.1, -1.3. **HRMS** calc. for $C_{16}H_{27}O_3N_2Si$ $[M+H]^+$, 323.17855 found, 323.17901. **IR ATR (cm^{-1}):** 3219, 2951, 1672, 1483, 1260, 1053, 745. **Mp:** 127 °C.

8.4.25. Synthesis of 3-chloro-5-((3-methyl-2-oxo-1-((2-(trimethylsilyl)ethoxy)methyl)-2,3-dihydro-1*H*-benzo[*d*]imidazol-4-yl)oxy)benzonitrile (63)

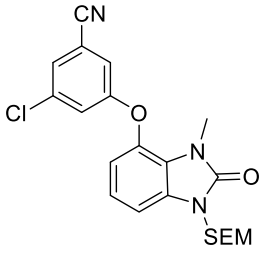

This reaction was carried out according to the procedure described for **52** using the following: **61** (200 mg, 679 µmol), Cs_2CO_3 (332 mg, 1.02 mmol) and **51** (159 mg, 1.02 mmol). This reaction yielded **63** as a clear oil (181 mg, 421 µmol, 64%).

Rf, 0.56 (30% EtOAc/Hexane) **^{1}H NMR (400 MHz, $CDCl_3$) δ** 7.36 – 7.35 (m, 1H, Ar*H*), 7.20 – 7.19 (m, 1H, Ar*H*), 7.12 – 7.07 (m, 3H, Ar*H*), 6.73 (dd, *J* = 6.1, 3.2 Hz, 1H, Ar*H*), 5.33 (s, 2H, CH_2), 3.66 – 3.61 (m, 2H, CH_2), 3.44 (s, 3H, CH_3), 0.96 – 0.91 (m, 2H, CH_2), -0.03 (s, 9H, Si(CH_3)$_3$). **^{13}C NMR (101 MHz, $CDCl_3$) δ** 159.4, 154.3, 137.6, 136.78, 131.5, 126.4, 122.5, 121.8, 118.3, 117.0, 114.9, 114.8, 106.7, 71.1, 66.5, 29.4, 17.9, -1.3. **HRMS** calc. for $C_{21}H_{24}ClO_3N_3Si$ [M+]$^+$, 427.12700 found, 429.12734. **IR ATR (cm^{-1}):** 2951, 2236, 1710, 1573, 1079, 833.

8.4.26. 3-chloro-5-((2-oxo-3-propyl-1-((2-(trimethylsilyl)ethoxy)methyl)-2,3-dihydro-1*H*-benzo[*d*]imidazol-4-yl)oxy)benzonitrile (64)

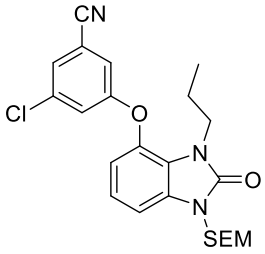

This reaction was carried out according to the procedure described for **52** using the following: **62** (172 mg, 533 µmol), Cs_2CO_3 (348 mg, 1.07 mmol) and **51** (166 mg, 1.07 mmol). This reaction yielded **64** as a clear oil (181 mg, 395 µmol, 74%).

Rf, 0.36 (20% EtOAc/Hexane) **^{1}H NMR (500 MHz, $CDCl_3$) δ** 7.37 – 7.36 (m, 1H, Ar*H*), 7.22 – 7.21 (m, 1H, Ar*H*), 7.14 – 7.13 (m, 1H, Ar*H*), 7.11 – 7.07 (m, 2H, Ar*H*), 6.74 – 6.69 (m, 1H, Ar*H*), 5.34 (s, 2H, CH_2), 3.85 – 3.80 (m, 2H, CH_2), 3.65 – 3.61 (m, 2H, CH_2), 1.72 – 1.64 (m, 2H, CH_2), 0.97 – 0.91 (m, 2H, CH_2), 0.86 (t, *J* = 7.4 Hz, 3H, CH_3), -0.03 (s, 9H, Si(CH_3)$_3$). **^{13}C NMR (126 MHz, $CDCl_3$) δ** 159.1, 154.3, 137.6, 136.9, 131.8, 126.5, 122.4, 121.9, 121.1, 118.4, 117.0, 115.0, 114.4, 106.5, 71.0, 66.5, 44.4, 23.3, 17.9, 11.1, -1.30. **HRMS** calc. for $C_{23}H_{28}O_3N_3ClSi$ [M+]$^+$, 458.16612 found, 458.16653. **IR ATR (cm^{-1}):** 2952, 2235, 1710, 1572, 1078, 833.

8.4.27. Synthesis of 3-chloro-5-((3-methyl-2-oxo-2,3-dihydro-1*H*-benzo[*d*]imidazol-4-yl)oxy)benzonitrile (53)

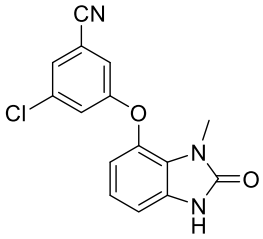

This reaction was carried out according to the procedure described for **22** using the following: **63** (139 mg, 0.323 mmol), BF_3OEt_2 (0.50 mL, 4.1 mmol) and NaOH (30 mg, 0.75 mmol). The reaction yielded **53** as a white solid (60 mg, 0.20 mmol, 62% over two steps).

Rf, 0.15 (40% EtOAc/Hexane) **^{1}H NMR (500 MHz, DMSO-*d*) δ** 11.13 (s, 1H, N*H*), 7.78 – 7.77 (m, 1H, Ar*H*), 7.48 – 7.47 (m, 1H, Ar*H*), 7.45 – 7.44 (m, 1H, Ar*H*), 7.04 – 7.00 (m, 1H, Ar*H*), 6.92 (dd, *J* = 7.8, 0.8 Hz, 1H, Ar*H*), 6.73 (dd, *J* = 8.2, 0.8 Hz, 1H, Ar*H*), 3.26 (s, 3H, CH_3). **^{13}C NMR (126 MHz, DMSO-*d*) δ** 159.2, 154.3, 137.2, 135.3, 131.0, 126.4, 122.4, 122.0, 121.8, 119.3, 117.0, 114.2, 113.3, 106.5, 28.4. **HRMS** calc. for $C_{15}H_{11}N_3O_2Cl$ $[M+H]^+$, 300.05343 found, 300.05322. **IR ATR (cm^{-1}):** 3065, 2215, 1686, 1574, 1230, 1105, 665. **Mp:** 267 °C.

8.4.28. Synthesis of 3-chloro-5-((2-oxo-3-propyl-2,3-dihydro-1*H*-benzo[*d*]imidazol-4-yl)oxy)benzonitrile (54)

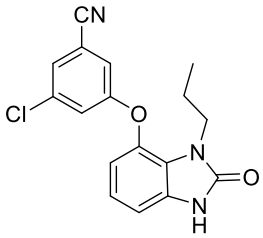

This reaction was carried out according to the procedure described for **22** using the following: **64** (176 mg, 0.384 mmol), BF_3OEt_2 (0.50 mL, 4.1 mmol) and NaOH (30 mg, 0.75 mmol). The reaction yielded **54** as a white solid (35 mg, 0.11 mmol, 29% over two steps).

Rf, 0.08 (40% EtOAc/Hexane) **^{1}H NMR (500 MHz, $CDCl_3$) δ** 10.48 (s, 1H, N*H*), 7.38 – 7.36 (m, 1H, Ar*H*), 7.23 – 7.22 (m, 1H, Ar*H*), 7.15 – 7.14 (m, 1H, Ar*H*), 7.08 – 7.04 (m, 2H, Ar*H*), 6.68 (dd, *J* = 7.4, 1.8 Hz, 1H, Ar*H*), 3.87 – 3.82 (m, 2H, CH_2), 1.74 – 1.68 (m, 2H, CH_2), 0.90 (t, *J* = 7.4 Hz, 3H, CH_3). **^{13}C NMR (126 MHz, $CDCl_3$) δ** 159.2, 155.8, 137.8, 136.9, 131.0, 126.5, 122.4, 121.90, 121.87, 118.5, 117.0, 115.0, 113.8, 107.4, 44.3, 23.4, 11.2. **HRMS** calc. for $C_{17}H_{15}ClO_2N_3$ $[M+H]^+$, 328.08473 found, 328.08450. **IR ATR (cm^{-1}):** 3064, 2210, 1700, 1571, 1427, 750. **Mp:** 210 °C.

8.4.29. 5-((3-ethyl-2-oxo-1-((2-(trimethylsilyl)ethoxy)methyl)-2,3-dihydro-1*H*-benzo[*d*]imidazole-4-yl)oxy)isophthalonitrile (71)

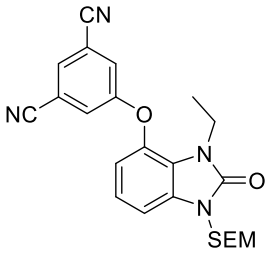

This reaction was carried out according to the procedure described for **52** using the following: **38** (100 mg, 324 µmol), Cs_2CO_3 (211 mg, 648 µmol) and 5-fluoroisophthalonitrile (**70**) (95 mg, 0.65 mmol). This reaction yielded **71** as a clear oil (132 mg, 304 µmol, 94%).

Rf, 0.53 (30% EtOAc/Hexane) **^{1}H NMR (500 MHz, $CDCl_3$) δ** 7.64 (t, *J* = 1.3 Hz, 1H, Ar*H*), 7.47 (d, *J* = 1.4 Hz, 2H, Ar*H*), 7.10 (dd, *J* = 4.7, 0.6 Hz, 2H, Ar*H*), 6.72 – 6.68 (m, 1H, Ar*H*), 5.32 (s, 2H, CH_2), 3.89 (q, *J* = 7.1 Hz, 2H, CH_2), 3.64 – 3.60 (m, 2H, CH_2), 1.21 (t, *J* = 7.1 Hz, 3H, CH_3), 0.94 – 0.91 (m, 2H, CH_2), -0.05 (s, 9H, Si(CH_3)$_3$). **^{13}C NMR (126 MHz, $CDCl_3$) δ** 158.9, 153.8, 136.9, 132.0, 129.5, 124.0, 122.5, 120.8, 116.1, 115.7, 114.2, 106.9, 70.9, 66.4, 37.8, 17.8, 15.1, -1.4. **HRMS** calc. for $C_{23}H_{26}O_3N_4Si$ $[M+]^+$, 434.17738 found, 434.17734.

8.4.30. Synthesis of 5-((3-ethyl-2-oxo-2,3-dihydro-1*H*-benzo[*d*]imidazol-4-yl)oxy)isophthalonitrile (65)

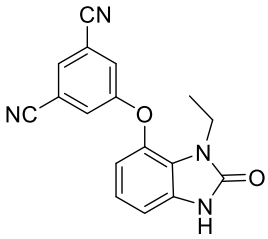

This reaction was carried out according to the procedure described for **22** using the following: **71** (132 mg, 0.304 mmol), BF_3OEt_2 (0.50 mL, 4.1 mmol) and NaOH (30 mg, 0.75 mmol). The reaction yielded **65** as a white solid (50 mg, 0.16 mmol, 54% over two steps).

Rf, 0.11 (40% EtOAc/Hexane) **^{1}H NMR (500 MHz, DMSO-*d*) δ** 11.14 (s, 1H, N*H*), 8.21 (t, *J* = 1.3 Hz, 1H, Ar*H*), 7.92 (d, *J* = 1.3 Hz, 2H, Ar*H*), 7.05 – 6.99 (m, 1H, Ar*H*), 6.92 (dd, *J* = 7.7, 0.8 Hz, 1H, Ar*H*), 6.71 (dd, *J* = 8.3, 0.7 Hz, 1H, Ar*H*), 3.74 (q, *J* = 7.1 Hz, 2H, CH_2), 1.10 (t, *J* = 7.1 Hz, 3H, CH_3). **^{13}C NMR (126 MHz, DMSO-*d*) δ** 158.1, 153.9, 137.1, 131.2, 130.7, 125.3, 121.8, 121.2, 116.6, 114.4, 112.8, 106.5, 36.6, 15.0. **HRMS** calc. for $C_{17}H_{13}N_4O_2$ $[M+H]^+$, 305.10330 found, 305.10302. **IR ATR (cm^{-1}):** 3067, 2244, 2237, 1690, 1583, 1223. **Mp:** 245 °C.

8.4.31. Synthesis of 3-ethyl-4-(naphthalen-1-yloxy)-1-((2-(trimethylsilyl)ethoxy)methyl)-1,3-dihydro-2*H*-benzo[*d*]imidazole-2-one (72)

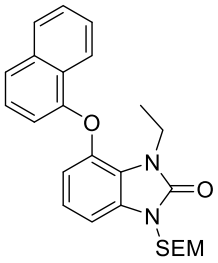

This reaction was carried out according to the procedure described for **39** using the following: **38** (15 mg, 48 µmol), K_3PO_4 (20 mg, 97µmol), 2-picolinic acid (12 mg, 9.7 µmol), iodonaphthalene (37 mg, 0.15 mmol) and CuI (9.0 mg, 4.8 µmol). The reaction yielded **40** as a clear oil (19 mg, 43 µmol, 91%).

Rf, 0.35 (20% EtOAc/Hexane) **^{1}H NMR (500 MHz, $CDCl_3$) δ** 8.34 – 8.30 (m, 1H, Ar*H*), 7.92 – 7.88 (m, 1H, Ar*H*), 7.63 – 7.60 (m, 1H, Ar*H*), 7.59 – 7.53 (m, 2H, Ar*H*), 7.37 – 7.33 (m, 1H, Ar*H*), 7.05 – 7.01 (m, 2H, Ar*H*), 6.87 – 6.84 (m, 1H, Ar*H*), 6.73 – 6.69 (m, 1H, Ar*H*), 5.37 (s, 2H, CH_2), 4.05 (q, *J* = 7.0 Hz, 2H, CH_2), 3.70 – 3.65 (m, 2H, CH_2), 1.30 (t, *J* = 7.1 Hz, 3H, CH_3), 1.00 – 0.95 (m, 2H, CH_2), 0.00 (s, H, Si(CH_3)$_3$). **^{13}C NMR (126 MHz, $CDCl_3$) δ** 154.1, 153.6, 140.5, 135.0, 131.4, 128.0, 126.9, 126.3, 126.2, 125.8, 123.3, 122.0, 121.7, 120.5, 113.9, 111.3, 105.0, 71.0, 66.4, 38.1, 18.0, 15.4, -1.3. **HRMS** calc. for $C_{25}H_{31}O_3N_2Si$ $[M+H]^+$, 435.20985 found, 435.21036. **IR ATR (cm^{-1}):** 2950, 1707, 1478, 1237, 1078, 769.

8.4.32. Synthesis of 1-ethyl-7-(naphthalen-1-yloxy)-1,3-dihydro-2*H*-benzo[*d*]imidazol-2-one (66)

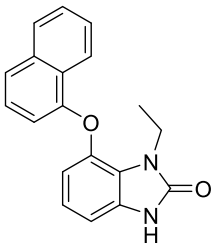

This reaction was carried out according to the procedure described for **22** using the following: **72** (71 mg, 0.16 mmol), BF_3OEt_2 (0.30 mL, 2.4 mmol) and NaOH (20 mg, 0.50 mmol). The reaction yielded **65** as a white solid (8.0 mg, 0.026 mmol, 16% over two steps).

Rf, 0.26 (50% EtOAc/Hexane) **^{1}H NMR (500 MHz, $CDCl_3$) δ** 10.31 (s, 1H, N*H*), 8.35 – 8.31 (m, 1H, Ar*H*), 7.92 – 7.88 (m, 1H, Ar*H*), 7.63 – 7.54 (m, 3H, Ar*H*), 7.38 – 7.34 (m, 1H, Ar*H*), 7.02 – 6.96 (m, 2H, Ar*H*), 6.87 – 6.83 (m, 1H, Ar*H*), 6.68 (dd, *J* = 7.1, 2.1 Hz, 1H, Ar*H*), 4.06 (q, *J* = 7.0 Hz, 2H, CH_2), 1.34 (t, *J* = 7.1 Hz, 3H, CH_3). **^{13}C NMR (126 MHz, $CDCl_3$) δ** 153.7, 140.6, 135.1, 130.5, 128.0, 127.0, 126.3, 126.2, 125.9, 123.2, 122.1, 121.7, 121.4, 113.3, 111.3, 105.9, 37.9, 15.5. **HRMS** calc. for $C_{19}H_{17}O_2N_2$ $[M+H]^+$, 305.12845 found, 305.12813. **IR ATR (cm^{-1}):** 3188, 1703, 1473, 1227, 728. **Mp:** 212 °C.

8.4.33. 4-((3-ethyl-2-oxo-1-((2-(trimethylsilyl)ethoxy)methyl)-2,3-dihydro-1*H*-benzo[*d*]imidazol-4-yl)oxy)picolinonitrile (76)

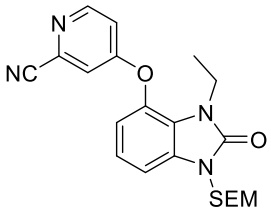

DMF (1 mL) was added to a Schlenk tube charged with **38** (200 mg, 648 µmol), K_2CO_3 (134 mg, 970 µmol) and 4-chloropicolinonitrile (**73**) (135 mg, 974 µmol) and the reaction was carried out for 18 hours at 90 °C under argon. The reaction mixture was subsequently cooled to room temperature, quenched with H_2O (50 mL) and extracted twice with EtOAc (2 × 100 mL). The organic phases were combined, washed with brine (200 mL) and dried over $MgSO_4$ before the solvent was removed *in vacuo*. The crude material was loaded onto silica gel and subsequently purified by column chromatography (5% EtOAc/hexane – 50% EtOAc/hexane) to yield the product as a clear oil. (251 mg, 611 µmol, 94%).

Rf, 0.61 (3% MeOH/DCM) **^{1}H NMR (400 MHz, $CDCl_3$) δ** 8.57 (d, *J* = 6.0 Hz, 1H, Ar*H*), 7.28 (d, *J* = 2.3 Hz, 1H, Ar*H*), 7.16 – 7.05 (m, 3H, Ar*H*), 6.80 – 6.76 (m, 1H, Ar*H*), 5.33 (s, 2H, CH_2), 3.86 (q, *J* = 7.1 Hz, 2H, CH_2), 3.68 – 3.58 (m, 2H, CH_2), 1.20 (t, *J* = 7.1 Hz, 3H, CH_3), 0.98 – 0.89 (m, 2H, CH_2), -0.03 (s, 9H, Si(CH_3)$_3$). **^{13}C NMR (101 MHz, $CDCl_3$) δ** 165.2, 153.8, 153.1, 135.9, 135.8, 132.0, 122.5, 121.0, 116.8, 116.6, 114.9, 114.5, 107.2, 71.0, 66.5, 37.8, 17.9, 15.1, -1.3. **HRMS** calc. for $C_{21}H_{27}O_3N_4Si$ $[M+H]^+$, 411.18469 found, 411.18478.

8.4.34. Synthesis of 4-((3-ethyl-2-oxo-2,3-dihydro-1*H*-benzo[*d*]imidazol-4-yl)oxy)picolinonitrile (67)

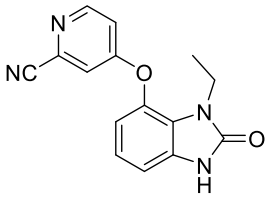

This reaction was carried out according to the procedure described for **22** using the following: **76** (118 mg, 0.287 mmol), BF_3OEt_2 (0.40 mL, 3.2 mmol) and NaOH (23 mg, 0.57 mmol). The reaction yielded **67** as a white solid (59 mg, 0.21 mmol, 74% over two steps).

Rf, 0.51 (60% EtOAc/Hexane) **^{1}H NMR (400 MHz, $CDCl_3$) δ** 10.76 (s, 1H, N*H*), 8.59 (d, *J* = 5.7 Hz, 1H, Ar*H*), 7.30 (d, *J* = 2.2 Hz, 1H, Ar*H*), 7.12 – 7.08 (m, 3H, Ar*H*), 6.81 – 6.74 (m, 1H, Ar*H*), 3.88 (q, *J* = 7.0 Hz, 2H, CH_2), 1.24 (t, *J* = 7.1 Hz, 3H, CH_3). **^{13}C NMR (101 MHz, $CDCl_3$) δ** 165.3, 155.5, 153.1, 136.0, 135.8, 131.2, 122.6, 121.7, 116.8, 116.6, 114.5, 114.3, 108.3, 37.6, 15.2. **HRMS** calc. for $C_{15}H_{13}O_2N_4$ $[M+H]^+$, 281.10330 found, 281.10297. **IR ATR (cm^{-1}):** 3135, 2980, 2243, 1701, 1634, 1579, 749. **Mp:** 198 °C.

8.4.35. Synthesis of 2-((3-ethyl-2-oxo-1-((2-(trimethylsilyl)ethoxy)methyl)-2,3-dihydro-1*H*-benzo[*d*]imidazol-4-yl)oxy)isonicotinonitrile (77)

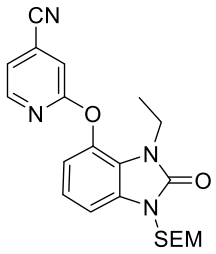

This reaction was carried out according to the procedure described for **76** using the following: **38** (100 mg, 324 µmol), K_2CO_3 (70 mg, 0.51 mmol) and 2-chloropicolinonitrile (**74**) (71 mg, 0.51 mmol). The reaction yielded **77** as a clear oil (121 mg, 295 µmol, 90%).

Rf, 0.51 (3% MeOH/DCM) **^{1}H NMR (500 MHz, $CDCl_3$) δ** 8.34 (dd, *J* = 5.1, 0.6 Hz, 1H, Ar*H*), 7.27 – 7.24 (m, 2H, Ar*H*), 7.12 – 7.07 (m, 2H, Ar*H*), 6.84 – 6.80 (m, 1H, Ar*H*), 5.31 (s, 2H, CH_2), 3.88 (q, *J* = 7.1 Hz, 2H, CH_2), 3.64 – 3.59 (m, 2H, CH_2), 1.18 (t, *J* = 7.1 Hz, 3H, CH_3), 0.95 – 0.90 (m, 2H, CH_2), -0.03 (s, 9H, Si(CH_3)$_3$). **^{13}C NMR (126 MHz, $CDCl_3$) δ** 163.9, 153.9, 149.5, 136.2, 131.5, 123.8, 121.8, 121.3, 120.2, 116.0, 115.9, 113.6, 106.5, 70.9, 66.3, 37.6, 17.8, 14.9, -1.4. **HRMS** calc. for $C_{21}H_{27}O_3N_4Si$ $[M+H]^+$, 411.18469 found, 411.18521. **IR ATR (cm^{-1}):** 2952, 2241, 1707, 1597, 1077.

8.4.36. Synthesis of 2-((3-ethyl-2-oxo-2,3-dihydro-1*H*-benzo[*d*]imidazol-4-yl)oxy)isonicotinonitrile (68)

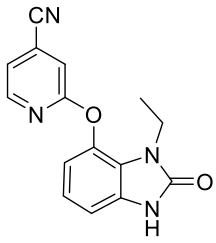

This reaction was carried out according to the procedure described for **22** using the following: **77** (121 mg, 0.295 mmol), BF_3OEt_2 (0.40 mL, 3.2 mmol) and NaOH (24 mg, 0.59 mmol). The reaction yielded **68** as a white solid (75 mg, 0.27 mmol, 90% over two steps).

Rf, 0.15 (60% EtOAc/Hexane) **^{1}H NMR (500 MHz, $CDCl_3$) δ** 10.74 (s, 1H, N*H*), 8.36 (d, *J* = 5.0 Hz, 1H, Ar*H*), 7.28 – 7.24 (m, 2H, Ar*H*), 7.09 – 7.03 (m, 2H, Ar*H*), 6.80 (dd, *J* = 7.7, 1.4 Hz, 1H, Ar*H*), 3.91 (q, *J* = 7.1 Hz, 2H, CH_2), 1.24 (t, *J* = 7.1 Hz, 3H, CH_3). **^{13}C NMR (126 MHz, $CDCl_3$) δ** 164.0, 155.6, 149.6, 136.4, 130.8, 123.9, 122.1, 121.9, 120.2, 116.0, 115.4, 113.6, 107.6, 37.4, 15.1. **HRMS** calc. for $C_{15}H_{13}O_2N_4$ $[M+H]^+$, 281.10330 found, 281.10298. **IR ATR (cm^{-1}):** 2969, 2241, 1697, 1636, 1596, 1117. **Mp:** 201 °C.

8.4.37. Synthesis of 4-((2-chloropyridin-4-yl)oxy)-3-ethyl-1-((2-(trimethylsilyl)ethoxy)methyl)-1,3-dihydro-2*H*-benzo[*d*]imidazol-2-one (78)

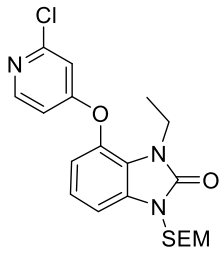

This reaction was carried out according to the procedure described for **76** using the following: **38** (150 mg, 486 µmol), K_2CO_3 (101 mg, 729 µmol) and 2,4-dichloropyridine (**75**) (86 mg, 0.58 mmol). The reaction yielded **77** as a yellow oil (126 mg, 300 µmol, 62%).

Rf, 0.62 (100% EtOAc) **^{1}H NMR (400 MHz, $CDCl_3$) δ** 8.28 – 8.25 (m, 1H, Ar*H*), 7.13 – 7.08 (m, 2H, Ar*H*), 6.89 – 6.77 (m, 3H, Ar*H*), 5.32 (s, 2H, CH_2), 3.87 (q, *J* = 7.1 Hz, 2H, CH_2), 3.66 – 3.59 (m, 2H, CH_2), 1.21 (t, *J* = 7.1 Hz, 3H, CH_3), 0.97 – 0.89 (m, 2H, CH_2), -0.04 (s, 9H, Si(CH_3)$_3$). **^{13}C NMR (101 MHz, $CDCl_3$) δ** 166.4, 153.9, 153.2, 151.2, 136.4, 131.8, 122.3, 121.0, 115.2, 111.6, 110.9, 106.9, 71.0, 66.5, 37.8, 17.9, 15.1, -1.3. **HRMS** calc. for $C_{20}H_{27}O_3N_3ClSi$ $[M+H]^+$, 420.15047 found, 420.15115.

8.4.38. Synthesis of 7-((2-chloropyridin-4-yl)oxy)-1-ethyl-1,3-dihydro-2*H*-benzo[*d*]imidazol-2-one (69)

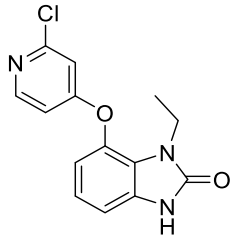

This reaction was carried out according to the procedure described for **22** using the following: **78** (120 mg, 0.286 mmol), BF_3OEt_2 (0.40 mL, 3.2 mmol) and NaOH (23 mg, 0.57 mmol). The reaction yielded **69** as a white solid (55 mg, 0.19 mmol, 66% over two steps).

Rf, 0.17 (100% EtOAc) **^{1}H NMR (400 MHz, $CDCl_3$) δ** 10.90 (s, 1H, N*H*), 8.29 (d, *J* = 5.7 Hz, 1H, Ar*H*), 7.11 – 7.03 (m, 2H, Ar*H*), 6.91 – 6.74 (m, 3H, Ar*H*), 3.91 (q, *J* = 7.1 Hz, 2H, CH_2), 1.26 (t, *J* = 7.1 Hz, 3H, CH_3). **^{13}C NMR (101 MHz, $CDCl_3$) δ** 166.5, 155.7, 153.2, 151.2, 136.5, 131.1, 122.4, 121.7, 114.5, 111.6, 110.9, 107.9, 37.6, 15.2. **HRMS** calc. for $C_{14}H_{13}ClO_2N_3$ $[M+H]^+$, 290.06908 found, 290.06895.

8.4.39. Synthesis of 2-aminoresorcinol (81)

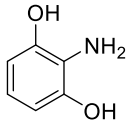

A mixture of 2-nitroresorcinol (**80**) (537 mg, 3.46 mmol) and a catalytic amount of palladium on activated charcoal in ethanol (10 mL) was vigorously stirred for 4 hours under an atmosphere of hydrogen. When the reaction had reached completion, the palladium was removed by filtration through celite. The filtrate was then concentrated *in vacuo* to yield the reduced product as a brown solid (414 mg, 3.31 mmol, 96%). This was taken to the next step crude.

Rf, 0.37 (60% EtOAc/Hexane) **^{1}H NMR (300 MHz, $CDCl_3$, CD_3OD) δ** 6.46 (t, *J* = 7.9 Hz, 1H, Ar*H*), 6.30 (d, *J* = 7.9 Hz, 2H, Ar*H*).**^{13}C NMR (75 MHz, $CDCl_3$, CD_3OD) δ** 146.2, 122.2, 119.0, 107.4. **HRMS** calc. for $C_6H_8NO_2$ $[M+H]^+$, 126.0555 found, 126.0552. **Mp:** 161 °C.

8.4.40. Synthesis of *N*-(2,6-dihydroxyphenyl)acetamide (82)

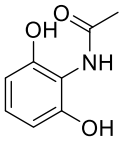

Triethylamine (2.2 mL, 16 mmol) was added to **81** (400 mg, 3.20 mmol) in THF (15 mL) at 0°C. After approximately 15 minutes acetyl chloride (0.30 mL, 3.5 mmol) was added to the reaction mixture at 0°C. The reaction was then allowed to warm to room temperature. After 18 hours the reaction mixture was basified with a 1M solution of KOH (50 mL) and stirred for 2 hours before 1M HCl (100 mL) was then added to acidify the reaction mixture to a pH of 2. The aqueous layer was extracted 3 times with EtOAc (3 × 100 mL), the combined organic layers where then washed with brine (300 mL), dried over $MgSO_4$, concentrated *in vacuo* and purified by silica gel column chromatography (40% – 100% EtOAc/Hexane) to yield the product **82** as an off-white solid (430 mg, 2.57 mmol, 80%)

Rf, 0.37 (60% EtOAc/Hexane) **^{1}H NMR (300 MHz, DMSO-*d*) δ** 9.33 (s, 3H, N*H*/O*H*), 6.87 (t, *J* = 8.1 Hz, 1H, Ar*H*), 6.35 (d, *J* = 8.1 Hz, 2H, Ar*H*), 2.11 (s, 3H, CH_3). **^{13}C NMR (75 MHz, DMSO-*d*) δ** 171.3, 153.0, 127.6, 115.0, 108.5, 23.7. **HRMS** calc. for $C_8H_{10}NO_3$ $[M+H]^+$, 168.0661 found, 168.0658. **IR ATR (cm^{-1}):** 3399, 3380, 3277, 1656, 1536, 1485, 1026. **Mp:** 175 °C.

8.4.41. Synthesis of 2-(ethylamino)benzene-1,3-diol (83)

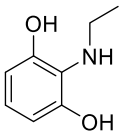

Aluminium trichloride (957 mg, 7.18 mmol) was added portionwise to lithium aluminium hydride (272 mg, 7.18 mmol) in THF (15 mL) at 0°C. The reaction was taken to room temperature and stirred for approximately 10 minutes before being once again cooled to 0°C at which point **82** (384 mg, 2.30 mmol) was added. The reaction was subsequently heated under reflux for 18 hours. After cooling the reaction was quenched with HCl (50 mL) and the crude product was extracted twice into EtOAc (2 × 100 mL). The organic phase was dried over $MgSO_4$, concentrated *in vacuo* and subsequently purified by column chromatography (20% – 80% EtOAc/Hexane) to afford the product **83** as a brown solid (214 mg, 1.40 mmol, 61%).

Rf, 0.25 (60% EtOAc/Hexane) **^{1}H NMR (300 MHz, DMSO-*d*) δ** 6.42 (t, *J* = 7.8 Hz, 1H, Ar*H*), 6.24 (d, *J* = 7.8 Hz, 2H, Ar*H*), 3.36 (s, 3H, O*H*/N*H*), 3.12 (q, *J* = 7.1 Hz, 2H, CH_2), 1.02 (t, *J* = 7.1 Hz, 3H, CH_3). **^{13}C NMR (75 MHz, DMSO-*d*) δ** 149.7, 125.6, 120.3, 107.8, 41.6, 17.0. **HRMS** calc. for $C_8H_{12}NO_2$ $[M+H]^+$, 154.0868 found, 154.0867. **IR ATR (cm^{-1}):** 3128, 2962, 1564, 1447, 1340, 1013. **Mp:** 153 °C.

8.4.42. Synthesis of 3-ethyl-4-hydroxybenzo[*d*]oxazol-2(3*H*)-one (84)

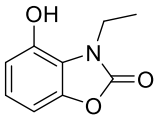

This reaction was carried out according to the procedure (conditions B) described for **36** using the following: CDI (159 mg, 9.79 mmol) and **83** (100 mg, 653 µmol). This reaction yielded **84** as a yellow solid (97 mg, 541 µmol, 83%).

Rf, 0.53 (60% EtOAc/Hexane) **^{1}H NMR (300 MHz, $CDCl_3$, CD_3OD) δ** 6.86 – 6.78 (m, 1H, Ar*H*), 6.65 (dd, *J* = 8.0, 0.8 Hz, 1H, Ar*H*), 6.57 (dd, *J* = 8.3, 0.8 Hz, 1H, Ar*H*), 3.99 (q, *J* = 7.1 Hz, 2H, CH_2), 1.30 (t, *J* = 7.1 Hz, 3H, CH_3). **^{13}C NMR (75 MHz, $CDCl_3$, CD_3OD) δ** 155.1, 144.1, 142.7, 122.6, 118.2, 111.4, 101.8, 38.9, 14.7. **HRMS** calc. for $C_9H_{10}NO_3$ $[M+H]^+$, 180.0661 found, 180.0654. **Mp:** 247 °C.

8.4.43. Synthesis of 3-chloro-5-((3-ethyl-2-oxo-2,3-dihydrobenzo[*d*]oxazol-4-yl)oxy)benzonitrile (79)

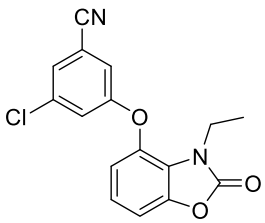

This reaction was carried out according to the procedure described for **52** using the following: **51** (113 mg, 728 µmol), **84** (87 mg, 0.49 mmol) and Cs_2CO_3 (237 mg, 728 µmol). This reaction yielded the desired product **79** as a yellow solid (67 mg, 0.21 mmol, 42%).

Rf, 0.51 (40% EtOAc/Hexane) **^{1}H NMR (400 MHz, $CDCl_3$) δ** 7.43 – 7.41 (m, 1H, Ar*H*), 7.27 – 7.24 (m, 1H, Ar*H*), 7.19 – 7.18 (m, 1H, Ar*H*), 7.15 – 7.09 (m, 2H, Ar*H*), 6.82 – 6.76 (m, 1H, Ar*H*), 3.90 (q, *J* = 7.2 Hz, 2H, CH_2), 1.30 (t, *J* = 7.2 Hz, 3H, CH_3). **^{13}C NMR (101 MHz, $CDCl_3$) δ** 158.3, 144.7, 137.8, 136.9, 127.0, 122.9, 122.5, 122.1, 118.6, 116.6, 115.8, 115.1, 110.6, 107.5, 39.0, 14.5. **HRMS** calc. for $C_{16}H_{12}N_2O_3Cl$ $[M+H]^+$, 315.0536 found, 315.0536. **IR ATR (cm^{-1}):** 3075, 2236, 1761, 1206, 857. **Mp:** 101 °C.

8.4.44. Synthesis of 3-ethyl-4-methoxy-1-((2-(trimethylsilyl)ethoxy)methyl)-1,3-dihydro-2*H*-benzo[*d*]imidazol-2-one (87)

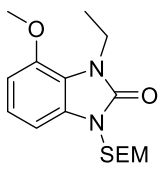

Methyl iodide (30 µL, 0.48) was added to a mixture of **38** (100 mg, 0.324 mmol) and NaH (60% in mineral oil, 20 mg, 0.83 mmol) in DMF (2 mL). After 2 hours at room temperature the reaction was quenched with a saturated solution of NH_4Cl (20 mL) and extracted twice with EtOAc (2 × 50 mL). The organic phases were combined, dried over $MgSO_4$ and concentrated *in vacuo*. Subsequent purification by column chromatography (5% – 30% EtOAc/Hexane) afforded **87** as a clear oil (96 mg, 0.30 mmol, 92%).

Rf, 0.38 (20% EtOAc/Hexane) **^{1}H NMR (400 MHz, $CDCl_3$) δ** 7.04 – 6.98 (m, 1H, Ar*H*), 6.84 – 6.80 (m, 1H, Ar*H*), 6.69 – 6.65 (m, 1H, Ar*H*), 5.29 (s, 2H, CH_2), 4.14 (q, *J* = 7.1 Hz, 2H, CH_2), 3.91 (s, 3H, CH_3), 3.62 – 3.55 (m, 2H, CH_2), 1.30 (t, *J* = 7.1 Hz, 3H, CH_3), 0.94 – 0.88 (m, 2H, CH_2), -0.05 (s, 9H, Si(CH_3)$_3$). **^{13}C NMR (101 MHz, $CDCl_3$) δ** 154.1, 145.1, 130.2, 121.8, 117.6, 105.1, 102.4, 70.8, 66.1, 55.9, 38.1, 17.9, 15.5, -1.3. **HRMS** calc. for $C_{16}H_{27}O_3N_2Si$ $[M+H]^+$, 323.17855 found, 323.17871.

8.4.45. Synthesis of 3-ethyl-4-((3-methylbut-2-en-1-yl)oxy)-1-((2-(trimethylsilyl)ethoxy)methyl)-1,3-dihydro-2*H*-benzo[*d*]imidazol-2-one (88)

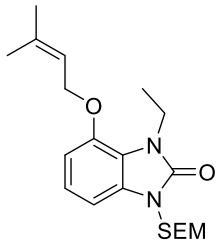

Prenylbromide (50 µL, 0.43 mmol) was added to a solution of **38** (100 mg, 0.324 mmol) and K_2CO_3 (54 mg, 0.39 mmol) in DMF (2 mL). After 18 hours at room temperature, the reaction was quenched with a saturated solution of NH_4Cl (20 mL))and extracted twice with EtOAc (2 × 50 mL). The organic phases were combined, dried over $MgSO_4$ and concentrated *in vacuo*. Subsequent purification by column chromatography (5% – 30% EtOAc/Hexane) afforded **88** as a clear oil (79 mg, 0.21 mmol, 65%).

Rf, 0.36 (20% EtOAc/Hexane) **^{1}H NMR (500 MHz, $CDCl_3$) δ** 7.01 – 6.97 (m, 1H, Ar*H*), 6.81 (dd, *J* = 7.9, 0.7 Hz, 1H, Ar*H*), 6.69 – 6.66 (m, 1H, Ar*H*), 5.51 – 5.47 (m, 1H, C*H*), 5.28 (s, 2H, CH_2), 4.61 (d, *J* = 6.6 Hz, 2H, CH_2), 4.15 (q, *J* = 7.1 Hz, 2H, CH_2), 3.62 – 3.56 (m, 2H, CH_2), 1.79 (s, 3H, CH_3), 1.75 (s, 3H, CH_3), 1.30 (t, *J* = 7.1 Hz, 3H, CH_3), 0.93 – 0.88 (m, 2H, CH_2), -0.05 (s, 9H, Si(CH_3)$_3$). **^{13}C NMR (126 MHz, $CDCl_3$) δ** 154.1, 144.3, 138.1, 130.4, 121.7, 119.6, 117.9, 106.3, 102.3, 70.8, 66.1, 65.6, 38.0, 25.8, 18.3, 17.9, 15.5, -1.3. **HRMS** calc. for $C_{20}H_{33}O_3N_2Si$ $[M+H]^+$, 377.22550 found, 377.22587.

8.4.46. Synthesis of 3-ethyl-4-hydroxy-1*H*-benzimidazol-2-one (89)

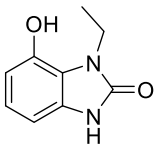

This reaction was carried out according to the procedure described for **38** using the following: **36** (116 mg, 0.651 mmol) and catalytic palladium on activated carbon. The reaction afforded **89** as a white solid (59 mg, 0.33 mmol, 77%).

Rf, 0.29 (40% EtOAc/Hexane) **^{1}H NMR (500 MHz, DMSO-*d*) δ** 10.66 (s, 1H, N*H* or O*H*), 9.66 (s, 1H, N*H* or O*H*), 6.78 – 6.73 (m, 1H, Ar*H*), 6.50 – 6.44 (m, 2H, Ar*H*), 3.94 (q, *J* = 7.0 Hz, 2H, CH_2), 1.20 (t, *J* = 7.0 Hz, 3H, CH_3). **^{13}C NMR (126 MHz, DMSO-*d*) δ** 153.9, 141.9, 130.0, 121.2, 117.1, 108.3, 100.7, 36.4, 15.6. **HRMS** calc. for $C_9H_{11}N_2O_2$ $[M+H]^+$, 179.0821 found, 179.0814. **IR ATR (cm^{-1}):** 3154, 2975, 1650, 1614. **Mp:** 218 °C.

8.4.47. Synthesis of 1-ethyl-7-methoxy-1,3-dihydro-2*H*-benzo[*d*]imidazol-2-one (85)

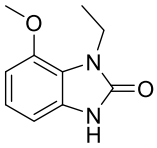

This reaction was carried out according to the procedure described for **87** using the following: **89** (30 mg, 0.17 mmol), methyl iodide (10 µL, 0.17 mmol) and NaH (60% in mineral oil, 7.0 mg, 0.29 mmol). This reaction afforded **85** as a white solid (7.0 mg, 0.036 mmol, 22%).

Rf, 0.14 (30% EtOAc/Hexane) **^{1}H NMR (500 MHz, $CDCl_3$) δ** 10.10 (s, 1H, N*H*), 7.01 – 6.96 (m, 1H, Ar*H*), 6.80 – 6.76 (m, 1H, Ar*H*), 6.65 – 6.62 (m, 1H, Ar*H*), 4.15 (q, *J* = 7.1 Hz, 2H, CH_2), 3.91 (s, 3H, OCH_3), 1.34 (t, *J* = 7.1 Hz, 3H, CH_3). **^{13}C NMR (126 MHz, $CDCl_3$) δ** 155.5, 145.2, 129.4, 121.9, 118.6, 104.5, 103.4, 55.9, 37.9, 15.7. **HRMS** calc. for $C_{10}H_{13}N_2O_2$ $[M+H]^+$, 193.09715 found, 193.09701. **IR ATR (cm^{-1}):** 3017, 2951, 1688, 1469, 1238. **Mp:** 124 °C.

8.4.48. Synthesis of 1-ethyl-7-((3-methylbut-2-en-1-yl)oxy)-1,3-2*H*-benzo[*d*]imidazole-2-one (86)

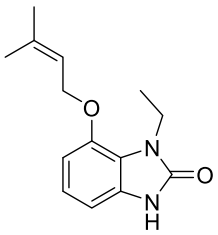

This reaction was carried out according to the procedure described for **88** using the following: prenylbromide (15 µL, 0.15 mmol) **89** (26 mg, 0.15 mmol) and K_2CO_3 (20 mg, 0.15 mmol). This reaction afforded the product **86** as a white solid (15 mg, 0.065 mmol, 44%).

Rf, 0.17 (40% EtOAc/Hexane) **^{1}H NMR (400 MHz, $CDCl_3$) δ** 10.41 (s, 1H, N*H*), 7.10 – 6.86 (m, 1H, Ar*H*), 6.78 (d, *J* = 7.8 Hz, 1H, Ar*H*), 6.63 (d, *J* = 8.3 Hz, 1H, Ar*H*), 5.50 (t, *J* = 5.6 Hz, 1H, C=C*H*), 4.61 (d, *J* = 6.6 Hz, 2H, CH_2), 4.17 (q, *J* = 7.0 Hz, 2H, CH_2), 1.80 (s, 3H, CH_3), 1.75 (s, 3H, CH_3), 1.34 (t, *J* = 7.1 Hz, 3H, CH_3). **^{13}C NMR (101 MHz, $CDCl_3$) δ** 155.6, 144.5, 138.1, 129.6, 121.8, 119.6, 118.7, 105.4, 103.3, 65.5, 37.8, 25.9, 18.4, 15.7. **HRMS** calc. for $C_{14}H_{19}N_2O_2$ $[M+H]^+$, 247.14410 found, 247.14393. **IR ATR (cm^{-1}):** 2968, 2926, 1687, 1627, 1237, 719. **Mp:** 135 °C.

8.5. Experimental pertaining to Chapter 4

8.5.1. Synthesis of 3-(3-fluorophenyl)propiolamide (94)

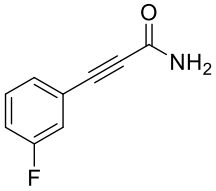

Conditions A: Toluene (3 mL) was added to an oven dried Schlenk tube and degassed under a positive pressure of argon for 15 minutes. To the toluene was added 3-fluoroiodobenzene (**92**) (0.20 mL, 1.8 mmol) and propiolamide (124 mg, 1.80 mmol), followed by $Pd(PPh_3)_4$ (62 mg, 54 µmol), copper iodide (31 mg, 0.16 mmol) and finally trimethylamine (0.25 mL, 1.8 mmol). The reaction was carried out for 18 hours at room temperature after which the reaction mixture was diluted with EtOAc (50 mL) and quenched with H_2O (50 mL). The organic phase was separated and washed with brine (50 mL). The organic phase was then dried over $MgSO_4$, concentrated in vacuo and purified on silica gel by column chromatography (40% – 100% EtOAc/hexane) to yield the product as a yellow solid (37 mg, 0.23 mmol, 13%).

Conditions B: To an oven dried Schlenk tube, DMF (3 mL) was added and degassed under a positive pressure of argon for 10 minutes. To the DMF was added **92** (0.11 mL, 0.90 mmol) and propiolamide (75 mg, 1.1 mmol) followed by triethylamine (0.60 mL, 4.5 mmol), triphenylphosphine (9.0 mg, 36 µmol) and finally $Pd(OAc)_2$ (4.0 mg, 18 µmol). Once all reagents had been added the reaction was heated to 70 °C. After 18 hours the reaction was cooled to room temperature and quenched with H_2O (30 mL). The reaction mixture was then extracted twice with EtOAc (2 × 50 mL), the organic phases were combined and washed with brine (100 mL) and then dried over $MgSO_4$ before being concentrated *in vacuo*. The crude product was then purified on silica gel by column chromatography (40% – 100% EtOAc/Hexane) to yield the product as a yellow solid (101 mg, 0.619 mmol, 69%).

Rf, 0.28 (60% EtOAc/Hexane) **^{1}H NMR (300 MHz, $CDCl_3$) δ** 7.39 – 7.29 (m, 2H, Ar*H*), 7.25 – 7.20 (m, 1H, Ar*H*), 7.18 – 7.09 (m, 1H, Ar*H*), 5.98 (2 × s, 2H, NH_2). **^{13}C NMR (75 MHz, $CDCl_3$) δ** 162.4 (d, J_{CF} = 248 Hz), 154.7, 130.5 (d, J_{CF} = 8.5 Hz), 128.7 (d, J_{CF} = 3.3 Hz), 121.9 (d, J_{CF} = 9.9 Hz), 119.5 (d, J_{CF} = 24 Hz), 118.0 (d, J_{CF} = 21 Hz), 84.5 (d, J_{CF} = 3.3 Hz), 82.9. **HRMS** calc. for C_9H_7FNO $[M+H]^+$, 164.0512 found, 164.0513. **IR ATR (cm^{-1}):** 3378, 3164, 2212, 1674, 1606, 1578. **Mp:** 112 °C.

8.5.2. Synthesis of ethyl 3-(3-fluorophenyl)propiolate (98)

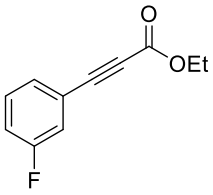

Sonogashira conditions: This reaction was carried out according to the procedure (conditions A) described for **94** using the following: 3-fluoroiodobenzene (**92**) (0.20 mL, 1.8 mmol), ethyl propiolate (0.18 mL, 1.80 mmol), $Pd(PPh_3)_4$ (62 mg, 54 µmol), copper iodide (31 mg, 0.16 mmol) and finally trimethylamine (0.25 mL, 1.8 mmol). This reaction yielded **98** as a yellow oil (15 mg, 0.078 mmol, 4%).

Negishi conditions: THF (5 mL) was added to an oven dried Schlenk tube and degassed under a positive pressure of argon for 15 minutes. *n*-BuLi (1.3 M in THF, 1.7 mL, 2.2 mmol) was then added to the THF followed by diisopropylamine (0.30 mL, 2.2 mmol) at -78 °C. To the reaction mixture was then added **92** (0.2 mL, 1.8 mmol), zinc (II) bromide (568 mg, 2.52 mmol), ethyl propiolate (0.26 mL, 2.5 mmol) and $Pd(PPh_3)_4$ (104 mg, 90.0 µmol). The reaction was allowed to warm to room temperature and after 18 hours the reaction mixture was quenched with a saturated NH_4Cl (40 mL) solution and extracted twice with Et_2O (2 × 50 mL). The organic phase was then washed with a saturated solution of $NaHCO_3$ (100 mL) followed by brine (100 mL). The organic phase was dried over $MgSO_4$, concentrated *in vacuo* and purified on silica by column chromatography (5% – 20% EtOAc/Hexane) to yield the product as a yellow oil (45 mg, 0.23 mmol, 13%).

Rf, 0.53 (20% EtOAc/Hexane) **^{1}H NMR (400 MHz, $CDCl_3$) δ** 7.40 – 7.32 (m, 2H, Ar*H*), 7.30 – 7.25 (m, 1H, Ar*H*), 7.20 – 7.13 (m, 1H, Ar*H*), 4.31 (q, *J* = 7.1 Hz, 2H, CH_2), 1.36 (t, *J* = 7.1 Hz, 3H, CH_3). **^{13}C NMR (75 MHz, $CDCl_3$) δ** 162.6 (d, J_{CF} = 248 Hz), 154.1, 130.7 (d, J_{CF} = 9 Hz), 129.2 (d, J_{CF} = 3 Hz), 121.8 (d, J_{CF} = 10 Hz), 120.0 (d, J_{CF} = 23 Hz), 118.4 (d, J_{CF} = 21 Hz), 84.6 (d, J_{CF} = 4 Hz), 81.5, 62.6, 14.4.

This spectroscopic data compares favourably with that in the literature.[228]

8.5.3. Synthesis of diethyl (*E*)-hex-2-en-4-ynedioate (99)

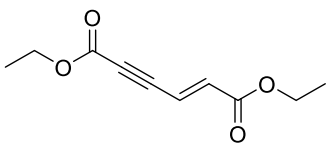

Compound **99** was formed under the Sonogashira conditions described for the synthesis of **98**. This product was obtained as an orange solid.

^{1}H NMR (400 MHz, $CDCl_3$) δ 6.74 (d, *J* = 16 Hz, 1H, C*H*), 6.42 (d, *J* = 16 Hz, 1H, C*H*), 4.27 – 4.18 (m, 4H, CH_2), 1.32 – 1.26 (m, 6H, CH_3). **^{13}C NMR (101 MHz, $CDCl_3$) δ** 164.7, 153.2, 135.5, 121.6, 87.1, 81.5, 62.5, 61.4, 14.2, 14.0.

This spectroscopic data compares favourably with that in the literature.[229]

8.5.4. Synthesis of ethyl (E)-3-(diisopropylamino)acrylate (100)

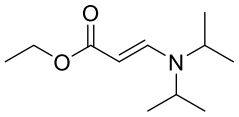

Compound **100** was formed under the Negishi conditions described for the synthesis of **98**. This product was obtained as a yellow oil.

^{1}H NMR (300 MHz, $CDCl_3$) δ 7.53 (d, *J* = 13.2 Hz, 1H, C*H*), 4.63 (d, *J* = 13.1 Hz, 1H, C*H*), 4.09 (q, *J* = 7.1 Hz, 2H, CH_2), 3.69 – 7.53 (m, 2H, C*H*), 1.22 (t, *J* = 7.1 Hz, 3H, CH_3), 1.17 (d, *J* = 6.8 Hz, 12H).

This spectroscopic data compares favourably with that in the literature.[234]

8.5.5. Synthesis of ((3-fluorophenyl)ethynyl)trimethylsilane (101)

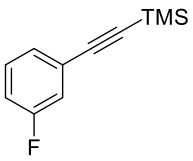

This reaction was carried out according to the procedure (conditions A) described for **94** using the following: **92** (0.11 mL, 0.90 mmol), ethynyltrimethysilane (0.13 mL, 0.90 mmol), $Pd(PPh_3)_4$ (31 mg, 27 µmol), copper iodide (15 mg, 81 µmol) and trimethylamine (0.13 mL, 0.90 mmol). This reaction afforded **101** as a colourless oil (174 mg, 0.90 mmol, quant.).

Rf, 0.59 (100% hexane) **^{1}H NMR (300 MHz, $CDCl_3$) δ** 7.28 – 7.19 (m, 2H, Ar*H*), 7.17 – 7.11 (m, 1H, Ar*H*), 7.04 – 6.96 (m, 1H, Ar*H*), 0.24 (s, 9H, Si(CH_3)). **^{13}C NMR (75 MHz, $CDCl_3$) δ** 162.4 (d, J_{CF} = 246 Hz), 129.9 (d, J_{CF} = 8.6 Hz), 128.0 (d, J_{CF} = 3.0 Hz), 125.1 (d, *J* = 9.1 Hz), 118.9 (d, J_{CF} = 23 Hz), 116.0 (d, J_{CF} = 21 Hz), 103.8 (d, J_{CF} = 3 Hz), 95.5, 0.0.

This spectroscopic data compares favourably with that in the literature.[228]

8.5.6. Synthesis of 3-(3-fluorophenyl)prop-2-yn-1-ol (107)

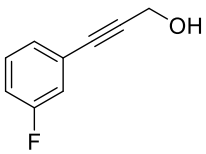

This reaction was carried out according to the procedure (conditions A) described for **94** using the following: **92** (0.22 mL, 1.8 mmol), propargyl alcohol (0.11 mL, 1.8 mmol), $Pd(PPh_3)_4$ (62 mg, 54 µmol), copper iodide (30 mg, 0.16 mmol) and trimethylamine (0.26 mL, 1.8 mmol). This reaction afforded **107** as a yellow oil (264 mg, 1.76 mmol, 97%).

Rf, 0.4 (40% EtOAc/Hexane) **^{1}H NMR (300 MHz, $CDCl_3$) δ** 7.30 – 7.18 (m, 2H, Ar*H*), 7.15 – 7.09 (m, 1H, Ar*H*), 7.06 – 6.98 (m, 1H, Ar*H*), 4.50 (d, *J* = 5.9 Hz, 2H, CH_2), 2.43 (t, *J* = 5.9 Hz, 1H, O*H*). **^{13}C NMR (75 MHz, $CDCl_3$) δ** 162.4 (d, J_{CF} = 245 Hz), 130.0 (d, J_{CF} = 9 Hz), 127.7 (d, J_{CF} = 3 Hz), 124.5 (d, J_{CF} = 9 Hz), 118.6 (d, J_{CF} = 23 Hz), 116.0 (d, J_{CF} = 21 Hz), 88.3, 84.5 (d, J_{CF} = 3 Hz), 51.5.

This spectroscopic data compares favourably with that in the literature.[284]

8.5.7. Synthesis of 3-(3-fluorophenyl)propiolonitrile (96)

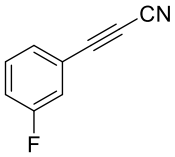

DMSO (0.25 mL, 3.4 mmol) in DCM (1 mL) was added to oxalyl chloride (70 µL, 0.80 mmol) in DCM (1 mL) in a Schlenk tube at -78 °C. After 15 minutes **94** (94 mg, 0.57 mmol) in a mixture of DCM (1 mL) and DMSO (0.2 mL) was added dropwise to the reaction mixture at -78 °C and the reaction mixture was stirred for 20 minutes. Finally, triethylamine (0.20 mL, 1.6 mmol) was added at -78 °C to the reaction mixture, after which the reaction was allowed to warm to room temperature. The reaction was monitored by TLC and after 1 hour all the starting material had been consumed. The reaction was quenched with NH_4Cl (40 mL) and extracted twice with DCM (2 × 50 mL). The organic layers were combined, washed with brine (100 mL), dried over $MgSO_4$ and concentrated *in vacuo*. The crude material was purified on silica gel by column chromatography (10% EtOAc/Hexane) to yield the dehydrated product **96** as a yellow solid (57 mg, 0.054 mmol, 69%).

Rf, 0.76 (60% EtOAc/Hexane) **^{1}H NMR (300 MHz, $CDCl_3$) δ** 7.47 – 7.38 (m, 2H, Ar*H*), 7.35 – 7.24 (m, 2H, Ar*H*). **^{13}C NMR (75 MHz, $CDCl_3$) δ** 162.29 (d, J_{CF} = 249 Hz), 130.92 (d, J_{CF} = 8.5 Hz), 129.64 (d, J_{CF} = 3.7 Hz), 120.32 (d, J_{CF} = 24 Hz), 119.78 (d, J_{CF} = 21 Hz), 119.44 (d, J_{CF} = 9.0 Hz), 105.26, 81.36 (d, J_{CF} = 3.3 Hz), 63.85. **IR ATR (cm^{-1}):** 3076, 2259, 2146, 1577, 1289, 1173. **Mp:** 53 °C.

8.5.8. Synthesis of (*E*)-3-((3-ethyl-2-oxo-1-((2-(trimethylsilyl)ethoxy)methyl)-2,3-dihydro-1*H*-benzo[*d*]imidazol-4-yl)oxy)-3-(3-fluorophenyl)acrylonitrile (115)

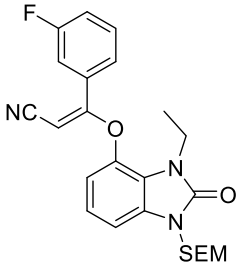

This reaction was carried out according to the procedure described for **52** using the following: **38** (50 mg, 0.16 mmol), **96** (35 mg, 0.24 mmol) and Cs_2CO_3 (87 mg, 0.24 mmol). Only trace amounts of **115** were obtained.

Rf, 0.43 (20% EtOAc/Hexane) **^{1}H NMR (300 MHz, CDCl3) δ** 7.90 – 7.84 (m, 1H, Ar*H*), 7.73 – 7.67 (m, 1H, Ar*H*), 7.57 – 7.49 (m, 1H, Ar*H*), 7.33 – 7.28 (m, 1H, Ar*H*), 7.17 – 7.09 (m, 2H, Ar*H*), 6.84 (dd, *J* = 6.7, 2.6 Hz, 1H, Ar*H*), 5.33 (s, 2H, CH_2), 4.72 (s, 1H, C*H*), 3.91 (q, *J* = 7.1 Hz, 2H, CH_2), 3.68 – 3.59 (m, 2H, CH_2), 1.25 (t, *J* = 7.1 Hz, 3H, CH_3), 0.99 – 0.90 (m, 2H, CH_2), -0.03 (s, 9H, Si(CH_3)$_3$). **^{13}C NMR (101 MHz, CDCl3) δ** 166.6 (d, J_{CF} = 2.9 Hz), 163.0 (d, J_{CF} = 248.3 Hz), 154.1, 139.6, 134.2 (d, J_{CF} = 7.7 Hz), 131.3, 131.1 (d, J_{CF} = 8.4 Hz), 122.3 (d, J_{CF} = 3.1 Hz), 121.9, 119.6, 119.1 (d, J_{CF} = 21.7 Hz),

114.0 (d, J_{CF} = 23.6 Hz), 113.6, 111.5, 105.9, 82.6, 71.0, 66.4, 38.3, 17.9, 15.5, -1.3. **HRMS** calc. for $C_{24}H_{29}FN_3O_3Si$ $[M+H]^+$, 454.1962 found, 454.1948. **IR ATR (cm^{-1}):** 3056, 2952, 2218, 1712, 1582, 1210, 1078.

8.5.9. Synthesis of (*E*)-3-(3-fluorophenyl)acrylamide (119)

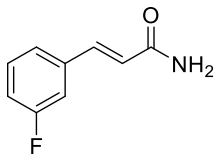

This reaction was carried out according to the procedure (conditions B) described for **94** using the following: **92** (0.11 mL, 0.90 mmol), acrylamide (77 mg, 1.1 mmol), triethylamine (0.60 mL, 4.5 mmol), triphenylphosphine (9.0 mg, 36 µmol) and $Pd(OAc)_2$ (4.0 mg, 18 µmol). This reaction afforded the product **119** as a brown solid (150 mg, 0.901 mmol, quant.).

Rf, 0.32 (100% EtOAc) **^{1}H NMR (300 MHz, $CDCl_3$) δ** 7.62 (d, *J* = 15.7 Hz, 1H, C*H*), 7.39 – 7.32 (m, 1H, Ar*H*), 7.31 – 7.26 (m, 1H, Ar*H*), 7.24 – 7.18 (m, 1H, Ar*H*), 7.11 – 7.04 (m, 1H, Ar*H*), 6.49 (d, *J* = 15.7 Hz, 1H, C*H*), 5.99 (2 × s, 2H, N*H*$_2$). **^{13}C NMR (75 MHz, $CDCl_3$) δ** 167.6, 164.5 (d, J_{CF} = 246 Hz), 141.2 (d, J_{CF} = 2.6 Hz), 136.8 (d, J_{CF} = 8.0 Hz), 130.4 (d, J_{CF} = 8.4 Hz), 124.0 (d, J_{CF} = 2.9 Hz), 120.9, 116.8 (d, J_{CF} = 21 Hz), 114.1, (d, J_{CF} = 22 Hz). **HRMS** calc. for C_9H_9FNO $[M+H]^+$, 166.0668 found, 166.0667. **IR ATR (cm^{-1}):** 3374, 3172, 1666, 1609, 1396, 1265.

8.5.10. Synthesis of (*E*)-3-(3-fluorophenyl)acrylonitrile (120)

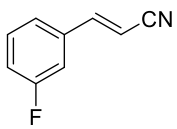

This reaction was carried out according to the procedure described for **96** using the following: DMSO (0.40 mL, 5.5 mmol), oxalyl chloride (0.11 mL, 1.3 mmol), **119** (150 mg, 0.908 mmol) and triethylamine (0.40 mL, 2.5 mmol) This reaction afforded **120** as a yellow solid (69 mg, 0.47 mmol, 45%).

Rf, 0.69 (60% EtOAc/Hexane) **^{1}H NMR (400 MHz, $CDCl_3$) δ** 7.42 – 7.33 (m, 2H, Ar*H* + C*H*), 7.25 – 7.21 (m, 1H, Ar), 7.18 – 7.07 (m, 2H, Ar), 5.89 (d, *J* = 16.6 Hz, 1H, C*H*). **^{13}C NMR (101 MHz, $CDCl_3$) δ** 163.1 (d, J_{CF} = 248 Hz), 149.3 (d, J_{CF} = 2.8 Hz), 135.7 (d, J_{CF} = 7.7 Hz), 130.9 (d, J_{CF} = 8.3 Hz), 123.6 (d, J_{CF} = 3 Hz), 118.3 (d, J_{CF} = 21 Hz), 117.7, 113.9 (d, J_{CF} = 22 Hz), 98.1. **HRMS** calc. for C_9H_7FN $[M+H]^+$, 148.0563 found, 148.0557. **IR ATR (cm^{-1}):** 3062, 2211, 1620, 1581, 1445, 1269, 965. **Mp:** 54 °C.

8.5.11. Synthesis of (*E*)-3-(3-cyano-5-fluorophenyl)acrylamide (122)

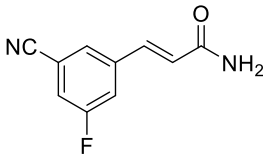

Copper-free conditions: This reaction was carried out according to the procedure (conditions B) described for **94** using the following: 3-bromo-5-fluorobenzonitrile (**91**) (100 mg, 0.50 mmol), acrylamide (42 mg, 0.60 mmol), triethylamine (0.40 mL, 2.4 µmol), triphenylphosphine (6.0 mg, 22 µmol) and $Pd(OAc)_2$ (2.0 mg, 9.0 µmol). This reaction afforded the product **122** as a yellow solid (16 mg, 0.079 mmol, 16%)

Phosphine-free conditions: DMF (2 mL) was added to a Schlenk tube charged with **91** (100 mg, 0.50 mmol), acrylamide (53 mg, 0.75 mmol) and N-phenylurea (14 mg, 0.10 mmol). The reaction mixture was then degassed under a positive pressure of argon for approximately 10 minutes. $Pd(OAc)_2$ (11 mg, 50 µmol) was then added to the reaction mixture followed by K_2CO_3 (138 mg, 1.00 mmol). The Schlenk tube was then placed in an oil bath preheated to 130 °C. After 2 hours the reaction was cooled to room temperature, quenched with H_2O (50 mL) and extracted with three times with EtOAc (3 × 50 mL). The organic phases were combined, washed with brine (150 mL), dried over $MgSO_4$ and concentrated *in vacuo*. The crude material was then purified by column chromatography (70% EtOAc/hexane – 100% EtOAc) to yield the desired product as a yellow solid (72 mg, 0.38 mmol, 76%).

Rf, 0.28 (100% EtOAc/Hexane) **^{1}H NMR (400 MHz, DMSO-*d*) δ** 7.96 – 7.92 (m, 1H, Ar*H*), 7.88 – 7.79 (m, 2H, Ar*H*), 7.58 (s, 1H, N*H*), 7.43 (d, *J* = 15.9 Hz, 1H, C*H*), 7.29 (s, 1H, N*H*), 6.77 (d, *J* = 15.9 Hz, 1H, C*H*). **^{13}C NMR (101 MHz, DMSO) δ** 166.0, 161.9 (d, J_{CF} = 247 Hz), 139.1 (d, J_{CF} = 8.9 Hz), 136.0 (d, J_{CF} = 3.0 Hz), 127.9 (d, J_{CF} = 3.3 Hz), 126.3, 119.6 (d, J_{CF} = 25.0 Hz), 119.1 (d, J_{CF} = 22.2 Hz), 117.5 (d, J_{CF} = 3.6 Hz), 113.5 (d, J_{CF} = 10.9 Hz). **HRMS** calc. for $C_{10}H_8FN_2$ $[M+H]^+$, 191.06152 found, 191.06146. **IR ATR (cm^{-1}):** 3367, 3172, 3078, 2235, 1669, 579. **Mp:** 115 °C.

8.5.12. Synthesis of (*E*)-3-(2-cyanovinyl)-5-fluorobenzonitrile (123)

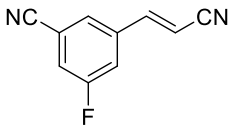

Conditions A: This reaction was carried out according to the procedure described for **96** using the following: DMSO (0.20 mL, 2.3 mmol), oxalyl chloride (0.11 mL, 50 µmol), **122** (66 mg, 0.35 mmol) and triethylamine (0.15 mL, 1.1 mmol) This reaction afforded **123** as a yellow solid (17 mg, 0.099 mmol, 29%).

Conditions B: **122** (193 mg, 1.02 mmol) was suspended in $POCl_3$ (2.0 mL, 21 mmol) at 0 °C for 30 minutes. The suspension was then allowed to warm to room temperature over 18 hours. The reaction mixture was cooled to 0 °C, quenched with H_2O (50 mL) and extracted twice with EtOAc (2 × 100 mL). The combined organic phases were washed with brine (200 mL), dried over $MgSO_4$ and concentrated *in vacuo*. The crude material was purified by column chromatography (10% EtOAc/hexane – 60% EtOAc/hexane) to yield the product as a white solid (133 mg, 0.77 mmol, 76%).

Rf, 0.81 (50% EtOAc/Hexane) **^{1}H NMR (400 MHz, $CDCl_3$) δ** 7.56 – 7.51 (m, 1H, Ar*H*), 7.44 – 7.37 (m, 2H, Ar*H*), 7.34 (d, *J* = 16.7 Hz, 1H, C*H*), 5.98 (d, *J* = 16.6 Hz, 1H, C*H*). **^{13}C NMR (101 MHz, $CDCl_3$) δ** 162.6 (d, J_{CF} = 253 Hz), 146.7 (d_{CF}, *J* = 2.7 Hz), 137.1 (d_{CF}, *J* = 8.2 Hz), 127.1 (d_{CF}, *J* = 3.5 Hz), 121.2 (d_{CF}, *J* = 25 Hz), 118.6 (d_{CF}, *J* = 22 Hz), 116.8, 116.7 (d_{CF}, *J* = 3.2 Hz), 115.2 (d_{CF}, *J* = 9.8 Hz), 101.1. **HRMS** calc. for $C_{10}H_6FN_2$ $[M+H]^+$, 173.05095 found, 173.05092. **IR ATR (cm^{-1}):** 3076, 2235, 2219, 1589, 1438, 970, 671. **Mp:** 141 °C.

8.5.13. Synthesis of 3-bromo-5-((3-ethyl-2-oxo-1-((2-(trimethylsilyl)ethoxy)methyl)-2,3-dihydro-1*H*-benzo[*d*]imidazol-4-yl)oxy)benzonitrile (125)

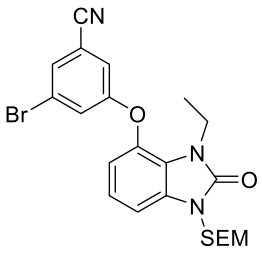

This reaction was carried out according to the procedure described for **52** using the following: **38** (400 mg, 1.30 mmol), **91** (519 mg, 2.60 mmol) and Cs_2CO_3 (634 mg, 1.95 mmol). This reaction afforded **125** as a clear oil. (609 mg, 1.25 mmol, 96%).

Rf, 0.56 (20% EtOAc/Hexane) **^{1}H NMR (300 MHz, $CDCl_3$) δ** 7.52 – 7.51 (m, 1H, Ar*H*), 7.40 – 7.38 (m, 1H, Ar*H*), 7.19 – 7.18 (m, 1H, Ar*H*), 7.13 – 7.06 (m, 2H, Ar*H*), 6.75 – 6.67 (m, 1H, Ar*H*), 5.34 (s, 2H, CH_2), 3.93 (q, *J* = 7.1 Hz, 2H, CH_2), 3.69 – 3.59 (m, 2H, CH_2), 1.24 (t, *J* = 7.1 Hz, 3H, CH_3), 0.99 – 0.90 (m, 2H, CH_2), -0.02 (s, 9H, Si(CH_3)$_3$). **^{13}C NMR (75 MHz, $CDCl_3$) δ** 158.9, 153.8, 131.7, 129.2, 124.7, 124.0, 122.3, 120.7, 118.8, 116.7, 115.2, 114.2, 106.4, 70.9, 66.4, 37.8, 17.8, 15.1, -1.4. **HRMS** calc. for $C_{22}H_{27}BrN_3O_3Si$ $[M+H]^+$, 488.1005 found, 488.0998. **IR ATR (cm^{-1}):** 3074, 2952, 2235, 1708, 1588, 1211.

8.5.14. Synthesis of (*E*)-3-(3-cyano-5-((3-ethyl-2-oxo-1-((2-(trimethylsilyl)ethoxy)methyl)-2,3-dihydro-1*H*-benzo[*d*]imidazol-4-yl)oxy)phenyl)acrylamide (126)

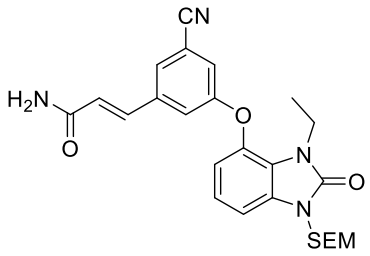

The reaction was carried out according to the procedure (phosphine-free conditions) described for **122** using the following: **125** (500 mg, 1.02 mmol), acrylamide (109 mg, 1.53 mmol), N-phenylurea (28 mg, 0.12 mmol), $Pd(OAc)_2$ (23 mg, 0.10 mmol) and K_2CO_3 (283 mg, 2.05 mmol). This reaction afforded **126** as a yellow solid (437 mg, 0.913 mmol, 89%).

Rf, 0.13 (60% EtOAc/Hexane) **^{1}H NMR (400 MHz, $CDCl_3$) δ** 7.59 – 7.50 (m, 2H, Ar*H*), 7.36 – 7.30 (m, 1H, Ar*H*), 7.24 – 7.21 (m, 1H, Ar*H*), 7.12 – 7.05 (m, 2H, Ar*H*), 6.75 – 6.68 (m, 1H, Ar*H*), 6.47 (d, *J* = 15.6 Hz, 1H, C*H*), 5.68 (s, 2H, CH_2), 5.34 (s, 2H, CH_2), 3.95 (q, *J* = 7.0 Hz, 2H, CH_2), 3.68 – 3.61 (m, 2H, CH_2), 1.24 (t, *J* = 7.0 Hz, 3H, CH_3), 0.98 – 0.93 (m, 2H, CH_2), -0.02 (s, 9H, Si(CH_3)$_3$). **^{13}C NMR (101 MHz, $CDCl_3$) δ** 166.7, 158.8, 153.9, 139.4, 138.2, 138.0, 131.7, 125.6, 123.2, 122.4, 120.8, 120.7, 120.6, 117.7, 114.6, 114.3, 106.3, 71.0, 66.5, 37.9, 17.9, 15.2, -1.3. **HRMS** calc. for $C_{25}H_{31}O_4N_4Si$ $[M+H]^+$, 479.21091 found, 479.21167. **IR ATR (cm^{-1}):** 3324, 2925, 2231, 1674, 1581, 1214, 834.

8.5.15. Synthesis of (*E*)-3-(3-cyano-5-((3-ethyl-2-oxo-2,3-dihydro-1*H*-benzo[*d*]imidazol-4-yl)oxy)phenyl)acrylamide (128)

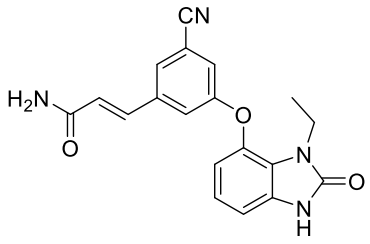

This reaction was carried out according to the procedure described for **21** using the following: **126** (415 mg, 0.867 mmol) and TBAF (3.5 mL, 13 mmol). The reaction yielded **128** as an off-white solid (97 mg, 0.28 mmol, 32%).

Rf, 0.33 (2% EtOAc/MeOH) **^{1}H NMR (500 MHz, CD_3OD) δ** 7.70 – 7.67 (m, 1H), 7.54 – 7.46 (m, *J* = 15.8 Hz, 2H), 7.35 – 7.32 (m, 1H), 7.09 – 7.05 (m, *J* = 8.5 Hz, 1H), 7.00 – 6.95 (m, *J* = 8.5 Hz, 1H), 6.73 – 6.63 (m, 2H), 3.92 (q, *J* = 7.0 Hz, 2H), 1.20 (t, *J* = 6.7 Hz, 3H). **^{13}C NMR (126 MHz, CD_3OD) δ** 166.3, 158.6, 155.0, 138.5, 138.4, 137.9, 131.0, 125.8, 124.0, 122.1, 121.1, 120.6, 120.1, 117.2, 114.2, 113.0, 106.3, 37.0, 14.0. **HRMS** calc. for $C_{19}H_{17}O_3N_4$ $[M+H]^+$, 349.12952 found, 349.12955. **IR ATR (cm^{-1}):** 3148, 3067, 2228, 1688, 1582, 1475, 1225. **Mp:** degrades at 256 °C.

8.5.16. Synthesis of (*E*)-3-(2-cyanovinyl)-5-((3-ethyl-2-oxo-2,3-dihydro-1*H*-benzo[*d*]imidazol-4-yl)oxy)benzonitrile (127)

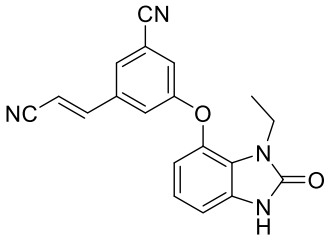

This reaction was carried out according to the procedure (conditions B) described for **123** using the following: **128** (135 mg, 0.388 mmol) and $POCl_3$ (0.80 mL, 8.6 mmol). The reaction afforded **127** as a white solid (52 mg, 0.16 mmol, 41%).

Rf, 0.33 (50% EtOAc/Hexane) **^{1}H NMR (500 MHz, $CDCl_3$) δ** 10.01 (s, 1H, N*H*), 7.47 – 7.45 (m, 1H, Ar*H*), 7.35 – 7.29 (m, 3H, Ar*H*), 7.09 – 7.02 (m, 2H, Ar*H*), 6.70 – 6.66 (m, 1H, Ar*H*), 5.94 (d, *J* = 16.6 Hz, 1H, C*H*), 3.95 (q, *J* = 7.1 Hz, 2H, CH_2), 1.28 (t, *J* = 7.1 Hz, 3H, CH_3). **^{13}C NMR (126 MHz, $CDCl_3$) δ** 159.1, 155.3, 147.3, 137.9, 136.9, 130.9, 125.2, 122.5, 122.0, 121.6, 119.7, 117.2, 116.9, 115.2, 113.6, 107.4, 100.7, 37.7, 15.4. **HRMS** calc. for $C_{19}H_{15}O_2N_4$ $[M+H]^+$, 331.11895 found, 331.11880. **IR ATR (cm^{-1}):** 3049, 2224, 1669, 1582, 1225, 749. **Mp:** 241 °C.

8.6. Experimental pertaining to Chapter 5

8.6.1. Synthesis of 1-(benzyloxy)-2-iodo-3-nitrobenzene (131)

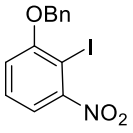

33 (500 mg, 2.05 mmol) was added to a mixture of DMSO (9 mL) and a 30% solution of H_sSO_4 (9 mL) and heated to 50 °C. After 2 hours, the reaction was cooled to 0 °C and $NaNO_2$ (212 mg, 3.07 mmol) in H_2O (1 mL) was added dropwise to the reaction mixture. After an hour at 0 °C potassium iodide (1.0 g, 6.0 mmol) in H_2O (1 mL) was added to the reaction mixture and the notable evolution of gas was indicative that displacement of the diazonium salt was transpiring. Following another hour additional potassium iodide (1.0 g, 6.0 mmol) was introduced into the reaction mixture and the reaction was left to run for 18 hours. The resulting product was subsequently extracted twice from the reaction mixture with EtOAc (2 × 100 mL). The organic phases were then combined and washed with sodium thiosulfate (200 mL), H_2O (200 mL) and brine (200 mL). The organic phase was then dried over $MgSO_4$, concentrated *in vacuo* and purified on silica gel by column chromatography (5% – 20% EtOAc/Hexane) to afford the desired product **131** as a yellow solid (441 mg, 1.24 mmol, 60%).

Rf, 0.36 (20% EtOAc/Hexane) **^{1}H NMR (400 MHz, $CDCl_3$) δ** 7.50 – 7.22 (m, 7H, Ar*H*), 6.99 (dd, *J* = 8.2, 1.0 Hz, 1H, Ar*H*), 5.21 (s, 2H, CH_2). **^{13}C NMR (101 MHz, $CDCl_3$) δ** 158.8, 135.5, 130.1, 128.9, 128.4, 127.1, 117.2, 115.2, 80.9, 71.9. **HRMS** calc. for $C_{13}H_{11}IO_3N$ $[M+H]^+$, 355.97781 found, 355.97812. **IR ATR (cm^{-1}):** 2361, 1521, 1337, 1260, 1015, 692, 566. **Mp:** 90 °C.

8.6.2. Attempted synthesis of 1-(2-(benzyloxy)-6-nitrophenyl)ethan-1-one (132)

n-BuLi (0.90 M in THF, 1.1 mL, 1.0 mmol) was added dropwise to **131** (300 mg, 845 µmol) in THF (3 mL) at -78 °C. After approximately 1 hour at this temperature, *N*-Methoxy-*N*-methylacetamide **139** (0.11 mL, 1.0 mmol) was added dropwise to the reaction mixture and the reaction was allowed to warm to room temperature. After 18 hours the reaction was quenched with a saturated solution of NH_4Cl (50 ml) and extracted twice with EtOAc (2 × 100 mL). The organic phases were combined, washed with brine (200 mL), dried over $MgSO_4$ and concentrated *in vacuo*. Purification by column chromatography (2% – 10% EtOAc/Hexane), however, afforded compounds **140** and **141** (or **142**) and not the desired product **132**.

For **140**:

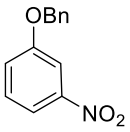

^{1}H NMR (400 MHz, $CDCl_3$) δ 7.87 – 7.80 (m, 2H, Ar*H*), 7.48 – 7.27 (m, 7H, Ar*H*), 5.15 (s, 2H, CH_2). **^{13}C NMR (101 MHz, $CDCl_3$) δ** 159.3, 135.8, 130.1, 128.9, 128.6, 127.7, 122.1, 116.2, 109.3, 70.7.

This spectroscopic data compares favourably with that in the literature.[285]

For **141** or **142**:

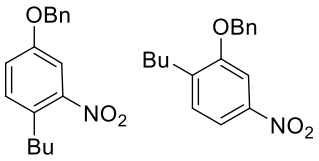

Rf, 0.78 (20% EtOAc/Hexane) **^{1}H NMR (400 MHz, $CDCl_3$) δ** 7.79 (dd, *J* = 8.2, 2.1 Hz, 1H, Ar*H*), 7.75 (d, *J* = 2.1 Hz, 1H, Ar*H*), 7.47 – 7.32 (m, 5H, Ar*H*), 7.27 (d, *J* = 8.2 Hz, 1H, Ar*H*), 5.15 (s, 2H, CH_2), 2.77 – 2.69 (m, 2H, CH_2), 1.65 – 1.54 (m, 2H, CH_2), 1.41 – 1.31 (m, 2H, CH_2), 0.92 (t, *J* = 7.3 Hz, 3H, CH_3). **^{13}C NMR (101 MHz, $CDCl_3$) δ** 196.4, 156.7, 140.0, 136.2, 130.0, 128.8, 128.3, 127.3, 116.1, 106.4, 70.4, 31.6, 30.3, 22.7, 14.1.

8.6.3. Attempted synthesis of 3-(benzyloxy)-2-iodoaniline (148)

The reaction was carried out according to the procedure (conditions B) described for **35** using the following: **131** (500 mg, 1.41 mmol) and $SnCl_2.2H_2O$ (2.7g, 9.0 mmol). However, in this instance the reduced product **149** was obtained and not the desired product **148**.

For **149**:

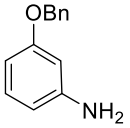

^{1}H NMR (500 MHz, $CDCl_3$) δ 7.46 – 7.31 (m, 5H, Ar*H*), 7.10 – 7.06 (m, 1H, Ar*H*), 6.44 – 6.41 (m, 1H, Ar*H*), 6.35 – 6.31 (m, 2H, Ar*H*), 5.04 (s, 2H, CH_2), 3.61 (s, 2H, NH_2). **^{13}C NMR (126 MHz, $CDCl_3$) δ** 160.1, 147.9, 137.3, 130.2, 128.7, 128.0, 127.6, 108.3, 105.0, 102.1, 69.9. **HRMS** calc. for $C_{13}H_{14}ON$ $[M+H]^+$, 200.10699 found, 200.10708. **IR ATR (cm^{-1}):** 3436, 3361, 1583, 1158, 1024. **Mp:** 57 °C.

8.6.4. Synthesis of tert-butyl (3-(benzyloxy)phenyl)carbamate (150)

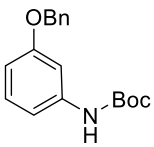

149 (526 mg, 2.64 mmol) was treated with Boc anhydride (576 mg, 2.64 mmol) and DMAP (32 mg, 0.26 mmol) in THF (10 mL). After 1 hour, TLC indicated that the reaction had reached completion. The reaction mixture was therefore concentrated *in vacuo* and

loaded onto silica gel. Subsequent purification by column chromatography (5% – 20% EtOAc/Hexane) afforded **150** as a clear oil (620 mg, 2.07 mmol, 90%).

^{1}H NMR (500 MHz, CDCl3) δ 10.96 (s, 1H, N*H*), 7.45 – 7.29 (m, 5H, Ar*H*), 7.22 – 7.18 (m, 1H, Ar*H*), 6.83 – 6.80 (m, 2H, Ar*H*), 6.73 – 6.70 (m, 1H, Ar*H*), 5.04 (s, 2H, CH_2), 1.36 (s, 9H, CH_3). **^{13}C NMR (126 MHz, $CDCl_3$) δ** 159.6, 152.0, 139.4, 129.7, 128.7, 128.0, 127.6, 121.5, 114.8, 112.4, 84.2, 70.1, 28.0. **HRMS** calc. for $C_{18}H_{22}O_3N$ $[M+H]^+$, 300.15942 found, 300.15968. **IR ATR (cm^{-1}):** 3283, 2922, 1722, 1287, 1151.

8.6.5. Synthesis of 1-(benzyloxy)-2-methyl-3-nitrobenzene (165)

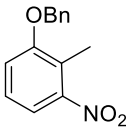

The reaction was carried out according to the procedure described for **33** using the following: 2-methyl-3-nitrophenol (**153**) (500 mg, 3.27 mmol), benzyl bromide (0.50 mL, 4.2 mmol) and K_2CO_3 (542 mg, 3.92 mmol). This reaction afforded **165** as a pale yellow solid (702 mg, 2.89 mmol, 88%).

Rf, 0.60 (20% EtOAc/Hexane) **^{1}H NMR (400 MHz, $CDCl_3$) δ** 7.43 – 7.31 (m, 6H, Ar*H*), 7.25 – 7.20 (m, 1H, Ar*H*), 7.10 – 7.06 (m, 1H, Ar*H*), 5.11 (s, 2H, CH_2), 2.41 (s, 3H, CH_3). **^{13}C NMR (101 MHz, $CDCl_3$) δ** 157.5, 151.2, 136.3, 128.8, 128.3, 127.2, 126.8, 122.5, 116.1, 115.4, 70.9, 11.9. **HRMS** calc. for $C_{14}H_{14}O_3N$ $[M+H]^+$, 244.09682 found, 244.09691. **IR ATR (cm^{-1}):** 1606, 1523, 1262, 703. **Mp:** 64 °C.

8.6.6. Synthesis of 2-(benzyloxy)-6-nitrobenzaldehyde (167)

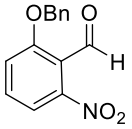

N,*N*-dimethylformamide dimethyl acetal (**162**) (0.35 mL, 2.5 mmol) was added to **165** (200 mg, 822 µmol) in DMF (2 mL) and the reaction was heated to 135 °C. After 18 hours the reaction was cooled to 0 °C and subsequently added to a vigorously stirring solution of $NaIO_4$ (528 mg, 2.47 mmol) in DMF (1.5 mL) and H_2O (3 mL) at 0 °C. The reaction was then allowed to warm to room temperature. After an additional 18 hours the reaction was filtered through a bed of celite and the resulting filtrate was subsequently washed with H_2O (40 mL) and brine (40 mL), dried over $MgSO_4$, concentrated *in vacuo* and then purified on silica gel by column chromatography to afford the benzaldehyde **167** as an orange solid (31 mg, 0.12 mmol, 15%).

Rf, 0.18 (20% EtOAc/Hexane) **^{1}H NMR (500 MHz, $CDCl_3$) δ** 10.43 (s, 1H, C*H*O), 7.58 – 7.53 (m, 1H, Ar*H*), 7.44 – 7.34 (m, 6H, Ar*H*), 7.30 – 7.27 (m, 1H, Ar*H*), 5.22 (s, H, CH_2). **^{13}C NMR (126 MHz, $CDCl_3$) δ** 187.7, 159.0, 148.9, 135.2, 133.6, 129.0, 128.7, 127.4, 117.8, 115.9, 110.1, 71.7. **HRMS** calc. for $C_{14}H_{12}O_4N$ $[M+H]^+$, 258.07608 found, 258.07613. **IR ATR (cm^{-1}):** 2910, 2864, 1705, 1276, 739. **Mp:** 67 °C.

8.6.7. Synthesis of 1-methoxy-2-methyl-3-nitrobenzene (168)

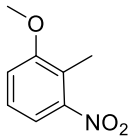

This reaction was carried out according to the procedure described for **87** using the following: **153** (500 mg, 2.99 mmol), methyl iodide (0.24 mL, 3.9 mmol) and NaH (154 mg, 6.4 mmol). This reaction afforded **168** as a pale yellow solid (502 mg, 2.55 mmol, 92%).

Rf, 0.37 (20% EtOAc/Hexane) **^{1}H NMR (500 MHz, $CDCl_3$) δ** 7.41 – 7.38 (m, 1H, Ar*H*), 7.28 – 7.24 (m, 1H, Ar*H*), 7.05 – 7.02 (m, 1H, Ar*H*), 3.89 (s, 3H, CH_3), 2.36 (s, 3H, CH_3). **^{13}C NMR (126 MHz, $CDCl_3$) δ** 158.6, 151.1, 126.8, 122.1, 115.9, 113.9, 56.4, 11.6. **HRMS** calc. for $C_8H_{10}O_3N$ $[M+H]^+$, 168.06552 found, 168.06555. **IR ATR (cm^{-1}):** 3015, 2841, 1519, 1466, 1262, 1064. **Mp:** 53 °C.

8.6.8. Synthesis of 2-methoxy-6-nitrobenzoic acid (169)

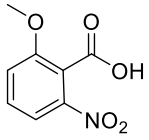

$KMnO_4$ (11 g, 70 mmol) was added to a suspension of **168** (1.98 g, 11.8 mmol) in *t*-BuOH (10 mL) and H_2O (20 mL) and reaction mixture was heated under reflux for 18 hours. The reaction mixture was then cooled to room temperature and filtered through a bed of celite. Following extraction of **169** from the filtrate, the resulting aqueous phase was acidified with 3N HCl (100 mL) and the product was extracted twice with EtOAc (2 × 100 mL). The organic phases containing the product were combined, dried over $MgSO_4$ and concentrated *in vacuo* to afford the desired carboxylic acid **169** as a white solid (784 mg, 3.98 mmol, 34%).

^{1}H NMR (500 MHz, DMSO-*d*) δ 7.76 – 7.54 (m, 3H, Ar*H*), 3.89 (s, 3H, CH_3). **^{13}C NMR (126 MHz, DMSO-*d*)** δ 165.1, 156.3, 145.4, 131.0, 120.4, 118.3, 115.6, 56.9. **HRMS** calc. for $C_8H_8O_5N$ $[M+H]^+$, 198.03970 found, 198.03974. **IR ATR (cm^{-1}):** 2851, 1703, 1530, 1477, 1351, 1269. **Mp:** degrades at 144 °C.

8.6.9. Synthesis of methyl 2-hydroxy-6-nitrobenzoate (170)

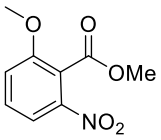

Methyl iodide (0.36 mL, 5.8 mmol) was added to a solution of **169** (750 mg, 3.80 mmol) and K_2CO_3 (789 mg, 5.71 mmol) in DMF (10 mL). After 2 hours the reaction was quenched with a saturated solution of NH_4Cl (50 mL) and extracted twice with EtOAc (2 × 100 mL). The organic phases were combined, dried over $MgSO_4$, concentrated *in vacuo* and purified by column chromatography to **170** as a yellow solid (773 mg, 3.66 mmol, 96%).

Rf, 0.29 (40% EtOAc/Hexane) **^{1}H NMR (500 MHz, $CDCl_3$) δ** 7.74 (dd, *J* = 8.3, 0.8 Hz, 1H, Ar*H*), 7.53 – 7.49 (m, 1H, Ar*H*), 7.27 – 7.24 (m, 1H, Ar*H*), 3.95 (s, 3H, CH_3), 3.90 (s, 3H, CH_3). **^{13}C NMR (126 MHz, $CDCl_3$) δ** 165.1, 157.3, 146.3, 131.0, 119.8, 117.1, 116.0, 56.9, 53.3. **HRMS** calc. for $C_9H_{10}O_5N$ $[M+H]^+$, 212.05535 found, 212.05542. **IR ATR (cm^{-1}):** 1734, 1530, 1347, 1264, 1110, 1072, 1050. **Mp:** 67 °C.

8.6.10. Synthesis of methyl 2-amino-6-methoxybenzoate (171)

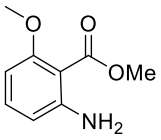

A catalytic amount of palladium on activated charcoal was added to a solution of **170** (773 mg, 3.66 mmol) in EtOH (20 mL) under an atmosphere of hydrogen. After 18 hours the reaction was filtered through a bed of celite. The resulting filtrate was concentrated *in vacuo*, loaded onto silica gel and then purified by column chromatography to afford **171** as a white solid (613 mg, 3.38 mmol, 93%).

Rf, 0.49 (40% EtOAc/Hexane) **^{1}H NMR (500 MHz, $CDCl_3$) δ** 7.12 – 7.08 (m, 1H, Ar*H*), 6.27 (dd, *J* = 8.2, 0.9 Hz, 1H, Ar*H*), 6.22 (dd, *J* = 8.3, 0.6 Hz, 1H, Ar*H*), 4.93 (s, 2H, NH_2), 3.87 (s, 3H, CH_3), 3.79 (s, H, CH_3). **^{13}C NMR (126 MHz, $CDCl_3$) δ** 168.6, 160.3, 149.8, 132.8, 109.4, 104.6, 100.3, 56.1, 51.8. **HRMS** calc. for $C_9H_{12}O_3N$ $[M+H]^+$, 182.08117 found, 182.08125. **IR ATR (cm^{-1}):** 3465, 3354, 1668, 1236, 1113, 1077. **Mp:** 59 °C.

8.6.11. Synthesis of 2-(2-amino-6-methoxyphenyl)propan-2-ol (172)

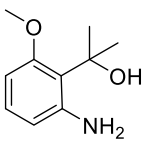

171 (511 mg, 2.82 mmol) was dissolved in THF (10 mL) and cooled to 0 °C. After methylmagnesium bromide (3.0 M in Et_2O, 4.7 mL, 41 mmol) was added to the reaction at 0 °C, the reaction mixture warmed to room temperature. After 4 hours, the reaction was taken back to 0 °C, slowly quenched with H_2O (100 ml) and then extracted twice with DCM (2 × 200 mL).

The organic phases were combined, dried over $MgSO_4$ and concentrated *in vacuo* to afford **172** as an orange solid (521 mg, 2.47 mmol, 91%).

Rf, 0.26 (40% EtOAc/Hexane) **^{1}H NMR (399 MHz, $CDCl_3$) δ** 6.97 – 6.92 (m, 1H, Ar*H*), 6.31 – 6.25 (m, 2H, Ar*H*), 4.00 (s, 2H, NH_2), 3.75 (s, 3H, CH_3), 1.71 (s, 6H, CH_3). **^{13}C NMR (100 MHz, $CDCl_3$) δ** 157.9, 146.8, 127.8, 119.2, 111.9, 102.0, 76.3, 55.5, 30.9. **HRMS** calc. for $C_{10}H_{16}O_2N$ $[M+H]^+$, 182.11756 found, 182.11766.

8.6.12. Synthesis of 5-methoxy-4,4-dimethyl-1,4-dihydro-2H-benzo[*d*][1,3]oxazin-2-one (173)

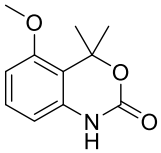

This reaction was carried out according to the procedure (conditions B) described for **36** using the following: **172** (464 mg, 2.56 mmol) and CDI (623 mg, 3.84 mmol). The reaction yielded **173** as a white solid (360 mg, 1.74 mmol, 68%).

Rf, 0.27 (40% EtOAc/Hexane) **^{1}H NMR (500 MHz, $CDCl_3$) δ** 9.47 (s, 1H, N*H*), 7.16 – 7.12 (m, 1H, Ar*H*), 6.58 – 6.55 (m, 1H, Ar*H*), 6.49 (dd, *J* = 7.9, 0.9 Hz, 1H, Ar*H*), 3.82 (s, 3H, CH_3), 1.78 (s, 6H, CH_3). **^{13}C NMR (126 MHz, $CDCl_3$) δ** 155.6, 152.5, 135.0, 129.4, 113.6, 107.8, 106.3, 84.8, 55.6, 28.5. **HRMS** calc. for $C_{11}H_{14}O_3N$ $[M+H]^+$, 208.09682 found, 208.09682. **IR ATR (cm^{-1}):** 3106, 2968, 1704, 1597, 1368, 1247, 780. **Mp:** 147 °C.

8.6.13. Synthesis of 5-hydroxy-4,4-dimethyl-1,4-dihydro-2H-benzo[*d*][1,3]oxazin-2-one (174)

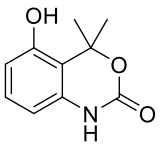

Boron tribromide (1.0 M in DCM, 2.0 mL, 21 mmol) was added to a solution of **173** (232 mg, 1.12 mmol) in DCM (6 mL) at 0 °C. After 4 hours the reaction was cooled to -10 °C (acetone/ice) and quenched slowly with H_2O (100 mL). Subsequent extraction with EtOAc (2 × 200 mL) and concentration *in vacuo* afforded **174** as a pale yellow solid (195 mg, 1.01 mmol, 90%).

Rf, 0.26 (50% EtOAc/Hexane) **^{1}H NMR (400 MHz, DMSO-*d*) δ** 9.98 (s, 1H, N*H* or O*H*), 9.85 (s, 1H, N*H* or O*H*), 7.00 – 6.94 (m, 1H, Ar*H*), 6.48 – 6.42 (m, 1H, Ar*H*), 6.33 – 6.28 (m, 1H, Ar*H*), 1.65 (s, 6H, CH_3). **^{13}C NMR (101 MHz, DMSO-*d*) δ** 153.3, 149.9, 135.9, 128.9, 111.5, 110.3, 105.2, 82.4, 28.0. **HRMS** calc. for $C_{10}H_{12}O_3N$ $[M+H]^+$, 194.08117 found, 194.08129. **IR ATR (cm^{-1}):** 3185, 3099, 2978, 2935, 1688, 1392, 1056, 784. **Mp:** 268 °C.

8.6.14. Synthesis of 3-chloro-5-((4,4-dimethyl-2-oxo-1,4-dihydro-2*H*-benzo[*d*][1,3]oxazin-5-yl)oxy)benzonitrile (130)

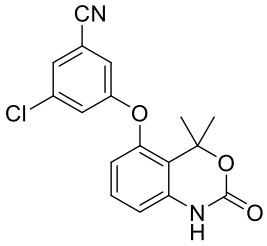

This reaction was carried out according to the procedure described for **52** using the following: **174** (72 mg, 0.37 mmol), **51** (59 mg, 0.38 mmol) and Cs_2CO_3 (122 mg, 0.374 mmol). However, in this instance the reaction was carried out at 70 °C. This reaction afforded **130** as a white solid (16 mg, 0.049 mmol, 13%)

Rf, 0.42 (50% EtOAc/Hexane) **^{1}H NMR (500 MHz, $CDCl_3$) δ** 9.41 (s, 1H, N*H*), 7.40 – 7.38 (m, 1H, Ar*H*), 7.25 – 7.21 (m, 2H, Ar*H*), 7.15 (dd, *J* = 2.3, 1.3 Hz, 1H, Ar*H*), 6.76 (dd, *J* = 8.0, 0.9 Hz, 1H, Ar*H*), 6.55 (dd, *J* = 8.2, 0.8 Hz, 1H, Ar*H*), 1.77 (s, 6H, C*H*$_3$). **^{13}C NMR (126 MHz, $CDCl_3$) δ** 158.2, 152.1, 150.8, 136.9, 136.4, 130.2, 126.9, 123.0, 119.5, 117.9, 116.9, 115.12, 115.02, 111.8, 83.6, 28.7. **HRMS** calc. for $C_{17}H_{14}ClO_3N_2$ $[M+H]^+$, 329.06875 found, 329.06869. **IR ATR (cm^{-1}):** 3090, 2992, 2940, 2228, 1709, 1572, 1058 **Mp:** 211 °C.

Addendum I: X-ray Crystallographic Data for 130

Crystal Data and Experimental

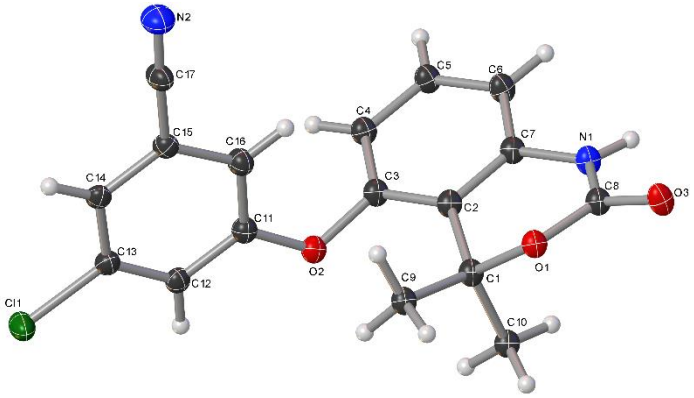

Crystal data was obtained by John Bacsa at the Emory University X-ray Crystallography Center

Experimental. Compound **130** was dissolved in hot ethanol and single colourless needle-shaped crystals formed on cooling the solution. A suitable crystal 0.35×0.10×0.05 mm^3 was selected and mounted on a loop with paratone oil on an XtaLAB Synergy, Dualflex, HyPix diffractometer. The crystal was cooled to T = 100(2) K during data collection. The structure was solved with the **ShelXT** structure solution program using the Intrinsic Phasing solution method and by using **Olex2** as the graphical interface.[286-287] The model was refined with version 2017/1 of **ShelXL** using Least Squares minimisation.[288]

Crystal Data. $C_{17}H_{13}ClN_2O_3$, M_r = 328.74, monoclinic, $P2_1/c$ (No. 14), a = 21.3495(13) Å, b = 5.2431(3) Å, c = 14.3162(12) Å, β = 106.429(8)°, α = γ = 90°, V = 1537.08(19) $Å^3$, T = 100(2) K, Z = 4, Z' = 1, $\mu(MoK_\alpha)$ = 0.265, 13778 reflections measured, 3225 unique (R_{int} = 0.0913) which were used in all calculations. The final wR_2 was 0.1830 (all data) and R_1 was 0.0788 (I > 2σ(I)).

Compound	130
Formula	$C_{17}H_{13}ClN_2O_3$
$D_{calc.}$/ g cm^{-3}	1.421
μ/mm^{-1}	0.265
Formula Weight	328.74
Colour	colourless
Shape	needle
Size/mm^3	0.35×0.10×0.05
T/K	100(2)
Crystal System	monoclinic
Space Group	$P2_1/c$
a/Å	21.3495(13)
b/Å	5.2431(3)
c/Å	14.3162(12)
α/°	90
β/°	106.429(8)
γ/°	90
V/$Å^3$	1537.08(19)
Z	4
Z'	1
Wavelength/Å	0.71073
Radiation type	MoK_α
Θ_{min}/°	2.850
Θ_{max}/°	26.732
Measured Refl.	13778
Independent Refl.	3225
Reflections with I > 2σ(I)	2899
R_{int}	0.0913
Parameters	293
Restraints	278
Largest Peak	0.535
Deepest Hole	-0.329
GooF	1.204
wR_2 (all data)	0.1830
wR_2	0.1799
R_1 (all data)	0.0853
R_1	0.0788

Structure Quality Indicators

Reflections:	d min (Mo) 0.79	I/σ 11.3	Rint 9.13%	complete at 2θ=56° 99%
Refinement:	Shift 0.000	Max Peak 0.5	Min Peak -0.3	GooF 1.204

A colourless needle-shaped crystal with dimensions 0.35×0.10×0.05 mm^3 was mounted on a loop with paratone oil. Data were collected using an XtaLAB Synergy, Dualflex, HyPix diffractometer equipped with an Oxford Cryosystems low-temperature device, operating at T = 100(2) K.

Data were measured using ω scans of 1/2° per frame for 15s using MoK_{α} radiation (micro-focus sealed X-ray tube, 50 kV, 1.0 mA). The total number of runs and images was based on the strategy calculation from the program **CrysAlisPro** (Rigaku, V1.171.39.35c, 2017). The maximum resolution that was achieved was Θ = 26.732°.

The diffraction patterns were indexed using **CrysAlisPro** (Rigaku, V1.171.39.35c, 2017) and the unit cells were refined using **CrysAlisPro** (Rigaku, V1.171.39.35c, 2017) on 6194 reflections, 45 % of the observed reflections. Data reduction, scaling and absorption corrections were performed using **CrysAlisPro** (Rigaku, V1.171.39.35c, 2017). A numerical absorption correction based on Gaussian integration over a multifaceted crystal model was applied. An empirical absorption correction using spherical harmonics, implemented in SCALE3 ABSPACK scaling algorithm was also used. The final completeness is 99.20% out to 26.732° in Θ. The absorption coefficient μ of this material is 0.265 mm^{-1} at this wavelength (λ = 0.71073Å) and the minimum and maximum transmissions are 0.672 and 1.000.

The structure was solved and the space group $P2_1/c$ (# 14) determined by the **ShelXT** structure solution program using Intrinsic Phasing and refined by Least Squares using version 2017/1 of **ShelXL**.[287-288] All non-hydrogen atoms were refined anisotropically. Hydrogen atom positions were calculated geometrically and refined using the riding model.

The chlorobenzonitrile group is disordered but can be satisfactorily resolved using two disorder components.

Images of the Crystal on the Diffractometer

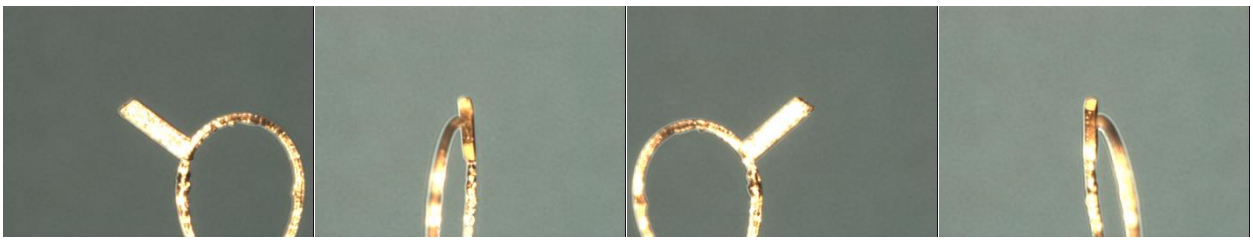

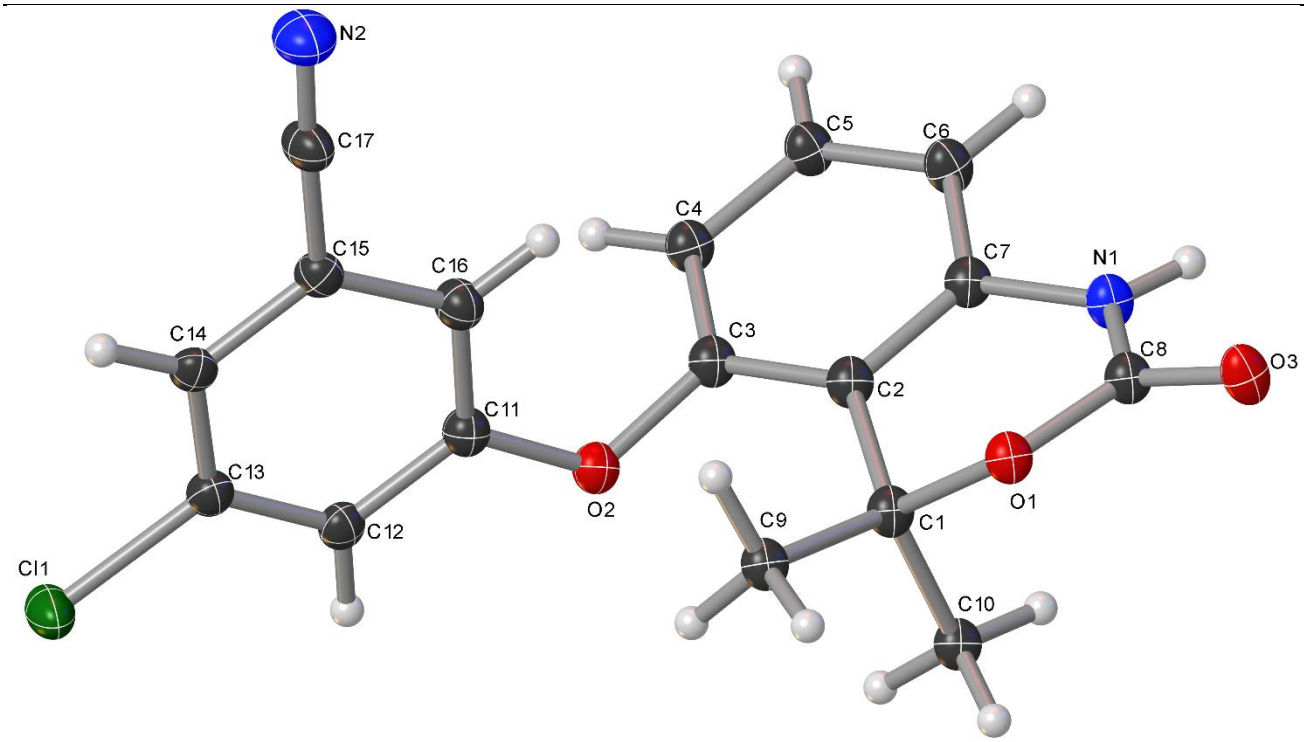

Figure 63: Plot of the asymmetric unit showing disorder component #1.

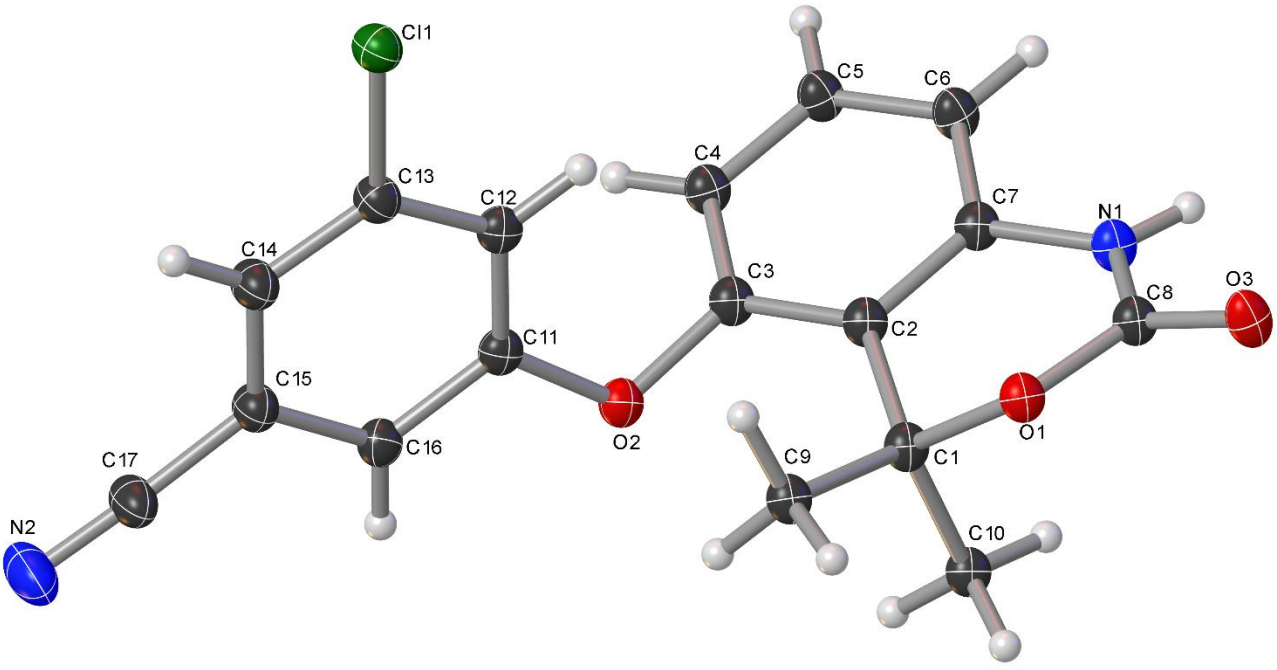

Figure 2: Plot of the asymmetric unit showing disorder component #2.

_exptl_absorpt_process_details: CrysAlisPro 1.171.39.35c (Rigaku Oxford Diffraction, 2017) Numerical absorption correction based on gaussian integration over a multifaceted crystal modelEmpirical absorption correction using spherical harmonics, implemented in SCALE3 ABSPACK scaling algorithm.

There is a single molecule in the asymmetric unit, which is represented by the reported sum formula. In other words: Z is 4 and Z' is 1.

Data Plots: Diffraction Data

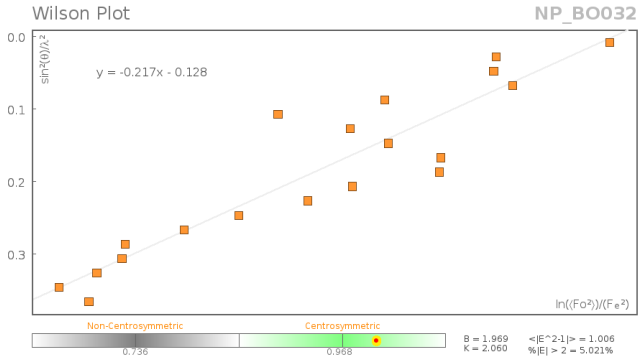

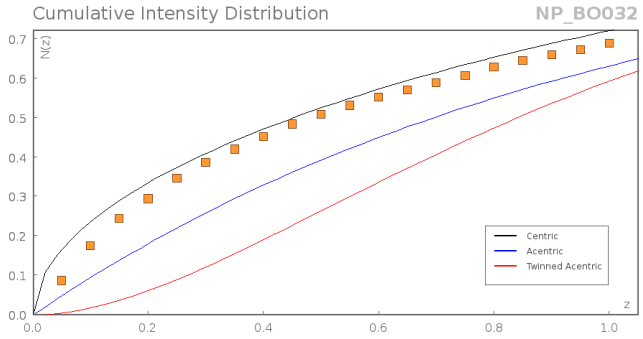

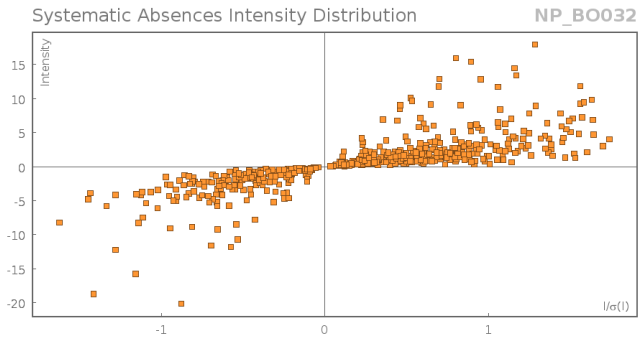

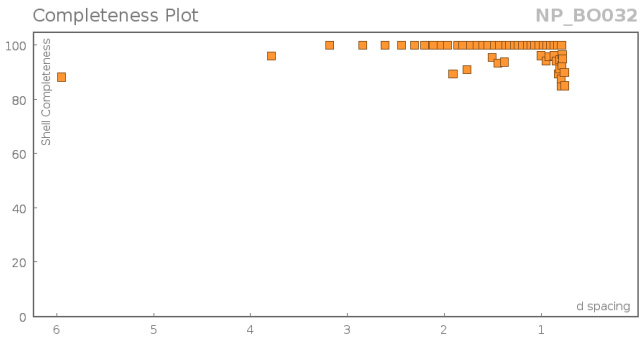

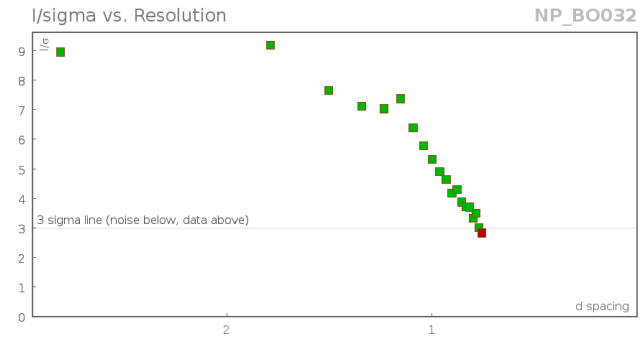

Data Plots: Refinement and Data

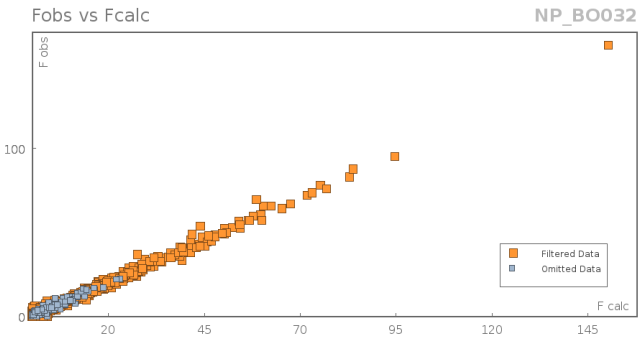

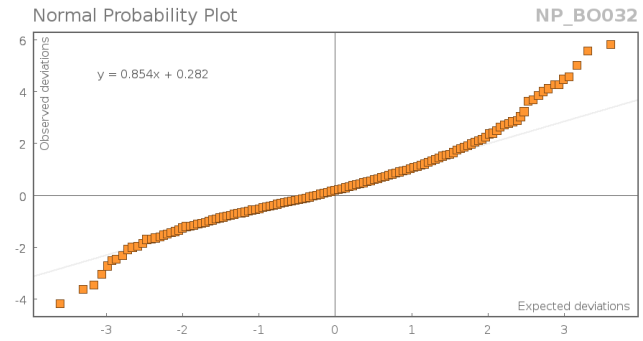

Reflection Statistics

Total reflections (after filtering)	14649	Unique reflections	3225
Completeness	0.988	Mean I/σ	11.29
hkl_{max} collected	(28, 6, 18)	hkl_{min} collected	(-28, -6, -18)
hkl_{max} used	(25, 6, 18)	hkl_{min} used	(-26, 0, 0)
Lim d_{max} collected	20.0	Lim d_{min} collected	0.79
d_{max} used	9.61	d_{min} used	0.79
Friedel pairs	3050	Friedel pairs merged	1
Inconsistent equivalents	10	R_{int}	0.0913
R_{sigma}	0.072	Intensity transformed	0
Omitted reflections	0	Omitted by user (OMIT hkl)	2
Multiplicity	(5306, 3176, 924, 311, 47, 6, 2)	Maximum multiplicity	12
Removed systematic absences	869	Filtered off (Shel/OMIT)	1310

Table 7: Fractional Atomic Coordinates (×10^4) and Equivalent Isotropic Displacement Parameters (Å^2×10^3) for **130**. U_{eq} is defined as 1/3 of the trace of the orthogonalised U_{ij}.

Atom	x	y	z	U_{eq}
C1	8011.3(15)	2740(6)	4616(2)	17.6(3)
C2	8198.1(15)	1422(6)	3790(2)	17.1(4)
C3	7802.1(15)	-156(6)	3089(2)	17.7(4)
C4	8032.0(16)	-1443(6)	2406(2)	20.3(5)
C5	8682.6(16)	-1202(6)	2423(2)	20.7(6)
C6	9095.4(16)	338(6)	3115(2)	21.2(6)
C7	8851.5(15)	1622(6)	3789(2)	16.7(5)
C8	9053.3(15)	4996(6)	4986(2)	17.2(5)
C9	7319.7(15)	3777(6)	4378(2)	19.1(4)
C10	8165.5(16)	1006(6)	5508(2)	19.2(4)
N8	9270.2(13)	3151(5)	4497(2)	19.5(5)
O1	8412.4(10)	5065(4)	4886.9(17)	18.7(4)
O2	7166.5(11)	-652(4)	3122.6(17)	20.3(4)
O3	9407.9(11)	6628(4)	5483.3(18)	22.6(5)
C11_2	6668(3)	450(20)	2343(7)	16.9(14)
C12_2	6749(4)	2390(20)	1734(9)	19.1(16)
C13_2	6213(3)	3313(19)	1054(7)	19.4(16)
C14_2	5589(3)	2444(16)	949(6)	24.2(16)
C15_2	5506(3)	489(17)	1561(7)	21.5(15)
C16_2	6051(4)	-550(20)	2276(9)	20.2(19)
C17_2	4872(3)	-419(17)	1506(6)	26.6(16)
Cl1_2	6305.6(10)	5867(4)	305.0(17)	22.5(5)
N2_2	4343(3)	-1116(17)	1419(6)	39.6(19)
C11_1	6645(3)	154(18)	2429(6)	18.4(12)
C12_1	6048(4)	-979(17)	2353(7)	18.0(13)
C13_1	5510(3)	-94(13)	1669(5)	19.5(11)
C14_1	5527(2)	1856(11)	1035(4)	18(1)
C15_1	6128(3)	3000(15)	1109(6)	18.9(12)
C16_1	6704(3)	2149(19)	1814(7)	20.3(14)
C17_1	6176(3)	5029(13)	479(5)	23.4(11)
Cl1_1	4748.1(8)	-1538(4)	1562.0(12)	29.5(5)
N2_1	6239(3)	6641(12)	-41(5)	31.2(14)

Table 8: Anisotropic Displacement Parameters ($\times 10^4$) **130**. The anisotropic displacement factor exponent takes the form: $-2\pi^2[h^2a^{*2} \times U_{11} + \ldots + 2hka^* \times b^* \times U_{12}]$

Atom	U_{11}	U_{22}	U_{33}	U_{23}	U_{13}	U_{12}
C1	18.0(6)	13.1(6)	20.9(6)	-0.9(4)	4.0(5)	0.6(4)
C2	18.4(5)	11.7(7)	19.9(6)	0.2(5)	3.3(4)	1.3(4)
C3	19.3(4)	12.8(8)	19.8(6)	0.1(5)	3.3(4)	0.1(4)
C4	22.4(6)	15.9(10)	21.9(8)	-2.4(8)	5.0(6)	-0.6(6)
C5	22.8(7)	16.6(11)	22.5(9)	-4.2(8)	5.9(6)	-0.7(6)
C6	21.5(7)	17.9(11)	23.9(8)	-5.6(8)	6.3(5)	-0.3(6)
C7	18.5(5)	11.3(9)	19.3(7)	-0.4(7)	3.5(4)	1.4(4)
C8	18.0(5)	12.9(7)	20.4(10)	-1.8(7)	4.7(5)	0.6(4)
C9	18.2(6)	13.8(9)	24.4(10)	-0.8(8)	4.5(6)	1.0(5)
C10	22.2(10)	14.2(8)	20.9(7)	-0.5(7)	5.6(7)	2.8(7)
N8	17.9(5)	16.1(7)	23.4(8)	-4.9(7)	4.2(4)	1.0(4)
O1	18.2(5)	13.1(6)	24.6(8)	-2.6(5)	5.6(5)	0.6(4)
O2	19.2(4)	18.7(8)	21.2(7)	1.1(5)	3.2(4)	-0.9(4)
O3	19.5(6)	19.2(7)	29.4(10)	-9.1(7)	7.2(6)	-1.9(6)
C11_2	19.0(5)	15(2)	16.8(18)	-3.1(18)	4.8(7)	1.1(8)
C12_2	20.1(7)	17(3)	20(2)	0(2)	5.1(10)	1(1)
C13_2	20.0(7)	19(2)	20(2)	0(2)	5.5(10)	1.3(9)
C14_2	20.1(7)	25(2)	27(2)	7(2)	4.4(10)	0.5(9)
C15_2	19.1(5)	21(3)	23(2)	3(2)	4.0(7)	0.5(9)
C16_2	19.1(5)	19(3)	21(3)	1(3)	3.9(8)	0.5(9)
C17_2	19.1(5)	27(3)	31(3)	10(2)	3.4(8)	0.2(11)
Cl1_2	23.1(9)	21.2(10)	24.3(10)	4.0(7)	8.2(7)	2.6(6)
N2_2	21.5(8)	50(4)	45(5)	13(4)	5.1(16)	-6.5(17)
C11_1	18.8(5)	18(2)	18.2(15)	-1.4(15)	4.4(6)	0.4(7)
C12_1	19.0(5)	19(2)	16(2)	-2.6(18)	4.5(7)	-0.3(8)
C13_1	18.5(5)	22.8(19)	17.1(17)	-0.2(15)	4.9(6)	-0.3(8)
C14_1	17.7(7)	21.2(17)	15.9(16)	-1.5(13)	6.0(8)	1.2(8)
C15_1	17.4(7)	20.9(19)	18.8(17)	0.3(16)	5.7(8)	1.7(8)
C16_1	18.0(7)	20(2)	21.5(19)	1.7(19)	4.4(9)	0.7(9)
C17_1	16.7(11)	27.1(18)	26.0(18)	7.0(15)	5.3(13)	1.7(12)
Cl1_1	20.0(5)	38.5(10)	27.4(8)	9.9(7)	2.6(5)	-5.4(6)
N2_1	32(3)	31.1(19)	30(2)	9.8(16)	9(2)	-1.3(17)

Table 9: Bond Lengths in Å for **130**.

Atom	Atom	Length/Å
C1	C2	1.518(4)
C1	C9	1.519(4)
C1	C10	1.525(4)
C1	O1	1.477(4)
C2	C3	1.388(4)
C2	C7	1.399(4)
C3	C4	1.387(4)
C3	O2	1.396(4)
C4	C5	1.388(4)
C5	C6	1.384(5)
C6	C7	1.393(4)
C7	N8	1.399(4)
C8	N8	1.350(4)
C8	O1	1.336(4)

Atom	Atom	Length/Å
C8	O3	1.228(4)
O2	C11_2	1.429(5)
O2	C11_1	1.334(5)
C11_2	C12_2	1.381(9)
C11_2	C16_2	1.396(9)
C12_2	C13_2	1.363(9)
C13_2	C14_2	1.374(7)
C13_2	Cl1_2	1.761(6)
C14_2	C15_2	1.392(7)
C15_2	C16_2	1.424(9)
C15_2	C17_2	1.417(9)
C17_2	N2_2	1.158(8)
C11_1	C12_1	1.381(9)
C11_1	C16_1	1.396(9)

Atom	Atom	Length/Å	Atom	Atom	Length/Å
C12_1	C13_1	1.363(9)	C15_1	C16_1	1.424(9)
C13_1	C14_1	1.374(7)	C15_1	C17_1	1.417(9)
C13_1	Cl1_1	1.761(6)	C17_1	N2_1	1.159(8)
C14_1	C15_1	1.392(7)			

Table 10: Bond Angles in ° for **130**.

Atom	Atom	Atom	Angle/°	Atom	Atom	Atom	Angle/°
C2	C1	C9	116.1(3)	C12_2	C11_2	C16_2	121.2(4)
C2	C1	C10	109.8(2)	C16_2	C11_2	O2	112.3(6)
C9	C1	C10	111.6(3)	C13_2	C12_2	C11_2	118.8(6)
O1	C1	C2	108.6(2)	C12_2	C13_2	C14_2	123.5(5)
O1	C1	C9	102.6(2)	C12_2	C13_2	Cl1_2	119.2(5)
O1	C1	C10	107.5(2)	C14_2	C13_2	Cl1_2	117.3(5)
C3	C2	C1	126.5(3)	C13_2	C14_2	C15_2	117.9(4)
C3	C2	C7	116.6(3)	C14_2	C15_2	C16_2	120.7(5)
C7	C2	C1	116.6(3)	C14_2	C15_2	C17_2	120.2(5)
C2	C3	O2	119.0(3)	C17_2	C15_2	C16_2	119.1(5)
C4	C3	C2	122.3(3)	C11_2	C16_2	C15_2	117.9(5)
C4	C3	O2	118.4(3)	N2_2	C17_2	C15_2	177.0(8)
C3	C4	C5	119.7(3)	O2	C11_1	C12_1	118.7(6)
C6	C5	C4	119.8(3)	O2	C11_1	C16_1	120.1(6)
C5	C6	C7	119.4(3)	C12_1	C11_1	C16_1	121.2(3)
C6	C7	C2	122.2(3)	C13_1	C12_1	C11_1	118.8(5)
C6	C7	N8	119.4(3)	C12_1	C13_1	C14_1	123.5(5)
N8	C7	C2	118.4(3)	C12_1	C13_1	Cl1_1	119.1(4)
O1	C8	N8	117.1(3)	C14_1	C13_1	Cl1_1	117.3(4)
O3	C8	N8	123.7(3)	C13_1	C14_1	C15_1	117.8(4)
O3	C8	O1	119.2(3)	C14_1	C15_1	C16_1	120.7(5)
C8	N8	C7	122.9(3)	C14_1	C15_1	C17_1	120.4(5)
C8	O1	C1	120.4(2)	C17_1	C15_1	C16_1	118.9(5)
C3	O2	C11_2	114.4(4)	C11_1	C16_1	C15_1	117.9(5)
C11_1	O2	C3	122.1(4)	N2_1	C17_1	C15_1	177.0(7)
C12_2	C11_2	O2	126.4(6)				

Table 11: Hydrogen Fractional Atomic Coordinates ($\times 10^4$) and Equivalent Isotropic Displacement Parameters ($Å^2 \times 10^3$) for **130**. U_{eq} is defined as 1/3 of the trace of the orthogonalised U_{ij}.

Atom	x	y	z	U_{eq}
H4	7745.67	-2485.54	1929.26	24
H5	8844.05	-2090.34	1960.92	25
H6	9540.93	518.31	3129.71	25
H9A	7215.94	4682.63	3753.8	29
H9B	7284.2	4954.48	4891.71	29
H9C	7012.8	2361.48	4333.33	29
H10A	7879.52	-491.73	5369.3	29
H10B	8093.81	1939.7	6061.92	29
H10C	8622.26	456.43	5665.85	29
H8	9693.89	2899.47	4629.99	23
H12_2	7169.75	3073.35	1787.58	23
H14_2	5226.97	3154.18	473.87	29

Atom	x	y	z	U_{eq}
H16_2	5997.5	-1888.7	2694.47	24
H12_1	6013.77	-2350.47	2768.85	22
H14_1	5142.06	2404.72	561.85	22
H16_1	7115.3	2915.01	1863.81	24

Table 12: Atomic Occupancies for all atoms that are not fully occupied in **130**.

Atom	Occupancy
C11_2	0.435(3)
C12_2	0.435(3)
H12_2	0.435(3)
C13_2	0.435(3)
C14_2	0.435(3)
H14_2	0.435(3)
C15_2	0.435(3)
C16_2	0.435(3)
H16_2	0.435(3)
C17_2	0.435(3)
Cl1_2	0.435(3)
N2_2	0.435(3)
C11_1	0.565(3)
C12_1	0.565(3)
H12_1	0.565(3)
C13_1	0.565(3)
C14_1	0.565(3)
H14_1	0.565(3)
C15_1	0.565(3)
C16_1	0.565(3)
H16_1	0.565(3)
C17_1	0.565(3)
Cl1_1	0.565(3)
N2_1	0.565(3)

References

1. L. Montagnier, A History of HIV Discovery. *Science* **2002**, *298*, 1727-1728.
2. R. C. Gallo, The Early Years of HIV/AIDS. *Science* **2002**, *298*, 1728-1730.
3. R. C. M. D. Gallo, L. M. D. Montagnier, The Discovery of HIV as the Cause of AIDS. *The New England Journal of Medicine* **2003**, *349*, 2283-2285.
4. R. C. Gallo, L. Montagnier, Historical Essay: Prospects for the Future. *Science* **2002**, *298*, 1730-1731.
5. R. C. Gallo, A Reflection on HIV/AIDS Research after 25 Years. *Retrovirology* **2006**, *3*, 72-77.
6. W. C. Greene, A History of AIDS: Looking Back to See Ahead. *European Journal of Immunology* **2007**, *37*, S94-S102.
7. Un Joint Programme on HIV/AIDS (UNAIDS) Data 2017, **2017**, available at http://www.UNAIDS.org/en/resources/documents/2017/2017_data_book.
8. S. G. Deeks, J. Overbaugh, A. Phillips, S. Buchbinder, HIV Infection. **2015**, *1*, 15035.
9. R. K. Jewkes, K. Dunkle, M. Nduna, N. Shai, Intimate Partner Violence, Relationship Power Inequity, and Incidence of HIV Infection in Young Women in South Africa: A Cohort Study. *The Lancet*, *376*, 41-48.
10. J. R. N. Nansseu, J. J. R. Bigna, Antiretroviral Therapy Related Adverse Effects: Can Sub-Saharan Africa Cope with the New "Test and Treat" Policy of the World Health Organization? *Infectious Diseases of Poverty* **2017**, *6*, 24.
11. UNAIDS Global AIDS Update, **2016**, available at http://www.UNAIDS.org/en/resources/documents/2016/Global-AIDS-update-2016.
12. UNAIDS 90-90-90 an Ambitious Treatment Target to Help End the AIDS Epidemic, **2014**, available at http://www.UNAIDS.org/en/resources/documents/2017/90-90-90.
13. Z. Shubber, E. J. Mills, J. B. Nachega, R. Vreeman, M. Freitas, P. Bock, S. Nsanzimana, M. Penazzato, T. Appolo, M. Doherty, N. Ford, Patient-Reported Barriers to Adherence to Antiretroviral Therapy: A Systematic Review and Meta-Analysis. *PLOS Medicine* **2016**, *13*, e1002183.
14. R. Bijker, A. Jiamsakul, C. Kityo, S. Kiertiburanakul, M. Siwale, P. Phanuphak, S. Akanmu, R. Chaiwarith, F. W. Wit, B. L. Sim, T. S. Boender, R. Ditangco, T. F. Rinke de Wit, A. H. Sohn, R. L. Hamers, Adherence to Antiretroviral Therapy for HIV in Sub-Saharan Africa and Asia: A Comparative Analysis of Two Regional Cohorts. *Journal of the International AIDS Society* **2017**, *20*, 21218.
15. T. B. Chan, C. A. Tsai, HIV Stigma Trends in the General Population During Antiretroviral Treatment Expansion: Analysis of 31 Countries in Sub-Saharan Africa, 2003–2013. *Journal of Acquired Immune Deficiency Syndromes* **2016**, *72*, 558-564.
16. A. P. Mahajan, J. N. Sayles, V. A. Patel, R. H. Remien, D. Ortiz, G. Szekeres, T. J. Coates, Stigma in the HIV/AIDS Epidemic: A Review of the Literature and Recommendations for the Way Forward. *AIDS (London, England)* **2008**, *22*, S67-S79.
17. UNAIDS Reduction of HIV-Related Stigma and Discrimination, **2014**, available at http://www.UNAIDS.org/en/resources/documents/2014/ReductionofHIV-relatedstigmaanddiscrimination.
18. T. Huet, R. Cheynier, A. Meyerhans, G. Roelants, S. Wain-Hobson, Genetic Organization of a Chimpanzee Lentivirus Related to HIV-1. *Nature* **1990**, *345*, 356-359.

19. F. Gao, E. Bailes, D. L. Robertson, Y. Chen, C. M. Rodenburg, S. F. Michael, L. B. Cummins, L. O. Arthur, M. Peeters, G. M. Shaw, P. M. Sharp, B. H. Hahn, Origin of HIV-1 in the Chimpanzee Pan Troglodytes Troglodytes. *Nature* **1999**, *397*, 436-441.
20. B. F. Keele, F. Van Heuverswyn, Y. Li, E. Bailes, J. Takehisa, M. L. Santiago, F. Bibollet-Ruche, Y. Chen, L. V. Wain, F. Liegeois, S. Loul, E. M. Ngole, Y. Bienvenue, E. Delaporte, J. F. Y. Brookfield, P. M. Sharp, G. M. Shaw, M. Peeters, B. H. Hahn, Chimpanzee Reservoirs of Pandemic and Nonpandemic HIV-1. *Science* **2006**, *313*, 523-526.
21. P. M. Sharp, B. H. Hahn, Origins of HIV and the AIDS Pandemic. *Cold Spring Harbor Perspectives in Medicine:* **2011**, *1*, a006841.
22. T. Mourez, F. Simon, J.-C. Plantier, Non-M Variants of Human Immunodeficiency Virus Type 1. *Clinical Microbiology Reviews* **2013**, *26*, 448-461.
23. F. Van Heuverswyn, Y. Li, C. Neel, E. Bailes, B. F. Keele, W. Liu, S. Loul, C. Butel, F. Liegeois, Y. Bienvenue, E. M. Ngolle, P. M. Sharp, G. M. Shaw, E. Delaporte, B. H. Hahn, M. Peeters, Human Immunodeficiency Viruses: SIV Infection in Wild Gorillas. *Nature* **2006**, *444*, 164-164.
24. J.-C. Plantier, M. Leoz, J. E. Dickerson, F. De Oliveira, F. Cordonnier, V. Lemee, F. Damond, D. L. Robertson, F. Simon, A New Human Immunodeficiency Virus Derived from Gorillas. *Nature Medicine* **2009**, *15*, 871-872.
25. M. D'arc, A. Ayouba, A. Esteban, G. H. Learn, V. Boué, F. Liegeois, L. Etienne, N. Tagg, F. H. Leendertz, C. Boesch, N. F. Madinda, M. M. Robbins, M. Gray, A. Cournil, M. Ooms, M. Letko, V. A. Simon, P. M. Sharp, B. H. Hahn, E. Delaporte, E. Mpoudi Ngole, M. Peeters, Origin of the HIV-1 Group O Epidemic in Western Lowland Gorillas. *Proceedings of the National Academy of Sciences* **2015**, *112*, E1343-E1352.
26. B. S. Taylor , M. E. Sobieszczyk , F. E. McCutchan , S. M. Hammer The Challenge of HIV-1 Subtype Diversity. *New England Journal of Medicine* **2008**, *358*, 1590-1602.
27. R. De Leys, B. Vanderborght, M. Vanden Haesevelde, L. Heyndrickx, A. van Geel, C. Wauters, R. Bernaerts, E. Saman, P. Nijs, B. Willems, et al., Isolation and Partial Characterization of an Unusual Human Immunodeficiency Retrovirus from Two Persons of West-Central African Origin. *Journal of Virology* **1990**, *64*, 1207-1216.
28. F. Simon, P. Mauclere, P. Roques, I. Loussert-Ajaka, M. C. Muller-Trutwin, S. Saragosti, M. C. Georges-Courbot, F. Barre-Sinoussi, F. Brun-Vezinet, Identification of a New Human Immunodeficiency Virus Type 1 Distinct from Group M and Group O. *Nature Medicine* **1998**, *4*, 1032-1037.
29. A. Vallari, P. Bodelle, C. Ngansop, F. Makamche, N. Ndembi, D. Mbanya, L. Kaptue, L. G. Gurtler, C. P. McArthur, S. G. Devare, C. A. Brennan, Four New HIV-1 Group N Isolates from Cameroon: Prevalence Continues to Be Low. *AIDS Research and Human Retroviruses* **2010**, *26*, 109-115.
30. C. Delaugerre, F. De Oliveira, C. Lascoux-Combe, J.-C. Plantier, F. Simon, HIV-1 Group N: Travelling Beyond Cameroon. *The Lancet* **2011**, *378*, 1894.
31. A. Vallari, V. Holzmayer, B. Harris, J. Yamaguchi, C. Ngansop, F. Makamche, D. Mbanya, L. Kaptué, N. Ndembi, L. Gürtler, S. Devare, C. A. Brennan, Confirmation of Putative HIV-1 Group P in Cameroon. *Journal of Virology* **2011**, *85*, 1403-1407.
32. V. M. Hirsch, R. A. Olmsted, M. Murphey-Corb, R. H. Purcell, P. R. Johnson, An African Primate Lentivirus (SIVsm) Closely Related to HIV-2. *Nature* **1989**, *339*, 389-392.
33. F. Gao, L. Yue, A. T. White, P. G. Pappas, J. Barchue, A. P. Hanson, B. M. Greene, P. M. Sharp, G. M. Shaw, B. H. Hahn, Human Infection by Genetically Diverse SIVsm-Related HIV-2 in West Africa. *Nature* **1992**, *358*, 495-499.
34. S. J. Popper, A. D. Sarr, A. Guèye-Ndiaye, S. Mboup, M. E. Essex, P. J. Kanki, Low Plasma Human Immunodeficiency Virus Type 2 Viral Load Is Independent of Proviral Load: Low Virus Production in Vivo. *Journal of Virology* **2000**, *74*, 1554-1557.

35. N. Berry, S. Jaffar, M. Schim van der Loeff, K. Ariyoshi, E. Harding, P. T. N'Gom, F. Dias, A. Wilkins, D. Ricard, P. Aaby, R. Tedder, H. Whittle, Low Level Viremia and High CD4% Predict Normal Survival in a Cohort of HIV Type-2-Infected Villagers. *AIDS Research and Human Retroviruses* **2002**, *18*, 1167-1173.
36. M. F. S. van der Loeff, A. A. Awasana, R. Sarge-Njie, M. van der Sande, A. Jaye, S. Sabally, T. Corrah, S. J. McConkey, H. C. Whittle, Sixteen Years of HIV Surveillance in a West African Research Clinic Reveals Divergent Epidemic Trends of HIV-1 and HIV-2. *International Journal of Epidemiology* **2006**, *35*, 1322-1328.
37. J. M. Brenchley, T. W. Schacker, L. E. Ruff, D. A. Price, J. H. Taylor, G. J. Beilman, P. L. Nguyen, A. Khoruts, M. Larson, A. T. Haase, D. C. Douek, CD4(+) T Cell Depletion During All Stages of HIV Disease Occurs Predominantly in the Gastrointestinal Tract. *The Journal of Experimental Medicine* **2004**, *200*, 749-759.
38. E. O. Freed, HIV-1 Replication. *Somatic Cell and Molecular Genetics* **2001**, *26*, 13-33.
39. F. Barre-Sinoussi, A. L. Ross, J.-F. Delfraissy, Past, Present and Future: 30 Years of HIV Research. *Nature Reviews Microbiology* **2013**, *11*, 877-883.
40. T. Malik, G. Chauhan, G. Rath, R. S. R. Murthy, A. K. Goyal, "Fusion and Binding Inhibition" Key Target for HIV-1 Treatment and Pre-Exposure Prophylaxis: Targets, Drug Delivery and Nanotechnology Approaches. *Drug Delivery* **2017**, *24*, 608-621.
41. C. B. Wilen, J. C. Tilton, R. W. Doms, HIV: Cell Binding and Entry. *Cold Spring Harbor Perspectives in Medicine* **2012**, *2*, a006866.
42. R. W. Doms, Beyond Receptor Expression: The Influence of Receptor Conformation, Density, and Affinity in HIV-1 Infection. *Virology* **2000**, *276*, 229-237.
43. R. Horuk, Chemokine Receptor Antagonists: Overcoming Developmental Hurdles. *Nature Reviews Drug Discovery* **2009**, *8*, 23-33.
44. E. A. Berger, R. W. Doms, E. M. Fenyo, B. T. M. Korber, D. R. Littman, J. P. Moore, Q. J. Sattentau, H. Schuitemaker, J. Sodroski, R. A. Weiss, A New Classification for HIV-1. *Nature* **1998**, *391*, 240-240.
45. R. I. Connor, K. E. Sheridan, D. Ceradini, S. Choe, N. R. Landau, Change in Coreceptor Use Correlates with Disease Progression in HIV-1–Infected Individuals. *The Journal of Experimental Medicine* **1997**, *185*, 621-628.
46. D. C. Chan, D. Fass, J. M. Berger, P. S. Kim, Core Structure of gp41 from the HIV Envelope Glycoprotein. *Cell* **1997**, *89*, 263-273.
47. G. B. Melikyan, Common Principles and Intermediates of Viral Protein-Mediated Fusion: The HIV-1 Paradigm. *Retrovirology* **2008**, *5*, 111.
48. Z. Ambrose, C. Aiken, HIV-1 Uncoating: Connection to Nuclear Entry and Regulation by Host Proteins. *Virology* **2014**, *454*, 371-379.
49. A. Telesnitsky, S. P. Goff, Reverse Transcriptase and the Generation of Retroviral DNA in *Retroviruses*, Cold Spring Harbor Laboratory Press, Cold Spring Harbor (NY), **1997**.
50. L. A. Kohlstaedt, J. Wang, J. M. Friedman, P. A. Rice, T. A. Steitz, Crystal Structure at 3.5 Å Resolution of HIV-1 Reverse Transcriptase Complexed with an Inhibitor. *Science* **1992**, *256*, 1783-1790.
51. R. Di Santo, Inhibiting the HIV Integration Process: Past, Present, and the Future. *Journal of Medicinal Chemistry* **2014**, *57*, 539-566.
52. W. Yang, J. Y. Lee, M. Nowotny, Making and Breaking Nucleic Acids: Two-Mg2+-Ion Catalysis and Substrate Specificity. *Molecular Cell* **2006**, *22*, 5-13.
53. A. Engelman, K. Mizuuchi, R. Craigie, HIV-1 DNA Integration: Mechanism of Viral DNA Cleavage and DNA Strand Transfer. *Cell* **1991**, *67*, 1211-1221.

54. R. Craigie, HIV Integrase, a Brief Overview from Chemistry to Therapeutics. *Journal of Biological Chemistry* **2001**, *276*, 23213-23216.
55. T. A. Steitz, J. A. Steitz, A General Two-Metal-Ion Mechanism for Catalytic RNA. *Proceedings of the National Academy of Sciences of the United States of America* **1993**, *90*, 6498-6502.
56. Y. Wu, J. W. Marsh, Gene Transcription in HIV Infection. *Microbes and Infection* **2003**, *5*, 1023-1027.
57. J. Karn, C. M. Stoltzfus, Transcriptional and Posttranscriptional Regulation of HIV-1 Gene Expression. *Cold Spring Harbor Perspectives in Medicine* **2012**, *2*, a006916.
58. O. Rohr, C. Marban, D. Aunis, E. Schaeffer, Regulation of HIV-1 Gene Transcription: From Lymphocytes to Microglial Cells. *Journal of Leukocyte Biology* **2003**, *74*, 736-749.
59. V. W. Pollard, M. H. Malim, The HIV-1 Rev Protein. *Annual Review of Microbiology* **1998**, *52*, 491.
60. S. de Breyne, R. Soto-Rifo, M. López-Lastra, T. Ohlmann, Translation Initiation Is Driven by Different Mechanisms on the HIV-1 and HIV-2 Genomic RNAs. *Virus Research* **2013**, *171*, 366-381.
61. S. Guerrero, J. Batisse, C. Libre, S. Bernacchi, R. Marquet, J.-C. Paillart, HIV-1 Replication and the Cellular Eukaryotic Translation Apparatus. *Viruses* **2015**, *7*, 199-218.
62. E. Z. Alkalaeva, A. V. Pisarev, L. Y. Frolova, L. L. Kisselev, T. V. Pestova, In Vitro Reconstitution of Eukaryotic Translation Reveals Cooperativity between Release Factors ERF1 and ERF3. *Cell* **2006**, *125*, 1125-1136.
63. K. Saito, K. Ito, Ribosome Recycling in *Encyclopedia of Systems Biology*, Springer New York, New York, NY, **2013**, 1857-1859.
64. E. O. Freed, HIV-1 Assembly, Release and Maturation. *Nature Reviews Microbiology* **2015**, *13*, 484-496.
65. W. I. Sundquist, H.-G. Kräusslich, HIV-1 Assembly, Budding, and Maturation. *Cold Spring Harbor Perspectives in Medicine* **2012**, *2*.
66. E. O. Freed, HIV-1 Gag Proteins: Diverse Functions in the Virus Life Cycle. *Virology* **1998**, *251*, 1-15.
67. J. S. Saad, J. Miller, J. Tai, A. Kim, R. H. Ghanam, M. F. Summers, Structural Basis for Targeting HIV-1 Gag Proteins to the Plasma Membrane for Virus Assembly. *Proceedings of the National Academy of Sciences of the United States of America* **2006**, *103*, 11364-11369.
68. N. M. Bell, A. M. L. Lever, HIV Gag Polyprotein: Processing and Early Viral Particle Assembly. *Trends in Microbiology* **2013**, *21*, 136-144.
69. S. B. Kutluay, P. D. Bieniasz, Analysis of the Initiating Events in HIV-1 Particle Assembly and Genome Packaging (Initiating Events in HIV-1 Assembly). *PLoS Pathogens* **2010**, *6*, e1001200.
70. D. S. Victoria, F. S. Michael, How Retroviruses Select Their Genomes. *Nature Reviews Microbiology* **2005**, *3*, 643.
71. S. D. Fuller, T. Wilk, B. E. Gowen, H.-G. Kräusslich, V. M. Vogt, Cryo-Electron Microscopy Reveals Ordered Domains in the Immature HIV-1 Particle. *Current Biology* **1997**, *7*, 729-738.
72. M. Prabu-Jeyabalan, E. Nalivaika, C. A. Schiffer, Substrate Shape Determines Specificity of Recognition for HIV-1 Protease. *Structure* **2002**, *10*, 369-381.
73. T. D. Hollingsworth, R. M. Anderson, C. Fraser, HIV-1 Transmission, by Stage of Infection. *Journal of Infectious Diseases* **2008**, *198*, 687-693.
74. A. T. Haase, Perils at Mucosal Front Lines for HIV and SIV and Their Hosts. *Nature Reviews Immunology* **2005**, *5*, 783.
75. C. Reynolds, C. B. de Koning, S. C. Pelly, W. A. L. van Otterlo, M. L. Bode, In Search of a Treatment for HIV - Current Therapies and the Role of Non-Nucleoside Reverse Transcriptase Inhibitors (NNRTIs). *Chemical Society Reviews* **2012**, *41*, 4657-4670.
76. R. F. Siliciano, W. C. Greene, HIV Latency. *Cold Spring Harbor Perspectives in Medicine:* **2011**, *1*, a007096.

77. B. Romani, E. Allahbakhshi, Underlying Mechanisms of HIV-1 Latency. *Virus Genes* **2017**, *53*, 329-339.
78. M. Yorchoan, The History of Zidovudine (AZT): Partnership and Conflict, **2012**, available at http://www.scribd.com/doc/92129927/The-History-of-Zidovudine-AZT-Partnership-and-Conflict
79. H. Mitsuya, K. J. Weinhold, P. A. Furman, M. H. St Clair, S. N. Lehrman, R. C. Gallo, D. Bolognesi, D. W. Barry, S. Broder, 3'-Azido-3'-deoxythymidine (BW A509U): An Antiviral Agent That Inhibits the Infectivity and Cytopathic Effect of Human T-Lymphotropic Virus Type III/Lymphadenopathy-Associated Virus in Vitro. *Proceedings of the National Academy of Sciences of the United States of America* **1985**, *82*, 7096.
80. L. M. Mansky, H. M. Temin, Lower in Vivo Mutation Rate of Human Immunodeficiency Virus Type 1 Than That Predicted from the Fidelity of Purified Reverse Transcriptase. *Journal of Virology* **1995**, *69*, 5087-5094.
81. E. J. Arts, D. J. Hazuda, HIV-1 Antiretroviral Drug Therapy. *Cold Spring Harbor Perspectives in Medicine* **2012**, *2*, a007161.
82. V. Pirrone, N. Thakkar, J. M. Jacobson, B. Wigdahl, F. C. Krebs, Combinatorial Approaches to the Prevention and Treatment of HIV-1 Infection. *Antimicrobial Agents and Chemotherapy* **2011**, *55*, 1831-1842.
83. WHO Consolidated Guidelines on the Use of Antiretroviral Drugs for Treating and Preventing HIV Infection, **2016**, available at http://www.who.int/HIV/pub/arv/arv-2016/en/.
84. T. Cihlar, A. S. Ray, Nucleoside and Nucleotide HIV Reverse Transcriptase Inhibitors: 25 Years after Zidovudine. *Antiviral Research* **2010**, *85*, 39-58.
85. E. De Clercq, Anti-HIV Drugs: 25 Compounds Approved within 25 Years after the Discovery of HIV. *International Journal of Antimicrobial Agents* **2009**, *33*, 307-320.
86. E. De Clercq, Strategies in the Design of Antiviral Drugs. *Nature Reviews Drug Discovery* **2002**, *1*, 13.
87. A. M. Margolis, H. Heverling, P. A. Pham, A. Stolbach, A Review of the Toxicity of HIV Medications. *Journal of Medical Toxicology* **2014**, *10*, 26-39.
88. E. L. Asahchop, M. A. Wainberg, R. D. Sloan, C. L. Tremblay, Antiviral Drug Resistance and the Need for Development of New HIV-1 Reverse Transcriptase Inhibitors. *Antimicrobial Agents and Chemotherapy* **2012**, *56*, 5000-5008.
89. G. Birkus, N. Kutty, G.-X. He, A. Mulato, W. Lee, M. McDermott, T. Cihlar, Activation of 9-[(R)-2-[[(S)-[[(S)-1-(Isopropoxycarbonyl)ethyl]amino]phenoxyphosphinyl]-methoxy]propyl]adenine (GS-7340) and Other Tenofovir Phosphonoamidate Prodrugs by Human Proteases. *Molecular Pharmacology* **2008**, *74*, 92-100.
90. B. D. Herman, N. Sluis-Cremer, Molecular Pharmacology of Nucleoside and Nucleotide HIV-1 Reverse Transcriptase Inhibitors in *Pharmacology*, InTech, **2012**, 63-80.
91. M.-P. de Béthune, Non-Nucleoside Reverse Transcriptase Inhibitors (NNRTIs), Their Discovery, Development, and Use in the Treatment of HIV-1 Infection: A Review of the Last 20 Years (1989–2009). *Antiviral Research* **2010**, *85*, 75-90.
92. Y. Hsiou, J. Ding, K. Das, J. A. D. Clark, S. H. Hughes, E. Arnold, Structure of Unliganded HIV-1 Reverse Transcriptase at 2.7 Å Resolution: Implications of Conformational Changes for Polymerization and Inhibition Mechanisms. *Structure* **1996**, *4*, 853-860.
93. E. De Clercq, HIV Life Cycle: Targets for Anti-HIV Agents in *HIV-1 Integrase: Mechanism and Inhibitor Design*, John Wiley & Sons, Inc., Hoboken, New Jersey, **2011**, 1-14.
94. T. Miyasaka, H. Tanaka, M. Baba, H. Hayakawa, R. T. Walker, J. Balzarini, E. De Clercq, A Novel Lead for Specific Anti-HIV-1 Agents: 1-[(2-Hydroxyethoxy)methyl]-6-(phenylthio)thymine. *Journal of Medicinal Chemistry* **1989**, *32*, 2507-2509.

95. R. Pauwels, K. Andries, J. Desmyter, D. Schols, M. J. Kukla, H. J. Breslin, A. Raeymaeckers, J. V. Gelder, R. Woestenborghs, J. Heykants, K. Schellekens, M. A. C. Janssen, E. D. Clercq, P. A. J. Janssen, Potent and Selective Inhibition of HIV-1 Replication in Vitro by a Novel Series of Tibo Derivatives. *Nature* **1990**, *343*, 470-474.
96. E. De Clercq, Non-Nucleoside Reverse Transcriptase Inhibitors (NNRTIs): Past, Present, and Future. *Chemistry & Biodiversity* **2004**, *1*, 44-64.
97. J. A. Esté, T. Cihlar, Current Status and Challenges of Antiretroviral Research and Therapy. *Antiviral Research* **2010**, *85*, 25-33.
98. I. Usach, V. Melis, J.-E. Peris, Non-Nucleoside Reverse Transcriptase Inhibitors: A Review on Pharmacokinetics, Pharmacodynamics, Safety and Tolerability. *Journal of the International AIDS Society* **2013**, *16*, 18567.
99. R. K. Gupta, D. Pillay, HIV Resistance and the Developing World. *International Journal of Antimicrobial Agents* **2007**, *29*, 510-517.
100. S. G. Sarafianos, K. Das, S. H. Hughes, E. Arnold, Taking Aim at a Moving Target: Designing Drugs to Inhibit Drug-Resistant HIV-1 Reverse Transcriptases. *Current Opinion in Structural Biology* **2004**, *14*, 716-730.
101. E. B. Lansdon, K. M. Brendza, M. Hung, R. Wang, S. Mukund, D. Jin, G. Birkus, N. Kutty, X. Liu, Crystal Structures of HIV-1 Reverse Transcriptase with Etravirine (TMC125) and Rilpivirine (TMC278): Implications for Drug Design. *Journal of Medicinal Chemistry* **2010**, *53*, 4295-4299.
102. J. Ren, J. Milton, K. L. Weaver, S. A. Short, D. I. Stuart, D. K. Stammers, Structural Basis for the Resilience of Efavirenz (DMP-266) to Drug Resistance Mutations in HIV-1 Reverse Transcriptase. *Structure* **2000**, *8*, 1089-1094.
103. Y. Hsiou, J. Ding, K. Das, A. D. Clark Jr, P. L. Boyer, P. Lewi, P. A. J. Janssen, J.-P. Kleim, M. Rösner, S. H. Hughes, E. Arnold, The Lys103Asn Mutation of HIV-1 RT: A Novel Mechanism of Drug Resistance. *Journal of Molecular Biology* **2001**, *309*, 437-445.
104. A. E. Basson, S.-Y. Rhee, C. M. Parry, Z. El-Khatib, S. Charalambous, T. De Oliveira, D. Pillay, C. Hoffmann, D. Katzenstein, R. W. Shafer, L. Morris, Impact of Drug Resistance-Associated Amino Acid Changes in HIV-1 Subtype C on Susceptibility to Newer Nonnucleoside Reverse Transcriptase Inhibitors. *Antimicrobial Agents and Chemotherapy* **2015**, *59*, 960-971.
105. P. A. J. Janssen, P. J. Lewi, E. Arnold, F. Daeyaert, M. de Jonge, J. Heeres, L. Koymans, M. Vinkers, J. Guillemont, E. Pasquier, M. Kukla, D. Ludovici, K. Andries, M.-P. de Béthune, R. Pauwels, K. Das, A. D. Clark, Y. V. Frenkel, S. H. Hughes, B. Medaer, F. De Knaep, H. Bohets, F. De Clerck, A. Lampo, P. Williams, P. Stoffels, In Search of a Novel Anti-HIV Drug: Multidisciplinary Coordination in the Discovery of 4-[[4-[[4-[(1e)-2-Cyanoethenyl]-2,6-dimethylphenyl]amino]-2-pyrimidinyl]amino]benzonitrile (R278474, Rilpivirine). *Journal of Medicinal Chemistry* **2005**, *48*, 1901-1909.
106. K. Das, A. D. Clark, P. J. Lewi, J. Heeres, M. R. de Jonge, L. M. H. Koymans, H. M. Vinkers, F. Daeyaert, D. W. Ludovici, M. J. Kukla, B. De Corte, R. W. Kavash, C. Y. Ho, H. Ye, M. A. Lichtenstein, K. Andries, R. Pauwels, M.-P. de Béthune, P. L. Boyer, P. Clark, S. H. Hughes, P. A. J. Janssen, E. Arnold, Roles of Conformational and Positional Adaptability in Structure-Based Design of TMC125-R165335 (Etravirine) and Related Non-Nucleoside Reverse Transcriptase Inhibitors That Are Highly Potent and Effective against Wild-Type and Drug-Resistant HIV-1 Variants. *Journal of Medicinal Chemistry* **2004**, *47*, 2550-2560.
107. J. D. Burch, B. D. Sherry, D. R. Gauthier, L.-C. Campeau, Discovery and Development of Doravirine: An Investigational Next Generation Non-Nucleside Reverse Transcriptase Inhibitor (NNRTI) for the Treatment of HIV in *Comprehensive Accounts of Pharmaceutical Research and Development: From Discovery to Late-Stage Process Development Volume 1, Vol. 1239*, American Chemical Society, Washington, DC, **2016**, 175-205.

108. S. I. Gubernick, N. Felix, D. Lee, J. J. Xu, B. Hamad, The HIV Therapy Market. *Nature Reviews Drug Discovery* **2016**, *15*, 451-452.
109. M. Feng, N. A. Sachs, M. Xu, J. Grobler, W. Blair, D. J. Hazuda, M. D. Miller, M.-T. Lai, Doravirine Suppresses Common Nonnucleoside Reverse Transcriptase Inhibitor-Associated Mutants at Clinically Relevant Concentrations. *Antimicrobial Agents and Chemotherapy* **2016**, *60*, 2241-2247.
110. A. M. J. Wensing, N. M. van Maarseveen, M. Nijhuis, Fifteen Years of HIV Protease Inhibitors: Raising the Barrier to Resistance. *Antiviral Research* **2010**, *85*, 59-74.
111. G. N. Kumar, A. D. Rodrigues, A. M. Buko, J. F. Denissen, Cytochrome P450-Mediated Metabolism of the HIV-1 Protease Inhibitor Ritonavir (ABT-538) in Human Liver Microsomes. *Journal of Pharmacology and Experimental Therapeutics* **1996**, *277*, 423-431.
112. E. Voigt, A. Wickesberg, J. C. Wasmuth, P. Gute, L. Locher, B. Salzberger, A. Wöhrmann, A. Adam, L. Weitner, J. K. Rockstroh, First-Line Ritonavir/Indinavir 100/800 mg Twice Daily Plus Nucleoside Reverse Transcriptase Inhibitors in a German Multicentre Study: 48-Week Results. *HIV Medicine* **2002**, *3*, 277-282.
113. E. K. Hester, H. V. Chandler, K. M. Sims, Fosamprenavir: Drug Development for Adherence. *Annals of Pharmacotherapy* **2006**, *40*, 1301-1310.
114. L. Doyon, S. Tremblay, L. Bourgon, E. Wardrop, M. G. Cordingley, Selection and Characterization of HIV-1 Showing Reduced Susceptibility to the Non-Peptidic Protease Inhibitor Tipranavir. *Antiviral Research* **2005**, *68*, 27-35.
115. A. K. Ghosh, H. L. Osswald, G. Prato, Recent Progress in the Development of HIV-1 Protease Inhibitors for the Treatment of HIV/AIDS. *Journal of Medicinal Chemistry* **2016**, *59*, 5172-5208.
116. D. J. Hazuda, P. Felock, M. Witmer, A. Wolfe, K. Stillmock, J. A. Grobler, A. Espeseth, L. Gabryelski, W. Schleif, C. Blau, M. D. Miller, Inhibitors of Strand Transfer That Prevent Integration and Inhibit HIV-1 Replication in Cells. *Science* **2000**, *287*, 646-650.
117. T. Fujishita, T. Yoshinaga, A. Sato, Aromatic Heterocycle Compounds Having HIV Integrase Inhibiting Activities, Patent, WO2000039086 A1, **2001**
118. D. J. McColl, X. Chen, Strand Transfer Inhibitors of HIV-1 Integrase: Bringing in a New Era of Antiretroviral Therapy. *Antiviral Research* **2010**, *85*, 101-118.
119. X. Chen, M. Tsiang, F. Yu, M. Hung, G. S. Jones, A. Zeynalzadegan, X. Qi, H. Jin, C. U. Kim, S. Swaminathan, J. M. Chen, Modeling, Analysis, and Validation of a Novel HIV Integrase Structure Provide Insights into the Binding Modes of Potent Integrase Inhibitors. *Journal of Molecular Biology* **2008**, *380*, 504-519.
120. FDA, Approval of Vitekta, **2014**, available at https://www.accessdata.fda.gov/drugsatfda_docs/nda/2014/203093Orig1VITEKTAtoc.cfm
121. J.-L. Blanco, V. Varghese, S.-Y. Rhee, J. M. Gatell, R. W. Shafer, HIV-1 Integrase Inhibitor Resistance and Its Clinical Implications. *The Journal of Infectious Diseases* **2011**, *203*, 1204-1214.
122. C. Garrido, J. Villacian, N. Zahonero, T. Pattery, F. Garcia, F. Gutierrez, E. Caballero, M. Van Houtte, V. Soriano, C. de Mendoza, Broad Phenotypic Cross-Resistance to Elvitegravir in HIV-Infected Patients Failing on Raltegravir-Containing Regimens. *Antimicrobial Agents and Chemotherapy* **2012**, *56*, 2873-2878.
123. C. Garrido, J. Villacian, N. Zahonero, T. Pattery, F. Garcia, F. Gutierrez, E. Caballero, M. Van Houtte, V. Soriano, C. de Mendoza, S. G. on behalf of the, Broad Phenotypic Cross-Resistance to Elvitegravir in HIV-Infected Patients Failing on Raltegravir-Containing Regimens. *Antimicrobial Agents and Chemotherapy* **2012**, *56*, 2873-2878.
124. L. Xu, H. Liu, B. P. Murray, C. Callebaut, M. S. Lee, A. Hong, R. G. Strickley, L. K. Tsai, K. M. Stray, Y. Wang, G. R. Rhodes, M. C. Desai, Cobicistat (GS-9350): A Potent and Selective Inhibitor of Human CYP3A as a Novel Pharmacoenhancer. *ACS Medicinal Chemistry Letters* **2010**, *1*, 209-213.

125. X. Z. Zhao, S. J. Smith, D. P. Maskell, M. Metifiot, V. E. Pye, K. Fesen, C. Marchand, Y. Pommier, P. Cherepanov, S. H. Hughes, T. R. Burke, HIV-1 Integrase Strand Transfer Inhibitors with Reduced Susceptibility to Drug Resistant Mutant Integrases. *ACS Chemical Biology* **2016**, *11*, 1074-1081.
126. S. Hare, S. J. Smith, M. Métifiot, A. Jaxa-Chamiec, Y. Pommier, S. H. Hughes, P. Cherepanov, Structural and Functional Analyses of the Second-Generation Integrase Strand Transfer Inhibitor Dolutegravir (S/GSK1349572). *Molecular Pharmacology* **2011**, *80*, 565.
127. D. A. Osterholzer, M. Goldman, Dolutegravir: A Next-Generation Integrase Inhibitor for Treatment of HIV Infection. *Clinical Infectious Diseases* **2014**, *59*, 265-271.
128. P. Dorr, B. Stammen, E. van der Ryst, Discovery and Development of Maraviroc, a CCR5 Antagonist for the Treatment of HIV Infection in *Case Studies in Modern Drug Discovery and Development*, The Royal Society of Chemistry, Cambridge, **2012**, 196-226.
129. C. Barber, D. Pryde, From Hts to Market: The Discovery and Development of Maraviroc, a CCR5 Antagonist for the Treatment of HIV in *Accounts in Drug Discovery: Case Studies in Medicinal Chemistry*, The Royal Society of Chemistry, Cambridge, **2011**, 183-214.
130. A. M. Thayer, New Antiretrovirals. *Chemical & Engineering News Archive* **2008**, *86*, 29-36.
131. C. Flexner, HIV Drug Development: The Next 25 Years. *Nature Reviews Drug Discovery* **2007**, *6*, 959-966.
132. C. V. Fletcher, Enfuvirtide, a New Drug for HIV Infection. *The Lancet*, *361*, 1577-1578.
133. D. Robertson, US FDA Approves New Class of HIV Therapeutics. *Nature Biotechnology* **2003**, *21*, 470-471.
134. J. A. Este, A. Telenti, HIV Entry Inhibitors. *Lancet* **2007**, *370*, 81-88.
135. T. Matthews, M. Salgo, M. Greenberg, J. Chung, R. DeMasi, D. Bolognesi, Enfuvirtide: The First Therapy to Inhibit the Entry of HIV-1 into Host CD4 Lymphocytes. *Nature Reviews Drug Discovery* **2004**, *3*, 215-225.
136. J. M. Kilby, S. Hopkins, T. M. Venetta, B. DiMassimo, G. A. Cloud, J. Y. Lee, L. Alldredge, E. Hunter, D. Lambert, D. Bolognesi, T. Matthews, M. R. Johnson, M. A. Nowak, G. M. Shaw, M. S. Saag, Potent Suppression of HIV-1 Replication in Humans by T-20, a Peptide Inhibitor of gp41-Mediated Virus Entry. *Nature Medicine* **1998**, *4*, 1302-1307.
137. M. Tom, S. Miklos, G. Michael, C. Jain, D. Ralph, B. Dani, Enfuvirtide: The First Therapy to Inhibit the Entry of HIV-1 into Host CD4 Lymphocytes. *Nature Reviews Drug Discovery* **2004**, *3*, 215.
138. HIV Treatment Bulletin: HIV Pipeline 2017, **2017**, available at http://i-base.info/pipeline-2017/.
139. M. S. Saag, New and Investigational Antiretroviral Drugs for HIV Infection: Mechanisms of Action and Early Research Findings. *Topics in antiviral medicine* **2012**, *20*, 162.
140. H. Chong, X. Yao, C. Zhang, L. Cai, S. Cui, Y. Wang, Y. He, Biophysical Property and Broad Anti-HIV Activity of Albuvirtide, a 3-Maleimimidopropionic Acid-Modified Peptide Fusion Inhibitor. *PLoS ONE* **2012**, *7*, e32599.
141. J. F. Kadow, Y. Ueda, N. A. Meanwell, T. P. Connolly, T. Wang, C.-P. Chen, K.-S. Yeung, J. Zhu, J. A. Bender, Z. Yang, D. Parker, P.-F. Lin, R. J. Colonno, M. Mathew, D. Morgan, M. Zheng, C. Chien, D. Grasela, Inhibitors of Human Immunodeficiency Virus Type 1 (HIV-1) Attachment 6. Preclinical and Human Pharmacokinetic Profiling of BMS-663749, a Phosphonooxymethyl Prodrug of the HIV-1 Attachment Inhibitor 2-(4-Benzoyl-1-piperazinyl)-1-(4,7-dimethoxy-1H-pyrrolo[2,3-c]pyridin-3-yl)-2-oxoethanone (Bms-488043). *Journal of Medicinal Chemistry* **2012**, *55*, 2048-2056.
142. B. Nowicka-Sans, Y.-F. Gong, B. McAuliffe, I. Dicker, H.-T. Ho, N. Zhou, B. Eggers, P.-F. Lin, N. Ray, M. Wind-Rotolo, L. Zhu, A. Majumdar, D. Stock, M. Lataillade, G. J. Hanna, J. D. Matiskella, Y. Ueda, T. Wang, J. F. Kadow, N. A. Meanwell, M. Krystal, In Vitro Antiviral Characteristics of HIV-1 Attachment Inhibitor BMS-626529, the Active Component of the Prodrug BMS-663068. *Antimicrobial Agents and Chemotherapy* **2012**, *56*, 3498-3507.

143. C. Dousson, F.-R. Alexandre, A. Amador, S. Bonaric, S. Bot, C. Caillet, T. Convard, D. da Costa, M.-P. Lioure, A. Roland, E. Rosinovsky, S. Maldonado, C. Parsy, C. Trochet, R. Storer, A. Stewart, J. Wang, B. A. Mayes, C. Musiu, B. Poddesu, L. Vargiu, M. Liuzzi, A. Moussa, J. Jakubik, L. Hubbard, M. Seifer, D. Standring, Discovery of the Aryl-phospho-indole IDX899, a Highly Potent Anti-HIV Non-Nucleoside Reverse Transcriptase Inhibitor. *Journal of Medicinal Chemistry* **2016**, *59*, 1891-1898.
144. Z. Zhao, S. E. Wolkenberg, M. Lu, V. Munshi, G. Moyer, M. Feng, A. V. Carella, L. T. Ecto, L. J. Gabryelski, M.-T. Lai, S. G. Prasad, Y. Yan, G. B. McGaughey, M. D. Miller, C. W. Lindsley, G. D. Hartman, J. P. Vacca, T. M. Williams, Novel Indole-3-Sulfonamides as Potent HIV Non-Nucleoside Reverse Transcriptase Inhibitors (NNRTIs). *Bioorganic & Medicinal Chemistry Letters* **2008**, *18*, 554-559.
145. F. R. de Sa Alves, E. J. Barreiro, C. A. Fraga, From Nature to Drug Discovery: The Indole Scaffold as a 'Privileged Structure'. *Mini Reviews in Medicinal Chemistry* **2009**, *9*, 782-793.
146. B. E. Evans, K. E. Rittle, M. G. Bock, R. M. DiPardo, R. M. Freidinger, W. L. Whitter, G. F. Lundell, D. F. Veber, P. S. Anderson, R. S. L. Chang, V. J. Lotti, D. J. Cerino, T. B. Chen, P. J. Kling, K. A. Kunkel, J. P. Springer, J. Hirshfield, Methods for Drug Discovery: Development of Potent, Selective, Orally Effective Cholecystokinin Antagonists. *Journal of Medicinal Chemistry* **1988**, *31*, 2235-2246.
147. R. Müller, I. Mulani, A. E. Basson, N. Pribut, M. Hassam, L. Morris, W. A. L. van Otterlo, S. C. Pelly, Novel Indole Based NNRTIs with Improved Potency against Wild Type and Resistant HIV. *Bioorganic & Medicinal Chemistry Letters* **2014**, *24*, 4376-4380.
148. M. Hassam, A. E. Basson, D. C. Liotta, L. Morris, W. A. L. van Otterlo, S. C. Pelly, Novel Cyclopropyl-Indole Derivatives as HIV Non-Nucleoside Reverse Transcriptase Inhibitors. *ACS Medicinal Chemistry Letters* **2012**, *3*, 470-475.
149. S. Brigg, N. Pribut, A. E. Basson, M. Avgenikos, R. Venter, M. A. Blackie, W. A. L. van Otterlo, S. C. Pelly, Novel Indole Sulfides as Potent HIV-1 NNRTIs. *Bioorg Med Chem Lett* **2016**, *26*, 1580-1584.
150. X. Li, P. Gao, P. Zhan, X. Liu, Substituted Indoles as HIV-1 Non-Nucleoside Reverse Transcriptase Inhibitors: A Patent Evaluation (WO2015044928). *Expert Opinion on Therapeutic Patents* **2016**, *26*, 629-635.
151. G. Schneider, W. Neidhart, T. Giller, G. Schmid, "Scaffold-Hopping" by Topological Pharmacophore Search: A Contribution to Virtual Screening. *Angewandte Chemie International Edition* **1999**, *38*, 2894-2896.
152. N. Brown, Identifying and Representing Scaffolds in *Scaffold Hopping in Medicinal Chemistry*, Wiley-VCH Verlag GmbH & Co. KGaA, Weinheim, Germany, **2013**, 1-14.
153. R. A. Friesner, R. B. Murphy, M. P. Repasky, L. L. Frye, J. R. Greenwood, T. A. Halgren, P. C. Sanschagrin, D. T. Mainz, Extra Precision Glide: Docking and Scoring Incorporating a Model of Hydrophobic Enclosure for Protein–Ligand Complexes. *Journal of Medicinal Chemistry* **2006**, *49*, 6177-6196.
154. M. L. Barreca, A. Rao, L. De Luca, M. Zappalà, A.-M. Monforte, G. Maga, C. Pannecouque, J. Balzarini, E. De Clercq, A. Chimirri, P. Monforte, Computational Strategies in Discovering Novel Non-Nucleoside Inhibitors of HIV-1 Rt. *Journal of Medicinal Chemistry* **2005**, *48*, 3433-3437.
155. A.-M. Monforte, P. Logoteta, L. D. Luca, N. Iraci, S. Ferro, G. Maga, E. De Clercq, C. Pannecouque, A. Chimirri, Novel 1,3-Dihydro-benzimidazol-2-ones and Their Analogues as Potent Non-Nucleoside HIV-1 Reverse Transcriptase Inhibitors. *Bioorganic & Medicinal Chemistry* **2010**, *18*, 1702-1710.
156. M. L. Barreca, A. Rao, L. D. Luca, N. Iraci, A.-M. Monforte, G. Maga, E. D. Clercq, C. Pannecouque, J. Balzarini, A. Chimirri, Discovery of Novel Benzimidazolones as Potent Non-Nucleoside Reverse Transcriptase Inhibitors Active against Wild-Type and Mutant HIV-1 Strains. *Bioorganic & Medicinal Chemistry Letters* **2007**, *17*, 1956-1960.

157. C. Battilocchio, J. M. Hawkins, S. V. Ley, A Mild and Efficient Flow Procedure for the Transfer Hydrogenation of Ketones and Aldehydes Using Hydrous Zirconia. *Organic Letters* **2013**, *15*, 2278-2281.
158. B. P. Bandgar, V. S. Sadavarte, L. S. Uppalla, An Expedient and Highly Selective Iodination of Alcohols Using a KI/BF_3·Et_2O System. *Tetrahedron Letters* **2001**, *42*, 951-953.
159. E. J. Stoner, D. A. Cothron, M. K. Balmer, B. A. Roden, Benzylation Via Tandem Grignard Reaction—Iodotrimethylsilane (TMSI) Mediated Reduction. *Tetrahedron* **1995**, *51*, 11043-11062.
160. A. B. Gamble, J. Garner, C. P. Gordon, S. M. J. O'Conner, P. A. Keller, Aryl Nitro Reduction with Iron Powder or Stannous Chloride under Ultrasonic Irradiation. *Synthetic Communications* **2007**, *37*, 2777-2786.
161. P. Cintas, J.-L. Luche, Organometallic Sonochemistry in *Synthetic Organic Sonochemistry*, Springer US, Boston, MA, **1998**, 167-234.
162. F. G. Bordwell, G. Z. Ji, Effects of Structural Changes on Acidities and Homolytic Bond Dissociation Energies of the Hydrogen-Nitrogen Bonds in Amidines, Carboxamides, and Thiocarboxamides. *Journal of the American Chemical Society* **1991**, *113*, 8398-8401.
163. F. G. Bordwell, D. J. Algrim, J. A. Harrelson, The Relative Ease of Removing a Proton, a Hydrogen Atom, or an Electron from Carboxamides Versus Thiocarboxamides. *Journal of the American Chemical Society* **1988**, *110*, 5903-5904.
164. D. E. Gomez, L. Fabbrizzi, M. Licchelli, E. Monzani, Urea Vs. Thiourea in Anion Recognition. *Organic & Biomolecular Chemistry* **2005**, *3*, 1495-1500.
165. R. K. Gupta, A. Kohli, A. L. McCormick, G. J. Towers, D. Pillay, C. M. Parry, Full-Length HIV-1 Gag Determines Protease Inhibitor Susceptibility within in-Vitro Assays. *AIDS* **2010**, *24*, 1651-1655.
166. C. M. Parry, A. Kohli, C. J. Boinett, G. J. Towers, A. L. McCormick, D. Pillay, Gag Determinants of Fitness and Drug Susceptibility in Protease Inhibitor-Resistant Human Immunodeficiency Virus Type 1. *Journal of Virology* **2009**, *83*, 9094-9101.
167. M. Tim, Rapid Colorimetric Assay for Cellular Growth and Survival: Application to Proliferation and Cytotoxicity Assays. *Journal of Immunological Methods* **1983**, *65*, 55-63.
168. D. Li, P. Zhan, E. De Clercq, X. Liu, Strategies for the Design of HIV-1 Non-Nucleoside Reverse Transcriptase Inhibitors: Lessons from the Development of Seven Representative Paradigms. *Journal of Medicinal Chemistry* **2012**, *55*, 3595-3613.
169. J. Ren, P. P. Chamberlain, A. Stamp, S. A. Short, K. L. Weaver, K. R. Romines, R. Hazen, A. Freeman, R. G. Ferris, C. W. Andrews, L. Boone, J. H. Chan, D. K. Stammers, Structural Basis for the Improved Drug Resistance Profile of New Generation Benzophenone Non-Nucleoside HIV-1 Reverse Transcriptase Inhibitors†. *Journal of Medicinal Chemistry* **2008**, *51*, 5000-5008.
170. H. Pelemans, R. Esnouf, E. De Clercq, J. Balzarini, Mutational Analysis of Trp-229 of Human Immunodeficiency Virus Type 1 Reverse Transcriptase (RT) Identifies This Amino Acid Residue as a Prime Target for the Rational Design of New Non-Nucleoside Rt Inhibitors. *Molecular Pharmacology* **2000**, *57*, 954-960.
171. M. Ghosh, J. Williams, M. D. Powell, J. G. Levin, S. F. J. Le Grice, Mutating a Conserved Motif of the HIV-1 Reverse Transcriptase Palm Subdomain Alters Primer Utilization. *Biochemistry* **1997**, *36*, 5758-5768.
172. C. Fattorusso, S. Gemma, S. Butini, P. Huleatt, B. Catalanotti, M. Persico, M. De Angelis, I. Fiorini, V. Nacci, A. Ramunno, M. Rodriquez, G. Greco, E. Novellino, A. Bergamini, S. Marini, M. Coletta, G. Maga, S. Spadari, G. Campiani, Specific Targeting Highly Conserved Residues in the HIV-1 Reverse Transcriptase Primer Grip Region. Design, Synthesis, and Biological Evaluation of Novel, Potent, and Broad Spectrum NNRTIs with Antiviral Activity. *Journal of Medicinal Chemistry* **2005**, *48*, 7153-7165.

173. R. Corbau, J. Mori, C. Phillips, L. Fishburn, A. Martin, C. Mowbray, W. Panton, C. Smith-Burchnell, A. Thornberry, H. Ringrose, T. Knöchel, S. Irving, M. Westby, A. Wood, M. Perros, Lersivirine, a Nonnucleoside Reverse Transcriptase Inhibitor with Activity against Drug-Resistant Human Immunodeficiency Virus Type 1. *Antimicrobial Agents and Chemotherapy* **2010**, *54*, 4451-4463.
174. B. Côté, J. D. Burch, E. Asante-Appiah, C. Bayly, L. Bédard, M. Blouin, L. C. Campeau, E. Cauchon, M. Chan, A. Chefson, N. Coulombe, W. Cromlish, S. Debnath, D. Deschênes, K. Dupont-Gaudet, J. P. Falgueyret, R. Forget, S. Gagné, D. Gauvreau, M. Girardin, S. Guiral, E. Langlois, C. S. Li, N. Nguyen, R. Papp, S. Plamondon, A. Roy, S. Roy, R. Seliniotakis, M. St-Onge, S. Ouellet, P. Tawa, J. F. Truchon, J. Vacca, M. Wrona, Y. Yan, Y. Ducharme, Discovery of MK-1439, an Orally Bioavailable Non-Nucleoside Reverse Transcriptase Inhibitor Potent against a Wide Range of Resistant Mutant HIV Viruses. *Bioorganic and Medicinal Chemistry Letters* **2014**, *24*, 917-922.
175. X. Li, P. Zhan, E. D. Clercq, X. Liu, The HIV-1 Non-Nucleoside Reverse Transcriptase Inhibitors (Part V): Capravirine and Its Analogues. *Current Medicinal Chemistry* **2012**, *19*, 6138-6149.
176. R. Esnouf, J. Ren, C. Ross, Y. Jones, D. Stammers, D. Stuart, Mechanism of Inhibition of HIV-1 Reverse Transcriptase by Non-Nucleoside Inhibitors. *Nature Structural Biology* **1995**, *2*, 303-308.
177. L. H. Jones, G. Allan, R. Corbau, D. S. Middleton, C. E. Mowbray, S. D. Newman, C. Phillips, R. Webster, M. Westby, Comparison of the Non-Nucleoside Reverse Transcriptase Inhibitor Lersivirine with Its Pyrazole and Imidazole Isomers. *Chemical Biology & Drug Design* **2011**, *77*, 393-397.
178. S. E. Nichols, R. A. Domaoal, V. V. Thakur, J. Tirado-Rives, K. S. Anderson, W. L. Jorgensen, Discovery of Wild-Type and Y181C Mutant Non-Nucleoside HIV-1 Reverse Transcriptase Inhibitors Using Virtual Screening with Multiple Protein Structures. *Journal of Chemical Information and Modeling* **2009**, *49*, 1272-1279.
179. A. L. Hopkins, J. Ren, H. Tanaka, M. Baba, M. Okamato, D. I. Stuart, D. K. Stammers, Design of MKC-442 (Emivirine) Analogues with Improved Activity against Drug-Resistant HIV Mutants. *Journal of Medicinal Chemistry* **1999**, *42*, 4500-4505.
180. D. Maiti, S. L. Buchwald, Orthogonal Cu- and Pd-Based Catalyst Systems for the O- and N-Arylation of Aminophenols. *Journal of the American Chemical Society* **2009**, *131*, 17423-17429.
181. F. G. Bordwell, D. J. Algrim, Acidities of Anilines in Dimethyl Sulfoxide Solution. *Journal of the American Chemical Society* **1988**, *110*, 2964-2968.
182. J. P. Whitten, D. P. Matthews, J. R. McCarthy, [2-(Trimethylsilyl)ethoxy]methyl (SEM) as a Novel and Effective Imidazole and Fused Aromatic Imidazole Protecting Group. *The Journal of Organic Chemistry* **1986**, *51*, 1891-1894.
183. B. H. Lipshutz, W. Vaccaro, B. Huff, Protection of Imidazoles as their B-Trimethylsilylethoxymethyl (SEM) Derivatives. *Tetrahedron Letters* **1986**, *27*, 4095-4098.
184. R. N. Nair, T. D. Bannister, Tale of Two Protecting Groups—Boc Vs SEM—for Directed Lithiation and C–C Bond Formation on a Pyrrolopyridazinone Core. *Organic Process Research & Development* **2016**, *20*, 1370-1376.
185. A. M. Palmer, V. Chiesa, A. Schmid, G. Münch, B. Grobbel, P. J. Zimmermann, C. Brehm, W. Buhr, W.-A. Simon, W. Kromer, S. Postius, J. Volz, D. Hess, Tetrahydrochromenoimidazoles as Potassium-Competitive Acid Blockers (P-CABs): Structure−Activity Relationship of Their Antisecretory Properties and Their Affinity toward the Herg Channel. *Journal of Medicinal Chemistry* **2010**, *53*, 3645-3674.
186. P. B. Sampson, Y. Liu, N. K. Patel, M. Feher, B. Forrest, S.-W. Li, L. Edwards, R. Laufer, Y. Lang, F. Ban, D. E. Awrey, G. Mao, O. Plotnikova, G. Leung, R. Hodgson, J. Mason, X. Wei, R. Kiarash, E. Green, W. Qiu, N. Y. Chirgadze, T. W. Mak, G. Pan, H. W. Pauls, The Discovery of Polo-Like Kinase 4 Inhibitors: Design and Optimization of Spiro[cyclopropane-1,3′[3*H*]Indol]-2′(1′*H*)-ones as Orally Bioavailable Antitumor Agents. *Journal of Medicinal Chemistry* **2015**, *58*, 130-146.

187. J. M. Gardiner, C. R. Loyns, Efficient One-Pot Conversion of 6-Methyl-2-nitroaniline into 1-Alkyloxy-2-alkyl-4-methyl-, 1-Benzyloxy-2-phenyl-4-methyl-, and 1-Allyloxy-4-methyl-2-vinyl-benzimidazole. *Synthetic Communications* **1995**, *25*, 819-827.
188. J. Machin, R. K. Mackie, H. McNab, G. A. Reed, A. J. G. Sagar, D. M. Smith, O-Nitroaniline Derivatives. Part V. Cyclisation of N-Acylated Derivatives of N-Benzyl- and N-p-Nitrobenzyl-O-nitroaniline: A Comparison of Carboxamides and Sulphonamides. *Journal of the Chemical Society, Perkin Transactions 1* **1976**, 394-399.
189. J. Machin, D. M. Smith, O-Nitroaniline Derivatives. Part 7. The Synthesis of 2-Alkoxybenzimidazole N-oxides (2-Alkoxy-N-hydroxybenzimidazoles) from O-Nitroanilines. *Journal of the Chemical Society, Perkin Transactions 1* **1979**, 1371-1378.
190. A. F. Andrews, D. M. Smith, H. F. Hodson, P. B. Thorogood, Synthetic Approaches to Some Aza-Analogues of Benzimidazole N-Oxides. Part 1. The Imidazo[4,5-b]pyridine Series. *Journal of the Chemical Society, Perkin Transactions 1* **1982**, 2995-3006.
191. J. M. Gardiner, C. R. Loyns, C. H. Schwalbe, G. C. Barrett, P. R. Lowe, Synthesis of 1-Alkoxy-2-Alkyl-Benzimidazoles from 2-Nitroanilines Via Tandem N-Alkylation-Cyclization-O-Alkylation. *Tetrahedron* **1995**, *51*, 4101-4110.
192. A. J. Parker, The Effects of Solvation on the Properties of Anions in Dipolar Aprotic Solvents. *Quarterly Reviews, Chemical Society* **1962**, *16*, 163-187.
193. R. Zahler, R. T. Wester, S. J. Brickner, Compounds Useful as Antibiotic Tolerance Inhibitors, Patent, WO2014176258 A1, **2014**
194. Y. Nagata, Phthalocyanine Compound, Process for Producing the Same, and Colored Composition Containing the Phthalocyanine Compound, Patent, EP1870438, **2007**
195. M. Ding, F. He, T. W. Hudyma, X. Zheng, M. A. Poss, J. F. Kadow, B. R. Beno, K. L. Rigat, Y.-K. Wang, R. A. Fridell, J. A. Lemm, D. Qiu, M. Liu, S. Voss, L. A. Pelosi, S. B. Roberts, M. Gao, J. Knipe, R. G. Gentles, Synthesis and Sar Studies of Novel Heteroaryl Fused Tetracyclic Indole-Diamide Compounds: Potent Allosteric Inhibitors of the Hepatitis C Virus NS5B Polymerase. *Bioorganic & Medicinal Chemistry Letters* **2012**, *22*, 2866-2871.
196. I. S. Cloudsdale, J. K. Dickson, T. E. Barta, B. S. Grella, E. D. Smith, J. L. Kulp, F. Guarnieri, J. L. Kulp, Design, Synthesis and Biological Evaluation of Renin Inhibitors Guided by Simulated Annealing of Chemical Potential Simulations. *Bioorganic & Medicinal Chemistry* **2017**, *25*, 3947-3963.
197. N. G. M. Davies, H. Browne, B. Davis, M. J. Drysdale, N. Foloppe, S. Geoffrey, B. Gibbons, T. Hart, R. Hubbard, M. R. Jensen, H. Mansell, A. Massey, N. Matassova, J. D. Moore, J. Murray, R. Pratt, S. Ray, A. Robertson, S. D. Roughley, J. Schoepfer, K. Scriven, H. Simmonite, S. Stokes, A. Surgenor, P. Webb, M. Wood, L. Wright, P. Brough, Targeting Conserved Water Molecules: Design of 4-Aryl-5-cyanopyrrolo[2,3-D]pyrimidine Hsp90 Inhibitors Using Fragment-Based Screening and Structure-Based Optimization. *Bioorganic & Medicinal Chemistry* **2012**, *20*, 6770-6789.
198. A. Chicca, R. Berg, H. J. Jessen, N. Marck, F. Schmid, P. Burch, J. Gertsch, K. Gademann, Biological Evaluation of Pyridone Alkaloids on the Endocannabinoid System. *Bioorganic & Medicinal Chemistry* **2017**, *25*, 6102-6114.
199. J. M. Muchowski, D. R. Solas, Protecting Groups for the Pyrrole and Indole Nitrogen Atom. The [2-(Trimethylsilyl)ethoxy]methyl Moiety. Lithiation of 1-[[2-(Trimethylsilyl)ethoxy]methyl]pyrrole. *The Journal of Organic Chemistry* **1984**, *49*, 203-205.
200. K. C. Nicolaou, X. Huang, N. Giuseppone, P. Bheema Rao, M. Bella, M. V. Reddy, S. A. Snyder, Construction of the Complete Aromatic Core of Diazonamide a by a Novel Hetero Pinacol Macrocyclization Cascade Reaction. *Angewandte Chemie International Edition* **2001**, *40*, 4705-4709.
201. K. C. Nicolaou, S. A. Snyder, N. Giuseppone, X. Huang, M. Bella, M. V. Reddy, P. B. Rao, A. E. Koumbis, P. Giannakakou, A. O'Brate, Studies toward Diazonamide A: Development of a Hetero-

Pinacol Macrocyclization Cascade for the Construction of the Bis-Macrocyclic Framework of the Originally Proposed Structure. *Journal of the American Chemical Society* **2004**, *126*, 10174-10182.

202. C. E. Mowbray, C. Burt, R. Corbau, M. Perros, I. Tran, P. A. Stupple, R. Webster, A. Wood, Pyrazole NNRTIs 1: Design and Initial Optimisation of a Novel Template. *Bioorganic and Medicinal Chemistry Letters* **2009**, *19*, 5599-5602.
203. C. E. Mowbray, R. Corbau, M. Hawes, L. H. Jones, J. E. Mills, M. Perros, M. D. Selby, P. A. Stupple, R. Webster, A. Wood, Pyrazole NNRTIs 3: Optimisation of Physicochemical Properties. *Bioorganic & Medicinal Chemistry Letters* **2009**, *19*, 5603-5606.
204. C. E. Mowbray, C. Burt, R. Corbau, S. Gayton, M. Hawes, M. Perros, I. Tran, D. A. Price, F. J. Quinton, M. D. Selby, P. A. Stupple, R. Webster, A. Wood, Pyrazole NNRTIs 4: Selection of UK-453,061 (Lersivirine) as a Development Candidate. *Bioorganic & Medicinal Chemistry Letters* **2009**, *19*, 5857-5860.
205. H. Amii, K. Uneyama, C−F Bond Activation in Organic Synthesis. *Chemical Reviews* **2009**, *109*, 2119-2183.
206. V. M. Vlasov, Fluoride Ion as a Nucleophile and a Leaving Group in Aromatic Nucleophilic Substitution Reactions. *Journal of Fluorine Chemistry* **1993**, *61*, 193-216.
207. W. Danikiewicz, T. Bieńkowski, D. Kozłowska, M. Zimnicka, Aromatic Nucleophilic Substitution (S_NAr) Reactions of 1,2- and 1,4-Halonitrobenzenes and 1,4-Dinitrobenzene with Carbanions in the Gas Phase. *Journal of the American Society for Mass Spectrometry* **2007**, *18*, 1351-1363.
208. T. F. Woiwode, C. Rose, T. J. Wandless, A Simple and Efficient Method for the Preparation of Hindered Alkyl−Aryl Ethers. *The Journal of Organic Chemistry* **1998**, *63*, 9594-9596.
209. L. H. Jones, G. Allan, O. Barba, C. Burt, R. Corbau, T. Dupont, T. Knöchel, S. Irving, D. S. Middleton, C. E. Mowbray, M. Perros, H. Ringrose, N. A. Swain, R. Webster, M. Westby, C. Phillips, Novel Indazole Non-Nucleoside Reverse Transcriptase Inhibitors Using Molecular Hybridization Based on Crystallographic Overlays. *Journal of Medicinal Chemistry* **2009**, *52*, 1219-1223.
210. D.-S. Su, J. J. Lim, E. Tinney, B.-L. Wan, M. B. Young, K. D. Anderson, D. Rudd, V. Munshi, C. Bahnck, P. J. Felock, M. Lu, M.-T. Lai, S. Touch, G. Moyer, D. J. DiStefano, J. A. Flynn, Y. Liang, R. Sanchez, R. Perlow-Poehnelt, M. Miller, J. P. Vacca, T. M. Williams, N. J. Anthony, Biaryl Ethers as Novel Non-Nucleoside Reverse Transcriptase Inhibitors with Improved Potency against Key Mutant Viruses. *Journal of Medicinal Chemistry* **2009**, *52*, 7163-7169.
211. C. Bissantz, B. Kuhn, M. Stahl, A Medicinal Chemist's Guide to Molecular Interactions. *Journal of Medicinal Chemistry* **2010**, *53*, 5061-5084.
212. R. A. Abramovitch, J. G. Saha, Substitution in the Pyridine Series: Effect of Substituents in *Advances in Heterocyclic Chemistry, Vol. 6*, Academic Press, New York, **1966**, 229-345.
213. P. Li, J. Yu, F. Hao, H. He, X. Shi, J. Hu, L. Wang, C. Du, X. Zhang, Y. Sun, F. Lin, Z. Gu, D. Xu, X. Chen, L. Shen, G. Hu, J. Li, S. Chen, W. Xiao, Z. Wang, Q. Guo, X. Chang, X. Tian, T. Lin, Discovery of Potent EV71 Capsid Inhibitors for Treatment of HFMD. *ACS Medicinal Chemistry Letters* **2017**, *8*, 841-846.
214. Z. Zhan, J. Ai, Q. Liu, Y. Ji, T. Chen, Y. Xu, M. Geng, W. Duan, Discovery of Anilinopyrimidines as Dual Inhibitors of C-Met and VEGFR-2: Synthesis, SAR, and Cellular Activity. *ACS Medicinal Chemistry Letters* **2014**, *5*, 673-678.
215. M. Schlosser, T. Rausis, C. Bobbio, Rerouting Nucleophilic Substitution from the 4-Position to the 2- or 6-Position of 2,4-Dihalopyridines and 2,4,6-Trihalopyridines: The Solution to a Long-Standing Problem. *Organic Letters* **2005**, *7*, 127-129.
216. D. J. Kleinhans, Studies in the Synthesis of Benzoxazole Compounds, Thesis, Stellenbosch: Stellenbosch University **2015**.
217. G. Chiellini, G. Nesi, S. Sestito, S. Chiarugi, M. Runfola, S. Espinoza, M. Sabatini, L. Bellusci, A. Laurino, E. Cichero, R. R. Gainetdinov, P. Fossa, L. Raimondi, R. Zucchi, S. Rapposelli, Hit-to-Lead Optimization of Mouse Trace Amine Associated Receptor 1 (MTAAR1) Agonists with a

Diphenylmethane-Scaffold: Design, Synthesis, and Biological Study. *Journal of Medicinal Chemistry* **2016**, *59*, 9825-9836.

218. R. Pasceri, D. Siegel, D. Ross, C. J. Moody, Aminophenoxazinones as Inhibitors of Indoleamine 2,3-Dioxygenase (IDO). Synthesis of Exfoliazone and Chandrananimycin A. *Journal of Medicinal Chemistry* **2013**, *56*, 3310-3317.
219. G. Chiellini, G. Nesi, M. Digiacomo, R. Malvasi, S. Espinoza, M. Sabatini, S. Frascarelli, A. Laurino, E. Cichero, M. Macchia, R. R. Gainetdinov, P. Fossa, L. Raimondi, R. Zucchi, S. Rapposelli, Design, Synthesis, and Evaluation of Thyronamine Analogues as Novel Potent Mouse Trace Amine Associated Receptor 1 (MTAAR1) Agonists. *Journal of Medicinal Chemistry* **2015**, *58*, 5096-5107.
220. J. Ding, K. Das, H. Moereels, L. Koymans, K. Andries, P. A. Janssen, S. H. Hughes, E. Arnold, Structure of HIV-1 RT/TIBO R 86183 Complex Reveals Similarity in the Binding of Diverse Nonnucleoside Inhibitors. *Nature Structural Biology* **1995**, *2*, 407-415.
221. M. Bollini, R. A. Domaoal, V. V. Thakur, R. Gallardo-Macias, K. A. Spasov, K. S. Anderson, W. L. Jorgensen, Computationally-Guided Optimization of a Docking Hit to Yield Catechol Diethers as Potent Anti-HIV Agents. *Journal of Medicinal Chemistry* **2011**, *54*, 8582-8591.
222. D. M. Himmel, K. Das, A. D. Clark, S. H. Hughes, A. Benjahad, S. Oumouch, J. Guillemont, S. Coupa, A. Poncelet, I. Csoka, C. Meyer, K. Andries, C. H. Nguyen, D. S. Grierson, E. Arnold, Crystal Structures for HIV-1 Reverse Transcriptase in Complexes with Three Pyridinone Derivatives: A New Class of Non-Nucleoside Inhibitors Effective against a Broad Range of Drug-Resistant Strains. *Journal of Medicinal Chemistry* **2005**, *48*, 7582-7591.
223. A. Jutand, A. Mosleh, Rate and Mechanism of Oxidative Addition of Aryl Triflates to Zerovalent Palladium Complexes. Evidence for the Formation of Cationic (σ-Aryl)Palladium Complexes. *Organometallics* **1995**, *14*, 1810-1817.
224. R. Chinchilla, C. Najera, Recent Advances in Sonogashira Reactions. *Chemical Society Reviews* **2011**, *40*, 5084-5121.
225. K. Sonogashira, Y. Tohda, N. Hagihara, A Convenient Synthesis of Acetylenes: Catalytic Substitutions of Acetylenic Hydrogen with Bromoalkenes, Iodoarenes and Bromopyridines. *Tetrahedron Letters* **1975**, *16*, 4467-4470.
226. R. Chinchilla, C. Nájera, The Sonogashira Reaction: A Booming Methodology in Synthetic Organic Chemistry. *Chemical Reviews* **2007**, *107*, 874-922.
227. L. Xue, Z. Lin, Theoretical Aspects of Palladium-Catalysed Carbon-Carbon Cross-Coupling Reactions. *Chemical Society Reviews* **2010**, *39*, 1692-1705.
228. J. A. Newby, D. W. Blaylock, P. M. Witt, J. C. Pastre, M. K. Zacharova, S. V. Ley, D. L. Browne, Design and Application of a Low-Temperature Continuous Flow Chemistry Platform. *Organic Process Research & Development* **2014**, *18*, 1211-1220.
229. I. G. Trostyanskaya, I. P. Beletskaya, A Copper (I or II)/Diethylphosphite Catalytic System for Base-Free Additive Dimerization of Alkynes. *Tetrahedron* **2017**, *73*, 148-153.
230. L. Anastasia, E.-i. Negishi, Highly Satisfactory Procedures for the Pd-Catalyzed Cross Coupling of Aryl Electrophiles with in Situ Generated Alkynylzinc Derivatives. *Organic Letters* **2001**, *3*, 3111-3113.
231. E.-i. Negishi, L. Anastasia, Palladium-Catalyzed Alkynylation. *Chemical Reviews* **2003**, *103*, 1979-2018.
232. Y. Norihiko, M. Shigeru, M. Norio, F. Tsuyoshi, S. Akira, Preparation of 1-Aryl- or 1-Alkenyl-2-(perfluoroalkyl)acetylenes. *Bulletin of the Chemical Society of Japan* **1990**, *63*, 2124-2126.
233. E. Negishi, Palladium- or Nickel-Catalyzed Cross Coupling. A New Selective Method for Carbon-Carbon Bond Formation. *Accounts of Chemical Research* **1982**, *15*, 340-348.
234. R. Li, X. Wang, Z. Wei, C. Wu, F. Shi, Reaction of Arynes with Vinylogous Amides: Nucleophilic Addition to the Ortho-Quinodimethide Intermediate. *Organic Letters* **2013**, *15*, 4366-4369.

235. Y. Li, D. Shi, P. Zhu, H. Jin, S. Li, F. Mao, W. Shi, Copper Mediated Oxidative Coupling between Terminal Alkynes and CuCN. *Tetrahedron Letters* **2015**, *56*, 390-392.
236. L. Fen-Tair, W. Ren-Tzong, A Novel Synthesis of Cyanoalkynes Via Iodide-Catalyzed Cyanation of Terminal Acetylenes with Cuprous Cyanide. *Tetrahedron Letters* **1993**, *34*, 5911-5914.
237. B. Desai, K. Dixon, E. Farrant, Q. Feng, K. R. Gibson, W. P. van Hoorn, J. Mills, T. Morgan, D. M. Parry, M. K. Ramjee, C. N. Selway, G. J. Tarver, G. Whitlock, A. G. Wright, Rapid Discovery of a Novel Series of ABL Kinase Inhibitors by Application of an Integrated Microfluidic Synthesis and Screening Platform. *Journal of Medicinal Chemistry* **2013**, *56*, 3033-3047.
238. E.-i. Negishi, M. Qian, F. Zeng, L. Anastasia, D. Babinski, Highly Satisfactory Alkynylation of Alkenyl Halides Via Pd-Catalyzed Cross-Coupling with Alkynylzincs and Its Critical Comparison with the Sonogashira Alkynylation. *Organic Letters* **2003**, *5*, 1597-1600.
239. G. Lai, N. K. Bhamare, W. K. Anderson, A One-Pot Method for the Efficient Preparation of Aromatic Nitriles from Aldehydes Using Ammonia, Magnesium Sulfate, and Manganese Dioxide. *Synlett* **2001**, *2001*, 0230-0231.
240. G. D. McAllister, C. D. Wilfred, R. J. K. Taylor, Tandem Oxidation Processes: The Direct Conversion of Activated Alcohols into Nitriles. *Synlett* **2002**, *2002*, 1291-1292.
241. O. Koniev, S. Kolodych, Z. Baatarkhuu, J. Stojko, J. Eberova, J.-Y. Bonnefoy, S. Cianférani, A. Van Dorsselaer, A. Wagner, Mapn: First-in-Class Reagent for Kinetically Resolved Thiol-to-Thiol Conjugation. *Bioconjugate Chemistry* **2015**, *26*, 1863-1867.
242. P. Reutenauer, M. Kivala, P. D. Jarowski, C. Boudon, J.-P. Gisselbrecht, M. Gross, F. Diederich, New Strong Organic Acceptors by Cycloaddition of Tcne and Tcnq to Donor-Substituted Cyanoalkynes. *Chemical Communications* **2007**, 4898-4900.
243. H. S. Han, Y. J. Lee, Y.-S. Jung, S. B. Han, Stereoselective Photoredox-Catalyzed Chlorotrifluoromethylation of Alkynes: Synthesis of Tetrasubstituted Alkenes. *Organic Letters* **2017**, *19*, 1962-1965.
244. A. Soheili, J. Albaneze-Walker, J. A. Murry, P. G. Dormer, D. L. Hughes, Efficient and General Protocol for the Copper-Free Sonogashira Coupling of Aryl Bromides at Room Temperature. *Organic Letters* **2003**, *5*, 4191-4194.
245. J. Clayden, N. Greeves, S. Warren, P. Wothers, Organometallic Chemistry in *Organic Chemistry*, Oxford University Press Inc., New York, **2001**, 1311 - 1343.
246. N. Nakajima, M. Ubukata, Preparation of Nitriles from Primary Amides under Swern Oxidation Conditions. *Tetrahedron Letters* **1997**, *38*, 2099-2102.
247. N. Nakajima, M. Saito, M. Ubukata, Activated Dimethyl Sulfoxide Dehydration of Amide and Its Application to One-Pot Preparation of Benzyl-Type Perfluoroimidates. *Tetrahedron* **2002**, *58*, 3561-3577.
248. T. T. Tidwell, Oxidation of Alcohols by Activated Dimethyl Sulfoxide and Related Reactions: An Update. *Synthesis* **1990**, *1990*, 857-870.
249. A. H. Fenselau, E. H. Hamamura, J. G. Moffatt, Carbodiimide-Sulfoxide Reactions. VIII. Reactions of Oximes and Hydroxylamines. *The Journal of Organic Chemistry* **1970**, *35*, 3546-3552.
250. M. Marx, T. T. Tidwell, Reactivity-Selectivity in the Swern Oxidation of Alcohols Using Dimethyl Sulfoxide-Oxalyl Chloride. *The Journal of Organic Chemistry* **1984**, *49*, 788-793.
251. F. F. Fleming, Q. Wang, Unsaturated Nitriles: Conjugate Additions of Carbon Nucleophiles to a Recalcitrant Class of Acceptors. *Chemical Reviews* **2003**, *103*, 2035-2078.
252. H. Azijn, I. Tirry, J. Vingerhoets, M.-P. de Béthune, G. Kraus, K. Boven, D. Jochmans, E. Van Craenenbroeck, G. Picchio, L. T. Rimsky, TMC278, a Next-Generation Nonnucleoside Reverse Transcriptase Inhibitor (NNRTI), Active against Wild-Type and NNRTI-Resistant HIV-1. *Antimicrobial Agents and Chemotherapy* **2010**, *54*, 718-727.

253. W. L. Jorgensen, M. Bollini, V. V. Thakur, R. A. Domaoal, K. A. Spasov, K. S. Anderson, Efficient Discovery of Potent Anti-HIV Agents Targeting the Tyr181Cys Variant of HIV Reverse Transcriptase. *Journal of the American Chemical Society* **2011**, *133*, 15686-15696.
254. I. P. Beletskaya, A. V. Cheprakov, The Heck Reaction as a Sharpening Stone of Palladium Catalysis. *Chemical Reviews* **2000**, *100*, 3009-3066.
255. A. Jutand, Mechanisms of the Mizoroki–Heck Reaction in *The Mizoroki–Heck Reaction*, John Wiley & Sons, Ltd, Hoboken, New Jersey, **2009**, 1-50.
256. M. Bruch, *NMR Spectroscopy Techniques, Second Edition*, Taylor & Francis, New York, **1996**.
257. A. Spencer, A Highly Efficient Version of the Palladium-Catalysed Arylation of Alkenes with Aryl Bromides. *Journal of Organometallic Chemistry* **1983**, *258*, 101-108.
258. X. Cui, Y. Zhou, N. Wang, L. Liu, Q.-X. Guo, N-Phenylurea as an Inexpensive and Efficient Ligand for Pd-Catalyzed Heck and Room-Temperature Suzuki Reactions. *Tetrahedron Letters* **2007**, *48*, 163-167.
259. T. Mino, Y. Shirae, Y. Sasai, M. Sakamoto, T. Fujita, Phosphine-Free Palladium Catalyzed Mizoroki−Heck Reaction Using Hydrazone as a Ligand. *The Journal of Organic Chemistry* **2006**, *71*, 6834-6839.
260. B. K. Allam, K. N. Singh, An Efficient Phosphine-Free Heck Reaction in Water Using Pd(L-proline)2 as the Catalyst under Microwave Irradiation. *Synthesis* **2011**, *2011*, 1125-1131.
261. W.-M. Dai, K. W. Lai, Chemistry of Aminophenols. Part 3: First Synthesis of Nitrobenzo[b]Furans Via a Coupling–Cyclization Approach. *Tetrahedron Letters* **2002**, *43*, 9377-9380.
262. X. Sun, W. Li, L. Zhou, X. Zhang, Enantioselective Hydrogenation of A-Dehydroamino Acid Esters Catalyzed by Rhodium Complexes with Chiral Bisaminophosphine Ligands. *Advanced Synthesis & Catalysis* **2010**, *352*, 1150-1154.
263. M. G. Banwell, M. T. Jones, D. T. J. Loong, D. W. Lupton, D. M. Pinkerton, J. K. Ray, A. C. Willis, A Pd[0]-Catalyzed Ullmann Cross-Coupling/Reductive Cyclization Approach to C-3 Mono-Alkylated Oxindoles and Related Compounds. *Tetrahedron* **2010**, *66*, 9252-9262.
264. C.-J. Wang, Z.-P. Xu, X. Wang, H.-L. Teng, Axial [6,6′-(2,4-pentadioxy)]-1,1′-biphenyl-2,2′-diamine (Pd-bipham): Practical Synthesis and Applications in Asymmetric Hydrogenation. *Tetrahedron* **2010**, *66*, 3702-3706.
265. G. Bartoli, Conjugate Addition of Alkyl Grignard Reagents to Mononitroarenes. *Accounts of Chemical Research* **1984**, *17*, 109-115.
266. A. Ricci, M. Fochi, Reactions between Organomagnesium Reagents and Nitroarenes: Past, Present, and Future. *Angewandte Chemie International Edition* **2003**, *42*, 1444-1446.
267. R. Dalpozzo, G. Bartoli, Bartoli Indole Synthesis. *Current Organic Chemistry* **2005**, *9*, 163-178.
268. Z. Li, H. Yu, C. Bolm, Dibenzothiophene Sulfoximine as an NH_3 Surrogate in the Synthesis of Primary Amines by Copper-Catalyzed C–X and C–H Bond Amination. *Angewandte Chemie International Edition* **2017**, *56*, 9532-9535.
269. M. G. Vetelino, J. W. Coe, A Mild Method for the Conversion of Activated Aryl Methyl Groups to Carboxaldehydes Via the Uncatalyzed Periodate Cleavage of Enamines. *Tetrahedron Letters* **1994**, *35*, 219-222.
270. S. Caron, E. Vazquez, R. W. Stevens, K. Nakao, H. Koike, Y. Murata, Efficient Synthesis of [6-Chloro-2-(4-chlorobenzoyl)-1*H*-indol-3-yl]-acetic Acid, a Novel COX-2 Inhibitor. *The Journal of Organic Chemistry* **2003**, *68*, 4104-4107.
271. S. C. Glossop, A Microwave-Assisted Alternative Synthesis of 8-Amino-2-methyl-3,4-dihydroisoquinoli-*N*-1-one. *Synthesis* **2007**, *2007*, 981-983.
272. R. E. TenBrink, W. B. Im, V. H. Sethy, A. H. Tang, D. B. Carter, Antagonist, Partial Agonist, and Full Agonist Imidazo[1,5-a]quinoxaline Amides and Carbamates Acting through the GABAA/Benzodiazepine Receptor. *Journal of Medicinal Chemistry* **1994**, *37*, 758-768.

273. N. Sawatari, S. Sakaguchi, Y. Ishii, Oxidation of Nitrotoluenes with Air Using *N*-Hydroxyphthalimide Analogues as Key Catalysts. *Tetrahedron Letters* **2003**, *44*, 2053-2056.
274. S. Yamada, D. Morizono, K. Yamamoto, Mild Oxidation of Aldehydes to the Corresponding Carboxylic Acids and Esters: Alkaline Iodine Oxidation Revisited. *Tetrahedron Letters* **1992**, *33*, 4329-4332.
275. J. Pospíšil, C. Müller, A. Fürstner, Total Synthesis of the Aspercyclides. *Chemistry – A European Journal* **2009**, *15*, 5956-5968.
276. R. Pappo, J. D. S. Allen, R. U. Lemieux, W. S. Johnson, Notes - Osmium Tetroxide-Catalyzed Periodate Oxidation of Olefinic Bonds. *The Journal of Organic Chemistry* **1956**, *21*, 478-479.
277. D. Kidjemet, N,N-Dimethylformamide Dimethyl Acetal. *Synlett* **2002**, *2002*, 1741-1742.
278. S. O. Simonetti, E. L. Larghi, T. S. Kaufman, A Convenient Approach to an Advanced Intermediate toward the Naturally Occurring, Bioactive 6-Substituted 5-Hydroxy-4-aryl-1*H*-quinolin-2-ones. *Organic & Biomolecular Chemistry* **2016**, *14*, 2625-2636.
279. C. Yoakim, E. Malenfant, B. Thavonekham, W. Ogilvie, R. Deziel, Non-Nucleoside Reverse Transcriptase Inhibitors, Patent, US20040106791 A1, **2004**
280. G. Tojo, M. Fernández, Permanganate in *Oxidation of Primary Alcohols to Carboxylic Acids: A Guide to Current Common Practice*, Springer New York, New York, NY, **2007**, 1-12.
281. I. Sapountzis, H. Dube, R. Lewis, N. Gommermann, P. Knochel, Synthesis of Functionalized Nitroarylmagnesium Halides Via an Iodine−Magnesium Exchange. *The Journal of Organic Chemistry* **2005**, *70*, 2445-2454.
282. I. Sapountzis, P. Knochel, General Preparation of Functionalized O-Nitroarylmagnesium Halides through an Iodine-Magnesium Exchange. *Angewandte Chemie - International Edition* **2002**, *41*, 1610 - 1611.
283. A. F. Burchat, J. M. Chong, N. Nielsen, Titration of Alkyllithiums with a Simple Reagent to a Blue Endpoint. *Journal of Organometallic Chemistry* **1997**, *542*, 281-283.
284. A. Dell'Isola, M. M. W. McLachlan, B. W. Neuman, H. M. N. Al-Mullah, A. W. D. Binks, W. Elvidge, K. Shankland, A. J. A. Cobb, Synthesis and Antiviral Properties of Spirocyclic [1,2,3]-Triazolooxazine Nucleosides. *Chemistry – A European Journal* **2014**, *20*, 11685-11689.
285. M. Zhang, D. L. Flynn, P. R. Hanson, Oligomeric Benzylsulfonium Salts: Facile Benzylation Via High-Load Romp Reagents. *The Journal of Organic Chemistry* **2007**, *72*, 3194-3198.
286. O. V. Dolomanov, L. J. Bourhis, R. J. Gildea, J. A. K. Howard, H. Puschmann, OLEX2: A Complete Structure Solution, Refinement and Analysis Program. *Journal of Applied Crystallography* **2009**, *42*, 339-341.
287. G. Sheldrick, SHELXT - Integrated Space-Group and Crystal-Structure Determination. *Acta Crystallographica Section A* **2015**, *71*, 3-8.
288. G. Sheldrick, Crystal Structure Refinement with SHELXL. *Acta Crystallographica Section C* **2015**, *71*, 3-8.